Eleftheria G. Kavousanaki

# Ultrafast Nonlinear Optical Response of the Quantum Hall System

A Doctoral Dissertation


University of Crete
Department of Physics

Heraklion, August 2007

Eleftheria G. Kavousanaki

# Ultrafast Nonlinear Optical Response of the Quantum Hall System

A Dissertation
submitted to the Department of Physics, University of Crete,
in partial fulfillment of the requirements for the Degree of
Doctor of Philosophy in Physics


Heraklion, August 2007

# Ultrafast Nonlinear Optical Response of the Quantum Hall System


| | |
|---|---|
| Thesis author | E. G. Kavousanaki |
| Thesis supervisor | I. E. Perakis |
| Thesis committee | E. N. Economou |
| | I. Giapintzakis |
| | A. Petkou |
| | G. Tsironis |
| | P. Tzanetakis |
| | X. Zotos |

Department of Physics, University of Crete



Heraklion, August 2007

# Contents

# List of Figures

# List of Tables

# List of Abbreviations

| | |
|---|---|
| **2DEG** | Two–dimensional Electron Gas |
| **2DEG$^*$** | Excited Two–dimensional Electron Gas |
| **DCTS** | Dynamics Controlled Truncation Scheme |
| **FWM** | Four Wave Mixing |
| **FWHM** | Full Width at Half Maximum |
| **LL** | Landau Level |
| **MP** | Magnetoplasmon |
| **MR** | Magnetoroton |
| **PSF** | Phase Space Filling |
| **QH** | Quantum Hall |
| **RPA** | Random Phase Approximation |
| **SBE** | Semiconductor Bloch Equations |
| **SR–FWM** | Spectrally Resolved Four Wave Mixing |
| **TI–FWM** | Time Integrated Four Wave Mixing |
| **X** | Exciton (Magnetoexciton) |

# Acknowledgments

Over the years I have been working on my PhD, but also on a longer scale, my interaction with many people has directly or indirectly contributed to the completion of this work. It is thus most appropriate to start by thanking them.

I am grateful to my advisor, Ilias Perakis, for introducing me into the physics of non–equilibrium phenomena and giving me the opportunity to work on such a fascinating subject as the ultrafast nonlinear optical response of the quantum Hall system. Our collaboration has affected deeply the way I work and do physics.

I feel particularly fortunate for my collaboration with the experimental group of Daniel Chemla at the University of California at Berkeley, a pioneering group in ultrafast spectroscopy in semiconductors. I have learned a lot through this collaboration, which helped me bridge theoretical and experimental physics. Keshav Dani performed the bulk of the experiments that are related to this thesis. I would like to thank him for our wonderful collaboration and his enthousiasm that kept us working hard at every odd hour. I would also like to thank Jerome Tignon for his advices and useful comments, as well as his hospitality at École Normale Supérieure in Paris.

An important part of my work is based on numerical calculations written in Fortran. My programs were based on the code that Thanos Karathanos offered me kindly at the beginning of my PhD. I thank him for this; he has saved me a lot of time. I also thank Dimitris Counalakis for his help when computer–related disasters occurred, usually at the most inappropriate times.

When starting my PhD I studied spin dynamics in diluted magnetic semiconductors and collaborated with Jaroslav Chovan. I thank him for our collaboration and friendship.

I have been at the Department of Physics, University of Crete long enough to feel it like home. I would like to thank all faculty members, postdocs and graduate students for our discussions and interaction. I have gained a lot. Stefanos Trahanas has affected me deeply as a physicist and a teacher. I am also indebted to T. Tomaras for his advices.

I would like to thank all my friends and officemates for their friendship and support. I am particularly thankful to Maria Eleftheriou, Maria Fyta and Marotesa Voultsidou for their support, moral and practical.

I am grateful to Grigoris Panotopoulos for our innumerous discussions on physics and life in general, as well as his everlasting support and patience.

Last but not least, I would like to express my gratitude to my parents and my sister Melina for their love and encouragement. I wouldn't be anywhere without them.

Let us now turn our attention to the ultrafast nonlinear optical response of the quantum Hall system.

# Abstract

In the present dissertation we discuss a theory of the ultrafast nonlinear optical response of the quantum Hall system. Our theory focusses on the role of the low energy collective electronic excitations of the cold, strongly correlated, two–dimensional electron gas (2DEG) present in the ground state. It takes into account ground state electron correlations and Pauli exchange and interaction effects between the photoexcited excitons and the collective electron gas excitations. Our formulation addresses both the initial coherent regime, where the dynamics is determined by exciton and 2DEG polarizations and quantum mechanical coherences, and the subsequent incoherent regime, dominated by population dynamics. We discuss the manifestations of intraband and interband coherences induced by the collective 2DEG excitations in the coupled photocarrier–quantum Hall system and compare to transient three–pulse four–wave–mixing experiments. In addition, we apply our theory to the case of an undoped quantum well in a magnetic field and describe the creation of intraband and interband coherences therein, created by the photoexcited carriers.

# Chapter 1

# Introduction

## 1.1 Motivation

The quasiparticle concept is a cornerstone of modern condensed matter physics. To first approximation, the properties of many physical systems can be described in terms of non–interacting quasiparticles and elementary excitations, which may differ substantially from the strongly interacting bare electrons [1]. However, beyond the first order, residual interactions among the quasiparticles remain. In many cases, the quasi–static, thermodynamic, linear, and ground state properties do not depend critically on the residual interactions. On the other hand, these interactions determine the dynamics in the system. For example, correlations among quasiparticles due to interactions create quantum coherences among the many–body states, but also lead to decoherence and dephasing and limit the lifetime of the collective excitations [2, 3]. Understanding the dynamics of a many–body system requires to go beyond the non-interacting quasiparticle picture. Moreover, from a technological point of view, understanding the coherent dynamics is essential for building the new generation of controllable quantum coherent devices in the future. In that sense, "clean" and well–characterized many–body systems, such as the quantum Hall system of interest here, provide an ideal laboratory for testing new ideas that may be useful for implementing such quantum coherent devices. From a fundamental physics point of view, the role of many–body interactions on the quantum dynamics during the very early time scales where the many–body system has not yet relaxed and where quantum mechanical coherences created by the interactions have not yet decayed presents a frontier of modern condensed matter physics. This very early temporal regimes typically lasts for hundreds of femtoseconds and can be explored by using ultrafast nonlinear spectroscopy.

Ultrafast nonlinear optical spectroscopy is a powerful tool to study both coherent and incoherent dynamics. Over the past decade, it has been used extensively to study the dynamics of photoexcited carriers in undoped semiconductors [2, 3]. To analyse such experiments, theories such as the Dynamics Controlled Truncation Scheme (DCTS) [4–6], the correlation expansion [7], or the Keldysh Green function technique [8, 9] have been developed. These studies revealed the important role of Coulomb correlations among the photoexcited electron–hole pairs. For example, in two–pulse four–wave–mixing (FWM) experiments [10, 11], Pauli blocking or phase space filling (PSF) effects do not contribute for negative time delays [12], while exciton–exciton (X–X) interactions dominate [2]. The time–dependent Hartree–Fock treatment of X–X interactions [8] predicts an asymmetric FWM temporal profile, with a negative time delay signal decaying twice as fast as the positive time delay signal [2, 3, 13]. The observation of strong deviations from this asymmetric temporal profile was interpreted as the signature of X–X correlations in undoped semiconductor quantum wells [2, 3].

In understanding the results of such experiments, one need not take into account correlations with the ground state. In undoped semiconductors, the lowest electronic excitations are high energy interband transitions that can react almost instantaneously to photoexcited carriers [14, 15]. Then the ground state can be considered as rigid, merely providing the band structure and dielectric screening. On the other hand, in doped semiconductors, the situation is quite different because of the presence of low energy excitations that can interact with photoexcited carriers. Several interesting systems fall in this category, like high temperature superconductors [16, 17], and the quantum Hall system [18–20]. The fundamental reaction time of these systems, typically the period of one oscillation of the lowest excited state, is slow and they respond unadiabatically to photoexcitation. The nonlinear response is then strongly influenced not just by the dynamics of photoexcited carriers, but also by the quantum dynamics of the entire system. For the quantum Hall system, the presence of strong many–body correlations in the ground state itself leads to the quantum Hall effects [21–24]. Naturally, one expects these strong many–body correlations to produce interesting dynamics as well, which in turn influence the nonlinear response of the system. Such dynamics was not studied until very recently.

In addition, the theories used to describe the nonlinear response of undoped semiconductors, like the DCTS [4–6], break down for doped semiconductors, like the quantum Hall system [25]. The DCTS truncates the hierarchy of density matrices generated by the interactions based on the fact that, in the undoped system, all Coulomb interactions occur between photoexcited $e$–$h$ pairs and are thus dynamically generated by the optical

excitation, treated with an expansion in terms of the optical field. It also assumes the absence of free carriers in the ground state [6], a condition that does not hold in the quantum Hall system. Thus, the almost unexplored dynamics of strongly correlated systems whose ground state electrons interact unadiabatically with the photo–excited $e$–$h$ pairs raises very fundamental questions. In the doped system, the direct X–X interactions are screened, and the nonlinear response is mainly determined by the Fermi sea and electron gas excitations [26–32]. The presence of collective low energy electronic excitations and the resulting non-Markovian dynamics and memory effects, as well as the strongly correlated ground state, raise formidable theoretical difficulties for describing the non-linear optical dynamics of the quantum Hall and doped semiconductor system. For example, standard diagrammatic expansions and DCTS factorizations that assume a Hartree–Fock reference state break down. In addition, the theory must address the quantum effects due to the Pauli correlations between the collective electronic excitations and the photoexcited carriers. One must thus develop sophisticated theoretical techniques and overcome fundamental issues in order to understand the nonlinear response to photoexcitation.

As our quantum Hall system we consider a GaAs quantum well doped with electrons, which form a two–dimensional electron gas (2DEG). In the presence of a large perpendicular magnetic field, this is a well known quantum Hall system [33, 34]. The confinement in the $z$–direction due to the quantum well structure and the quasi–confinement in the $x$–$y$ plane due to the magnetic field exacerbate the quantum properties of the system. This confinement results in discrete, equally spaced, equally degenerate eigenstates known as Landau levels (LL) [21], which in the ground state are partially filled with the 2DEG. The ratio of occupied states to LL degeneracy gives the filling factor $\nu$. The LL degeneracy increases with magnetic field, and above a threshold value ($\nu \leq 2$), the ground state electrons only occupy the lowest LL (LL0) states; all the higher LLs (LL1, ...) are then empty in the ground state. The coupling of the degenerate LL states by the Coulomb interaction results in a strongly correlated incompressible quantum liquid, with low energy collective excitations such as the magnetoplasmons (MP) and the magnetorotons (MR) [35–37], whose properties depend on the filling factor. Exchange Coulomb interactions can stabilize a ground state with polarized electron spins for certain integer values of $\nu$ or certain fractional values of $\nu = 1/m$, where $m$ is an integer [21, 22].

The study of the ultrafast nonlinear optical dynamics of the quantum Hall system transcends across the boundaries of two communities largely disconnected up to now. Indeed, the transient optical properties of this system are governed by (i) the interband (exciton (X)) excitations (with the 2DEG at

rest), which consist of 1 $e$–$h$, 2 $e$–$h$, ... pairs created in the LLs (studied by the nonlinear optics community), and (ii) the intraband 2DEG excitations (with unexcited quantum well and full valence band), e.g. the 1–MP, 2–MP, ... and incoherent pair excitations (studied by the quantum Hall community). The ensemble of states that determine the nonlinear optical spectra to $(2\ell-1)$–th order in the optical field consist of products of up to $\ell$ $e$–$h$ pairs and $n$ 2DEG excitations. One can then draw an analogy with the X+phonon states that determine the ultrafast optical dynamics in undoped semiconductors [6, 7, 9]. However, there are some important differences. In the quantum Hall system, the 2DEG excitations are electronic in nature, and therefore subject to Pauli correlations with the photoexcited excitons, while the ground state electrons are strongly correlated. On the other hand, in the undoped system, the X operators commute with the collective excitation (phonon) operators, while the ground state correlations can be neglected. Thus the theoretical formulations used to study the nonlinear optical response in undoped semiconductors must be extended in order to treat correlations in the doped system. Despite the impressive work in the past on the ultrafast nonlinear optical response of undoped semiconductors and the properties of the quantum Hall system, so far these two fields are disconnected. The recent ultrafast wave mixing experiments on the quantum Hall system and the quantum coherent ultarfast dynamics that they reveal, which must be attributed to the many–body interactions, point out the need to develop a theoretical formulation that treats the effects of both intreband and intraband collective excitations in the very early coherent temporal regime.

Recent time–resolved four–wave–mixing experiments have shed new light into the dynamics of this strongly correlated system [25, 38–48]. The 2DEG correlations and collective electronic excitations dominate the dephasing of the photoexcited excitons for low photoexcitation intensities [25, 38–48], while the time and frequency dependence of the FWM spectra revealed new dynamical features that could not be explained within the random phase approximation (RPA). Of particular interest is the dynamics of the quantum Hall system during time scales comparable to the characteristic time it takes the cold 2DEG "bath" system to react to the introduction of photoexcited excitons. The dephasing times of the two lowest LL excitons in the quantum Hall system range from a few picoseconds (LL0) to a few hundreds of femtoseconds (LL1), while the 2DEG responds to the X–2DEG interactions within a time interval comparable to the period of its low energy excitations. The period of the lowest inter–LL magnetoplasmon collective modes [21, 49] is $T_{MP} = 2\pi\hbar/\Omega_M$, where $\Omega_M \sim 15 - 20$ meV is the MP excitation energy. Therefore, $T_{MP}$ is of the order of a few hundreds of femtoseconds, longer than the duration of the $\sim$100fs optical pulses used to probe this system. As a

result, strong quantum kinetic effects in the ultrafast non-linear optical dynamics are expected in this regime, and well–established pictures such as the semiclassical Boltzmann picture of dephasing and relaxation (which assumes instantaneous X–2DEG scattering) and the Markov approximation need to be revisited [2, 3, 7, 9, 50, 51].

This thesis is the result of a close collaboration with the experimental group of Daniel Chemla at the University of California Berkeley, who performed the first ultrafast four wave mixing experiments in the quantum Hall system. To interpret these experiments, a new theoretical formulation had to be developed, which extends the previous theoretical treatments of the ultrafast coherent dynamics of excitons in undoped semiconductors to include the collective excitations and ground state correlations of the quantum Hall system. The work presented here is the first theoretical attempt that addresses these problems. As we discuss in more detail later on, the comparison with the experiments allowed us to develop approximations from the full theoretical formulation that highlight the important non–equilibrium many–body physics that these experiments were able to access for the first time. Our theoretical formulation describes the ultrafast third–order nonlinear optical response of the quantum Hall system at zero temperature and addresses both the coherent and incoherent regimes. Our approach is based on the projection of the exciton states and the separation of the uncorrelated contributions to the third–order nonlinear optical response from the contributions due to correlations among the interband and intraband elementary excitations. Similar to the DCTS [4–6], we use an expansion in terms of the optical field in order to eliminate the number of independent dynamical variables that need to be considered. The X–2DEG correlations however do not allow the complete factorization of the intraband density matrix into products of interband coherences as in the case of the DCTS. We were able to separate out the correlated contributions, which lead to the incoherent effects, without assuming a Hartree–Fock ground state, as in the case of the DCTS. Although our theory can be used to treat the general case, we are interested is the spin–$\uparrow$ polarized LL0 2DEG, motivated by recent three–pulse FWM experiments [45–47, 52]. We derive an average polarization model from the full theoretical formulation to explain the experimental results, and show we can access the interband and intraband dynamics of the system. We also discuss a microscopic treatment of the scattering between of X+MP and X+MR states. As a special case, we also apply our theory in the case of an undoped semiconductor quantum well, where our approach reduces to the DCTS.

## 1.2 Structure of Thesis

In Chapter 2 we present the background scientific material that is necessary to understand the ultrafast nonlinear optical response of the quantum Hall system. We first review the quantum Hall system. We discuss the GaAs band structure and the creation of a 2DEG in a GaAs/AlGasAs heterostructure. We then discuss the energy spectrum of a doped GaAs quantum well in a large magnetic field, i.e. the eigenstructure of the quantum Hall system, as well as its low energy collective excitations, which are important in the system's nonlinear optical response. In the second part of this chapter, we discuss ultrafast nonlinear optical spectroscopy and review three–pulse four–wave–mixing, in order to understand the experimental results that we will present at a later stage. We also study four–wave–mixing in a non–interacting ensemble of two–level systems, which when compared to our many–body theory will allow us to distinguish the experimental features of the many–body interactions. We finish by discussing Coulomb interactions in undoped semiconductors, and describing the theories used for this study: the semiconductor Bloch equations and the DCTS.

In Chapter 3, we present our theoretical formulation that describes the ultrafast third–order nonlinear optical response of the quantum Hall system. We first setup the general problem and discuss the nature of the exciton and magnetoplasmon states that determine the optical spectra. We then present the equations of motion for the nonlinear polarizations and photoexcited carrier populations and identify the contributions due to the many–body correlations. We then present a decoupling scheme for treating the interaction effects, which is motivated by a decomposition of the photoexcited many–body states that separates out the uncorrelated and excitonic contributions from the correlated and incoherent contributions. We use this approach to devise a factorization scheme and identify the intraband and interband correlated contributions to the density matrix. We also discuss the linear absorption spectra. We finish by briefly discussing the coherent X–X interactions and scattering effects.

In Chapter 4 we apply the above theoretical framework to derive an average polarization model and explain a recent three–pulse FWM experiment on the quantum Hall system [45]. We first briefly describe the experiment and the experimental results. We then present the average polarization model, with which we calculate the FWM signal for the excitation conditions of the experiment. We also show that we can access the dynamics of both interband and intraband excitations of the system. We then present simple analytical solutions of our model, which will give us an intuitive picture about the dominant physical mechanisms in the ultrafast dynamics of the system. Finally,

we present full numerical calculations of the spectrally resolved FWM signal, which when compared with the experiment, will allow us to identify the trace of X–X+MP coherences and put an upper bound on their dephasing rate.

In Chapter 5, we apply our theory in the special case of an undoped quantum well in a perpendicular magnetic field, motivated by a very recent FWM experiment on this system [53]. In this case, our approach reduces to the DCTS if phonons are included. We begin by describing the main experimental results of a recent FWM and presenting an average polarization model derived from our theory. We then discuss some simple analytical solutions of the model, which by comparing to the experiment, will allow us to identify the signature of a Raman coherence and will extract its dephasing rate. We finish by discussing our numerical calculations and explaining the contributions of the different physical mechanisms to the nonlinear response of the undoped quantum well.

In Chapter 6 we return to the quantum Hall system and discuss in more detail the role of X+MP states in its linear and nonlinear response for filling factor $\nu = 1$. We first discuss the linear response and derive the equations of motion for the linear polarizations. We also study the energy dispersion of the X+MP states. We then calculate the linear absorption spectrum and we show that it is strongly affected by X+MP states with non–zero momentum and by rescattering many–body processes. We also discuss the nonlinear response by deriving the equations of motion for the nonlinear polarizations, which are coupled to X–X, X–X+MP and X+MP–X+MP coherences. We end by calculating the FWM signal and discussing the role of X+MP states therein.

Finally, in Chapter 7, we summarize our work and discuss its perspectives.

## 1.3 Related Publications

Parts of this dissertation have been published in the following journals:

- I. E. Perakis, E. G. Kavousanaki, *Theory of ultrafast exciton dynamics in the Quantum Hall system*, Chemical Physics **318**, 118-136 (2005); arXiv:cond-mat/0508322.

- K. M. Dani, J. Tignon, M. Breit, D. S. Chemla, E. G. Kavousanaki, and I. E. Perakis, *Dynamics of the collective excitations of the quantum Hall system*, Physica E **34**, 206-209 (2006).

- E. G. Kavousanaki, K. M. Dani, J. Tignon, D. S. Chemla and I. E. Perakis, *Correlation Effects in the Ultrafast Dynamics of the Quantum*

*Hall System close to* $\nu = 1$, Phys. Stat. Sol. (b) **243**, No. 10, 2397-2404 (2006).

- K. M. Dani, E. G. Kavousanaki, J. Tignon, D. S. Chemla and I. E. Perakis, *Nonlinear Optical studies of the Transient Coherence in the Quantum Hall System*, Solid State Communications **140**, 72-82 (2006); arXiv:cond-mat/0607550.

- K. M. Dani, J. Tignon, M. Breit, D. S. Chemla, E. G. Kavousanaki and I. E. Perakis, *Ultrafast dynamics of coherences in a quantum Hall system*, Phys. Rev. Lett. **97**, 057401 (2006); arXiv:cond-mat/0607545.

  This article was selected for the September 2006 issue of Virtual Journal of Ultrafast Science.

- K. M. Dani, I. A. Cotoros, J. Wang, J. Tignon, D. S. Chemla, E. G. Kavousanaki, I. E. Perakis, *Observation of Inter-Landau-level Quantum Coherence in Semiconductor Quantum Wells*, in preparation.

# Chapter 2

# The quantum Hall system & ultrafast nonlinear optics

## 2.1 Outline

In this chapter, we briefly discuss the background scientific material that is necessary to understand the nonlinear optical response of the quantum Hall system. We begin by reviewing the physics of the quantum Hall system. We first discuss the band structure of GaAs, and explain how a 2DEG is created in a GaAs/AlGaAs heterostructure. We also discuss the 2D exciton eigenstates and calculate the energy spectrum of a 2D electron in a perpendicular magnetic field. We then study the 2DEG in a magnetic field and review its low energy collective excitations.

In the second part of this chapter, we explain the ultrafast nonlinear spectroscopic technique of four–wave–mixing. We then discuss an ensemble of two–level systems, which will give us a good sense of the physics that is probed by FWM experiments, but also, when compared to our results in the following chapters, will show the effects of many–body interactions. Finally we discuss theories that have been developed to treat the nonlinear response of semiconductors: the semiconductor Bloch equations and the Dynamics Controlled Truncation Scheme. We end by discussing the limits of the DCTS and by explaining why we need to extend it in order to understand the nonlinear optical response of the quantum Hall system.

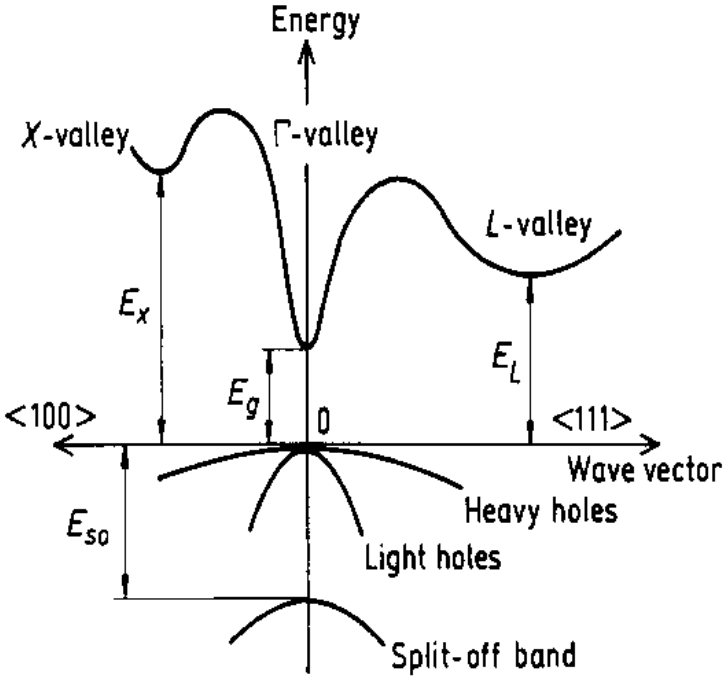


**Figure 2.1:** Schematic of the band structure of GaAs around the Γ point. $E_g = 1.519$ eV and $E_{so} = 0.34$ eV at low temperature. From [54].

## 2.2 The quantum Hall system

### 2.2.1 GaAs quantum wells

Today, GaAs and GaAs/AlGaAs heterostructures can be grown with remarkable purity using molecular beam epitaxy, leading to sharp resonances and long lifetimes for transitions. Such systems are excellent venues for studying thr ultrafast many-body correlations in semiconductors.

The band structure of bulk GaAs near the Γ-point is well described by the effective mass approximation (Fig. 2.1). There are 2 degenerate $s$-like conduction bands, and 6 $p$-like valence bands. The low temperature bandgap is $E_g = 1.519$ eV. The total angular momentum is a good quantum number, and thus the bands can be labeled by $|J, m_J\rangle$. The lowest lying valence bands, $|1/2, \pm 1/2\rangle$, called the split–off bands, are seperated from the other valence bands by the splin–orbit coupling. The large splitting between these bands and the other valence bands ($\approx 0.34$ eV at low temperature) allows us to neglect the split–off bands altogether. The $J = 3/2$ bands are called the heavy hole (hh, $m_J = \pm 3/2$) bands and light hole (lh, $m_J = \pm 1/2$)

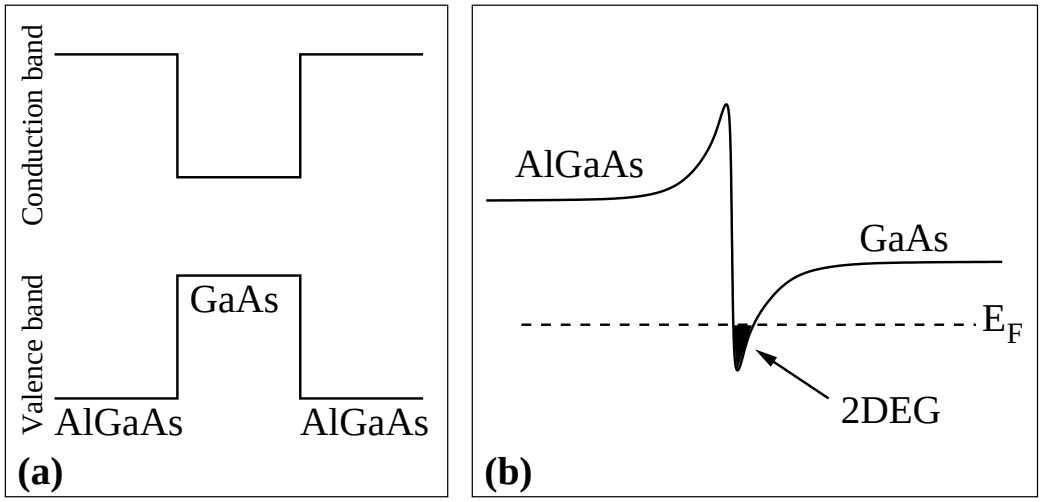


**Figure 2.2:** (a) Schematic of the GaAs/AlGaAs altentative layers. (b) Confinement of the 2DEG at the GaAs/AlGaAs interface.

bands. In bulk GaAs, they are degenerate at $k = 0$, but they have different curvature and therefore different energies away from the zone center. Within the effective mass approximation, this simply means that heavy holes and light holes have different effective masses: $m^*_{hh} = 0.5m_e$, $m^*_{lh} = 0.082m_e$, where $m_e$ is the bare effective mass. The conduction bands have $S = 1/2$, $m_S = \pm 1/2$ and $m^*_e = 0.0665m_e$.

An important advantage of GaAs/AlGaAs heterostructures is that while the band gap for AlGaAs is much higher than that of GaAs, the lattice constants for the two compounds is almost identical. As a result, alternating layers of GaAs and AlGaAs can be grown on top of one another with very little strain induced at the interfaces. By sandwiching a layer of GaAs between two layers of AlGaAs, a quantum well, i.e. a finite potential well is created in the growth direction (Fig. 2.2a). Moreover, if donors are added in the AlGaAs layer, known as modulation doping, the electrons get trapped in a small area at the interface of the two compounds, as shown in Fig. 2.2b. As a result a quasi–two dimensional electron gas is created with the additional advantage of being spacially seperated from the charged impurities.

The electronic states of the quantum well are modified from that of bulk GaAs by the confinement potential. To first approximation, we can think of the confinement potential as an infinite quantum well along the $z$-direction. Consequently, this discretizes the $k_z$ momentum states. Since the discrete energy levels of a particle in a box depend on the mass, the degeneracy of the heavy–hole and light-hole bands is lifted and the hh-conduction band

transition is at a lower energy than the lh transition.

In addition to the continuum of states of the band structure, there are also excitonic eigenstates just below the band edge. These states comprise of an electron in the conduction band and a hole in the valence band with energy the energy of the band gap minus the binding energy of the exciton. The latter is due to Coulomb attraction between the electron and the hole. To obtain the energy levels of a 2D excitonic state, we solve the relative Schrödinger equation for a 2D electron–hole pair:

$$\left[\frac{\mathbf{p}^2}{2m} - \frac{e^2}{\epsilon r}\right]\phi_n(r) = E_n\phi_n(r) \tag{2.1}$$

where $r = |\mathbf{r}_e - \mathbf{r}_h|$ is the electron–hole separation, $\mathbf{p} - \mathbf{p}_e - \mathbf{p}_h$ is the relative momentum and $m$ is the reduced mass, $1/m = 1/m_e^* + 1/m_h^*$. The energy levels $E_n$ are given by

$$E_n = E_g - \frac{R}{(n+1/2)^2}, \qquad n = 0, 1, ... \tag{2.2}$$

and the wavefunction for the lowest exciton state ($1s$) is

$$\phi_{1s}(r) = \left(\frac{2}{\pi}\right)^2 \frac{2}{\alpha} e^{-2r/\alpha} \tag{2.3}$$

where $R = me^4/2\epsilon^2\hbar^2$ is the 3D Rydberg energy and $\alpha = \epsilon\hbar^2/me^2$ is the Bohr radius.

In our study we will consider the quantum well as an ideal 2D system, although this is not the case, as the band gap of AlGaAs is larger than that of GaAs but not infinite. This implies that in the $z$–direction, the electron and hole wavefunctions are not entirely confined within the quantum well, but rather they penetrate into the barrier regions. Also, the quantum well itsself has a finite thickness in the $z$–direction. In our study we will treat the quantum well as purely two–dimensional, although there are effects due to deviations from this ideal picture.

### 2.2.2 2D Electron in a magnetic field

We will begin with the problem of a free electron (with effective mass $m_e^*$) in a uniform magnetic field $\mathbf{B} = B\mathbf{z}$, which is described by the Hamiltonian

$$H = \frac{1}{2m_e^*}\left(-i\hbar\boldsymbol{\nabla} + \frac{e}{c}\mathbf{A}\right)^2 = \frac{1}{2m_e^*}\left(\Pi_x^2 + \Pi_y^2\right) \tag{2.4}$$

where $\mathbf{A}$ is the vector potential related to the magnetic field as $\mathbf{B} = \boldsymbol{\nabla} \times \mathbf{A}$, and $\boldsymbol{\Pi}$ the kinetic momentum. It is straightforward to verify that the $x$ and $y$ componets of $\boldsymbol{\Pi}$ do not commute:

$$[\Pi_x, \Pi_y] = -i\frac{e\hbar B}{c} \tag{2.5}$$

In analogy with the harmonic oscillator, one may define operators $a$ and $a^\dagger$ as a linear compination of $\Pi_x$ and $\Pi_y$, for which $\left[a, a^\dagger\right] = 1$:

$$a = \sqrt{\frac{c}{2e\hbar B}}\left(\Pi_x - i\Pi_y\right) \tag{2.6}$$

$$a^\dagger = \sqrt{\frac{c}{2e\hbar B}}\left(\Pi_x + i\Pi_y\right) \tag{2.7}$$

Using these ladder operators, Eq. (2.4) becomes the same as in the harmonic oscillator:

$$H = \hbar\Omega_c\left(a^\dagger a + \frac{1}{2}\right) \tag{2.8}$$

where

$$\Omega_c = \frac{eB}{m_e^* c} \tag{2.9}$$

is the cyclotron energy. Thus, the eigenenergies are discrete states, known as *Landau levels*:

$$E_n = \hbar\Omega_c\left(n + \frac{1}{2}\right), \qquad n = 0, 1, 2, ... \tag{2.10}$$

By choosing the Landau gauge, for which $\mathbf{A} = Bx\mathbf{y}$, the Hamiltonian becomes

$$H = \frac{1}{2m_e^*}\left[p_x^2 + \left(p_y + \frac{eB}{c}x\right)^2\right] \tag{2.11}$$

The variables are easily separable and the eigenfunction is written as

$$\psi = e^{iky}\chi(x) \tag{2.12}$$

where $\hbar k$ is the eigenvalue of the $p_y$ operator, taking into account that $[p_y, H] = 0$. The function $\chi(x)$ is the eigenfunction of the time-independent Schrödinger equation,

$$-\frac{\hbar^2}{2m_e^*}\chi'' + \frac{1}{2}m_e^*\Omega_c^2(x - x_k)^2\chi = E\chi(x) \tag{2.13}$$

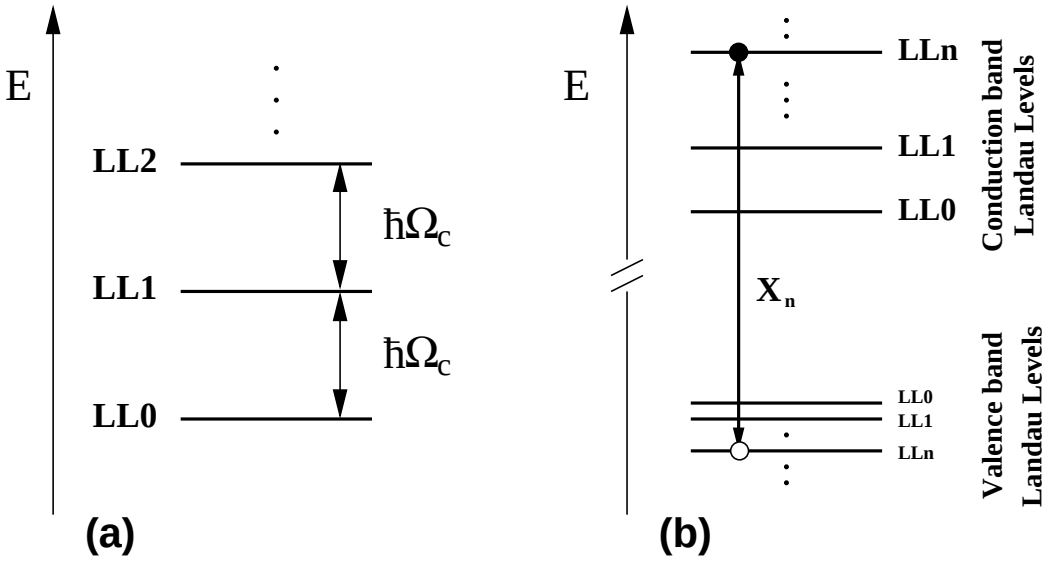


**Figure 2.3:** (a) The energy spectrum of a 2D electron in a perpendicular magnetic field consists of discrete, equally spaced and highly degenerate Landau levels. (b) The conduction and valence bands in a two–band quantum well in a magnetic field are split seperately into Landau levels for electrons and holes respectively. The inter–LL energy $\hbar\Omega_c$ is different for electrons and holes due to the difference in masses. A magnetoexciton $X_n$ is optically excited by creating a LLn electron and a LLn hole.

where $x_k = -k\ell^2$, and $\ell$ the magnetic length (cyclotron radius),

$$\ell = \sqrt{\frac{\hbar c}{eB}} \tag{2.14}$$

Eq. (2.13) is easily recognised as the Schrödinger equation corresponding to a harmonic oscillator of spring constant $\hbar\Omega_c = \hbar^2/m_e^*\ell^2$, with equilibrium point at $x_k$. Thus, the eigenfunction (ignoring the normalization factor) is

$$\psi_{nk}(x,y) = e^{iky} H_n\left[(x-x_k)/\ell\right] e^{-(x-x_k)^2/2\ell^2} \tag{2.15}$$

where $H_n$ the Hermite polynomial. The functions are extended in the $y$ direction and localized in $x$.

When the system is confined in a square cell of side $L$, the degeneracy of each Landau level (i.e. the number of allowd states) is the number of allowed values of $k$, such that the center $x_k$ lies between 0 and $L$. Using periodic boundary conditions we get $k = 2\pi m/L$, with $m$ an integer. The allowed values of $m$ are then determined by the condition

$$x_k = \frac{2\pi m}{L}\ell^2, \qquad 0 < x_k < L \tag{2.16}$$

The degeneracy $N$ of each Landau level is

$$N = \frac{L^2}{2\pi\ell^2} \tag{2.17}$$

The above equation can also be expressed in terms of the magnetic flux $\Phi = BL^2$ and the flux quantum $\Phi_0 = B2\pi\ell^2 = hc/e$ as

$$N = \frac{e}{hc}\Phi = \frac{\Phi}{\Phi_0} \tag{2.18}$$

Thus, the Landau level degeneracy is the total number of flux quanta in the external magnetic field. Another important quantity is the dimensionless density of the electrons expressed as the *filling factor* of the Landau level,

$$\nu = \frac{N_e}{N} = 2\pi\ell^2 n_e \tag{2.19}$$

where $N_e$ ($n_e$) is the number (density) of electrons in the system.

### 2.2.3 Quantum well in a magnetic field

To understand the effect of a magnetic field applied to a quantum well structure, we will first consider a two–band semiconductor quantum well that has just a conduction and valence band with effective masses $m_e^*$ and $m_h^*$ respectively. If we ignore the Coulomb interaction between the carriers in the system, the application of a magnetic field simply splits each band into its own series of Landau levels (Fig. 2.3b). The only difference between the conduction band and the valence band LLs is the inter–LL spacing: because of the different effective masses, the cyclotron energy, Eq. (2.9), is $\hbar\Omega_c^c = eB/m_e^*c$ for the former and $\hbar\Omega_c^v = eB/m_h^*c$ for the latter. As a result and due to the large hole mass in GaAs, the valence band LLs are much closer to each other than the conduction band LLs, as illustrated in Fig. 2.3b.

When an incoming photon is absorbed, a LLn electron and a LLn hole are created, because of the Coulomb attraction, form a bound electron–hole pair, i.e. an exciton (also called a magnetoexciton to denote the existence of the magnetic field). The strength of the $e$–$h$ Coulomb interaction may be characterized by the 3D Rydberg energy $R$ and the Bohr radius $\alpha$, and that of the magnetic field by the cyclotron energy $\hbar\Omega_c$ and the magnetic length $\ell$. The dimensionless parameter traditionally used to compare the relative importance of these two energy and length scales is $\lambda = (\alpha/\ell)^2 = \hbar\Omega_c/2R$, i.e. the ratio of the magnetic and Coulombic zero–point energies. For $\lambda \ll 1$, the Coulomb interaction dominates; one may think of the electron and hole being

closer to each other than the radius of their cyclotron obrits. For $\lambda \gg 1$, the distance between the electron and hole is large enough to not affect the individual obrits significantly, and thus the magnetic field dominates. In GaAs, the cross–over field where $\lambda = 1$ is $B \simeq 3.5$ T, and consequently both regimes are easily accessible.

When $\lambda \ll 1$, the magnetic field acts as a perturbation to the excitonic states. In this case, the energy levels of the exciton system depend quadratically on the applied field [55],

$$E_n \approx -\frac{R}{(n+1/2)^2} + \frac{\hbar^2 e^2}{8mc^2}\langle r^2\rangle_n B^2 + O(B^4) \tag{2.20}$$

When $\lambda \gg 1$, the Coulomb interaction can be thought as a perturbation of the Landau level spectrum. In this case,

$$E_n \approx \hbar\Omega_c(n+1/2) + A\frac{\pi}{2}\sqrt{R}\sqrt{\hbar\Omega_c} + O(B^0) \tag{2.21}$$

where $A$ a dimensionless constant [55]. The Coulomb correction increases like $\sqrt{B}$, so that for large magnetic fields, we asymptotically approach the bare energies of the Landau levels. In our study we will consider the high magnetic field limit, where the carriers can be thought of as being in their particular Landau levels.

In the realistic system, multiple bands exist and there is a strong coupling of different valence band spin states in a magnetic field. Moreover, the confinement at the interfaces of the quantum well structures changes the coupling between the bands. Many authors have treated these topics in detail [55–64].

For the $s$–like conduction band states, the interaction between the electron spin and the magnetic field does not change the picture significantly. The Zeeman Hamiltonian is $H_{Zeeman} = g^*\mu_B \mathbf{S}\cdot\mathbf{B}$ where $g^*$ is the electron $g$–factor in the material. In the conduction band we can seperate the wavefunction $\psi(r,\sigma_z) = \phi(r)\chi(\sigma_z)$, and the Zeeman splitting can be super–imposed over the Landau level structure.

However, the valence band structure is more complicated. There is a doubly degenerate pair of $p$–like bands at the $\Gamma$–point in the bulk material. Luttinger [65] introduced a Hamiltonian with the full symmetry of the heavy–hole and light–hole bands and exact to second order in $k$ and first order in the magnetic field, which provides an accurate description of the dispersion of the valence band for energies significantly smaller than the split–off energy (0.34 meV). The Luttinger Hamiltonian is

$$H = H_h + H_m \tag{2.22}$$

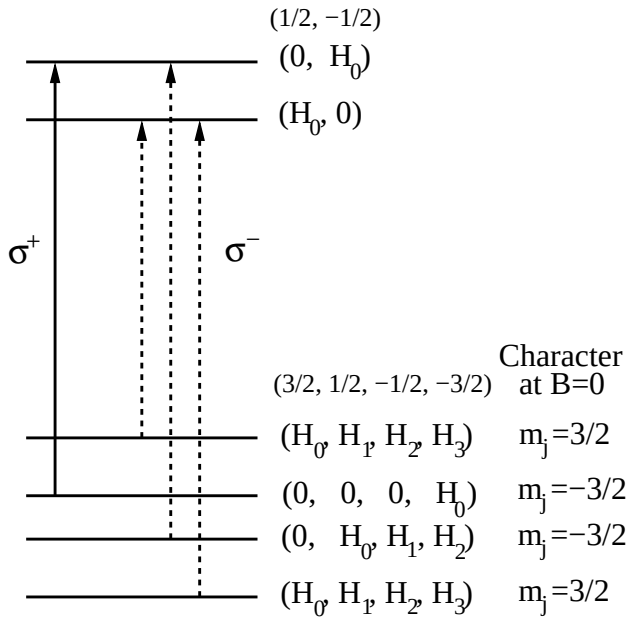


**Figure 2.4:** Selection rules for optical transitions of a GaAs quantum well in a magnetic field. Transitions are only made from $h$–LLn to $e$–LLn and must satisfy $\Delta m_j = \pm 1$. For given $n$, only one possible transition is allowed with $\sigma_+$ polarized light.

where

$$\begin{aligned} H_h = &-\frac{\gamma_1}{2m_0}k^2 \\ &+\frac{\gamma_2}{m_0}\left[\left(J_x^2-\frac{1}{3}J^2\right)k_x^2+\left(J_y^2-\frac{1}{3}J^2\right)k_y^2+\left(J_z^2-\frac{1}{3}J^2\right)k_z^2\right] \\ &-2\frac{\gamma_3}{m_0}\left(\{k_y,k_z\}\{J_y,J_z\}+\{k_z,k_x\}\{J_z,J_x\}+\{k_x,k_y\}\{J_x,J_y\}\right) \end{aligned} \quad (2.23)$$

is the kinetic term, and

$$H_m = \beta_4\left(B_xJ_x+B_yJ_y+B_zJ_z\right)+\beta_5\left(B_xJ_x^3+B_yJ_y^3+B_zJ_z^3\right) \quad (2.24)$$

is the magnetic term, and $\{J_a, J_b\}$ are symmetrized products of operators. The parameters $\beta$ and $\gamma$ describe the effective masses and magnetic field dispersion of the valence band. For bulk material in the absence of a amgnetic field, the Hamiltonian can be diagonalized to give the exact eigenvalues and eigenvectors of the valence band. For a zinc–blende semiconductor such as GaAs, the energy levels are

$$E = -\frac{1}{m_0}\left[\frac{1}{2}\gamma_1K^2 \pm \sqrt{\gamma_2^2k^4+3(\gamma_3^2-\gamma_2^2)(k_y^2k_z^2+k_z^2k_x^2+k_x^2k_y^2)}\right] \quad (2.25)$$

Often, the simplifying assumption that the band structure is isotropic within the plane, called the axial approximation, is made. This is accomplished by setting $\gamma_2 = \gamma_3$ in the above equations. We can then find solutions at finite magnetic fields. The wavefunctions in the valence band will be a combination of the different heavy–hole and light–ole subbands, with a different Landau level associated with each spin subband [64]. The eigenvectors take the 4–component spinor form $(F_{3/2,n-2}, F_{1/2,n-1}, F_{-1/2,n}, F_{-3/2,n+1})$, where the first subscript is the $z$–component of the angular momentum $m_J$, and the second is th eharmonic oscillator index which describes the nature of the Landau level associated with that $m_J$ state. The solution of this system is a tedious numerical calculation, which must be carried out for the specific samples used. The selection rules require $\Delta m_j = \pm 1$. Given angular momentum considerations from the Landau level wavefunctions of electrons and holes, a photon can couple only states with the same Landau level index $n$. Fig. 2.4 shows the optical transitions into the lowest conduction band Landau level, LL0 [64]. All valence band states shown are heavy hole states at $B = 0$. We see that there are several transitions excited by $\sigma_-$ polarized light, but only one excited by $\sigma_+$ light. Thus, in the case of right–circularly polarized light, we only need to consider the $|J, m_j\rangle = |3/2, -3/2\rangle$ band of the four valence bands. In this case, the optical field excites spin–$\downarrow$ electrons into the $|J, m_j\rangle = |3/2, -3/2\rangle$ conduction band. The experiments we will discuss in the following chapters are performed with right–circularly polarized light and consequently, we will be able to describe them adequately by making a two–band approximation.

### 2.2.4 2DEG in a magnetic field

In §2.2.1 we discussed the formation of a 2DEG in a modulation doped aAs/AlGaAs heterostructure: because of the larger band gap of AlGasAs as opposed to GaAs, the doped electrons get traped in a small area in the GaAs quantum well and form the 2DEG. When a large magnetic field is applied perpendicular to the 2DEG plane, the conduction and valence bands split into Landau levels, which are now populated by the 2DEG. For non–interacting electrons, the ground state of the system is obtained by putting each electron in the lowest available energy state. So first we fill all LL0 spin–$\uparrow$ states, followed by the LL0 spin–$\downarrow$ states. As we continue filling in more electrons, they start occupyning states in LL1 and so on. The filling factor $\nu$, defined as the ratio of the number of doped electrons to the degeneracy of the LLs, Eq. (2.19), shows the percentage of occupied states. For $\nu = 1$, all LL0 spin–$\uparrow$ states are occupied; for $\nu = 2$ all LL0 spin–$\uparrow$ and spin–$\downarrow$ states are occupied, etc.

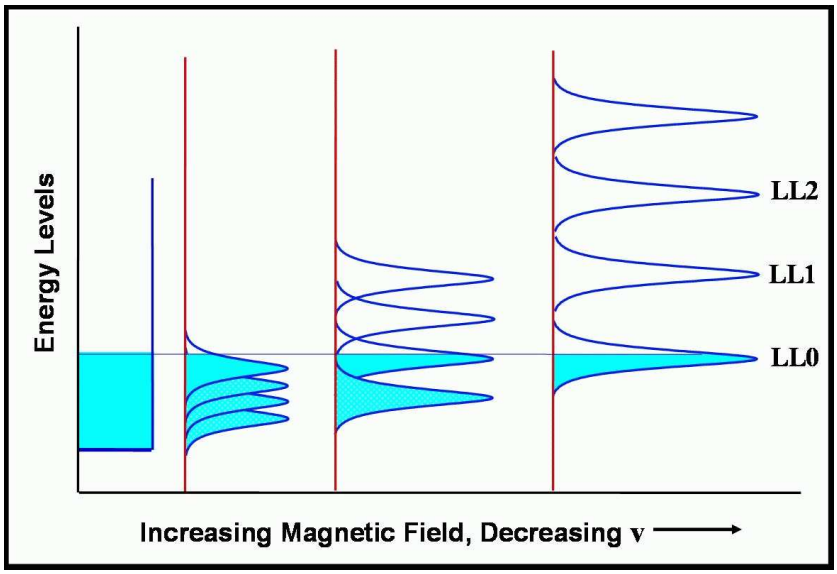


**Figure 2.5:** Filling factor decreases with increasing magnetic field: As the magnetic field is increased, the degeneracy of each Landau level increases and more electrons fit into the lower Landau levels.

As shown in Eq. (2.19), the filling factor can be changed not only by changing the number of doped electrons at a fixed magnetic field, but also by changing the magnetic field for a fixed doping concentration. By increasing the magnetic field, the degeneracy of the Landau levels is larger and more electron can fit in the lower LLs (Fig. 2.5). In our calculations, we will consider the filling factor to be $\sim 1$, i.e. the 2DEG resides in LL0 and mostly in the $|1/2, 1/2\rangle$ states, with spin–$\uparrow$.

When taking into account Coulomb interactions, the above discussion is valid in the large magnetic field limit, since cyclotron energy inceases linearly to B, while the characteristic Coulomb interaction energy, $e^2/\epsilon\ell$, increases as $\sqrt{B}$. As a result, for large enough magnetic fields, Landau level mixing due to Coulomb interactions is negligible and the non–interacting picture described above is valid. However, the presence of Coulomb interactions are important for the low energy collective excitations of the 2DEG, which affect its ultrafast nonlinear optical response.

### 2.2.5 Collective Excitations

The typical low energy collective excitation of the quantum Hall system are the intra- and inter-Landau level excitations. The spectrum due to these excitations has been studied theoretically [35, 66, 67]. However, only a few

experiments in electron tunneling or Raman scattering [68–70] have successfully accessed this information.

The intra-Landau level excitations exist entirely within a single Landau level. It has been shown [66] that the same theory used by Feynman to explain the excitations of liquid Helium [71] can also be used to explain the intra-Landau level excitations of the 2DEG in a large field. The dispersion curve for these excitations exhibits a minimum at a characteristic energy, in parallel with the roton mode made in superfluid helium [66]. In the quantum Hall community, these objects are called magnetorotons, and can be thought of as an excitation in which the electron density remains essentially constant, but there is a circular modulation built up from the phase of the single electron orbits.

The more relevant excitations for the experiments of interest here, will be the inter-Landau level excitations. At high field, when the Landau levels are well separated from one another, it costs an energy $\sim \Omega_c$ to create an inter-Landau level excitation. These excitations are known as magnetoplasmons.

Promoting an electron from a full Landau level to the next highest empty level costs energy $\Omega_c$. However, the removal of an electron leaves behind a hole in first level, which can interact with the promoted electron, similar to a magnetoexciton. This interaction must be taken into account to understand the structure of the excitation. The dispersion curve when LL0 is full ($\nu = 1$) has been calculated in Ref. [67].

The theory of intra-Landau level excitations has been extended to the calculation of the magnetoplasmon dispersion at partial filling [35]. If we think of the full level case as the creation of an electron-hole pair, similar to a magnetoexciton, than in a partially full level of magnetoplasmon is like an electron–hole pair accompanied by a shake–up of the electron gas.

For all filling factors, the excitation energy at long wavelength approaches the cyclotron energy. This is Kohn's theorem [72], a direct consequence of the translational invariance of the system in the $x$–$y$ plane.

## 2.3 Ultrafast Nonlinear Optical Spectroscopy

Optical spectroscopy is a powerful tool for investigating the electronic and vibrational properties of a variety of systems, like atoms, molecules and solids. In semiconductors, the techniques of absorption, reflection, luminescence, and light-scattering spectroscopies have provided invaluable information about such diverse aspects as the electronic band structure, phonons, single particle excitation spectra of electrons and holes, and properties of defects, surfaces and interfaces.

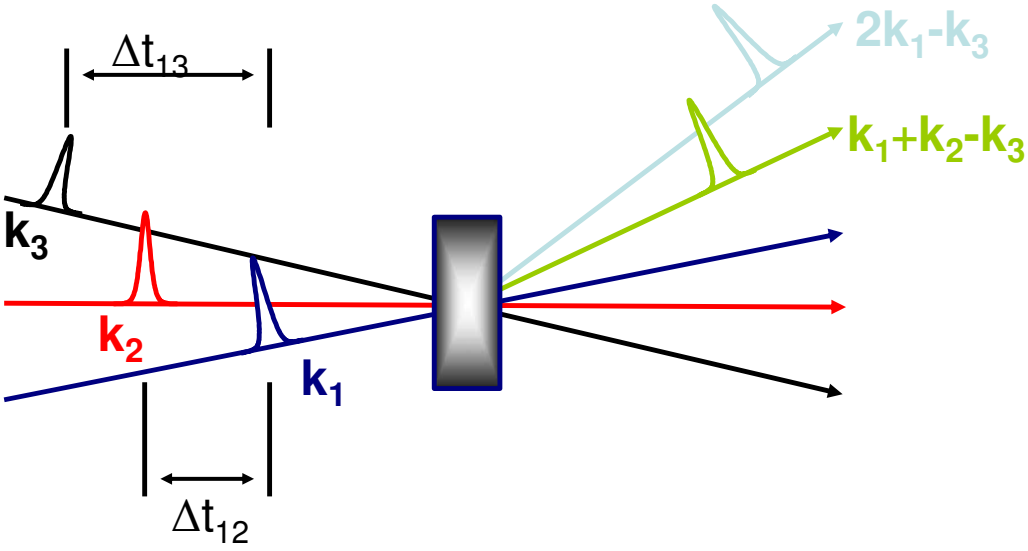


**Figure 2.6:** Schematic of a 2–pulse and 3–pulse FWM experiment.

However, optical spectroscopy has unique stengths since it can provide information about the non–equilibrium and nonlinear properties of semiconductors, in combination with picosecond and femtosecond laser pulses. It provides the best means of determining the non–equilibrium distribution functions of excitations created by the optical field. Moreover, optical techniques provide the ability to investigate the nonlinear properties, including coherent effects, in semiconductors, and thus provide insights into different aspects of semiconductors, such as many–body effects, coherent effects and dephasing phenomena.

Typical linear spectroscopic measurements are absorption, photoluminescence, etc. Standard nonlinear optical experiments are pumb–probe, four–wave–mixing, six–wave–mixing, etc. In the following, we will focus on the four–wave–mixing technique, which is relevant to the experiments of interest [45, 52].

### 2.3.1 Four–Wave–Mixing Spectroscopy

In a FWM experiment, we study the third order response of the system. Three optical pulses excite the ssystem under investigation. Two of the pulses create a second order excitation, and the third pulse is scattered by the excited state in a new direction. Thus this scattered pulse, which is the FWM signal, reflects the third–order nonlinear response of the system. The signal can be studied in different ways. For example, one may study

the intensity of the signal versus the time delays between the pulses, or can study the spectrum of the signal, etc. A FWM experiment can be done with two pulses (two–pulse FWM) or three pulses (three–pulse FWM), as shown in Fig. 2.6.

In two–pulse FWM, two pulses impinge on the sample in directions $\mathbf{k}_1$ and $\mathbf{k}_3$. The signal is measured in the background free direction $2\mathbf{k}_1 - \mathbf{k}_3$, and one can study the signal as a function of the time delay between the two pulses. In three–pulse FWM, the system is excited with three pulses that propagate in directions $\mathbf{k}_1$, $\mathbf{k}_2$, and $\mathbf{k}_3$. The signal is measured in the direction $\mathbf{k}_1+\mathbf{k}_2-\mathbf{k}_3$ and can now be studied as a function of two time delays in the system: $\Delta t_{12}$ betweeen pulses $\mathbf{k}_1$ and $\mathbf{k}_2$, and $\Delta t_{13}$ between pulses $\mathbf{k}_1$ and $\mathbf{k}_3$.

In the experiments we will discuss in the following chapters, three–pulse FWM is performed on the samples under investigation and the FWM signal is measured in the $\mathbf{k}_1 + \mathbf{k}_2 - \mathbf{k}_3$ direction in two different cases: (i) when pulses $\mathbf{k}_1$ and $\mathbf{k}_2$ arrive together, i.e. $\Delta t_{12} = 0$, which will be called "the $\Delta t_{13}$ axis", since the signal in this case depends only on the $\Delta t_{13}$, and (ii) when pulses $\mathbf{k}_1$ and $\mathbf{k}_3$ arrive together, i.e. when $\Delta t_{13} = 0$, which will be called "the $\Delta t_{12}$ axis", as the signal now depends only on $\Delta t_{12}$. Later on, we will show that the $\Delta t_{13}$ axis accesses the interband dynamics in the system, while the $\Delta t_{12}$ axis accesses the intraband dynamics.

In the following section, we will discuss the FWM signal in an ensemble of two–level systems, which will give us an intuition about the physics that is probed with such experiments.

### 2.3.2 An ensemble of independent two–level systems

The coherent phenomena in atoms and molecules are generally analyzed for an ensemble of independent two–level systems. The independent two–level model assumes that the photon is nearly resonant with the transition between $|a\rangle$ and $|b\rangle$ and far off resonance with respect to all other transitions. It further assumes that there is no interaction between various two–level atoms or molecules making up the ensemble. The electronic states in a semiconductor are considerably more complicated than those in atoms. However, each exciton in a semiconductor can be considered as a two–level system in the simplest approximation. For this reason, we will now discuss the predictions of the independent two–level model.

The quantum mechanics of transition probabilities in a two–level system by a near–resonant excitation is well known. If the wavefunctions of the two states are known, then one can describe the transition probabilities as bilinear combinations of transition amplitudes. Since the expectation value of any

observable involves such bilinear combinations, the density matrix method dealing directly with the bilinear combinations has been developed. The density matrix formalism facilitates the treatment of interacting quantum systems. We are interested not in a single two–level system but an ensemble of two–level systems. In such cases, the wavefunction of the ensemble of two–level systems is generally not known but certain statistical properties of the ensemble may be known. Such statistical properties are conveniently described in terms of the general density matrix operator:

$$\rho = \sum_j P_j |\Psi_j\rangle\langle\Psi_j| \tag{2.26}$$

where $P_j$ is the fraction of the systems which has the state vector $|\Psi_j\rangle$. The density matrix obeys the Liouville variant of the Schrödinger equation,

$$i\hbar\dot{\rho} = [H, \rho] \tag{2.27}$$

where $H$ is the Hamltonian operator of the system given by

$$H = H_0 + H_{\text{int}} + H_R \tag{2.28}$$

$H_0$ is the Hamiltonian of the isolated two–level system, $H_{\text{int}}$ is the Hamiltonian that describes the interaction between the radiation field and the two–level system, and the relaxation Hamiltonian $H_R$ describes all the processes that return the ensemble to thermal equilibrium. The expectation value of an operator $\hat{O}$ is given by

$$\langle\hat{O}\rangle = Tr\{\hat{O}\rho\} \tag{2.29}$$

For a two–level system with the ground state with state vector $|a\rangle$ and energy $E_a$ and an excited state with the state vector $|b\rangle$ and energy $E_b$ the density operator is written as

$$\rho = \begin{bmatrix} \rho_{bb} & \rho_{ba} \\ \rho_{ab} & \rho_{aa} \end{bmatrix} \tag{2.30}$$

The diagonal elements of the density matrix represent the probability of finding the system in the two energy eigenstates, i.e. the populations in the two eigenstates. The off–diagonal elements represent the coherence intrinsic to a superposition state.

In a closed two–level system, the diagonal components are related by

$$\rho_{aa} + \rho_{bb} = 1 \tag{2.31}$$

since the sum of the populations in the lower and upper states is constant. Because of the complexity of electronic states in a semiconductor, the assumption of a closed system may be difficult to satisfy in a semiconductor.

### The unperturbed Hamiltonian

The state vector $|\Psi_j\rangle$ obeys the time dependent Schrödinger equation

$$i\hbar|\dot{\Psi}_j\rangle = H|\Psi_j\rangle \tag{2.32}$$

For an isolated two–level system in the absence of any interactions $H = H_0$, and $H_0$ has no explicit time dependence so that for the system at position $\mathbf{R}$

$$\Psi_k(\mathbf{R}, t) = u_k(\mathbf{R})e^{-iE_k t/\hbar} \tag{2.33}$$

where $k = a, b$. Thus the unperturbed Hamiltonian $H_0$ is given by

$$H_0 = \begin{bmatrix} E_b & 0 \\ 0 & E_a \end{bmatrix} \tag{2.34}$$

For an ensemble of two–level systems, the state vector of the $j$–th system is

$$|\Psi_j(t)\rangle = C_{aj}|a\rangle + C_{bj}|b\rangle \tag{2.35}$$

and the density matrix can be written in the more familiar form

$$\rho = \sum_j P_j \begin{bmatrix} |C_{bj}|^2 & C_{bj}C_{aj}^* \\ C_{aj}C_{bj}^* & |C_{aj}|^2 \end{bmatrix} \tag{2.36}$$

where $P_j$ is the probability of being at the state $j$. If the state vectors for all $j$'s are identical (i.e. $C_{aj}$ and $C_{bj}$ are the same for all $j$'s), but the phases of the coherent superposition are radomly distributed between 0 and $2\pi$, then the off–diagonal elements vanish and there is no coherence in the ensemble. On the other hand, if there is a well defined phase relationship for different $j$, the ensemble has coherence.

### The Interaction Hamiltonian

For an electric dipole allowed transition, one generally neglects the electric quadrupole and magnetic dipole interactions (since they are smaller by the fine structure constant $\sim 1/137$) in the interaction Hamiltonian. In this dipole approximation,

$$H_{\text{int}} = -\mathbf{d} \cdot \mathbf{E}(\mathbf{R}, t) \tag{2.37}$$

where $\mathbf{d}$ is the dipole moment operator and $\mathbf{E}(\mathbf{R}, t)$ the electric field of the light. The components of the dipole moment operator are given by

$$\mathbf{d}_{nm} = -e \int dV u_n^* \mathbf{r} u_m = -e\mathbf{r}_{nm} \tag{2.38}$$

where $\mathbf{r}$ is the electron coordinate with respect to the location of the nucleus at $\mathbf{R}$. The components of $H_{\text{int}}$ are

$$\Delta_{nm} = -\mathbf{d}_{nm} \cdot \mathbf{E}(\mathbf{R}, t) \tag{2.39}$$

The diagonal components of $\mathbf{d}_{nm}$ and $\Delta_{nm}$ are zero because $\mathbf{d}$ is an odd parity operator.

For a monochromatic plane wave at angular frequency $\omega_0$ and linearly polarized in the direction $\hat{\varepsilon}$, the electric field can be written as the sum of two fields

$$\mathbf{E}(\mathbf{R}, t) = \mathbf{E}^{+}(\mathbf{R}, t) + \mathbf{E}^{-}(\mathbf{R}, t) \tag{2.40}$$

where

$$\mathbf{E}^{+}(\mathbf{R}, t) = \hat{\varepsilon} E_0 e^{i[\mathbf{q}\cdot\mathbf{R} - (\omega_0 t + \phi)]}, \qquad \mathbf{E}^{-}(\mathbf{R}, t) = \mathbf{E}^{+*}(\mathbf{R}, t) \tag{2.41}$$

where $E_0$ is the (real) electric field amplitude and $\phi$ a phase factor. In calculating the transition probabilities, one generally makes the rotating–wave approximation in which the term with the rapidly varying phase factor $e^{i(\omega_0+\Omega)t}$ (where $\hbar\Omega = E_b - E_a$) and the large denominator $\omega_0 + \Omega$, corresponding to $\mathbf{d} \cdot \mathbf{E}^{-}$ is neglected. In this approximation,

$$\Delta_{ba} = \hbar\chi_R e^{i[\mathbf{q}\cdot\mathbf{R} - (\omega_0 t + \phi)]} = \Delta_{ab}^{*} \tag{2.42}$$

where $\hbar\chi_R = e\mathbf{r}_{ba} \cdot \hat{\varepsilon} E_0$ is the Rabi energy at resonance $\omega_0 = \Omega$. The matrix form of $H_{\text{int}}$ can thus be written as

$$H_{\text{int}} = \begin{bmatrix} 0 & \Delta_{ba} \\ \Delta_{ba}^{*} & 0 \end{bmatrix} \tag{2.43}$$

The linear and nonlinear response of the system to the electromagnetic field is determined by the macroscopic polarization, which is connected to the macroscopic dielctric polarization density as

$$\mathbf{P} = NTr\{\mathbf{d}\rho\} \tag{2.44}$$

where $N$ is the number density in the ensemble.

### The Relaxation Hamiltonian

The processes which bring the ensemble back to thermal equilibrium include recombination, collisions with phonons and interaction with other electronic states. The relative time scales of these processes, and their relation to other characteristic times in the system such as the laser pulse duration, determine the correct treatment of these relaxation processes.

The most general approach to the description of non–equilibrium properties of semiconductors excited by laser pulses is the quantum kinetic equations approach based on non–equilibrium Green's functions [73]. These methods have been applied to the description of excitation and relaxation processes in laser–excited semiconductors. Numerical solutions of these equations have shown that non–Markovian behavior becomes important for time scales that are small compared to the dephasing times, a condition that is easily achieved for femtosecond photoexcitation not too far from resonance. Under these conditions, the interband polarizations do not follow the pulse adiabatically and the dephasing time is not an instantaneous function of its environment but depends on the "history" of the environment.

A simpler approach to the problem is to make the Markovian approximation under which the relaxation times are determined by the instantaneous distribution and polarization functions, and hence are time dependent. This approximation forms the basis for the classical Boltzmann equation approach to transport in semiconductors.

The simplest approach to the problem is to assume that the dynamical self energies in the non–equilibrium Green's function approach can be replaced by constant phenomenological transverse and longitudinal relaxation rates for the relevant relaxation processes in the problem and simplify the relaxation Hamiltonian accordingly. Analysis of most coherent experiments and the semiconductor Bloch equations are based on this assumption. In this approach, one approximates the relaxation Hamiltonian by

$$[H_R, \rho]_{bb} = -\rho_{bb}/T_1 \qquad \text{and} \qquad [H_R, \rho]_{ba} = -\rho_{ba}/T_2 \tag{2.45}$$

where $T_1$ is the lifetime of the state $b$ and $1/T_2$, the transverse relaxation rate, is the sum of the recombination rate $1/T_1$ and the pure dephasing rate. One can think of $T_2$ as the lifetime of the coherent superposition state.

The relaxation time approximation is valid in the limit that the response of the medium in which the system under study is embedded is either very fast or very slow compared to the system–medium interaction. It can be shown that the linear absorption shape is a Lorentzian (corresponding to a homogeneously broadened line) in the limit of very fast response of the medium, and a Gaussian (corresponding to an inhomogeneously broadened line) in the limit of very slow response of the medium.

### Optical Bloch equations

The coupled equations of motion for the polarization and the population of an ensemble of independent two–level systems are known as the optical Bloch equations, in analogy with the equations first derived by Bloch for the

spin systems. For simplification, we introduce a new notation and substitute $n = \rho_{bb}$, $1 - n = \rho_{aa}$, and $p = \rho_{ba}$. Using the Liouville equation and the above definitions, one gets

$$\rho = \begin{bmatrix} n & p \\ p^* & 1-n \end{bmatrix} \tag{2.46}$$

$$i\dot{n} = -i\frac{1}{T_1}n + \frac{1}{\hbar}(\Delta_{ba}p^* - p\Delta_{ba}^*) \tag{2.47}$$

$$i\dot{p} = \left(\Omega - i\frac{1}{T_2}\right)p + \frac{1}{\hbar}\Delta_{ba}(1-2n) \tag{2.48}$$

Eqs. (2.47) and (2.48) are known as the optical Bloch equations and form the basis for analyzing coherent transient experiments in independent two–level systems.

The coupled optical Bloch equations cannot be solved analytically in the general case. One generally resorts to expanding the density matrix into a Taylor series in the incident field amplitudes and obtains a solution to the desired order. Numerical techniques have to be employed in the general case. We formally write the density $n$ and polarization $p$ as

$$n = n^{(0)} + n^{(1)} + n^{(2)} + n^{(3)} + ... \tag{2.49}$$

$$p = p^{(0)} + p^{(1)} + p^{(2)} + p^{(3)} + ... \tag{2.50}$$

with $n^{(0)} = 0$ and $p^{(0)} = 0$. For the usual initial conditions of $n = 0$ and $p = 0$, it can be shown that the odd powers of $n$ and the even powers of $p$ are zero. The low order components of $n$ and $p$ are given by

$$i\dot{p}^{(1)} = \left(\Omega - i\frac{1}{T_2}\right)p^{(1)} + \frac{1}{\hbar}\Delta_{ba} \tag{2.51}$$

$$i\dot{n}^{(2)} = -i\frac{1}{T_1}n^{(2)} + \frac{1}{\hbar}(\Delta_{ba}p^{(1)*} - p^{(1)}\Delta_{ba}^*) \tag{2.52}$$

$$i\dot{p}^{(3)} = \left(\Omega - i\frac{1}{T_2}\right)p^{(3)} - 2\frac{1}{\hbar}\Delta_{ba}n^{(2)} \tag{2.53}$$

**Analysis of a three–pulse FWM experiment**

As discussed in §2.3.1, in a three–pulse FWM experiment the sample is excited by three pulses travelling in directions $\mathbf{k}_1$, $\mathbf{k}_2$ and $\mathbf{k}_3$ respectively, with time delay $\Delta t_{12} = t_1 - t_2$ between pulses 1 and 2 and $\Delta t_{13} = t_1 - t_3$ between pulses 1 and 3, and create a FWM signal in the $\mathbf{k}_s = \mathbf{k}_1 + \mathbf{k}_2 - \mathbf{k}_3$

direction. Assuming that the first pulse arrives at the sample at time $t = 0$,

$$\begin{aligned} E(\mathbf{R},t) =& \mathcal{E}(\mathbf{R},t)e^{i(\mathbf{k}_1\cdot\mathbf{R}-\omega_0 t)} + \mathcal{E}(\mathbf{R},t+\Delta t_{12})e^{i(\mathbf{k}_2\cdot\mathbf{R}-\omega_0 t)} \\ &+ \mathcal{E}(\mathbf{R},t+\Delta t_{13})e^{i(\mathbf{k}_3\cdot\mathbf{R}-\omega_0 t)} \end{aligned} \tag{2.54}$$

where $\mathcal{E}(\mathbf{R},t)$ is the electric field pulse shape at $\mathbf{R}$, and $\omega_0$ corresponds to the peak of the mode–locked laser spectrum. For this electric field,

$$\begin{aligned} \Delta_{ba}/\hbar =& (e/\hbar)r_{ba}e^{-i\omega_0 t} \times \big[\mathcal{E}(\mathbf{R},t)e^{i\mathbf{k}_1\cdot\mathbf{R}} + \\ & \mathcal{E}(\mathbf{R},t+\Delta t_{12})e^{i\mathbf{k}_2\cdot\mathbf{R}} + \mathcal{E}(\mathbf{R},t+\Delta t_{13})e^{i\mathbf{k}_3\cdot\mathbf{R}}\big] \\ \equiv& ie^{-i\omega_0 t}f(t) \end{aligned} \tag{2.55}$$

If we define $p^{(1)} = p^{(1)}(t)e^{-i\omega_0 t}$, then

$$\dot{p}^{(1)}(t) + Gp^{(1)}(t) = f(t) \tag{2.56}$$

which has the solution

$$p^{(1)} = \int_{-\infty}^{t} dt' e^{-G(t-t')} f(t') e^{-i\omega_0 t} \tag{2.57}$$

where $G = 1/T_2 + i(\Omega - \omega_0)$. The signal along $\mathbf{k}_s = \mathbf{k}_1 + \mathbf{k}_2 - \mathbf{k}_3$ results either from the diffraction of pulse 1 from a grating created by pulses 2 and 3, or from the diffraction of pulse 2 from a grating created by pulses 1 and 3 i.e., it is related to either $p^{(3)}_{123}$ or $p^{(3)}_{213}$. We therefore need to calculate only the $\mathbf{k}_2 - \mathbf{k}_3$ and $\mathbf{k}_1 - \mathbf{k}_3$ components in the density $n^{(2)}$, i.e., $n^{(2)}_{23}$ and $n^{(2)}_{13}$ which using Eq. (2.47), can be shown to be given by

$$n^{(2)}_{i3} = \int_{-\infty}^{t} dt'' e^{-(t-t'')/T_1} f_{i3}(t'') \qquad (i = 1, 2) \tag{2.58}$$

where

$$\begin{aligned} f_{13}(t) =& \frac{e^2|r_{ba}|^2}{\hbar^2} e^{i(\mathbf{k}_1-\mathbf{k}_3)\cdot\mathbf{R}} \Bigg[\mathcal{E}(\mathbf{R},t)\int_{-\infty}^{t} dt' \mathcal{E}(\mathbf{R},t'+\Delta t_{13})e^{-G^*(t-t')} \\ & + \mathcal{E}(\mathbf{R},t+\Delta t_{13})\int_{-\infty}^{t} dt' \mathcal{E}(\mathbf{R},t')e^{-G(t-t')}\Bigg] \end{aligned} \tag{2.59}$$

$$\begin{aligned} f_{23}(t) =& \frac{e^2|r_{ba}|^2}{\hbar^2} e^{i(\mathbf{k}_2-\mathbf{k}_3)\cdot\mathbf{R}} \Bigg[\mathcal{E}(\mathbf{R},t+\Delta t_{12})\int_{-\infty}^{t} dt' \mathcal{E}(\mathbf{R},t'+\Delta t_{13})e^{-G^*(t-t')} \\ & + \mathcal{E}(\mathbf{R},t+\Delta t_{13})\int_{-\infty}^{t} dt' \mathcal{E}(\mathbf{R},t'+\Delta t_{12})e^{-G(t-t')}\Bigg] \end{aligned} \tag{2.60}$$

The third order polarizations $p^{(3)}_{123}$ and $p^{(3)}_{213}$ can be obtained from Eq. (2.48)

$$\begin{aligned} p^{(3)}_{123} =& -2i(e|r_{ba}|/\hbar)^3 e^{-i\Omega t} e^{-t/T_2} \int_{-\infty}^{t} dt''' \int_{-\infty}^{t'''} dt'' \int_{-\infty}^{t''} dt' e^{Gt'''} e^{-(t'''-t'')/T_1} \\ & \times \mathcal{E}(\mathbf{R}, t''') \Big[ \mathcal{E}(\mathbf{R}, t''+\Delta t_{12}) \mathcal{E}(\mathbf{R}, t'+\Delta t_{13}) e^{-G^*(t''-t')} \\ & + \mathcal{E}(\mathbf{R}, t''+\Delta t_{13}) \mathcal{E}(\mathbf{R}, t'+\Delta t_{12}) e^{-G(t''-t')} \Big] \end{aligned} \tag{2.61}$$

$$\begin{aligned} p^{(3)}_{213} =& -2i(e|r_{ba}|/\hbar)^3 e^{-i\Omega t} e^{-t/T_2} \int_{-\infty}^{t} dt''' \int_{-\infty}^{t'''} dt'' \int_{-\infty}^{t''} dt' e^{Gt'''} e^{-(t'''-t'')/T_1} \\ & \times \mathcal{E}(\mathbf{R}, t'''+\Delta t_{12}) \Big[ \mathcal{E}(\mathbf{R}, t'') \mathcal{E}(\mathbf{R}, t'+\Delta t_{13}) e^{-G^*(t''-t')} \\ & + \mathcal{E}(\mathbf{R}, t''+\Delta t_{13}) \mathcal{E}(\mathbf{R}, t') e^{-G(t''-t')} \Big] \end{aligned} \tag{2.62}$$

In order to determine the signal at a given point in space and time, the Maxwell's propagation equations have to be solved in general. However, for an optically thin sample with thickness small compared to the wavelength of light, the signal diffracted signal along $\mathbf{k}_s$ can be approximated by

$$P^{(3)}_{ij3} = N \mathrm{Tr}\{d\rho\} \tag{2.63}$$

with appropriate order and component of $\rho$.

These equations can be numerically integrated to obtain the spectrally–resolved FWM signal (SR–FWM) in the $\mathbf{k}_s$ direction

$$S^{(3)}_{ij3}(\Delta t_{12}, \Delta t_{13}, \omega) = | \int_{-\infty}^{\infty} P^{(3)}_{ij3}(t) e^{i\omega t} dt|^2 \tag{2.64}$$

and the time-integrated (TI–FWM) signal

$$I^{(3)}_{ij3}(\Delta t_{12}, \Delta t_{13}) = \int_{-\infty}^{\infty} |P^{(3)}_{ij3}(t)|^2 dt \tag{2.65}$$

as a function of the time delays $\Delta t_{12}$ and $\Delta t_{13}$.

**Analytic Solutions for Delta Pulses.**

The iterative equations can be solved numerically for a given pulse shape. However, we consider in this section a simpler case of pulses that can be described by the Dirac $\delta$-functions in time, i.e. $\mathcal{E}(\mathbf{R}, t) = E_0 \delta(t)$. We also assume that the sample is thin and the propagation effects can be neglected. In this case, Eq. (2.56) gives

$$p^{(1)} = \frac{e r_{ba}}{i\hbar} E_0 \left[ e^{-Gt} \theta(t) + e^{-G(t+\Delta t_{12})} \theta(t+\Delta t_{12}) + e^{-G(t+\Delta t_{13})} \theta(t+\Delta t_{13}) \right] e^{i\omega t} \tag{2.66}$$

where $\theta(t)$ is the Heaviside step function, and we recall that $G = (1/T_2) + i(\Omega - \omega_0)$. Thus, at resonance ($\Omega = \omega_0$), the first order polarization is a sum of three damped oscillations at $\omega_0$ displaced by the time delays $\Delta t_{12}$ and $\Delta t_{13}$.

Similarly, Eq. (2.58) can be integrated and give e.g. for $n_{13}^{(2)}$

$$n_{13}^{(2)} = \frac{e^2|r_{ba}|^2}{\hbar^2} E_0^2 \left[\theta(t)\theta(\Delta t_{13}) e^{-t/T_1} e^{-G^* \Delta t_{13}} + \theta(t + \Delta t_{13})\theta(-\Delta t_{13}) e^{-(t+\Delta t_{13})/T_1} e^{G\Delta t_{13}}\right] \tag{2.67}$$

There are two terms of which only one is non-zero for a given $\Delta t_{13}$: the first term is non-zero only when $\Delta t_{13} > 0$, i.e., for positive time delays, whereas the second term is non-zero only for negative time delays ($\Delta t_{13} < 0$). This equation simply states that, after the arrival of the second pulse (pulse 1 if $\Delta t_{13} > 0$, and pulse 3 if $\Delta t_{13} < 0$), $n_{13}^{(2)}$ decreases exponentially with $\Delta t_{13}$. For a given $\Delta t_{13}$, $n_{13}^{(2)}$ decreases with the population decay constant $T_1$ as a function of time. Similar results are obtained for negative $\Delta t_{13}$, as well as for $n_{23}^{(2)}$.

This process can be repeated to obtain an expression for the third–order polarization in the $\mathbf{k}_s$ direction from Eq. (2.62). For example, for $p_{213}^{(3)}$ we obtain

$$\begin{aligned} p_{213}^{(3)} = &- i\frac{e^3|r_{ba}|^3}{\hbar^3} E_0^3 e^{-i\omega t} e^{-t/T_2} e^{i(\mathbf{k}_1+\mathbf{k}_2-\mathbf{k}_3)\cdot\mathbf{R}} \theta(t + \Delta t_{12}) e^{-G\Delta t_{12}} \\ &\times \left[\theta(\Delta t_{13})\theta(-\Delta t_{12}) e^{\Delta t_{12}/T_1} e^{-G^*\Delta t_{13}} \right. \\ &\left. + \theta(-\Delta t_{13})\theta(\Delta t_{13} - \Delta t_{12}) e^{(\Delta t_{12}-\Delta t_{13})/T_1} e^{-G\Delta t_{13}}\right] \end{aligned} \tag{2.68}$$

from which we obtain the decay of the third–order polarization for given time delays $\Delta t_{12}$ and $\Delta t_{13}$.

## 2.4 Coulomb correlations in semiconductors

Semiconductors are a highly complex, interacting many-body system. Incoming photons excite electrons and holes. If we neglect the Coulomb interactions between them, we can treat each state in k-space as a separate two level system. Optical experiments in semiconductors have been explained using multi-level models (see e.g. Refs. [74, 75]). However, the Coulomb interaction has drastic effects even on the linear optical properties of the semiconductor. Ignoring these interactions, or including them in a ad hoc manner, is a poor way to explain the nonlinear results.

To account for the interactions between photo–excited electrons and holes, we begin from the Hamiltonian for the electron-hole subsystem of the semiconductor [9]:

$$\begin{aligned} H_{tot} = &\sum_{\mathbf{k}} [E_{c\mathbf{k}} \hat{e}^{\dagger}_{\mathbf{k}} \hat{e}_{\mathbf{k}} + E_{v\mathbf{k}} \hat{h}^{\dagger}_{\mathbf{k}} \hat{h}_{\mathbf{k}}] \\ &+ \frac{1}{2} \sum_{\mathbf{k} \neq \mathbf{k}'} v_{\mathbf{q}} [\hat{e}^{\dagger}_{\mathbf{k}+\mathbf{q}} \hat{e}^{\dagger}_{\mathbf{k}'-\mathbf{q}} \hat{e}_{\mathbf{k}'} \hat{e}_{\mathbf{k}} + \hat{h}^{\dagger}_{\mathbf{k}+\mathbf{q}} \hat{h}^{\dagger}_{\mathbf{k}'-\mathbf{q}} \hat{h}_{\mathbf{k}'} \hat{h}_{\mathbf{k}} - 2\hat{e}^{\dagger}_{\mathbf{k}+\mathbf{q}} \hat{h}^{\dagger}_{\mathbf{k}'-\mathbf{q}} \hat{h}_{\mathbf{k}'} \hat{e}_{\mathbf{k}}] \\ &- \sum_{\mathbf{k}} [\mu_{cv} E(t) \hat{e}^{\dagger}_{\mathbf{k}} \hat{h}^{\dagger}_{-\mathbf{k}} + \mu^{*}_{cv} E^{*}(t) \hat{h}^{\dagger}_{-\mathbf{k}} \hat{e}^{\dagger}_{\mathbf{k}}], \end{aligned} \tag{2.69}$$

where $E_{c\mathbf{k}}$ ($E_{v\mathbf{k}}$) gives the dispersion of the conduction (valence) band, $\hat{e}^{\dagger}_{\mathbf{k}}$ ($\hat{h}^{\dagger}_{\mathbf{k}}$) is the creation operator of an electron in the conduction band (hole in the valence band) with wavevector $\mathbf{k}$, $v_{\mathbf{q}}$ is the Coulomb potential in $\mathbf{k}$–space, and $\mu_{cv}$ is the dipole moment. The first line of Eq. (2.69) gives the single particle energies of the electrons and holes, the second line describes $e$–$e$, $h$–$h$ and $e$–$h$ Coulomb interactions, while the last line describes the optical field–semiconductor interaction. We consider the band dispersions to be parabolic, and given by the effective mass approximation ($\hbar = 1$):

$$E_{c\mathbf{k}} = E_g + \frac{k^2}{2m^*_e} \qquad \text{and} \qquad E_{v\mathbf{k}} = \frac{k^2}{2m^*_h}. \tag{2.70}$$

The band gap $E_g$ contains the Coulomb interaction of the full valence band.

The polarization is given by

$$\vec{P} = \sum_{\mathbf{k}} \mu^{*} \langle \hat{P}_{\mathbf{k}} \rangle = \sum_{\mathbf{k}} \mu^{*} \langle \hat{h}^{\dagger}_{-\mathbf{k}} \hat{e}^{\dagger}_{\mathbf{k}} \rangle \tag{2.71}$$

If we write the Heisenberg equation of motion for the operator $\hat{P}_{\mathbf{k}}$, we find that in addition to being driven by other two–particle correlations (polarizations and electron or hole populations), the Coulomb interaction couples the two–particle correlations to four–particle correlations (products of four operators). To solve our equation, we must then solve equations of motion for these four-particle correlations. These are in turn driven by six-particle correlations, and so on in an infinite hierarchy. We thus must make some approximations which truncate this hierarchy and give a closed set of equations.

### 2.4.1 The semiconductor Bloch equations

The most common method for dealing with this problem has been to factorize the four-particle correlations into products of two-particle correlations,

and then make the random phase approximation (RPA), which neglects the terms which oscillate rapidly due to large momentum differences. The RPA is also called the time-dependent Hartee-Fock approximation. This leads to a closed set of equations for the two-particle density matrix elements ($n_{e,\mathbf{k}}, n_{h,\mathbf{k}}$ and $P_{\mathbf{k}}$), well known as semiconductor Bloch equations (SBE) [76], given here within the relaxation time approximation:

$$\begin{aligned} i\frac{\partial}{\partial t}P_{\mathbf{k}} =&(E_{c,\mathbf{k}} + E_{h,\mathbf{k}} - i\gamma)P_{\mathbf{k}} - \sum_{\mathbf{q}\neq\mathbf{k}} V_{\mathbf{k}-\mathbf{q}}P_{\mathbf{q}} - \mu_{cv}E(t)[1 - n_{e,\mathbf{k}} - n_{h,\mathbf{k}}] \\ &+ \sum_{\mathbf{q}\neq\mathbf{k}} V_{\mathbf{k}-\mathbf{q}}[P_{\mathbf{q}}(n_{e,\mathbf{k}} + n_{h,\mathbf{k}}) - P_{\mathbf{k}}(n_{e,\mathbf{q}} + n_{h,\mathbf{q}})] \end{aligned} \tag{2.72}$$

$$\frac{\partial}{\partial t}n_{j,\mathbf{k}} = -2Im\left\{P^*_{\mathbf{k}}[\mu_{cv}E(t) + \sum_{\mathbf{q}\neq\mathbf{k}} V_{\mathbf{k}-\mathbf{q}}P_{\mathbf{q}}]\right\} - \frac{1}{T_1}n_{j,\mathbf{k}} \ (j = e, h) \tag{2.73}$$

The density matrix elements in Eqs. (2.72) and (2.73) are driven by both the electric field of the laser and a term due to the polarization from all other $\mathbf{k}$ states. The SBE have been quite successful in explaining many experiments in semiconductors, such as the AC stark effect [77, 78], time–rsolved FWM effects [79], and photon echoes from continuum states [80, 81].

One very important effect of the Coulomb interaction is the existence of a FWM signal for $\Delta t < 0$, seen in experiments on GaAs quantum wells [82, 83]. The prediction of rise time of $T_2/4$ is a general result of the SBE, independent of the excitation or the material, assuming the system is homogeneously broadened. For an inhomogeneous system there is a weaker signal for $\Delta t < 0$ [84].

It is possible to transform the SBE from $\mathbf{k}$-space into the exciton basis [3]. A useful model can be extracted by averaging over the lowest lying exciton states, and generating an equation of the motion for a single average polarization $P$. The average polarization model was first introduced to clarify the RPA theory of FWM, since it captured the essential physics while simplifying the equations to keep the interpretation transparent [83]. In addition to the averaging, we will make the assumption that we are in the coherent regime, and that the length of the Bloch vector is constant $n \approx |P|^2$. We then have only a single equation to solve perturbatively:

$$i\frac{\partial}{\partial t}P(t) = (\Omega - i\gamma)P(t) - \mu E(t)[1 - \frac{|P(t)|^2}{P_s^2}] + VP(t)|P(t)|^2 \tag{2.74}$$

Here, $P_s$ is a saturation parameter and $V$ is an effective Coulomb coupling parameter. It is straightforward to generalize Eq. (2.74) to include several levels [3], for example the different hole states. The average polarization

model has been useful in explaining a number of experiments at the RPA level [83**?** **?** ]. However, for a quantitatively accurate simulation of experiments, it is necessary to use the full numerical solutions of the SBE, including all band structure and selection rules.

We can also apply the RPA factorization technique in the case of a magnetic field applied to the sample. We start by expanding the magnetoexciton states in terms of the Landau levels, and generate a set of equations for $P_n$ and $n_n$, the polarization and excited population of LL$n$ respectively [85]:

$$i\frac{\partial}{\partial t}P_n = (E_n - 2\sum_{n'} V_{n,n'} n_{n'})P_n - (1-2n_n)(\mu_{cv}E(t) + \sum_{n'} V_{n,n'}P_{n'}) \quad (2.75)$$

$$\frac{\partial}{\partial t}n_n = 2Im\left\{P_n(\mu^*_{cv}E^*(t) + \sum_{n'} V_{n,n'}P^*_{n'})\right\} \quad (2.76)$$

The Coulomb interaction $V_{n,n'}$ couples different Landau levels together. Eqs. (2.75) and (2.76) have been solved numerically for up to 1000 Landau levels [85, 86]. An average polarization model can be generated from this system as well, by keeping only the few Landau levels which are directly excited.

### 2.4.2 The Dynamics–Controlled Truncation Scheme

Over the past several years, numerous experiment effects have been measured which require a theoretical description beyond the RPA, such as the contribution of biexcitons to the nonlinear optical response [87–89]. The correct interpretation of these experiments requires a formalism in which the Coulomb interaction is accounted for consistently, and to arbitrary order. One such formalism which naturally extends the SBE is the Dynamics–Controlled Truncation Scheme (DCTS) [4–6].

Calculating the optical response starts, as before, with the many-body Hamiltonian, Eq. (2.69), and the equation of motion for the polarization. However, unlike the RPA treatment, the four–particle correlations are not factorized, The results of the DCTS theory are several mathematical theorems which show that certain higher correlations contribute to higher order in the electric field and can thus be neglected for a calculation of the optical response to a given order [4, 90]. This can be accomplished because of the correspondence between the number of electron-hole pairs in the system and the sequence of photon absorption and emission. The theory systematically includes all correlations which contribute to a specific order. In the limit of third order processes ($\chi^{(3)}$–truncation), and within the coherent limit, there

is only one four–particle correlation function which must be taken into account, the biexciton creation operator $B$ [90, 91]. The effects of additional four–particle correlations, such as the exciton density, and correlations which contribute to fifth order in the electric field, have been investigated as well [92, 93].

The necessary four–particle correlation $B^{ehe'h'} = \langle \hat{e}\hat{h}\hat{e}'\hat{h}'\rangle - \langle \hat{e}\hat{h}\rangle\langle \hat{e}'\hat{h}'\rangle + \langle \hat{e}\hat{h}'\rangle\langle \hat{e}'\hat{h}\rangle$, gives the biexcitonic structure, both the bound and unbound states. By subtracting the factorized components, we let $B$ characterize the deviation from the RPA theory [91]. The DCTS equations will then contain several driving terms: (1) the Pauli blocking nonlinearity present even in the atomic systems, (2) the Coulomb interaction of the RPA theory, and (3) a new source term which describes the coupling between excitons and the full spectrum of two-exciton states. This final driving term is beyond the RPA, and has a dramatic effect on the FWM signal.

To understand the effect of this correlation, we can update the average polarization model to include higher order correlations, based on the DCTS microscopic theory [91, 94]. For the case of co-circularly polarized laser pulses (which cannot excite a bound biexciton), the new equation of motion for the polarization is [94]:

$$i\frac{\partial}{\partial t}P(t) = (\Omega - i\gamma)P(t) - \mu E(t)[1 - \frac{|P(t)|^2}{P_s^2}] + VP(t)|P(t)|^2 + V_B B(t)P^*(t) \tag{2.77}$$

where the function $B$ is an effective four–particle correlation function describing the continuum of unbound biexciton states, and satisfying the equations

$$i\frac{\partial}{\partial t}B(t) = (2\Omega - i\Gamma)B(t) + P(t)^2 \tag{2.78}$$

Unlike the Pauli blocking nonlinearity which exists only for $\Delta t > 0$, or even the mean-field X–X nonlinearity for which the rise time is half of the decay time, a new source term due to exciton-exciton correlations grows in a non-exponential fashion, and for $\Delta t < 0$ can dominate the signal.

These equations can easily be generalized to include the four Zeemman–split heavy hole and light hole transitions in a magnetic field [95]. This model has also been used to explain the effects of the bound biexciton on the pump–probe spectrum of ZnSe QWs and microcavities [96, 97]. The functional form of the model is directly related to the full microscopic theory, which makes it qualitatively different from a simple multi–level scheme.

Several different formalisms have been developed which are able to account for the higher order correlations, and many are in fact equivalent to the DCTS [98–101]. Recently, a theory has been presented which bridges

the gap between the DCTS and theories based on Green functions which explain the build-up of screening effects [102]. Within this theory is possible to simulate with remarkable accuracy the results of FWM in bulk GaAs in a high magnetic field.

**Limits of the DCTS**

The DCTS is successful because in many semiconductor systems, there is a correspondence between the number of electron-hole pairs in the system and the absorption of photons. In semiconductor systems where this scheme is applicable, we have been able to explain the experimental results with incredible accuracy. However, if this correspondence breaks down, the DCTS fails. This is the case, for instance, in modulation doped quantum wells where a high mobility 2DEG exists in the sample before excitation, and can react to photons and photo-excited carriers. In the following chapter, we will develop a theory that extends the DCTS and addresses the nonlinear response of systems with such a strongly correlated ground state.

## 2.5 Conclusions

In this chapter, we reviewed the background scientific material that is necessary to study the ultrafast nonlinear optical dynamics of the quantum Hall system. We first over-viewed the properties of GaAs quantum wells and discussed the physics of the 2DEG in a magnetic field. We then discussed ultrafast nonlinear spectroscopic experiments, and in particular four–wave–mixing experiments. To illustrate the physics that can be accessed with such experiments we also discussed the case of a two–level system. We then reviewed the theoretical methods that have been used to explain such experiments and more specifically we discussed the Semiconductor Bloch equations and Dynamics–Controlled Truncation Scheme. We concluded by pointing out that the DCTS cannot be applied in systems with a strongly correlated ground state, such as the quantum Hall system.

# Chapter 3

# Theoretical framework

## 3.1 Outline

As discussed in Chapter 2, the nonlinear optical response of undoped semiconductors has been treated extensively in the past using different theoretical approaches, such as the DCTS [5, 6]. However, in the quantum Hall system, the presence of the 2DEG leads to strong Coulomb correlations in the ground state itself, which result in long range charge and spin order at sufficiently low temperatures and to collective electronic excitations. As a result, the main DCTS assumption of an uncorrelated Hartree–Fock ground state breaks down. In this chapter, we will develop a theoretical formulation that goes beyond the DCTS by not relying on a Hartree–Fock or other specific ground state, in analogy with Feynman's theory of liquid helium [21, 49, 71, 103**?** , 104], and allows us to study the ultrafast nonlinear optical response of the quantum Hall system.

In §3.2, we set up the general problem, and in §3.3 we introduce the excitations that dominate the ultrafast dynamics, the magnetoexcitons (X) and the magnetoplasmons (MP). We also discuss the X+MP states created by the interactions of the photoexcited excitons and 2DEG carriers. In §3.4, we derive the equations of motion for the polarizations and the photoexcited carrier populations, and we identify the contributions due to the many–body interactions. In §3.5, we present a decoupling scheme for treating the interaction effects, which is motivated by a decomposition of the photoexcited many–body states that separates out the uncorrelated and excitonic contributions from the correlated and incoherent contributions. We use this approach to devise a factorization scheme and identify the intraband and interband correlated contributions to the density matrix. We also discuss the linear absorption spectrum. Finally, in §3.6 we briefly discuss the coherent

X–X interaction and scattering effects. At this point, our theory is set up and we are able to derive an average polarization model to describe the ultrafast nonlinear optical response of the system and identify the experimental signatures of the 2DEG dynamics, which will be discussed in Chapter 4. In here, we will present a general solution.

## 3.2 Hamiltonian

To describe the quantum Hall system, we adopt a two–band many–body Hamiltonian of interacting electrons and holes subject to a magnetic field that splits the conduction and valence bands into discrete electron ($e$) and hole ($h$) LLs [9] ($\hbar = 1$):

$$H = \sum_{kn\sigma} [E_g + \Omega_c^c(n+1/2)]\, \hat{e}^\dagger_{kn\sigma}\hat{e}_{kn\sigma} + \sum_{kn\sigma} \Omega_c^v(n+1/2)\, \hat{h}^\dagger_{kn\sigma}\hat{h}_{kn\sigma} + H_{int} \quad (3.1)$$

where $E_g$ is the bandgap, $\Omega_c^{c,v} = eB/m_{e,h}$, are the electron and heavy hole cyclotron energies, $\hat{e}^\dagger_{kn\sigma}$ is the creation operator of the spin $\sigma$ LL$n$ conduction band electron state, Eq. (2.15), and similarly, $\hat{h}^\dagger_{kn\sigma}$ is the creation operator of the spin $\sigma$ LL$n$ valence band heavy hole state $\bar{\psi}$. In the ideal two–dimensional system the hole wavefunction is related to the electron one as $\bar{\psi}_{kn} = \psi^*_{-kn}$, which leads to an electron–hole symmetry that strongly affects the nonlinear optical properties [105]. In the realistic system, this symmetry is partially lifted due to lateral confinement, the different band offsets, confinement between the electrons and the holes, valence band mixing, etc.

The Hamiltonian $H_{int}$ describes the $e$–$e$, $e$–$h$, and $h$–$h$ Coulomb interactions,

$$H_{int} = \frac{1}{2} \sum_{\alpha_1\alpha_2\alpha_3\alpha_4} \Big[ v^{ee}_{\alpha_1\alpha_2,\alpha_3\alpha_4} \hat{e}^\dagger_{\alpha_3}\hat{e}^\dagger_{\alpha_1}\hat{e}_{\alpha_2}\hat{e}_{\alpha_4} + v^{hh}_{\alpha_1\alpha_2,\alpha_3\alpha_4} \hat{h}^\dagger_{\alpha_3}\hat{h}^\dagger_{\alpha_1}\hat{h}_{\alpha_2}\hat{h}_{\alpha_4} - v^{eh}_{\alpha_1\alpha_2,\alpha_3\alpha_4} \hat{h}^\dagger_{\alpha_3}\hat{e}^\dagger_{\alpha_1}\hat{e}_{\alpha_2}\hat{h}_{\alpha_4} - v^{he}_{\alpha_1\alpha_2,\alpha_3\alpha_4} \hat{e}^\dagger_{\alpha_3}\hat{h}^\dagger_{\alpha_1}\hat{h}_{\alpha_2}\hat{e}_{\alpha_4} \Big] \quad (3.2)$$

where $\alpha = (k, n, \sigma)$. In the ideal two–dimensional system, the Coulomb interaction matrix elements $v^{ij}_{\alpha_1\alpha_2,\alpha_3\alpha_4}$ (with $i, j = e, h$) are given by

$$v^{ij}_{\alpha_1\alpha_2,\alpha_3\alpha_4} = \int \frac{d\mathbf{q}}{(2\pi)^2}\, v_q\, F^i_{\alpha_1\alpha_2}(\mathbf{q}) F^j_{\alpha_3\alpha_4}(-\mathbf{q}) \quad (3.3)$$

where

$$v_q = \frac{2\pi e^2}{\epsilon q} \quad (3.4)$$

is the Fourier transformed 2D Coulomb potential [9], $\epsilon$ the material dielectric constant, $q = \sqrt{q_x^2 + q_y^2}$, and

$$F^e_{\alpha_1\alpha_2}(\mathbf{q}) = \phi_{n_1 n_2}(\mathbf{q}) e^{iq_x(k_1+k_2)\ell^2/2}\delta_{k_1,k_2+q_y}\delta_{\sigma_1,\sigma_2} \quad F^h_{\alpha_1\alpha_2}(\mathbf{q}) = F^e_{-\alpha_2,-\alpha_1}(\mathbf{q}) \tag{3.5}$$

where $-\alpha = (-k, n, \sigma)$, and

$$\phi_{mn}(\mathbf{q}) = \frac{n!}{m!}\left[\frac{(-q_y + iq_x)l}{\sqrt{2}}\right]^{m-n} L_n^{m-n}\left(\frac{q^2\ell^2}{2}\right)e^{-q^2\ell^2/4} \tag{3.6}$$

for $m \geq n$ and $\phi_{mn}(\mathbf{q}) = \phi^*_{nm}(-\mathbf{q})$ for $m < n$. $L_n^{m-n}$ is the generalized Laguerre polynomial

$$L_n^{m-n}(x) = \sum_{r=0}^{n} \frac{(-1)^r m!\; x^r}{(n-r)!(m-n+r)!r!} \tag{3.7}$$

Because of the symmetry of the Coulomb potential, Eq. (3.6) is often useful in polar coordinates, obtained by substituting $q_x = q\cos\theta$ and $q_y = q\sin\theta$:

$$\phi_{mn}(\mathbf{q}) = \frac{n!}{m!}\left(\frac{iql}{\sqrt{2}}\right)^{m-n} e^{i(m-n)\theta} L_n^{m-n}\left(\frac{q^2\ell^2}{2}\right)e^{-q^2\ell^2/4} \tag{3.8}$$

In the following, all energies are measured with respect to the ground state energy, i.e. $H|G\rangle = 0$.

The coupling to an external electric field $E(t)$ can be described, within the dipole approximation, by the Hamiltonian [9]

$$H_{\text{tot}}(t) = H - \mu E(t)\hat{X}^\dagger - \mu E^*(t)\hat{X} \tag{3.9}$$

where $\mu$ is the interband transition matrix element and $\hat{X}^\dagger$ the interband optical transition operator, given by

$$\hat{X}^\dagger = \sum_{nk} \hat{e}^\dagger_{kn\downarrow}\hat{h}^\dagger_{-kn\downarrow} \tag{3.10}$$

when the system is excited with right–circularly polarized light.

## 3.3 Magnetoexcitons and Magnetoplasmons

In this section we briefly discuss the magnetoexciton (X) and magnetoplasmon (MP) excitations that govern the ultrafast nonlinear optical dynamics. In the case of photoexcitation with right–circularly polarized light, which

excites spin–$\downarrow$ $e$–$h$ pairs, the dipole transition operator $\hat{X}^\dagger$ can be expanded in terms of the exciton creation operators $\hat{X}_i$ that create the allowed optical transitions for given LLs. In particular, the creation operator of a LL$m \rightarrow$ LL$n$ magnetoexciton with total momentum $\mathbf{q}$ is

$$\hat{X}^\dagger_{\mathbf{q}nm} = \frac{1}{\sqrt{N}} \sum_k e^{ikq_x\ell^2} \hat{e}^\dagger_{k+q_y/2,n,\downarrow} \hat{h}^\dagger_{-k+q_y/2,m,\downarrow} \tag{3.11}$$

In the absence of disorder, momentum is conserved and only $\mathbf{q} = 0$ excitons are photoexcited directly. Furthermore, in the ideal system, the only allowed optical transitions correspond to $m = n$. We then have that

$$\hat{X}^\dagger = \sqrt{N} \sum_n \hat{X}^\dagger_n \qquad \hat{X}^\dagger_n = \hat{X}^\dagger_{0nn} = \frac{1}{\sqrt{N}} \sum_k \hat{e}^\dagger_{kn\downarrow} \hat{h}^\dagger_{-kn\downarrow} \tag{3.12}$$

In the realistic system, the disorder can relax the momentum conservation condition [20, 37, 70, 106], thus mixing exciton states with different momenta, while the valence band mixing couples the $n \neq m$ valence hole states and magnetoexcitons [20, 63, 64, 106].

The states $|X_n\rangle = \hat{X}^\dagger_n |G\rangle$ are the magnetoexciton states in the 2DEG system. The difference from undoped semiconductors is that here the exciton operators $\hat{X}^\dagger_n$ act on the strongly correlated state $|G\rangle$, which is the ground state of the many–body Hamiltonian $H$ that describes the correlated 2DEG at rest.

The following orthogonality relation holds for the exciton states:

$$\langle X_n | X_m \rangle = (1 - \nu_n)\delta_{nm}, \tag{3.13}$$

where

$$\nu_n = \frac{1}{N} \sum_k \langle G | \hat{e}^\dagger_{kn\downarrow} \hat{e}_{kn\downarrow} | G \rangle \tag{3.14}$$

is the ground state filling factor of the LL$n$ spin–$\downarrow$ 2DEG electron states. In the strong magnetic field limit, $\nu_n = 0$.

The Pauli exchange effects between the excitons are described – as already known from undoped semiconductors – by the deviation of the commutator of the X operators from bosonic behavior due to the underlying Fermi statistics. Using Eq. (3.12) we obtain that

$$[\hat{X}_n, \hat{X}^\dagger_m] = \delta_{nm} \left(1 - \nu_n - \Delta\hat{\nu}_n\right), \tag{3.15}$$

where

$$\Delta\hat{\nu}_n = \frac{1}{N} \sum_k \left( \hat{h}^\dagger_{-kn\downarrow} \hat{h}_{-kn\downarrow} + \hat{e}^\dagger_{kn\downarrow} \hat{e}_{kn\downarrow} - \langle G | \hat{e}^\dagger_{kn\downarrow} \hat{e}_{kn\downarrow} | G \rangle \right) \tag{3.16}$$

describes the change in the LL$n$ filling factor due to the photoexcited electron and hole populations.

The magnetoplasmon modes dominate over quasi-electron – quasi-hole pair excitations for momenta $q < 1/l$. A LL$m$ →LL$n$ MP may be thought of as an $e$–$h$ pair, or exciton, formed by an electron in LL$n$ and a hole in the LL$m$ 2DEG. The creation operator of this MP is given to first approximation by the LL$m$ →LL$n$ contribution to the collective density operator [21, 35, 49, 67, 103]:

$$\hat{\rho}^{e}_{\mathbf{q}nm\sigma} = \frac{1}{\sqrt{N}} \sum_{k} e^{iq_x k\ell^2} \hat{e}^{\dagger}_{k+q_y/2,n,\sigma} \hat{e}_{k-q_y/2,m,\sigma}. \tag{3.17}$$

in analogy with the magnetoexciton creation operator, Eq. (3.11). It is convenient to also introduce a similar collective operator for the hole states [105],

$$\hat{\rho}^{h}_{\mathbf{q}nm\sigma} = \frac{1}{\sqrt{N}} \sum_{k} e^{iq_x k\ell^2} \hat{h}^{\dagger}_{-k+q_y/2,n,\sigma}\ \hat{h}_{-k-q_y/2,m,\sigma}, \tag{3.18}$$

The creation and annihilation operators are related as

$$\hat{\rho}^{i\dagger}_{\mathbf{q}nm\sigma} = \hat{\rho}^{i}_{-\mathbf{q}mn\sigma}\ ,\ i = e, h \tag{3.19}$$

Here we focus on photoexcitation of the LL0 and LL1 optical transitions only, which are dynamically coupled by the LL0 → LL1 inter–LL MPs [25, 38, 40–43]. These MPs are the lowest–energy neutral charge excitations of the $\nu = 1$ quantum Hall ferromagnet, where the intra–LL charge excitations are suppressed since all spin–↑ LL0 states are occupied in the ground state [107–109].

Similar to Feynmann's theory of the collective charge excitation spectrum of liquid helium [21, 35, 49, 71, 103, 104], a good variational approximation of the MP eigenstates of the Hamiltonian $H$ is given by the state (single–mode approximation) [21, 49]

$$|M_{\mathbf{q}}\rangle = \sum_{\sigma nm} C_{nm\sigma}(\mathbf{q}) \phi_{nm}(\mathbf{q}) \hat{\rho}^{e}_{\mathbf{q}nm\sigma} |G\rangle, \tag{3.20}$$

where $C_{nm\sigma}(\mathbf{q})$ are variational parameters. The mixing of the different LL states, which is due to the interactions, is suppressed in the strong magnetic field limit [49] by a factor $\propto B^{-1/2}$ since the characteristic 2DEG Coulomb interaction energy $e^2/\ell \propto \sqrt{B}$ is smaller than the energy separation between the electron LLs, $\Omega^c_c \propto B$. Even though in the realistic system $e^2/\ell \sim \Omega^c_c$, calculations have shown that the LL mixing does not change qualitatively the MP properties [35, 103, 110].

Excitons and magnetoplasmons are both made of electrons, and therefore the X–MP Pauli exchange effects must be considered. Similar to the case of Xs, these are described by the commutators

$$[\hat{\rho}^{e}_{\mathbf{q}nm\sigma}, \hat{X}^{\dagger}_{l}] = \frac{1}{\sqrt{N}}\delta_{lm}\delta_{\sigma\downarrow}\hat{X}^{\dagger}_{\mathbf{q}nm} \qquad [\hat{\rho}^{h}_{\mathbf{q}nm\sigma}, \hat{X}^{\dagger}_{l}] = \frac{1}{\sqrt{N}}\delta_{lm}\delta_{\sigma\downarrow}\hat{X}^{\dagger}_{\mathbf{q}mn} \quad (3.21)$$

obtained by using the second quantization expressions for $\hat{\rho}$ and $\hat{X}$. In the case of a spin–polarized ground state 2DEG of spin–$\uparrow$ electrons, the MP and X operators commute since right–circularly polarized light only creates spin–$\downarrow$ electrons.

In addition to the Pauli exchange effects, the optical properties are strongly affected by the interactions between the photoexcited excitons $\hat{X}_n$ and the 2DEG carriers. We can describe such X–2DEG interactions, which scatter the X into X+MP final states, by considering the action of the Hamiltonian $H$ on $|X_n\rangle$ [25]:

$$H|X_n\rangle = \Omega_n|X_n\rangle - (1-\nu_n)\sum_{m\neq n} V_{mn}|X_m\rangle + |Y_n\rangle. \quad (3.22)$$

The above equation defines the state $|Y_n\rangle$ by the requirement that it is orthogonal to all exciton states, $\langle X_m|Y_n\rangle = 0$, and therefore describes an excited 2DEG configuration (denoted as 2DEG$^*$ from now on).

The above orthogonality requirement, as well as the orthogonality among the X states, gives

$$\Omega_n = \frac{\langle X_n|H|X_n\rangle}{\langle X_n|X_n\rangle} \quad (3.23)$$

the energy of the X$_n$ state, and

$$V_{nm} = -\frac{\langle X_n|H|X_m\rangle}{(1-\nu_n)(1-\nu_m)} = V^{*}_{mn} \quad (3.24)$$

the static Coulomb–induced coupling of the different LL Xs. Based on the above we introduce the operator

$$\hat{Y}_n = [\hat{X}_n, H] - \Omega_n\hat{X}_n + (1-\nu_n)\sum_{m\neq n} V_{nm}\hat{X}_m \quad (3.25)$$

that describes the interactions between $X_n$ and all the other carriers: Xs, MPs, or ground state 2DEG.

An explicit expression for the operator $\hat{Y}_n$ can be obtained by calculating the commutator $[\hat{X}_n, H]$:

$$\begin{aligned}[\hat{X}_n, H] = &\left[E_g + (n+1/2)\left(\Omega^{c}_{c} + \Omega^{v}_{c}\right)\right]\hat{X}_n \\ &- \sum_{m}\hat{X}_m\int\frac{d\mathbf{q}}{(2\pi)^2}\,v_q\,|\phi_{mn}(q)|^2 + \hat{Y}^{\mathrm{int}}_{n}\end{aligned} \quad (3.26)$$

The first two terms give the X energies and Coulomb–induced couplings similar to the undoped system [85, 111], while the interaction contributions are described by the operator

$$\hat{Y}_n^{\rm int} = \frac{1}{2\pi\ell^2\sqrt{N}} \sum_{\mathbf{q}m} v_q \hat{\rho}_{\mathbf{q}} \left[ \phi_{nm}(-\mathbf{q}) \hat{X}_{\mathbf{q}mn} - \phi_{mn}(-\mathbf{q}) \hat{X}_{\mathbf{q}nm} \right] \tag{3.27}$$

where we defined for simplicity

$$\hat{\rho}_{\mathbf{q}} = \sum_{mm'\sigma} \phi_{mm'}(\mathbf{q}) \left( \hat{\rho}^e_{\mathbf{q}mm'\sigma} - \hat{\rho}^h_{\mathbf{q}m'm\sigma} \right). \tag{3.28}$$

The operator $\hat{Y}_n$ can be obtained from Eq. (3.25) by subtracting from the above expression for $\hat{Y}_n^{\rm int}$ the contributions to the X energies and couplings, Eqs. (3.23) and (3.24), which are $\propto \langle X_m | \hat{Y}_n^{\rm int\dagger} | G \rangle$. After some algebra,

$$\begin{aligned} \hat{Y}_n = \hat{Y}_n^{\rm int} &+ \sum_{m\neq n} \frac{\hat{X}_n}{1-\nu_n} \int \frac{d\mathbf{q}}{(2\pi)^2} v_q \phi_{nm}(-\mathbf{q}) \langle G | \hat{\rho}_{\mathbf{q}} \hat{\rho}^e_{-\mathbf{q}nm\downarrow} | G \rangle \\ &- \sum_{m\neq n} \frac{\hat{X}_m}{1-\nu_m} \int \frac{d\mathbf{q}}{(2\pi)^2} v_q \phi_{mn}(-\mathbf{q}) \langle G | \hat{\rho}_{\mathbf{q}} \hat{\rho}^e_{-\mathbf{q}mn\downarrow} | G \rangle \end{aligned} \tag{3.29}$$

In the undoped system, $\hat{Y}_n^\dagger |G\rangle = 0$ (since $\hat{\rho}_{\mathbf{q}} |G\rangle = 0$) and $\hat{Y}_n = \hat{Y}_n^{\rm int}$ describes the X–X interaction effects. In the doped system, $\hat{Y}_n^{\rm int}$ renormalizes the exciton energies and couplings due to the exciton interactions with the ground state 2DEG. In addition to X–X interactions, here $\hat{Y}_n^{\rm int}$ describes X+MP scattering effects. This can be seen from Eqs. (3.27) and (3.28) by recalling that the operators $\hat{\rho}^e_{\mathbf{q}mm'\sigma}$ create and annihilate the MPs. In the special case of spin–$\uparrow$ polarized 2DEG, there is no change in the X energies and couplings, as $\hat{\rho}^e_{-\mathbf{q}nm\downarrow} |G\rangle = 0$. Furthermore, the X–X and X+MP contributions can be distinguished, since the MPs are excitations of the spin–$\uparrow$ electrons that populate the ground state, while all $\sigma = \downarrow$ carriers are induced by the right–circularly polarized optical pulses. As a result, in this case the $\sigma = \uparrow$ contribution to Eq. (3.28) describes the MP interaction effects, while the $\sigma = \downarrow$ term describes the X–X interactions.

To make the analogy to the case of phonons in undoped semiconductors [5, 7], the density matrix $\langle \hat{Y}_n \rangle$ describes the contribution of the MP–assisted interband density matrices and the X–X interactions. The results of [5, 7] for the polarization equation of motion are reproduced if we add to the Hamiltonian $H$ the electron–phonon interaction and use Eq. (3.25). The difference here is that both the X–X interactions and the interactions between

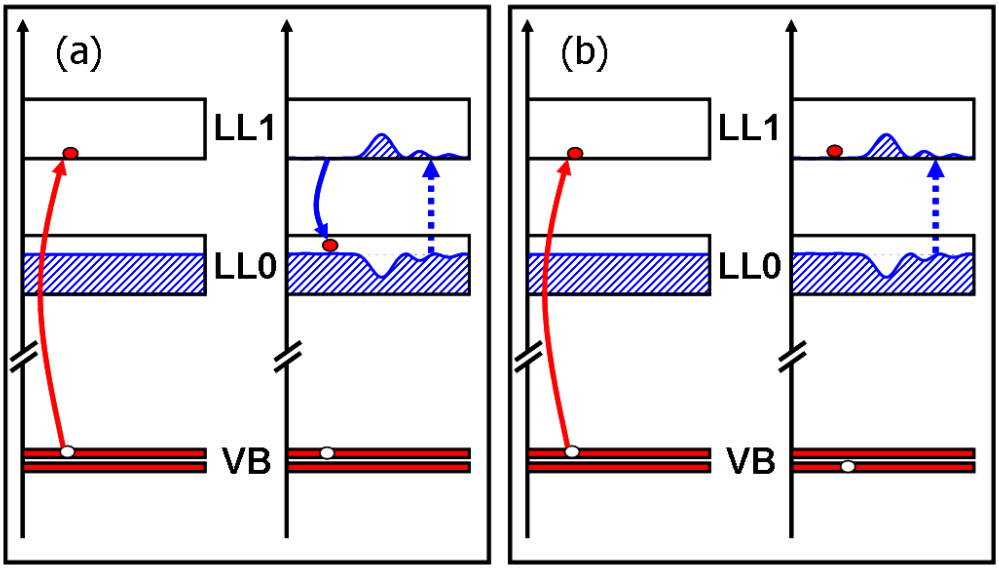


**Figure 3.1:** Scattering of the LL1 exciton to (a) a {1-MP + 1-LL0-$e$ + 1-LL1-$h$} and (b) a {1-MP + 1-LL1-$e$ + 1-LL0-$h$} four–particle excitation of the ground state.

the photoexcited carriers and the collective 2DEG excitations are described by the same electronic Hamiltonian Eq. (3.2).

By retaining contributions from the photoexcited LLs (LL0 and LL1) only, we obtain the simple property

$$\hat{Y}_1 = -\hat{Y}_0 = \hat{Y} \tag{3.30}$$

where

$$\begin{aligned}\hat{Y} = \hat{Y}_{\rm int} &+ \frac{\hat{X}_1}{1-\nu_1}\int \frac{d\mathbf{q}}{(2\pi)^2} v_q \phi_{10}(-\mathbf{q}) \langle G|\hat{\rho}_{\mathbf{q}}\hat{\rho}^e_{-\mathbf{q}10\downarrow}|G\rangle \\ &- \frac{\hat{X}_0}{1-\nu_0}\int \frac{d\mathbf{q}}{(2\pi)^2} v_q \phi_{01}(-\mathbf{q}) \langle G|\hat{\rho}_{\mathbf{q}}\hat{\rho}^e_{-\mathbf{q}01\downarrow}|G\rangle \end{aligned} \tag{3.31}$$

and

$$\hat{Y}_{\rm int} = \frac{1}{2\pi\ell^2\sqrt{N}} \sum_{\mathbf{q}} v_q \hat{\rho}_{\mathbf{q}} \left[\phi_{10}(-\mathbf{q})\hat{X}_{\mathbf{q}01} - \phi_{01}(-\mathbf{q})\hat{X}_{\mathbf{q}10}\right] \tag{3.32}$$

As is shown in the above expression, the state $\hat{Y}^\dagger_{\rm int}|G\rangle$ is a linear combination of {1-MP + 1-LL0-$e$ + 1-LL1-$h$} and {1-MP + 1-LL1-$e$ + 1-LL0-$h$}

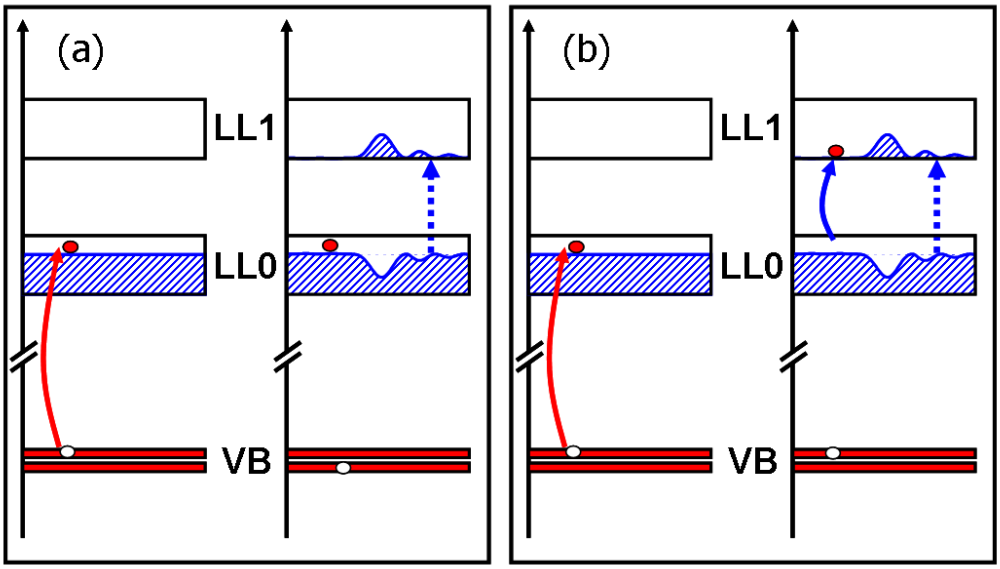


**Figure 3.2:** Scattering of the LL0 exciton to (a) a {1-MP + 1-LL1-$e$ + 1-LL0-$h$} and (b) a {1-MP + 1-LL0-$e$ + 1-LL1-$h$} four–particle excitation of the ground state.

four–particle excitations, into which both the LL0 and the LL1 excitons can scatter by interacting with the 2DEG. In the case of $X_1$, the LL1 electron can scatter to LL0 by emitting a LL0 $\rightarrow$ LL1 MP, as illustrated in Fig. 3.1a. Since the MP energy is close to the $e$–LL0 $\rightarrow$ $e$–LL1 energy spacing, this scattering process is almost resonant and therefore provides an efficient decay channel of the LL1 exciton to a {1-MP + 1-LL0-$e$ + 1-LL1-$h$} four–particle excitation of the ground state $|G\rangle$. All other allowed scattering processes are non-resonant. For example, the $X_1$ hole can scatter to LL0 by emitting a MP, which leads to a {1-MP + 1-LL1-$e$ + 1-LL0-$h$} four–particle excitation (Fig. 3.1b). The latter state however has energy that is significantly higher, by an amount of the order of $\sim \Omega_c^c + \Omega_c^v$, from that of the initial $X_1$ state. In the case of $X_0$, the LL0 electron can scatter to LL1 by emitting a MP, so that $X_0 \rightarrow$ {1-MP + 1-LL1-$e$ + 1-LL0-$h$} (Fig. 3.2a), or the LL1 hole can scatter to LL0, in which case $X_0 \rightarrow$ {1-MP + 1-LL0-$e$ + 1-LL1-$h$} (Fig. 3.2b). $|Y_0\rangle$ is thus a linear combination of the same final states as $|Y_1\rangle$, also seen from Eq. (3.30). However, in this case the energy of all final states is significantly higher than that of the initial state $|X_0\rangle$. Therefore, the decay of the LL0 exciton is suppressed as compared to that of the LL1 (or higher) exciton. As discussed below, this difference in the dephasing of the two LL excitons

already plays an important role in the linear absorption spectra, and has even more profound effects on the nonlinear optical spectra.

## 3.4 Ultrafast Nonlinear Optical Response

In this section we obtain the equations of motion for the interband polarizations and the intraband populations that determine the nonlinear optical response and identify the contributions due to the many–body interactions.

Within the dipole approximation, the optical spectra are determined by the polarization of the photo–excited system,

$$P(t) = \frac{\mu}{\sqrt{N}} \sum_n P_n(t) \qquad P_n = \langle \hat{X}_n \rangle \tag{3.33}$$

which may be obtained from the equations of motion for the $X_n$ polarizations $P_n$. The time evolution of any operator $\hat{O}$ is determined by the full many–body Hamiltonian $H_{tot}(t)$:

$$i\partial_t \langle \hat{O} \rangle = \langle [\hat{O}, H] \rangle - d(t) \sum_m \langle [\hat{O}, \hat{X}_m^\dagger] \rangle - d^*(t) \sum_m \langle [\hat{O}, \hat{X}_m] \rangle. \tag{3.34}$$

where $d(t) = \mu E(t)\sqrt{N}$ is the Rabi energy. Substituting $\hat{O} = \hat{X}_n$ in the above equation and using the property $[\hat{X}_n, \hat{X}_m] = 0$, Eq. (3.25) for the commutator $[\hat{X}_n, H]$ and Eq. (3.15) for the commutator $[\hat{X}_n, \hat{X}_m^\dagger]$ we obtain the equation of motion for the polarization:

$$i\partial_t P_n(t) - \Omega_n P_n(t) + (1-\nu_n) \sum_{m \neq n} V_{nm} P_m(t) = -d(t)[1 - \nu_n - \Delta\nu_n] + \langle \hat{Y}_n \rangle \tag{3.35}$$

where $\Delta\nu_n = \langle \Delta\hat{\nu}_n \rangle$. The lhs of the above equation describes the static exciton energies and Coulomb–induced LL couplings, while the rhs describes two sources of nonlinearity. The first term describes the Pauli blocking effects (PSF), which are determined by the ground state spin–$\downarrow$ electron populations, with filling factor $\nu_n$, and by the photo–induced carrier populations in the spin–$\downarrow$ electron system, described by $\langle \Delta\hat{\nu}_n \rangle$, (see Eq. (3.16)). The second term on the rhs of Eq. (3.35), $\langle \hat{Y}_n \rangle$, includes the interactions between $X_n$ and the rest of the carriers in the system: X–X, X–MP, and X–2DEG interactions.

The equation of motion for $\Delta\hat{\nu}_n$ may be obtained by substituting $\hat{O} = \Delta\hat{\nu}_n$ in Eq. (3.34) and recalling Eq. (3.15), which gives $\Delta\hat{\nu}_n = 1 - \nu_n - [\hat{X}_n, \hat{X}_n^\dagger]$. The commutator $[H, [\hat{X}_n, \hat{X}_n^\dagger]]$ can be easily calculated using the property

$$[A, [B, C]] + [C, [A, B]] + [B, [C, A]] = 0 \tag{3.36}$$

which holds for any operators $A$, $B$, $C$ and Eq. (3.25) for the commutators $[\hat{X}_n, H]$. The commutator $[\Delta\hat{\nu}_n, \hat{X}_m^\dagger]$ is obtained using Eqs. (3.12) and (3.16):

$$[\Delta\hat{\nu}_n, \hat{X}_m^\dagger] = \frac{2}{N}\delta_{nm}\hat{X}_n^\dagger, \tag{3.37}$$

We therefore have the equation of motion:

$$i\partial_t \Delta\nu_n = \frac{2}{N}\left[d^*(t)P_n - d(t)P_n^*\right] + \langle\hat{M}_n\rangle^* - \langle\hat{M}_n\rangle \tag{3.38}$$

where we introduced the operator

$$\hat{M}_n = [\hat{Y}_n, \hat{X}_n^\dagger] \tag{3.39}$$

This intra–band density matrix describes a redistribution of the photoexcited carrier populations between the LLs that is assisted by the MP and the interactions. Analogous phonon–assisted effects in the case of undoped semiconductors are discussed e.g. in [7] and [5]. The corresponding physical processes become clear by calculating the above commutator using Eqs. (3.12), (3.29) and (3.27):

$$\begin{aligned}
\hat{M}_n &= \frac{1}{2\pi\ell^2\sqrt{N}}\sum_{\mathbf{q}m} v_q\hat{\rho}_{\mathbf{q}}\left[\phi_{nm}(-\mathbf{q})\langle X_{\mathbf{q}mn}|X_n\rangle - \phi_{mn}(-\mathbf{q})\langle X_{\mathbf{q}nm}|X_n\rangle\right] \\
&+ \sum_{\mathbf{q}mn'}\frac{v_q}{L^2}\left[\phi_{n'n}(\mathbf{q})\hat{X}^\dagger_{\mathbf{q}n'n} - \phi_{nn'}(\mathbf{q})\hat{X}^\dagger_{\mathbf{q}nn'}\right]\left[\phi_{nm}(-\mathbf{q})\hat{X}_{\mathbf{q}mn} - \phi_{mn}(-\mathbf{q})\hat{X}_{\mathbf{q}nm}\right] \\
&- \sum_{\mathbf{q}m\neq n}\frac{v_q}{L^2}\left[\phi_{nm}(-\mathbf{q})\hat{\rho}_{\mathbf{q}}\hat{\rho}^e_{-\mathbf{q}nm\downarrow} - \phi_{mn}(-\mathbf{q})\hat{\rho}_{\mathbf{q}}\hat{\rho}^h_{-\mathbf{q}nm\downarrow}\right] \\
&+ \frac{[\hat{X}_n, \hat{X}_n^\dagger]}{1-\nu_n}\sum_{\mathbf{q}m\neq n}\frac{v_q}{L^2}\phi_{nm}(-\mathbf{q})\langle G|\hat{\rho}_{\mathbf{q}}\hat{\rho}^e_{-\mathbf{q}nm\downarrow}|G\rangle
\end{aligned} \tag{3.40}$$

The first term on the rhs describes the photoexcitation of coherent MPs and is analogous to the coherent phonon contribution in undoped semiconductors [7]. Similar to the latter case, it vanishes in the ideal system, but is known to contribute in the realistic quantum Hall system due to disorder, inhomogeneities, and valence band mixing [20, 37, 70, 106]. The second term describes a contribution due to X populations and inter–LL exciton coherences, described by the density matrices $\langle\hat{X}^\dagger_{\mathbf{q}nm}\hat{X}_{\mathbf{q}n'm'}\rangle$. As in the undoped system, these exciton coherences and populations come from the photoexcited carriers. The third term describes interactions among the photoexcited carriers similar to the undoped system [7], as well as the scattering and correlations between MPs and spin–$\downarrow$ carriers, which lead to the relaxation of the photoexcited carriers due to MP emission and absorption.

As can be seen from Eq. (3.40), the intraband scattering processes are described by density matrices of the form $\langle \hat{X}^\dagger \hat{X} \rangle$, $\langle \hat{\rho}^e_\sigma \hat{\rho}^e_\downarrow \rangle$, $\langle \hat{\rho}^e_\sigma \hat{\rho}^h_\downarrow \rangle$, and $\langle \hat{\rho}^h_\downarrow \hat{\rho}^h_\downarrow \rangle$. In the case of the spin–$\uparrow$ polarized 2DEG, the MP contributions are described by the density matrices $\langle \hat{\rho}^e_\uparrow \hat{\rho}^e_\downarrow \rangle$ and $\langle \hat{\rho}^e_\uparrow \hat{\rho}^h_\downarrow \rangle$, which vanish in the undoped system in the case of right–circularly polarized light and are analogous to the phonon–assisted intraband density matrices [7]. They relate an initial state consisting of a photoexcited electron or hole to a final state consisting of an electron or hole plus a MP and describe the effects of carrier scattering by MP emission or absorption.

The number of independent density matrices can be reduced by noting that the $e$–$h$ pair creation operators may be expressed in terms of exciton operators:

$$\hat{e}^\dagger_{kn\downarrow} \hat{h}^\dagger_{-k'm\downarrow} = \frac{1}{\sqrt{N}} \sum_{\mathbf{q}} \hat{X}^\dagger_{\mathbf{q}nm} e^{-iq_x(k+k')\ell^2/2} \delta_{q_y,k-k'}, \tag{3.41}$$

obtained from Eq. (3.11). Similar to the DCTS, further reductions can be obtained by noting that, as discussed below, only many–body states with one valence band hole contribute to the above intraband density matrices in the case of the third–order nonlinear optical response, and thus the density matrix $\langle \hat{h}^\dagger \hat{h}^\dagger \hat{h} \hat{h} \rangle$ can be neglected to this order. Furthermore, in the case of the spin–$\uparrow$ polarized 2DEG excited with right–circularly polarized light, spin–$\downarrow$ carriers are only created via the photexcitation, and thus the density matrix $\langle \hat{e}^\dagger_\downarrow \hat{e}^\dagger_\downarrow \hat{e}_\downarrow \hat{e}_\downarrow \rangle$ contributes to higher order, similar to the undoped system. In this case, only states with one spin–$\downarrow$ electron or hole contribute, and we obtain by using Eq. (3.41) and denoting by $n_{e\downarrow}$ and $n_{h\downarrow}$ the number operators of the spin–$\downarrow$ carriers that

$$\hat{\rho}^e_{\mathbf{q}nn'\downarrow} = \hat{\rho}^e_{\mathbf{q}nn'\downarrow} n_{h\downarrow} = \frac{1}{\sqrt{N}} \sum_{\mathbf{q}'m} e^{i(\mathbf{q}\times\mathbf{q}')_z \ell^2/2} \hat{X}^\dagger_{\mathbf{q}'nm} \hat{X}_{\mathbf{q}'-\mathbf{q}n'm} \tag{3.42}$$

and

$$\hat{\rho}^h_{\mathbf{q}nn'\downarrow} = \hat{\rho}^h_{\mathbf{q}nn'\downarrow} n_{e\downarrow} = \frac{1}{\sqrt{N}} \sum_{\mathbf{q}'m} e^{-i(\mathbf{q}\times\mathbf{q}')_z \ell^2/2} \hat{X}^\dagger_{\mathbf{q}'mn} \hat{X}_{\mathbf{q}'-\mathbf{q}mn'}. \tag{3.43}$$

The above expressions can be used to show that, in the case of spin–polarized 2DEG (e.g. for filling factors $\nu = 1/m$ ($m$ = integer) or integer $\nu$) and right–circular polarization, the independent intraband density matrices have the form $\langle \hat{X}^\dagger \hat{X} \rangle$ and $\langle \hat{\rho}^e_\uparrow \hat{X}^\dagger \hat{X} \rangle$. For other filling factors, all density matrices that enter in Eq. (3.40) must be calculated to obtain the third–order response, with the exception of $\langle \hat{h}^\dagger \hat{h}^\dagger \hat{h} \hat{h} \rangle$ which contributes to higher order.

To conclude this section, we note from the above equations of motion that the effects of the interactions on the nonlinear optical response are described by the interband density matrix $\langle \hat{Y} \rangle$ and the intraband density matrix $\langle \hat{M}_n \rangle$. Due to the many–body nature of this strongly correlated system, approximations are needed in order to calculate these interaction–induced effects. In the undoped system, the DCTS cumulant expansions separate the coherent from the incoherent and the correlated from the uncorrelated contributions. In the case of the 2DEG, we need an analogous decoupling scheme that we will present in the following section.

## 3.5 Interaction Effects

In this section we discuss a decomposition of the photoexcited many–body wavefunction into correlated and uncorrelated contributions, which we use in the next section to devise approximations for treating the interaction–induced density matrices $\langle \hat{Y}_n \rangle$ and $\langle \hat{M}_n \rangle$. Similar to the DCTS, we expand in terms of the optical field and calculate the third–order polarization, which is expected to describe the nonlinear optical signal when the photoexcited carrier density is small and the X–cold 2DEG correlations prevail.

As in the theoretical approaches of [5, 112], we note the one to one correspondence between the photon absorption / emission processes and the $e$–$h$ pair creation/destruction. However, since here a 2DEG is present prior to the photoexcitation, when following the effects of the applied fields we count the number of valence band holes in a given state. Therefore, we use the shorthand notation 0–$h$, 1–$h$, 2–$h$ ... to label the states, and it is clear that states with three or more holes do not contribute to the third–order nonlinear polarization [99]. We can then decompose the optically–excited state $|\psi\rangle$ according to

$$|\psi\rangle = |\psi_0\rangle + |\psi_1\rangle + |\psi_2\rangle \tag{3.44}$$

where $|\psi_n\rangle$, $n = 0, 1, 2$, describes the contribution of the $n$–$h$ states. From now on, we refer to operators that change the number of holes as interband and to operators that leave the number of holes unchanged as intraband.

Substituting Eq. (3.44) into the Schrödinger equation for the Hamiltonian $H_{tot}$, Eq. (3.9), we obtain up to third order in the optical field that

$$i\partial_t|\psi_0\rangle - H|\psi_0\rangle = -\mu E^*(t)\hat{X}|\psi_1\rangle \tag{3.45}$$

$$i\partial_t|\psi_1\rangle - H|\psi_1\rangle = -\mu E(t)\hat{X}^\dagger|\psi_0\rangle - \mu E^*(t)\hat{X}|\psi_2\rangle \tag{3.46}$$

$$i\partial_t|\psi_2\rangle - H|\psi_2\rangle = -\mu E(t)\hat{X}^\dagger|\psi_1\rangle \tag{3.47}$$

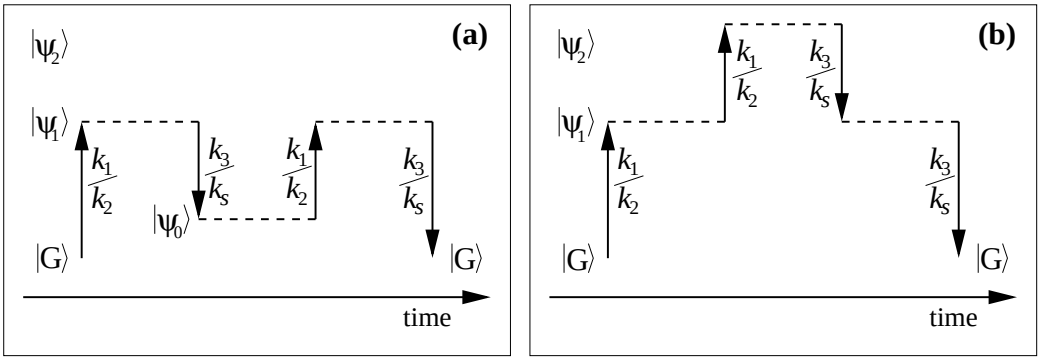


**Figure 3.3:** Photoexcitation of the (a) 0–$h$ ($|\psi_0\rangle$), and (b) 2–$h$ ($|\psi_2\rangle$) states via the nonlinear optical processes that contribute to the FWM signal. To third order in the optical fields, the emission of a $\mathbf{k}_s$ photon in the FWM direction $\mathbf{k}_s = \mathbf{k}_1 + \mathbf{k}_2 - \mathbf{k}_3$ is determined by the excitation of one $e$–$h$ by pulse $\mathbf{k}_1$, the excitation of one $e$–$h$ pair by pulse $\mathbf{k}_2$ and the deexcitation of one $e$–$h$ pair by the optical field $\mathbf{k}_3$. Although in a coherent FWM experiment the nonlinear excitation process must begin and end with the ground state $|G\rangle$, the intermediate 0–$h$ state $|\psi_0\rangle$ does not need to be the ground state and may contain excitations of the 2DEG.

with initial condition $|\psi_n(-\infty)\rangle = \delta_{n,0}|G\rangle$. The Hamiltonian $H$ includes the degrees of freedom which lead to dephasing. The physics of the above equations is clearly displayed: $|\psi_0\rangle$ is coupled to $|\psi_1\rangle$ by the destruction of one $e$–$h$ pair, $|\psi_1\rangle$ is coupled to $|\psi_0\rangle$ by the creation of one $e$–$h$ pair and to $|\psi_2\rangle$ by the destruction of one $e$–$h$ pair, and $|\psi_2\rangle$ is coupled to $|\psi_1\rangle$ by the creation of one $e$–$h$ pair. Fig. 3.3 shows the optical transitions that determine the FWM signal up to third order in the optical field. It is worth noting that one can extend Eqs. (3.45), (3.46) and (3.47) to treat higher order nonlinear processes by retaining states with higher hole numbers in the expansion Eq. (3.44).

### 3.5.1 Linear response

To lowest order in the optical field, only the 1–$h$ state $|\psi_1\rangle$ is photoexcited. We separate out the magnetoexciton contribution to this state by introducing the decomposition

$$|\psi_{1L}\rangle = \sum_n \frac{P_n^L}{1-\nu_n}|X_n\rangle + |\bar{\psi}_{1L}\rangle \tag{3.48}$$

where $|\bar{\psi}_{1L}\rangle$ is the $\{1\text{-}h/2\text{DEG}^*\}$ contribution, defined by the requirement $\langle X_n|\bar{\psi}_1\rangle = 0$, that describes the incoherent contributions due to the X–2DEG

interactions. The exciton amplitude

$$P_n^L = \langle X_n|\psi_{1L}\rangle \tag{3.49}$$

coincides with the linear polarization, whose equation of motion is obtained by linearizing Eq. (3.35):

$$i\partial_t P_n^L = (\Omega_n - i\Gamma_n)P_n^L - (1-\nu_n)\sum_{m\neq n} V_{nm}P_m^L - d(t)(1-\nu_n) + \bar{P}_n^L \tag{3.50}$$

where we introduced an exciton dephasing rate $\Gamma_n$. The amplitude

$$\bar{P}_n^L = \langle \hat{Y}_n\rangle_L = \langle Y_n|\psi_{1L}\rangle = \langle Y_n|\bar{\psi}_{1L}\rangle \tag{3.51}$$

describes the time evolution of the X+MP states that contribute to $|Y_n\rangle$ and corresponds to a X+MP coherence, analogous to the X+phonon coherence in undoped semiconductors [5, 7].

By substituting Eq. (3.48) in Eq. (3.46), using Eqs. (3.50) and (3.22), and noting that up to first order in the optical field $|\psi_0\rangle = |G\rangle$ and $|\psi_2\rangle$ does not contribute, we obtain the equation of motion for $|\bar{\psi}_{1L}\rangle$:

$$i\partial_t|\bar{\psi}_{1L}\rangle - H|\bar{\psi}_{1L}\rangle = \sum_n \frac{1}{1-\nu_n}\left[P_n^L|Y_n\rangle - \bar{P}_n^L|X_n\rangle\right] \tag{3.52}$$

The first term in the rhs of the above equation describes the scattering of $X_n$ with the 2DEG, while the second term is responsible for the dephasing of $P_n^L$.

If we restrict to the LL0 and LL1 states, Eq. (3.30) applies and thus

$$\bar{P}_1^L = -\bar{P}_0^L = \bar{P}^L \tag{3.53}$$

To obtain the equation of motion for $\bar{P}^L$, a basis of X+MP states must be introduced. A simple basis can be created by considering the action of the Hamiltonian on the state $|Y\rangle$ introduced in §3.3. Similar to Eq. (3.22) that defines the latter state, we introduce a new state $|Z\rangle$ orthogonal to all the $|X_n\rangle$ states as well as to $|Y\rangle$ as follows [25]:

$$H|Y\rangle = \bar{\Omega}|Y\rangle + W\left(\frac{|X_1\rangle}{1-\nu_1} - \frac{|X_0\rangle}{1-\nu_0}\right) + |Z\rangle \tag{3.54}$$

where

$$\bar{\Omega} = \frac{\langle Y|H|Y\rangle}{\langle Y|Y\rangle} \quad \text{and} \quad W = \langle Y|Y\rangle \tag{3.55}$$

obtained by using the above orthogonality requirements and Eqs. (3.13), (3.22) and (3.30).

By substituting $\hat{O} = \hat{Y}$ in Eq. (3.34), keeping terms up to first order to the optical field and using Eq. (3.54), we obtain the equation of motion for $\bar{P}^L$:

$$i\partial_t \bar{P}^L = (\bar{\Omega} - i\gamma)\bar{P}^L + W\left(\frac{P_1^L}{1-\nu_1} - \frac{P_0^L}{1-\nu_0}\right) + Z^L \tag{3.56}$$

where $Z^L = \langle Z|\bar{\psi}_{1L}\rangle$ and $\gamma$ is the dephasing rate.

By continuing the above orthogonalization procedure, we create a Lanczos basis [8, 113] of strongly correlated orthogonal states $|Z^{(n)}\rangle$, where $|Z^{(0)}\rangle = |Y\rangle$ and $|Z^{(1)}\rangle = |Z\rangle$, from the recursive relation obtained by acting with the Hamiltonian $H$ on the previous state, and then orthogonalizing the result with respect to all the existing basis states [25, 113]:

$$H|Z^{(n)}\rangle = \bar{\Omega}^{(n)}|Z^{(n)}\rangle + W^{(n)}|Z^{(n-1)}\rangle + |Z^{(n+1)}\rangle \tag{3.57}$$

where

$$\bar{\Omega}^{(n)} = \frac{\langle Z^{(n)}|H|Z^{(n)}\rangle}{\langle Z^{(n)}|Z^{(n)}\rangle}\ ,\ W^{(n)} = \frac{\langle Z^{(n)}|Z^{(n)}\rangle}{\langle Z^{(n-1)}|Z^{(n-1)}\rangle}. \tag{3.58}$$

By substituting $\hat{O} = \hat{Z}^{(n)}$ in Eq. (3.34) and keeping terms up to first order to the optical field we obtain the equations of motion for the coherences $Z^{(n)L} = \langle Z^{(n)}|\bar{\psi}_{1L}\rangle$:

$$i\partial_t Z^{(n)L} = \left(\bar{\Omega}^{(n)} - i\gamma_n\right) Z^{(n)L} + W^{(n)} Z^{(n-1)L} + Z^{(n+1)L} \tag{3.59}$$

As discussed in [25], by taking the Fourier transform of the above system of equations, we can obtain a continued fraction expansion of the polarization, which describes a non–Markovian dephasing. This approach is analogous to the numerical calculations of the 2DEG dynamical structure factor [21, 49]. The above hierarchy can be truncated when convergence is reached, which becomes more rapid with increasing damping rates or, in the case of an $N$–electron system, after performing $N$ iterations. In the quantum Hall effect literature, numerical calculations of the $N$–electron spectral functions have been shown to extrapolate to the $N \to \infty$ limit for a relatively small $N$ [21, 105]. Compared to an expansion in terms of non–interacting X+MP states, as in Eq. (3.27), the correlated Lanczos states are advantageous when the different momentum contributions are strongly coupled, or for obtaining a simple solution such as the average polarization model discussed in §4.3.

### Linear Absorption Spectrum

By retaining only the $|X_0\rangle$, $|X_1\rangle$, and $|Y\rangle$ states, and using Eqs. (3.50) and (3.56), we can calculate the linear absorption spectrum. In Chapter 6, we

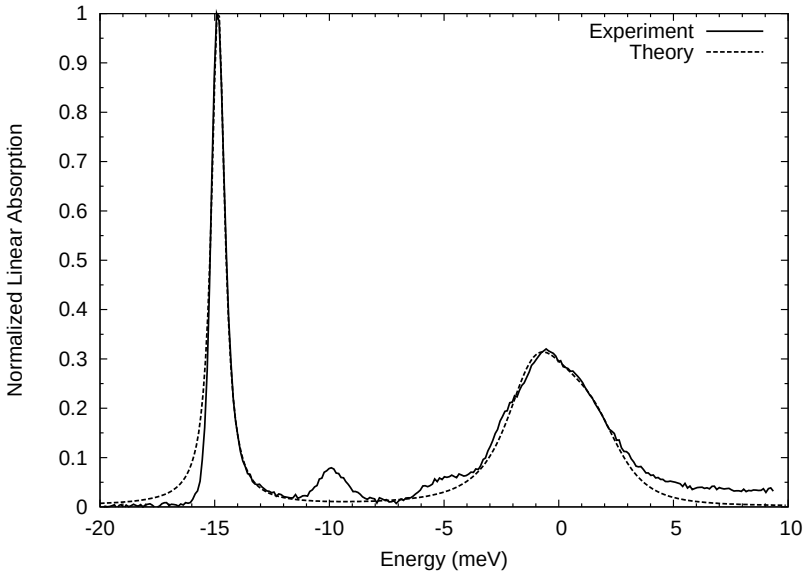


**Figure 3.4:** Normalized linear absorption spectrum of the quantum Hall system at $B = 7$ T. The zero of energy was taken to be at $\omega = \Omega_1$. Solid line: experiment [52]. Dashed line: theoretical calculation by retaining the $|X_0\rangle$, $|X_1\rangle$, and $|Y\rangle$ states and with parameters chosen to fit the experiment: $\Omega_0 - \Omega_1 = 14.3$ meV, $\Gamma_0 = \Gamma_1 = 0.28$ meV, $V_{01} = V_{10} = 2.3$ meV, $\bar{\Omega} - \Omega_1 = 0.1$ meV, $\gamma = 3.5$ meV, $\sqrt{W} = 2$ meV, $\nu_0 = 0.34$, $\nu_1 = 0$. The small peak at $-10$ meV in the experiment is due to the light–hole band, which is not taken into account in our theoretical model.

will discuss our exact calculation for $\nu = 1$, where we retain the $|X_0\rangle$, $|X_1\rangle$, and $\hat{X}^\dagger_{\mathbf{q}01}\hat{\rho}^e_{-\mathbf{q}10\uparrow}|G\rangle$ states and calculate all energies and couplings. Here, we use parameters that fit the experimental data. Our results do not depend on their precise value. Fig. 3.4 shows the calculated spectrum in comparison with the experiment for $B = 7$ T. The effect of the higher Lanczos states, which describe the "bath" that leads to exciton dephasing and do not couple directly to the exciton, is taken into account by introducing the dephasing rate $\gamma$ of $\bar{P}^L$ that describes the coupling between the exciton and the "bath". This dephasing is due to X+MP scattering (see Eq. (3.27)) and the emission of other 2DEG excitations.

Noting the analogy between a MP and an X, one can make an analogy between the X–MP scattering described by Eq. (3.27) and the X–X scattering in undoped semiconductors. As shown in [111], in the case of magnetoexcitons the latter can be described by a dephasing rate for strong X–X interactions and leads to the average polarization model [3, 91, 111]. The main feature

in Fig. 3.4 is the strong LL1 broadening and asymmetric lineshape, which is due to $\bar{P}^L$ and cannot be obtained by introducing a polarization dephasing time. Even though the time evolution of the X+MP states, described by $\bar{P}^L$, determines the lineshape of the LL1 peak, it only plays a small role at the LL0 frequency. To interpret this difference we note that, as can be seen by using Eq. (3.32) to calculate the state $|Y\rangle$, the main contribution to $\bar{P}^L$ comes from $\{1\text{–MP} + 1\text{–LL0–}e + 1\text{–LL1–}h\}$ four–particle excitations, while all other contributions are non-resonant with the LL0 and LL1 excitons. Even though $\bar{P}^L$ couples equally to both X amplitudes $P_0^L$ and $P_1^L$, it dominates the dephasing of $P_1^L$ since the above four–particle states have energy comparable to that of $X_1$ in the case of an inter–LL MP. In contrast, $X_0$ has significantly smaller energy, and thus the inter–LL MP plays a minor role in the broadening of the LL0 exciton peak.

### 3.5.2 Second order processes

In this section we consider the two–photon nonlinear optical processes that lead to the photoexcitation of the 2–$h$ state $|\psi_2\rangle$ and the 0–$h$ state $|\psi_0\rangle$. By separating out the contribution of the states $|X_nX_m\rangle = \hat{X}_n^\dagger \hat{X}_m^\dagger |G\rangle$, which describe a pair of non-interacting Xs, and $\hat{X}_n^\dagger|\bar{\psi}_{1L}\rangle$, which describes a non-interacting pair of X and X+MP 1–$h$ states, we arrive at the decomposition to $O(E^4)$

$$|\psi_2\rangle = \frac{1}{2}\sum_{nm}\frac{P_n^L P_m^L}{(1-\nu_n)(1-\nu_m)}|X_nX_m\rangle + \sum_n \frac{P_n^L}{1-\nu_n}\hat{X}_n^\dagger|\bar{\psi}_{1L}\rangle + |\bar{\psi}_2\rangle \quad (3.60)$$

where $|\bar{\psi}_2\rangle$ describes the correlated X–X and X–X+MP contributions and satisfies the equation of motion

$$\begin{aligned} i\partial_t|\bar{\psi}_2\rangle - H|\bar{\psi}_2\rangle =& \frac{1}{2}\sum_{nm}\frac{P_n^L P_m^L}{(1-\nu_n)(1-\nu_m)}[\hat{Y}_n^\dagger, \hat{X}_m^\dagger]|G\rangle \\ &+ \sum_n \frac{1}{1-\nu_n}\left[P_n^L\hat{Y}_n^\dagger - \bar{P}_n^L\hat{X}_n^\dagger\right]|\bar{\psi}_1\rangle \end{aligned} \quad (3.61)$$

obtained by substituting Eq. (3.60) into Eq. (3.47) and using Eqs. (3.50), (3.52) and (3.22). We note that, in the above equation of motion, there are no terms proportional to $d(t)$ and therefore the decomposition Eq. (3.60) eliminates all contributions to $|\psi_2\rangle$ that are proportional to the excitonic amplitudes $P_n^L$ (whose time derivative is proportional to $d(t)$).

In addition to the photoexcitation of the above 2–$h$ many–body state, the two–photon process of excitation of a 1–$h$ state and then de-excitation

of an $e$–$h$ pair (possibly accompanied by the scattering of 2DEG excitations) leads to a second order contribution to the 0–$h$ state $|\psi_0\rangle$. We split the latter state into the contribution of the ground state $|G\rangle$, with amplitude $\langle G|\psi\rangle$, where the 2DEG is not excited during the excitation–deexcitation process, and the photoexcited $\{0\text{–}h/2\text{DEG}^*\}$ contribution. We further decompose the latter contribution into an uncorrelated part $\propto \hat{X}_n|\bar{\psi}_{1L}\rangle$, where the deexcited exciton $\hat{X}_n$ does not interact with the $|\bar{\psi}_{1L}\rangle$ carriers, and a correlated contribution $|\bar{\psi}_0\rangle$:

$$|\psi_0\rangle = \langle G|\psi\rangle|G\rangle - \sum_n \frac{P_n^{L*}}{1-\nu_n}\hat{X}_n|\bar{\psi}_{1L}\rangle + |\bar{\psi}_0\rangle + O(E^4) \tag{3.62}$$

where the 2DEG$^*$ state $|\bar{\psi}_0\rangle$ is orthogonal to the ground state, $\langle G|\bar{\psi}_0\rangle = 0$, and up to second order in the optical field satisfies the equation of motion

$$\begin{aligned} i\partial_t|\bar{\psi}_0\rangle - H|\bar{\psi}_0\rangle = &\sum_{nm}\frac{P_n^{L*}P_m^L}{(1-\nu_n)(1-\nu_m)}\hat{X}_n|Y_m\rangle + \sum_n \frac{P_n^{L*}\hat{Y}_n - \bar{P}_n^{L*}\hat{X}_n}{1-\nu_n}|\bar{\psi}_{1L}\rangle \\ &- \sum_{nm}\frac{P_n^{L*}\bar{P}_m^L}{(1-\nu_n)(1-\nu_m)}\hat{X}_n|X_m\rangle + d^*(t)\ \sum_n \frac{P_n^L}{1-\nu_n}\Delta\hat{\nu}_n|G\rangle \end{aligned} \tag{3.63}$$

obtained by substituting Eq. (3.62) into Eq. (3.45) and using Eqs. (3.50), (3.52) and (3.22).

The first term in Eq. (3.63) describes the photo–excitation of the 2DEG via the second–order interaction–assisted process where the exciton $\mathrm{X}_m$, photo–excited with amplitude $P_m^L$, scatters with the 2DEG into the state $|Y_m\rangle$, and then the exciton $\mathrm{X}_n$ is deexcited with amplitude $P_n^L$. The above process leaves the system in a 2DEG$^*$ 0–$h$ state. It is analogous to the photo–excitation of coherent phonons in undoped semiconductors, and dominates the inelastic light scattering spectra of the 2DEG [20, 70]. The second term on the rhs of Eq. (3.63) describes the scattering of $\mathrm{X}_n$ with the carriers in $|\bar{\psi}_1\rangle$ during its de–excitation. The rest of the terms describe the possibility to create 2DEG excitations by photoexciting an exciton whose hole then recombines with a 2DEG electron (Raman process). In the case of the spin–$\uparrow$ polarized 2DEG and right–circularly polarized light, the latter Raman process vanishes since there are no spin–$\downarrow$ electrons in the ground state.

In the following we use the above decompositions of the photoexcited many–body wavefunction $|\psi\rangle$, Eqs. (3.48), (3.60) and (3.62), in order to describe the interaction–induced contributions to Eqs. (3.35) and (3.38). These decompositions provide a way of separating out the uncorrelated from the correlated parts in a general correlated system, where a Hartree–Fock non–interacting state may not be an appropriate reference state as in undoped

semiconductors. This separation also motivates a factorization of the corresponding density matrices that applies not only to undoped semiconductors, but also to systems with strongly correlated ground states, where Wick's theorem does not apply. Similar to the DCTS, our method provides a systematic way of identifying the parts that can be factorized and the new intraband dynamical variables that cannot be expressed in terms of interband coherences due to the incoherent processes. Importantly, it allows us to treat both coherent and incoherent processes in strongly correlated systems, where the coupling between the photoexcited carriers and the "bath" (here the 2DEG) leads to new dynamics governed by slow/low energy "bath" collective excitations. Finally, our method raises the possibility of devising new approximations, obtained by projecting the many–body wavefunctions in an appropriate basis of strongly correlated states or operators, and then using this expansion to evaluate the correlated contributions to the density matrices.

### 3.5.3 Intraband density matrix

In this section we turn to the equation of motion for the density matrix $\langle\hat{M}\rangle$, where $\hat{M}$ is any intraband operator that does not change the number of holes. Furthermore, we assume that $\langle G|\hat{M}|G\rangle = 0$, as is the case for the operator $\hat{M}_n = [\hat{Y}_n, \hat{X}_n^\dagger]$ discussed in §3.4.

Substituting the decomposition of the many–body state $|\psi\rangle$, Eq. (3.44), together with Eqs. (3.48), (3.60) and (3.62), and keeping terms up to second order in the optical field, we obtain for the average value $\langle\psi|\hat{M}|\psi\rangle$:

$$\begin{aligned}\langle\hat{M}\rangle = \langle\hat{M}\rangle_c &+ \sum_{nm} \frac{P_n^{L*} P_m^L}{(1-\nu_n)(1-\nu_m)} \langle X_n|\hat{M}|X_m\rangle \\ &+ \sum_n \frac{P_n^{L*}}{1-\nu_n} \langle G|[\hat{X}_n, \hat{M}]|\bar{\psi}_{1L}\rangle + \sum_n \frac{P_n^L}{1-\nu_n} \langle\bar{\psi}_{1L}|[\hat{M}, \hat{X}_n^\dagger]|G\rangle \quad (3.64)\end{aligned}$$

where $\langle\hat{M}\rangle_c$ is the correlated contribution, given by

$$\langle\hat{M}\rangle_c = \langle G|\hat{M}|\bar{\psi}_0\rangle + \langle\bar{\psi}_0|\hat{M}|G\rangle + \langle\bar{\psi}_{1L}|\hat{M}|\bar{\psi}_{1L}\rangle. \quad (3.65)$$

This above result corresponds to an intraband density matrix decomposition into a factorizable part and a correlated part $\langle\hat{M}\rangle_c$. The second term on the rhs of Eq. (3.64) is the coherent contribution, which similar to the undoped system can be expressed as a product of exciton polarizations, while the rest of the terms describe the incoherent contributions and 2DEG photoexcitation

processes. This decomposition corresponds to a projection of the exciton states $|X_n\rangle$.

We can obtain the equation of motion for $\langle\hat{M}\rangle_c$ by substituting the decomposition of $\langle\hat{M}\rangle$, Eq. (3.64) in Eq. (3.34) and using Eqs. (3.35) and (3.52):

$$
\begin{aligned}
&i\partial_t\langle\hat{M}\rangle_c - \langle[\hat{M},H]\rangle_c + i\gamma_M\langle\hat{M}\rangle_c = \sum_{nm}\frac{P_n^{L*}P_m^L}{(1-\nu_n)(1-\nu_m)} \\
&\times\left[i(\Gamma_n+\Gamma_m-\gamma_M)\langle X_n|\hat{M}|X_m\rangle + \langle Y_n|\hat{X}_m^\dagger\hat{M}|G\rangle - \langle G|\hat{M}\hat{X}_n|Y_m\rangle\right] \\
&+\sum_n\frac{i(\Gamma_n+\gamma-\gamma_M)}{1-\nu_n}\left[P_n^L\langle\bar{\psi}_{1L}|[\hat{M},\hat{X}_n^\dagger]|G\rangle + P_n^{L*}\langle G|[\hat{X}_n,\hat{M}]|\bar{\psi}_{1L}\rangle\right] \\
&+\sum_{nm}\frac{P_n^L\bar{P}_m^{L*}}{(1-\nu_n)(1-\nu_m)}\langle X_m|\hat{X}_n^\dagger\hat{M}|G\rangle - \sum_{nm}\frac{\bar{P}_n^L P_m^{L*}}{(1-\nu_n)(1-\nu_m)}\langle G|\hat{M}\hat{X}_m|X_n\rangle \\
&+\sum_n\frac{P_n^L}{1-\nu_n}\langle\bar{\psi}_{1L}|[\hat{M},\hat{Y}_n^\dagger]|G\rangle + \sum_n\frac{P_n^{L*}}{1-\nu_n}\langle G|[\hat{M},\hat{Y}_n]|\bar{\psi}_{1L}\rangle \\
&+\sum_n\frac{\bar{P}_n^{L*}}{1-\nu_n}\langle G|[\hat{X}_n,\hat{M}]|\bar{\psi}_{1L}\rangle + \sum_n\frac{\bar{P}_n^L}{1-\nu_n}\langle\bar{\psi}_{1L}|[\hat{X}_n^\dagger,\hat{M}]|G\rangle \\
&+\sum_{nm}\frac{d(t)P_m^{L*}}{1-\nu_m}\langle G|[\hat{X}_m,\hat{X}_n^\dagger]\hat{M}|G\rangle - \sum_{nm}\frac{d^*(t)P_m^L}{1-\nu_m}\langle G|\hat{M}[\hat{X}_n,\hat{X}_m^\dagger]|G\rangle
\end{aligned}
\tag{3.66}
$$

where we introduced a new dephasing rate $\gamma_M$ for the correlated contribution $\langle\hat{M}\rangle_c$, since it has its own dynamics that cannot be described by the polarization dephasing.

The above equation of motion applies for any intraband operator $\hat{M}$, for which $\langle G|\hat{M}|G\rangle = 0$, such as the operators that contribute to Eq. (3.40). It includes contributions due to the possible photoexcitation of a 2DEG coherence associated with the 2DEG$^*$ state $\hat{M}|G\rangle$, as well as due to deviations from the factorization Eq. (3.64), induced by incoherent processes that involve the photoexcited carriers. The intraband density matrix $\langle\hat{M}_n\rangle$, defined in Eq. (3.39), can be calculated either by direct use of Eqs. (3.64) and (3.66), or by expanding $\hat{M}_n$ in the strongly correlated basis $|X_m\rangle\langle X_n|$, $|X_m\rangle\langle Z^{(n)}|$ and $|Z^{(m)}\rangle\langle Z^{(n)}|$ and write equations of motion for the corresponding density matrices.

By substituting $\hat{M} = |X_m\rangle\langle X_n|$ in Eq. (3.64), we seperate the coherent contribution in the X populations (for $n = m$) and X$\leftrightarrow$X coherences (for $n \neq m$) from the correlated one:

$$
\langle|X_m\rangle\langle X_n|\rangle = P_n^L P_m^{L*} + \langle|X_m\rangle\langle X_n|\rangle_c \tag{3.67}
$$

The equation of motion of the latter is easily obtained by using Eqs. (3.66) and (3.22) and taking into account that $\langle X_n|\bar{\psi}_{1L}\rangle = 0$:

$$\begin{aligned} i\partial_t\langle|X_m\rangle\langle X_n|\rangle_c &= (\Omega_n - \Omega_m - i\Gamma_{nm})\,\langle|X_m\rangle\langle X_n|\rangle_c \\ &+ (1-\nu_m)\sum_{m'\neq m} V_{m'm}\langle|X_{m'}\rangle\langle X_n|\rangle_c - (1-\nu_n)\sum_{n'\neq n} V_{nn'}\langle|X_m\rangle\langle X_{n'}|\rangle_c \\ &+ i(\Gamma_n + \Gamma_m - \Gamma_{nm})P_n^L P_m^{L*} + \langle|X_m\rangle\langle Y_n|\rangle_c - \langle|X_n\rangle\langle Y_m|\rangle_c^* \end{aligned} \tag{3.68}$$

As can be seen from the above equation, incoherent X populations and X↔X coherences can be photoexcited due to (i) the difference between the intraband relaxation rate $\Gamma_{nm}$ and the sum of the exciton dephasing rates $\Gamma_n+\Gamma_m$, and (ii) the coupling between the X and X+MP states described by the last two terms on the rhs. The former is the only source in the undoped system, while the latter X↔X+MP coupling dominates in the doped system and is described by the equation of motion

$$\begin{aligned} i\partial_t\langle|X_n\rangle\langle Y|\rangle_c &= \left(\bar{\Omega} - \Omega_n - i\gamma_n\right)\langle|X_n\rangle\langle Y|\rangle_c + i(\Gamma_n + \gamma - \gamma_n)P_n^{L*}\bar{P}^L \\ &+ W\left[\frac{\langle|X_n\rangle\langle X_1|\rangle_c}{1-\nu_1} - \frac{\langle|X_n\rangle\langle X_0|\rangle_c}{1-\nu_0}\right] + (1-\nu_n)\sum_{m\neq n} V_{mn}\langle|X_m\rangle\langle Y|\rangle_c \\ &+ (\delta_{n1} - \delta_{n0})\left(\bar{P}^{L*}\bar{P}^L - \langle|Y\rangle\langle Y|\rangle_c\right) + \langle|X_n\rangle\langle Z|\rangle_c \end{aligned} \tag{3.69}$$

### 3.5.4 Interband density matrix

We now consider the equation of motion for the density matrix $\langle\hat{Y}\rangle$, where $\hat{Y}$ is any interband operator that creates an $e$–$h$ pair with the simultaneous scattering of any number of other electrons or holes (e.g. the operator $\hat{Y}_n^{\rm int}$ defined in Eq. (3.27)). By using the decomposition of the photoexcited many–body state $|\psi\rangle$ and keeping terms up to third order in the optical field, we obtain after some algebra the following decomposition of the interband density matrix $\langle\hat{Y}\rangle$ into correlated and uncorrelated contributions [25]:

$$\begin{aligned} \langle\hat{Y}\rangle = &\sum_n \frac{P_n^{L*}}{1-\nu_n}\langle G|[\hat{X}_n,\hat{Y}]|\psi_2\rangle + \sum_n \frac{P_n^L}{1-\nu_n}\langle[\hat{Y},\hat{X}_n^\dagger]\rangle_c \\ &+ \frac{1}{2}\sum_{nm}\frac{P_n^L P_m^L}{(1-\nu_n)(1-\nu_m)}\langle\bar{\psi}_{1L}|[[\hat{Y},\hat{X}_n^\dagger],\hat{X}_m^\dagger]|G\rangle + \langle\hat{Y}\rangle_c \end{aligned} \tag{3.70}$$

where

$$\langle\hat{Y}\rangle_c = \langle\psi|G\rangle\bar{P}^L + \langle Y|\bar{\psi}_{1NL}\rangle + \langle\bar{\psi}_0|\hat{Y}|\bar{\psi}_{1L}\rangle + \langle\bar{\psi}_{1L}|\hat{Y}|\bar{\psi}_2\rangle \tag{3.71}$$

and we introduced the nonlinear 1–$h$ state

$$|\bar{\psi}_{1NL}\rangle = |\psi_1\rangle - |\psi_{1L}\rangle + \sum_n \frac{P_n^{L*}}{1-\nu_n}\hat{X}_n|\psi_2\rangle - \sum_n \frac{P_n^{L}}{1-\nu_n}\hat{X}_n^\dagger|\bar{\psi}_0\rangle \qquad (3.72)$$

The first term on the rhs of Eq. (3.70) describes the coherent X–X interaction and correlation effects analogous to the undoped system, discussed in the following section. The second term describes the contribution due to the interaction of the optical polarization with the correlated intraband contributions, i.e. the intraband coherences and incoherent populations discussed above. The above two terms treat the effects of coherent X–X interactions and the intraband excitation and incoherent population processes. The third term in Eq. (3.70) describes X–X interactions accompanied by the shake–up of 2DEG excitations, while the last term describes the correlated contribution to the nonlinear polarization. As can be seen from Eq. (3.71), the dynamics of the first two terms of the latter contribution is governed by the dephasing of the X+MP state $|Y\rangle$ while the last two nonlinear terms are determined by the $\{1\text{-}h/2\text{DEG}^*\}$ state $|\bar{\psi}_{1L}\rangle$ and describe incoherent correlated interband contributions. The equation of motion for $\langle\hat{Y}\rangle_c$ can be obtained as above and describes the X dephasing.

## 3.6 Coherent X–X correlations

In this section we make the connection between the above result for the coherent X–X interaction contribution to the nonlinear polarization (first term on the rhs of Eq. (3.70)), described by the amplitude of the 2–$h$ state $\langle G|[\hat{X}_n,\hat{Y}]|\psi_2\rangle = \langle[\hat{X}_n,\hat{Y}]\rangle + O(E^5)$, and the familiar expressions that describe X–X correlations in undoped semiconductors [5, 6]. Using Eq. (3.32) and restricting to the first two LLs, we obtain for $\hat{B} = [\hat{X}_1,\hat{Y}] = -[\hat{X}_0,\hat{Y}]$

$$\begin{aligned}\hat{B} =& \sum_{\mathbf{q}} \frac{v_q}{L^2}\Big[\phi_{01}(-\mathbf{q})\hat{X}_{-\mathbf{q}01} - \phi_{10}(-\mathbf{q})\hat{X}_{-\mathbf{q}10}\Big]\Big[\phi_{01}(\mathbf{q})\hat{X}_{\mathbf{q}01} - \phi_{10}(\mathbf{q})\hat{X}_{\mathbf{q}10}\Big] \\ =& \sum_{\mathbf{q}} \frac{v_q}{L^2}\Big[\phi_{01}(-\mathbf{q})\phi_{01}(\mathbf{q})\hat{X}_{-\mathbf{q}01}\hat{X}_{\mathbf{q}01} + \phi_{10}(-\mathbf{q})\phi_{10}(\mathbf{q})\hat{X}_{-\mathbf{q}10}\hat{X}_{\mathbf{q}10} \\ & -2|\phi_{10}(\mathbf{q})|^2\hat{X}_{-\mathbf{q}01}\hat{X}_{\mathbf{q}10}\Big] = \hat{B}_{01}^{01} + \hat{B}_{10}^{10} + \hat{B}_{10}^{01} \end{aligned} \qquad (3.73)$$

where $\hat{B}_{nm}^{n'm'\dagger}|G\rangle$ describes the 4–particle state $\{1\text{–LL}n'\text{–}e + 1\text{–LL}m'\text{–}h + 1\text{–LL}n\text{–}e + 1\text{–LL}m\text{–}h\}$. As can be seen from the above equation, the coherent X–X interactions are determined by 2–X density matrices of the form

$\langle \hat{X}_n \hat{X}_m \rangle$, similar to the undoped system, where $n$, $m$ describe excitons with finite total momentum. Using the decomposition Eq. (3.60) we obtain for any 2–h state $|B\rangle$ (e.g. the states $[\hat{Y}^\dagger, \hat{X}_n^\dagger]|G\rangle$ that determine the coherent X–X contribution to the nonlinear polarization)

$$\langle B|\psi_2\rangle = \frac{1}{2}\sum_{nm} \frac{\langle B|X_n X_m\rangle P_n^L\ P_m^L}{(1-\nu_n)(1-\nu_m)} + \sum_n \frac{P_n^L}{1-\nu_n}\langle B|\hat{X}_n^\dagger|\bar{\psi}_{1L}\rangle + B_c \quad (3.74)$$

where $B_c = \langle B|\bar{\psi}_2\rangle$ describes the X–X and X–X+MP correlations. The first term in the above equation describes the familiar Hartree–Fock X–X interactions, while the second term describes the analogous interactions between the exciton $\hat{X}_n$ and the $\{1\text{–}h/2\text{DEG}^*\}$ state $|\bar{\psi}_{1L}\rangle$. By using Eq. (3.73) for $\hat{B}$ to calculate the overlap $\langle G|\hat{B}|X_n X_m\rangle$ and taking into account that the 2DEG populates only LL0 (i.e. $\nu < 2$),

$$\langle B|\psi_2\rangle = \frac{2V_{10}}{N} P_0^L P_1^L + \sum_n \frac{P_n^L}{1-\nu_n}\langle B|\hat{X}_n^\dagger|\bar{\psi}_{1L}\rangle + B_{01}^{01} + B_{10}^{10} + B_{10}^{01} \quad (3.75)$$

where $B_{nm}^{n'm'} = \langle B_{nm}^{n'm'}|\bar{\psi}_2\rangle$. In the X–phonon system, $\langle G|\hat{B}\hat{X}_n^\dagger|\bar{\psi}_{1L}\rangle = 0$, and thus we reproduce the results obtained in [5, 6] for the undoped system by using the cumulants.

We now turn to the equation of motion for the correlated X–X amplitude $B_c$. By projecting the state $\langle B|$ to Eq. (3.61), restricting to the LL0 and LL1 states, and using Eq. (3.30) we obtain that

$$\begin{aligned} i\partial_t B_c = \langle B|H|\bar{\psi}_2\rangle + \frac{\langle B|\hat{B}^\dagger|G\rangle}{2}\left(\frac{P_1^L}{1-\nu_1} - \frac{P_0^L}{1-\nu_0}\right)^2 \\ + \left(\frac{P_1^L}{1-\nu_1} - \frac{P_0^L}{1-\nu_0}\right)\langle B|\hat{Y}^\dagger|\bar{\psi}_{1L}\rangle - \left[\frac{\langle B|\hat{X}_1^\dagger|\bar{\psi}_{1L}\rangle}{1-\nu_1} - \frac{\langle B|\hat{X}_0^\dagger|\bar{\psi}_{1L}\rangle}{1-\nu_0}\right]\bar{P}^L \end{aligned} \quad (3.76)$$

By using the Lanczos recursive method [113], one can generate a basis of strongly correlated 2–$h$ states similar to §3.5.1. By describing the effects of the higher Lanczos states by introducing a dephasing rate we recover the average polarization model results used to describe X–X correlations and biexciton effects in undoped semiconductors [3, 91, 111]. Thus the Lanczos method can be used to derive such a model, which, in the case of 2D magnetoexcitons, was shown in [111] to be a good approximation in the case of attractive or strong repulsive X–X interactions with appropriate range. The Lanczos basis leads to a continued fraction expression of the X–X amplitude $B_c$, similar to the linear response of the 2DEG [25], and is advantageous in the case of strong coupling between the different X momentum states, e.g. due to an antibound continuum resonance or a bound biexciton [111].

## 3.7 Conclusions

In summary, we discussed a theory [46, 114] that can describe the ultrafast non-linear optical response of magnetoexcitons in both doped and undoped semiconductors, including systems with a strongly correlated many–electron ground state, like the quantum Hall system. We discussed a method for describing the interaction contributions to the density matrix equation of motion, which gives the third–order non-linear polarization measured in pumb–probe and FWM experiments.

Similar to the DCTS, we use an expansion in terms of the optical field in order to eliminate the number of independent dynamical variables that need to be considered. The X–2DEG correlations do not allow the complete factorization of the intraband density matrix into products of interband coherences. We thus use a decomposition of the photoexcited many–body wavefunction into correlated and uncorrelated contributions to obtain a factorization scheme for the density matrix. Our expansion in terms of the optical field is valid for sufficiently short pulses and/or weak excitation conditions, where the correlations are most pronounced. In undoped semiconductors, our approach reduces to the DCTS if phonons are included.

In the following chapter, we will apply our theory to the case of the photoexcitation of the quantum Hall system with three right–circularly polarized optical pulses and we will derive an average polarization model to describe the nonlinear optical dynamics of the system.

# Chapter 4

# Interband and intraband dynamics

## 4.1 Outline

In this chapter we will use the theory developed in Chapter 3 to derive an average polarization model and explain a recent three–pulse FWM experiment on a quantum Hall system, as well as on an undoped well for comparison [45]. In §4.2 we briefly describe the experiment and the experimental results. In the doped quantum well, a large off–resonant signal with striking oscillations is observed, which is not present in the undoped system. We will then present an average polarization model derived from the theory of Chapter 3, which we will use to calculate the FWM signal for the excitation conditions of the experiment. We will show that the signal along the $\Delta t_{13}$ axis gives us information about the dynamics of interband excitations of the system, while the signal along the $\Delta t_{12}$ axis accesses the dynamics of intraband coherences. We will also present simple analytical solutions of our model, which will give us an intuitive picture about the dominant physical mechanisms in the ultrafast dynamics of the quantum Hall system. Finally, we will present full numerical calculations of the FWM signal along both axes, which when compared with the experiment, will allow us to identify the trace of X–X+MP coherences and put an upper bound on their dephasing rate.

## 4.2 Experimental results

In this section we briefly describe one of the first experiments that studies the ultrafast dynamics of the quantum Hall system. These experiments motivated the present work, which will be used to interpret them.

In the experiment described in Refs. [45, 52], the quantum Hall system is excited with three 100 fs $\sigma_+$ circularly polarized pulses along directions $\mathbf{k}_1$, $\mathbf{k}_2$, and $\mathbf{k}_3$. Pulses $\mathbf{k}_1$ and $\mathbf{k}_2$ ($\mathbf{k}_3$) are separated by a time delay $\Delta t_{12}$ ($\Delta t_{13}$), where pulse $\mathbf{k}_1$ arrives first for negative values of the delay (see Fig. 2.6). The FWM response is obtained in the background–free direction $\mathbf{k}_1 + \mathbf{k}_2 - \mathbf{k}_3$. Using an interference filter, the signal is spectrally resolved so as to separate out the contribution from each Landau level and then the intensity from each Landau level is measured as a function of the time delays. In particular, measurements are taken along the $\Delta t_{12}$ axis ($\Delta t_{13} = 0$) and along the $\Delta t_{13}$ axis ($\Delta t_{12} = 0$).

The sample under investigation is a modulation–doped quantum well structure consisting of 10 periods of 12 nm GaAs wells and 42 nm AlGaAs barrier layers with Si doped at their centers. The doped carrier (2DEG) density is $2.1 \times 10^{11}$ cm$^{-2}$. The magnetic field is $B = 7$ T, which corresponds to filling factor $\nu = 1.3$, i.e. only the lowest Landau level (LL0) is occupied and the 2DEG is mostly spin–$\uparrow$ polarized. The temperature is maintained between 1.5–4 K. The frequency of the optical pulses is tuned such that LL1 is largely excited over LL0. For comparison, the FWM signal from a similar undoped quantum well (i.e. without a 2DEG) is measured. Low and high intensity measurements are also compared. For low intensity, the photo–excited carriers density ($5 \times 10^9$ cm$^{-2}$) is kept much smaller than the 2DEG density in order to weakly perturb the quantum Hall system. For high intensity, the two densities are comparable, so the photoexcited carrier contribution is strong. More details about the samples and the experimental setup can be found in Ref. [52].

### 4.2.1 Results along the $\Delta t_{13}$ axis

Fig. 4.1a shows the measured LL0 and LL1 FWM signals from the doped quantum well along the $\Delta t_{13}$ axis. The back panel shows the LL0 and LL1 peaks in the linear absorption spectrum (in yellow), and the optical pulse intensity (in red), centered on the LL1 peak. Fig. 4.1b shows the FWM signal from the undoped quantum well. A striking difference between the two responses is the large off-resonant signal from LL0 in the doped sample, despite the large LL1/LL0 excitation ratio. One would expect a strong signal from the states that are photo–excited, i.e. from LL1 in our case, which is exactly what we observe in the undoped sample.

Besides the unexpectedly large off–resonant signal, there exist other important differences in the LL0 signal as compared to the undoped sample. In the latter, one sees an asymmetric profile with oscillations at the inter–LL frequency. On the other hand, the LL0 signal from the doped sample

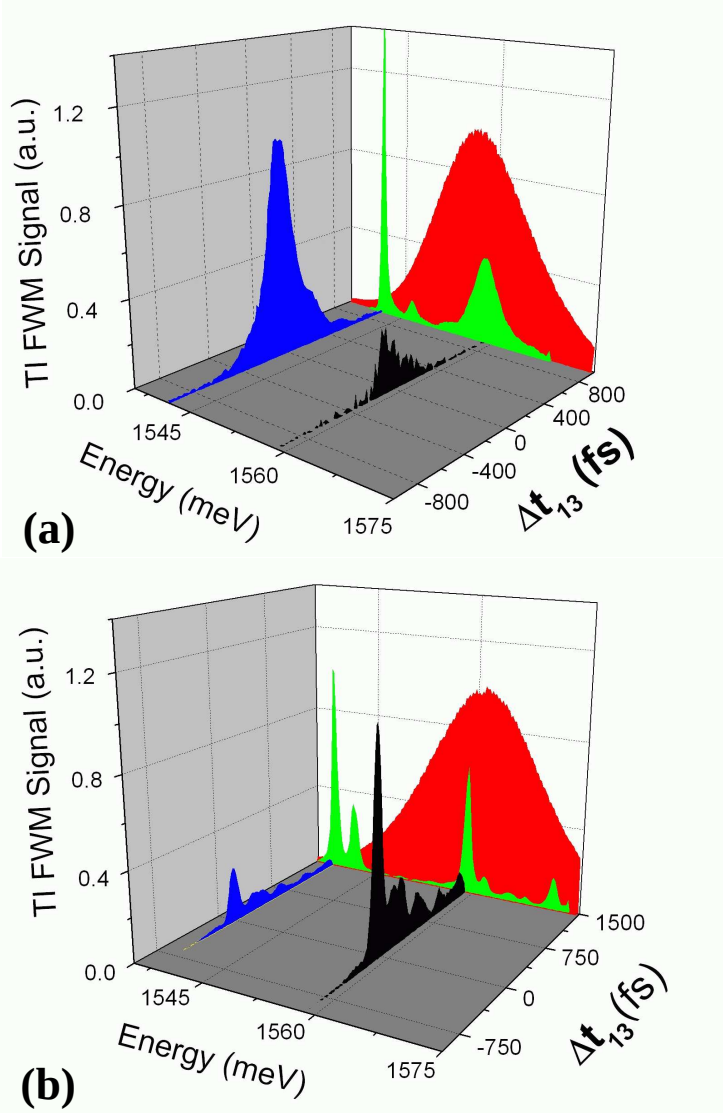


**Figure 4.1:** SR–FWM signal of the (a) doped and (b) undoped quantum well along the $\Delta t_{13}$ axis and for mostly LL1 excitation. The doped sample shows a large off–resonant signal from LL0, in contrast with the undoped well, and a symmetric profile contrary to the RPA theory. Back panel: Linear absorption spectrum and optical pulse intensity, showing the largely LL1 excitation conditions.

shows an unusually symmetric profile, in contrast with the RPA theory [38]. Moreover, there are no oscillations.

These differences between the LL0 signals from the doped and the undoped quantum wells indicate that the presence of the 2DEG in the former strongly affects the nonlinear response of the system. An easy test of this is to increase the ratio of photoexcited over ground state carriers by increasing the photoexcitation intensity. For low intensity, the number of the photo–excited carriers is much smaller than the number of the 2DEG carriers. Thus one is studying the quantum Hall system peturbatively. However, at large intensity, the number of photo–excited carriers becomes comparable or higher that that of the 2DEG, and consequently the nonlinear response will be mostly determined by the photo–induced carriers. Thus one expects that at large intensity the signal from the doped sample should be similar to the undoped system. Fig. 4.2 shows the profiles of the LL0 signals for low and high intensity for both the doped and the undoped samples. It is clear that at high intensity the differences between the two systems diminish.

Based on the above observations, we conclude that the off–resonant signal from LL0 is due to the presence of the 2DEG in the doped quantum well. We expect that the magnetoplasmon excitations of the 2DEG lead to a resonant coupling between the two Landau levels. This causes a transfer of oscillator strength from LL1 to LL0 which may give rise to a large off–resonant signal. In the following sections, we will use our theory to study this hypothesis. We will see that the creation of X–X+MP coherences lead to such coupling with the observed temporal profile, but before discussing the interpretation, we will summarize the experimental results along the $\Delta t_{12}$ axis.

### 4.2.2 Results along the $\Delta t_{12}$ axis

Fig. 4.3 shows the SR–FWM signal of the doped quantum well along the $\Delta t_{12}$ axis, for mostly LL1 photoexcitation. As in the case of the $\Delta t_{13}$ axis, there is a large off–resonant LL0 signal despite of largely exciting LL1. Moreover, this signal exhibits strong oscillations at the inter-LL exciton frequency. There are no oscillations in the LL1 signal. One would expect to observe oscillations at the inter-LL energy because of the interference of the LL0 and LL1 signals, but this cannot be the case here since the LL1 signal is much smaller than the LL0 one. Moreover, if this was true, the LL1 signal should also exhibit oscillations.

The LL0 oscillations are present for both positive and negative $\Delta t_{12}$ and decay symmetrically on both sides of the axis. As explained in Ref. [52], by subtracting a decaying exponential background from the $\Delta t_{12} > 0$ signal and then taking the Fourier transform, a single peak at $15.5 \pm 0.1$ meV with a

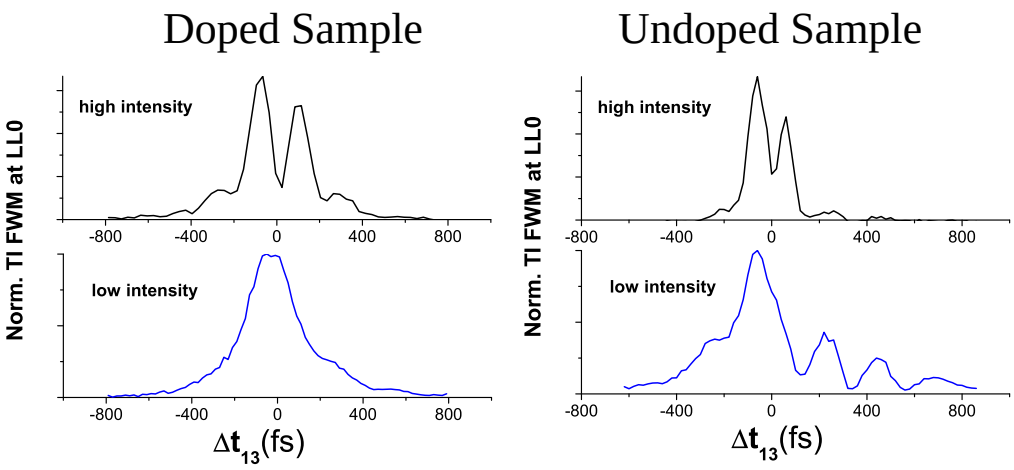


**Figure 4.2:** Photoexcitation intensity dependence of the LL0 signal from doped and undoped quantum wells. At low photoexcitation the doped signal shows the symmetric temporal profile. The undoped signal shows the standard RPA profile with oscillations. At high intensity, both signals look similar.

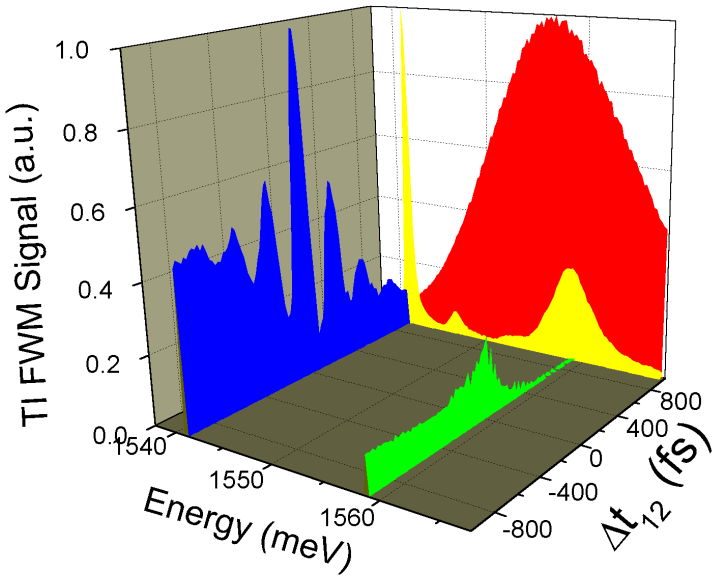


**Figure 4.3:** SR–FWM signal of the doped quantum well along the $\Delta t_{12}$ axis and for mostly LL1 excitation. The signal from LL0 exhibits oscillations that decay symmetrically about $\Delta t_{12} = 0$. Back panel: Linear absorption spectrum and optical pulse intensity, showing the largely LL1 excitation conditions.

linewidth of $6.8 \pm 0.5$ meV is obtained by fitting the peak with a Lorentzian. The linewidth of the peak gives an estimate of the decay of the oscillations. Similarly for the negative $\Delta t_{12}$ axis, a peak at $16.0 \pm 0.4$ meV with a linewidth of $7.8 \pm 1.0$ meV was obtained. From the nearly equal linewidths of the oscillations on both sides of the $\Delta t_{12}$ axis, we conclude that the oscillations decay symmetrically. This will be important later on, in order to identify the source of the oscillations. In the following section, we will present our average polarization model, derived from the theory of Chapter 3, which we will use to calculate the FWM signal and understand the above results.

## 4.3 Average Polarization Model

To derive a generalized average polarization model from the theoretical formulation of the previous chapter, we retain the $|X_0\rangle$, $|X_1\rangle$ and $|Y\rangle$ states and restrict to the photo–excited Landau levels, LL0 and LL1. We expand the intraband density matrix $\langle \hat{M}_n \rangle$, Eq. (3.40), on our basis consisting of the X–X coherences and densities $\langle |X_n\rangle\langle X_m| \rangle$ $(n, m = 0, 1)$, and the X–X+MP coherences $\langle |X_n\rangle\langle Y| \rangle$ $(n = 0, 1)$. We ignore the density matrix $\langle |Y\rangle\langle Y| \rangle$, since it describes X+MP–X+MP coherences and thus is expected to dephase quickly. By using this expansion in Eq. (3.70) for $\hat{Y}$ and keeping only the Hartree–Fock term of the X–X interactions (first term of Eq. (3.75)), we end up with the following equations of motion for the LL0 and LL1 polarizations:

$$
\begin{aligned}
&i\partial_t P_0 - (\Omega_0 - i\Gamma_0)P_0 + (1-\nu_0)V_{01}P_1 + \bar{P} = \\
&\quad = 2\mu E(t)\left(P_0^L P_0^{L*} + N_0\right) - 2V_{01}P_0^L P_1^L\left(\frac{P_1^{L*}}{1-\nu_1} - \frac{P_0^{L*}}{1-\nu_0}\right) \\
&\qquad - 2V_{01}\left[\frac{P_0^L}{1-\nu_1}\left(\frac{N_1}{1-\nu_1} - \frac{N_{10}}{1-\nu_0}\right) - \frac{P_1^L}{1-\nu_0}\left(\frac{N_0}{1-\nu_0} - \frac{N_{01}}{1-\nu_1}\right)\right] \\
&\qquad - \frac{P_0^L P_1^L \bar{P}^{L*}}{(1-\nu_0)(1-\nu_1)} - \left[\frac{P_0^L M_1^*}{1-\nu_1} - \frac{P_0^L M_0}{1-\nu_0} + \frac{P_1^L M_0^*}{1-\nu_0} - \frac{P_1^L M_1}{1-\nu_1}\right] \qquad (4.1)
\end{aligned}
$$

$$
\begin{aligned}
&i\partial_t P_1 - (\Omega_1 - i\Gamma_1)P_1 + (1-\nu_1)V_{10}P_1 - \bar{P} = \\
&\quad = 2\mu E(t)\left(P_1^L P_1^{L*} + N_1\right) + 2V_{10}P_0^L P_1^L\left(\frac{P_1^{L*}}{1-\nu_1} - \frac{P_0^{L*}}{1-\nu_0}\right) \\
&\qquad + 2V_{10}\left[\frac{P_0^L}{1-\nu_1}\left(\frac{N_1}{1-\nu_1} - \frac{N_{10}}{1-\nu_0}\right) - \frac{P_1^L}{1-\nu_0}\left(\frac{N_0}{1-\nu_0} - \frac{N_{01}}{1-\nu_1}\right)\right] \\
&\qquad + \frac{P_0^L P_1^L \bar{P}^{L*}}{(1-\nu_0)(1-\nu_1)} + \left[\frac{P_0^L M_1^*}{1-\nu_1} - \frac{P_0^L M_0}{1-\nu_0} + \frac{P_1^L M_0^*}{1-\nu_0} - \frac{P_1^L M_1}{1-\nu_1}\right] \qquad (4.2)
\end{aligned}
$$

where we used the definitions

$$N_n = \langle |X_n\rangle\langle X_n| \rangle_c \tag{4.3}$$

for the incoherent LL$n$ populations,

$$N_{nm} = \langle |X_m\rangle\langle X_n| \rangle_c \tag{4.4}$$

with $n \neq m$ for the intraband X–X coherences and

$$M_n = \langle |X_n\rangle\langle Y| \rangle_c \tag{4.5}$$

for the intraband X–X+MP coherences. The first term in the right–hand side of Eqs. (4.1) and (4.2) describes Pauli blocking effects (PSF), the second descibes the mean-field X–X interactions, the third one is the contribution of incoherent densities $N_n$ and X–X coherences $N_{nm}$, while the last two terms describe X–X+MP coherences.

The dynamics of the incoherent densities $N_0$ and $N_1$ is described by the following equations of motion, derived from Eq. (6.30):

$$\begin{aligned} i\partial_t N_0 =& -i\gamma_D N_0 + (1-\nu_0)V_{10}N_{01} - (1-\nu_0)V_{01}N_{10} \\ &+ i(2\Gamma_0 - \gamma_D)P_0^L P_0^{L*} - M_0 + M_0^* \end{aligned} \tag{4.6}$$

$$\begin{aligned} i\partial_t N_1 =& -i\gamma_D N_1 + (1-\nu_1)V_{01}N_{10} - (1-\nu_1)V_{10}N_{01} \\ &+ i(2\Gamma_1 - \gamma_D)P_1^L P_1^{L*} + M_1 - M_1^* \end{aligned} \tag{4.7}$$

where $\gamma_D$ is the incoherent density relaxation rate, which is expected to be very long (hundreds of picoseconds), as determined by radiation decay [115].

Similarly, the X–X coherences $N_{10} = N_{01}^*$ are described by:

$$\begin{aligned} i\partial_t N_{10} =& (\Omega_1 - \Omega_0 - i\gamma_{10})N_{10} + (1-\nu_0)V_{10}N_1 - (1-\nu_1)V_{10}N_0 \\ &+ i(\Gamma_0 + \Gamma_1 - \gamma_{10})P_1^L P_0^{L*} + M_0 + M_1^* \end{aligned} \tag{4.8}$$

where we introduced the X↔X coherence dephasing rate, $\gamma_{10}$, which is expected to be much shorter than the population relevant of $N_{10}$ relaxation rate [115].

By using Eq. (3.69) we obtain the equation of motion for the X↔X+MP coherences $M_0$ and $M_1$:

$$\begin{aligned} i\partial_t M_0 =& (\bar{\Omega} - \Omega_0 - i\gamma_{M_0})M_0 + (1-\nu_0)V_{10}M_1 \\ &+ i(\Gamma_0 + \gamma - \gamma_{M_0})\bar{P}^L P_0^{L*} + W\left(\frac{N_{10}}{1-\nu_1} - \frac{N_0}{1-\nu_0}\right) \end{aligned} \tag{4.9}$$

$$i\partial_t M_1 = (\bar{\Omega} - \Omega_1 - i\gamma_{M_1})M_1 + (1-\nu_1)V_{01}M_0 + i(\Gamma_1 + \gamma - \gamma_{M_1})\bar{P}^L P_1^{L*} + W\left(\frac{N_1}{1-\nu_1} - \frac{N_{01}}{1-\nu_0}\right) \tag{4.10}$$

where again, $\gamma_{M_n}$ is the X↔X coherence dephasing time.

Finally, the dynamics of the third–order X+MP excitation $\bar{P} = \langle \hat{Y} \rangle_c - \bar{P}^L$ can be described in a first approximation by

$$i\partial_t \bar{P} = (\bar{\Omega} - i\gamma)\bar{P} + W\left(\frac{P_1}{1-\nu_1} - \frac{P_0}{1-\nu_0}\right) \tag{4.11}$$

in analogy with Eq. (3.56). This approximation neglects the excitation induced changes in the exciton dephasing, which for large $\gamma$ are expected to lead to nonlinearities smaller than the ones considered above.

Eqs. (4.1)–(4.11), together with the equations for the linear polarizations $P_n^L$ and $\bar{P}^L$, Eqs. (3.50) and (3.56), consitute our model. To obtain the FWM spectrum, we consider an optical field similar to experiment,

$$E(t) = E_p(t)e^{i\mathbf{k}_1\cdot\mathbf{r}} + E_p(t+\Delta t_{12})e^{i\mathbf{k}_2\cdot\mathbf{r}} + E_p(t+\Delta t_{13})e^{i\mathbf{k}_3\cdot\mathbf{r}} \tag{4.12}$$

where $E_p(t) = E_0 e^{-(t/t_p)^2}$ is the Gaussian envelope of the pulses emitted by the laser, with amplitude $E_0$ and pulse intensity FWHM $t_p$. We then solve Eqs. (4.1)–(4.11) as a function of time $t$ and the time delays $\Delta t_{12}$ and $\Delta t_{13}$, with the initial condition that all quantities are zero at $t \to -\infty$, and by keeping only terms that give a nonlinear signal in the $\mathbf{k}_1 + \mathbf{k}_2 - \mathbf{k}_3$ direction. The SR–FWM signal is obtained by performing a Fourier transform of the nonlinear polarizations,

$$S(\omega, \Delta t_{12}, \Delta t_{13}) = |(1-\nu_0)P_0(\omega) + (1-\nu_1)P_1(\omega)|^2 \tag{4.13}$$

which at $\omega = \Omega_0$ and $\omega = \Omega_1$ gives the LL0 and LL1 signal respectively. In the following sections, we will discuss the results of our analytical and numerical calculations.

## 4.4 Simple analytical solutions

The system of Eqs. (4.1)–(4.11) is already too complicated to be solved analytically and a numerical computation is necessary in order to calculate the FWM signal. However, before discussing the full numerical calculations of our model, it is helpful to solve these equations in some simplified form analytically. Such analytical solutions will give us an intuition about the role of each term and will help us identify their signatures in the FWM signal,

which in comparison with the experimental results and the full numerical calculations, will guide us to the processes that dominate the nonlinear optical response of the quantum Hall system.

In the following, we will calculate the linear absorption spectrum and the FWM contribution of PSF, X–X interactions and X–X and X–X+MP coherences by making a few simplifications that will allow us to produce analytical expressions. In particular, we assume delta–function pulses instead of Gaussian ones, which is relatively justified by the fact that the Gaussian pulses used in experiment are of $\sim$ 100 fs duration, while the shortest dephasing times / oscillation periods are a few hundreds of fs.[1] Furthermore, we can ignore all non–resonant terms in our equations, since resonant terms will mainly drive the dynamics. This results in e.g. ignoring the $V_{nm}$ term in Eq. (3.50) and the coupling between the LL0 polarization and $\bar{P}$, since the latter is almost resonant with LL1. Thus, we will approximately describe the linear response of the system with the following simplified form of Eqs. (3.50) and (3.56):

$$i\partial_t P_0^L = (\Omega_0 - i\Gamma_0)P_0^L - \mu E_0\delta(t) \tag{4.14}$$

$$i\partial_t P_1^L = (\Omega_1 - i\Gamma_1)P_1^L - \mu E_0\delta(t) + \bar{P}^L \tag{4.15}$$

$$i\partial_t \bar{P}^L = (\bar{\Omega} - i\gamma)\bar{P}^L + \frac{W}{1-\nu_1}P_1^L \tag{4.16}$$

the solution of which is

$$P_0^L(t) \propto e^{-i\Omega_0 t}e^{-\Gamma_0 t}\,\theta(t) \tag{4.17}$$

$$P_1^L(t) \propto \left(e^{-i\omega_1 t} + c\, e^{-i\omega_2 t}\right)\,\theta(t) \tag{4.18}$$

$$\bar{P}^L(t) \propto W\left(e^{-i\omega_1 t} - e^{-i\omega_2 t}\right)\,\theta(t) \tag{4.19}$$

where $\theta(t)$ is the step function, $c$ a constant and $\omega_{1,2}$ the solutions of the quadratic equation $(\omega - \Omega_1 + i\Gamma_1)(\omega - \bar{\Omega} + i\gamma) - W = 0$. Assuming that $\bar{\Omega} \simeq \Omega_1$ and $\nu_1 = 0$ for the experiment of Refs. [45, 52], we obtain

$$\omega_{1,2} \simeq \Omega_1 \pm \sqrt{W - \left(\frac{\gamma - \Gamma_1}{2}\right)^2} - i\frac{\gamma + \Gamma_1}{2} \equiv (\Omega_1 \pm \delta) - i\gamma_1 \tag{4.20}$$

i.e. $P_1^L$ and $\bar{P}^L$ describe two almost degenerate states of which the separation $2\delta$ depends on the coupling strength $W$. If $\delta$ is negligible, $\omega_1 = \omega_2$, and the LL1 polarization can be described by a single Lorentzian with an effective

[1] However, an important difference between delta and Gaussian pulses is that in the latter case we can excite e.g. only LL1, while in the former case, all LLs are equally excited.

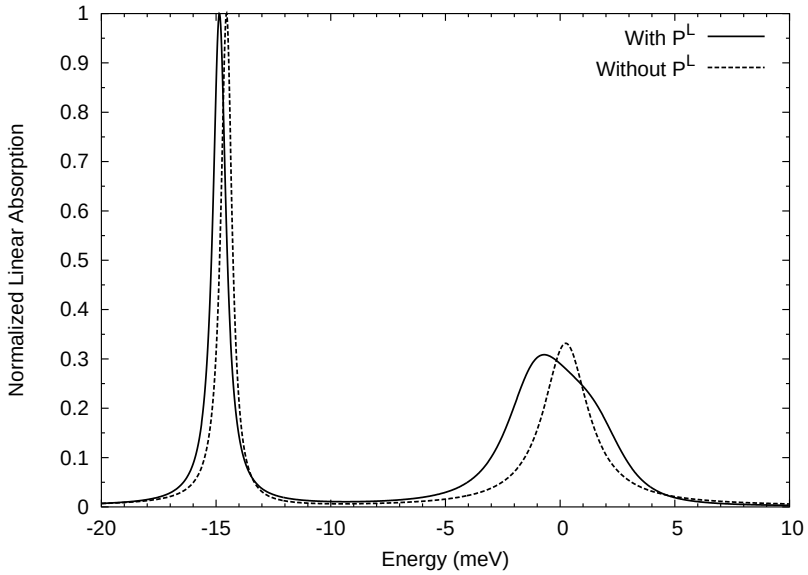


**Figure 4.4:** Theoretical calculation of the linear absorption spectrum with and without $\bar{P}^L$, with parameters chosen to fit experiment of Ref. [52] at $B = 7$ T. The solid line ($\bar{P}^L \neq 0$) is the same as in Fig. 3.4. The dashed line ($\bar{P}^L = 0$) is obtained by setting $W = 0$ and $\Gamma_1 = 1.2$ meV, as an effective dephasing rate for $P_1^L$. The LL0 peak is slightly changed because of the non–resonant $P_0^L$–$\bar{P}^L$ coupling.

dephasing rate $\gamma_1$. This is shown in Fig. 4.4, where the linear absorption spectrum with and without $\bar{P}^L$ is calculated. The presence of $\bar{P}^L$ affects the LL1 peak in a way that cannot be described with a single Lorentzian. Moreover, because of the strong dephasing of the X+MP states described by $\bar{P}^L$, the LL1 exciton decays faster that the LL0 exciton, which is what is observed in the experiment (see Fig. 3.4).

Using the above approximations and solutions for the $P_n^L$ and $\bar{P}^L$ we can obtain the time and time delay dependence of the second order densities $N_n$ and coherences $N_{nm}$ and $M_n$, and then calculate their contributions to the LL0 and LL1 third order polarizations. In order to compare with the experiment, we study the two axes $\Delta t_{13}$ and $\Delta t_{12}$ separately. As will become clear from the following discussion, the former accesses the interband dynamics of the system, while the latter accesses the intraband dynamics.

### 4.4.1 The $\Delta t_{13}$ axis: interband dynamics

To obtain a simple solution for the third order polarizations $P_n$ along the $\Delta t_{13}$ axis, we first solve Eqs. (4.6)–(4.10) vs. time $t$ and time delay $\Delta t_{13}$ by using Eqs. (4.17), (4.18) and (4.19) and the approximations discussed above.

Contributions to $P_0(\Omega_0)$ along the $\Delta t_{13}$ axis

| Term | if $\Delta t_{13} > 0$ | if $\Delta t_{13} < 0$ |
|---|---|---|
| $E(t)P_0^L P_0^{L*}$ | $e^{i\Omega_0\Delta t_{13}}e^{-\Gamma_0\Delta t_{13}}$ | 0 |
| $E(t)N_0$ | $e^{i\Omega_0\Delta t_{13}}e^{-\Gamma_0\Delta t_{13}}$ | 0 |
| $P_0^L P_1^L P_1^{L*}$ | $e^{i\Omega_1\Delta t_{13}}e^{-\gamma_1\Delta t_{13}}$ | $e^{i\Omega_1\Delta t_{13}}e^{(\Gamma_0+\gamma_1)\Delta t_{13}}$ |
| $P_0^L N_1$ | $e^{i\Omega_1\Delta t_{13}}e^{-\gamma_1\Delta t_{13}}$ | $e^{i\Omega_1\Delta t_{13}}e^{(\Gamma_0+\gamma_1)\Delta t_{13}}$ |
| $P_1^L N_{01}$ | $e^{i\Omega_1\Delta t_{13}}e^{-\gamma_1\Delta t_{13}}$ | $e^{i\Omega_1\Delta t_{13}}e^{(\Gamma_0+\gamma_1)\Delta t_{13}}$ |
| $P_0^L M_1^*$ | $e^{i\Omega_1\Delta t_{13}}e^{-\gamma_1\Delta t_{13}}$ | $e^{i\Omega_1\Delta t_{13}}e^{(\Gamma_0+\gamma_1)\Delta t_{13}}$ |
| $P_1^L M_0^*$ | $e^{i\Omega_1\Delta t_{13}}e^{-\gamma_1\Delta t_{13}}$ | $e^{i\Omega_1\Delta t_{13}}e^{(\Gamma_0+\gamma_1)\Delta t_{13}}$ |
| $P_0^L P_1^L \bar{P}^{L*}$ | $e^{i\Omega_1\Delta t_{13}}e^{-\gamma_1\Delta t_{13}}$ | $e^{i\Omega_1\Delta t_{13}}e^{(\Gamma_0+\gamma_1)\Delta t_{13}}$ |

**Table 4.1:** Contributions of the resonant terms in the equation of motion Eq. (4.1) to the LL0 third order polarization $P_0(\omega = \Omega_0)$ along the $\Delta t_{13}$ axis ($\Delta t_{12} = 0$). The dependence on $\delta \ll \Omega_1 - \Omega_0$ is ignored for clarity. The first two terms describe Pauli blocking (PSF), the third one X–X interactions, the next two are the contributions of X populations and X–X coherences, and the last three are the contributions of X–X+MP coherences.

For example, Eq. (4.6) is simplified to

$$i\partial_t N_0 = -i\gamma_D N_0 + i(2\Gamma_0 - \gamma_D)P_0^L(t)P_0^{L*}(t + \Delta t_{13}) \tag{4.21}$$

The time delay dependence appears by recalling that we are interested in the FWM signal in the $\mathbf{k}_1 + \mathbf{k}_2 - \mathbf{k}_3$ direction, in which a term of the form e.g. $P_n^L P_m^L P_l^{L*}$ gives two contributions: $P_n^L(t)P_m^L(t + \Delta t_{12})P_l^{L*}(t + \Delta t_{13})$ and $P_n^L(t + \Delta t_{12})P_m^L(t)P_l^{L*}(t + \Delta t_{13})$, depending on which pulse creates each polarization. In the $\Delta t_{13}$ axis, $\Delta t_{12} = 0$ and thus, the two FWM contributions collapse into one. However, as we will see in the following section, the two contributions in the $\Delta t_{12}$ axis are different and interfere with each other, giving rise to interesting dynamics.

The solution of Eq. (4.21) is

$$N_0 \propto \begin{cases} e^{i\Omega_0\Delta t_{13}}e^{-\Gamma_0\Delta t_{13}}\left(e^{-\gamma_D t} - e^{-2\Gamma_0 t}\right)\theta(t) & \text{if } \Delta t_{13} > 0 \\ e^{i\Omega_0\Delta t_{13}}e^{\Gamma_0\Delta t_{13}}\left[e^{-\gamma_D(t+\Delta t_{13})} - e^{-2\Gamma_0(t+\Delta t_{13})}\right]\theta(t + \Delta t_{13}) & \text{if } \Delta t_{13} < 0 \end{cases} \tag{4.22}$$

which shows clearly the physical process that takes place. When the first pulse comes in, it creates a polarization that decays as $\Gamma_0$ for time $|\Delta t_{13}|$ until the second pulse comes in. Then, there are two possibilities: either the

Contributions to $P_1(\Omega_1)$ along the $\Delta t_{13}$ axis

| Term | if $\Delta t_{13} > 0$ | if $\Delta t_{13} < 0$ |
|---|---|---|
| $E(t)P_1^L P_1^{L*}$ | $e^{i\Omega_1 \Delta t_{13}} e^{-\gamma_1 \Delta t_{13}}$ | 0 |
| $E(t)N_1$ | $e^{i\Omega_1 \Delta t_{13}} e^{-\gamma_1 \Delta t_{13}}$ | 0 |
| $P_1^L P_0^L P_0^{L*}$ | $e^{i\Omega_0 \Delta t_{13}} e^{-\Gamma_0 \Delta t_{13}}$ | $e^{i\Omega_0 \Delta t_{13}} e^{(\Gamma_0+\gamma_1) \Delta t_{13}}$ |
| $P_0^L N_{10}$ | $e^{i\Omega_0 \Delta t_{13}} e^{-\Gamma_0 \Delta t_{13}}$ | $e^{i\Omega_0 \Delta t_{13}} e^{(\Gamma_0+\gamma_1) \Delta t_{13}}$ |
| $P_1^L N_0$ | $e^{i\Omega_0 \Delta t_{13}} e^{-\Gamma_0 \Delta t_{13}}$ | $e^{i\Omega_0 \Delta t_{13}} e^{(\Gamma_0+\gamma_1) \Delta t_{13}}$ |
| $P_0^L M_0$ | $e^{i\Omega_0 \Delta t_{13}} e^{-\Gamma_0 \Delta t_{13}}$ | $e^{i\Omega_0 \Delta t_{13}} e^{(\Gamma_0+\gamma_1) \Delta t_{13}}$ |
| $P_1^L M_1$ | $e^{i\Omega_1 \Delta t_{13}} e^{-\gamma_1 \Delta t_{13}}$ | $e^{i\Omega_1 \Delta t_{13}} e^{2\gamma_1 \Delta t_{13}}$ |

**Table 4.2:** Contributions of the resonant terms in the equation of motion Eq. (4.2) to the LL1 third order polarization $P_1(\omega = \Omega_1)$ along the $\Delta t_{13}$ axis ($\Delta t_{12} = 0$). The dependence on $\delta \ll \Omega_1 - \Omega_0$ is ignored for clarity. The first two terms describe Pauli blocking (PSF), the third one X–X interactions, the next two are the contributions of X populations ans X–X coherences, and the last two are contributions of X–X+MP coherences.

density $N_0$ is created, which then decays with its own rate $\gamma_D$, or nothing happens and the two polarizations decay with rate $2\Gamma_0$.

We repeat the same process for all second order densities and intraband coherences and then substitute the obtained expressions into the Fourier transformed Eqs. (4.1) and (4.2) to calculate their contribution to the LL0 ($P_0$) and LL1 ($P_1$) polarizations at the LL0 ($\omega = \Omega_0$) and LL1 ($\omega = \Omega_1$) energy respectively. Tables 4.1 and 4.2 list these contributions along the positive and negative $\Delta t_{13}$ axis. The first two terms describe Pauli blocking (PSF), which does not contribute for negative time delays, as predicted from the standard mean field theory. The third term is the contribution of the mean field X–X interactions and the rest are contributions of X–X and X–X+MP coherences. These simple expressions can already give us an explanation of the experimental results along the $\Delta t_{13}$ axis. Since mostly LL1 is photoexcited in the experiment, PSF is expected to dominate the LL1 signal and be insignificant for the LL0 signal. Thus the LL1 signal will approximately follow the decay of the PSF contribution, which is $-\gamma_1 \Delta t_{13}$ for $\Delta t_{13} > 0$ and zero for $\Delta t_{13} < 0$, i.e. it will be almost *asymmetric* about $\Delta t_{13} = 0$. On the other hand, the LL0 signal will not be affected by the PSF contribution. Since all other terms give the same decay rate, $\gamma_1$ for $\Delta t_{13} > 0$ and $\Gamma_0 + \gamma_1$ for $\Delta t_{13} < 0$, the full LL0 signal will follow these decay rates. As

discussed earlier, $\gamma_1$ is the effective decay rate of the LL1 exciton, enhanced by the strong dephasing of the X+MP states, and is much larger than the decay rate of the LL0 exciton. As a result $\Gamma_0 + \gamma_1 \approx \gamma_1$, i.e the LL0 signal will be *symmetric* about $\Delta t_{13} = 0$. Moreover, since all terms (except for PSF) in Table 4.1 have the same phase $\Omega_1 \Delta t_{13}$, there will be no significant oscillations in the signal.

It is important to note that all contributions decay with the interband polarization decaying rates in both the positive and negative $\Delta t_{13}$ axis, i.e. we do not obtain any information about the dephasing rates of densities and intraband coherences that are created in the system. We can only obtain the decay rate of *interband* excitations, like the polarizations. This is a direct consequence of the physical processes that can create a FWM signal in the $\mathbf{k}_1 + \mathbf{k}_2 - \mathbf{k}_3$ direction along the $\Delta t_{13}$ axis. We thus state that "the $\Delta t_{13}$ axis accesses the interband dynamics of the system". To illustrate this, we will discuss a typical process of creating a FWM signal along the positive and the negative $\Delta t_{13}$ axis.

### Positive $\Delta t_{13}$ axis

Fig. 4.5 shows the creation of the FWM signal along the positive $\Delta t_{13}$. In this case, pulse $\mathbf{k}_3$ arrives first and creates a polarization, i.e. an interband coherence. If both Landau levels, LL0 and LL1 are excited, the excited polarization can be either LL0$^*$ or LL1$^*$. The wavevector of this polarization is $-\mathbf{k}_3$[2]. The excited polarization evolves in the sample for a time $\Delta t_{13}$ with a phase $-\Omega_n \Delta t_{13}$, where $n = 0, 1$ depending on whether it is a LL0$^*$ or a LL1$^*$ polarization. The evolving polarization also decays over this time interval with a rate $\Gamma_n$. After time $t = \Delta t_{13}$, pulses $\mathbf{k}_1$ and $\mathbf{k}_2$ arrive simultaneously. One of them creates an intraband excitation via a second order process, and the other probes it at the same time. As a result, the decay and the phase of the resulting FWM signal reflects the decay and phase accumulated by the polarization during its evolution for time $\Delta t_{13}$, while the instantaneously created second order excitation does not affect the decay of the measured signal. Thus, by measuring the intensity of the decaying signal along the positive $\Delta t_{13}$ axis, one can only obtain the decoherence rate of an interband polarization.

[2]Pulse $\mathbf{k}_3$ also creates second order excitations, like intraband coherences between LL0 and LL1 or LL0 and LL1 populations. However, these second order quantities will have wavevectors $\mathbf{k}_3 - \mathbf{k}_3 = 0$ or $\pm(\mathbf{k}_3 + \mathbf{k}_3) = \pm 2\mathbf{k}_3$. Thus, when probed by pulses $\mathbf{k}_1$ and $\mathbf{k}_2$ they cannot contribute to the nonlinear signal in the $\mathbf{k}_1 + \mathbf{k}_2 - \mathbf{k}_3$ direction.

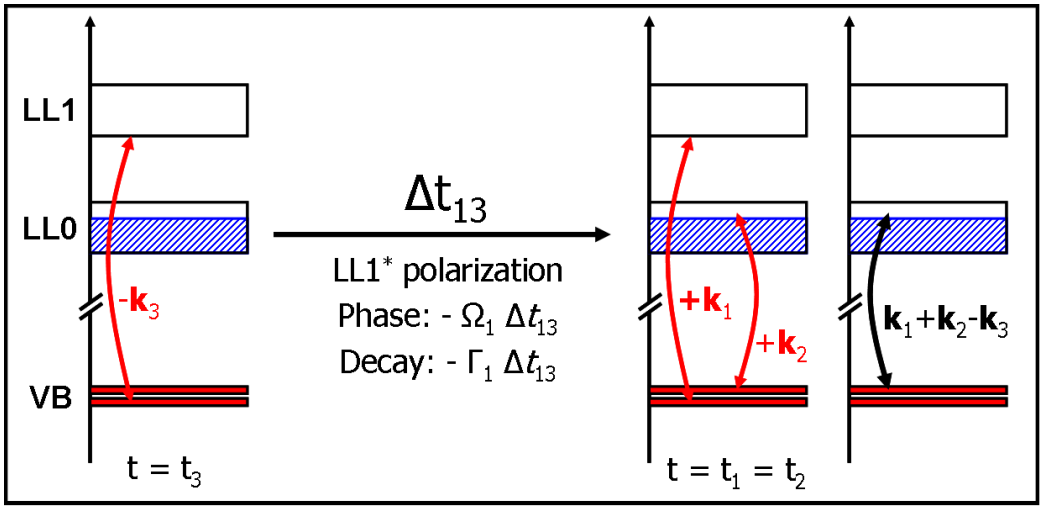


**Figure 4.5:** Interband dynamics along the $\Delta t_{13} > 0$ axis: Pulse $\mathbf{k}_3$ comes first, creates an interband polarization (LL1* in this figure), which accumulates a phase $-\Omega_1 \Delta t_{13}$ and decay $-\Gamma_1 \Delta t_{13}$. Pulses $\mathbf{k}_1$ and $\mathbf{k}_2$ then arrive and produce the FWM signal, which reflects the phase $-\Omega_1 \Delta t_{13}$ and decay $-\Gamma_1 \Delta t_{13}$.

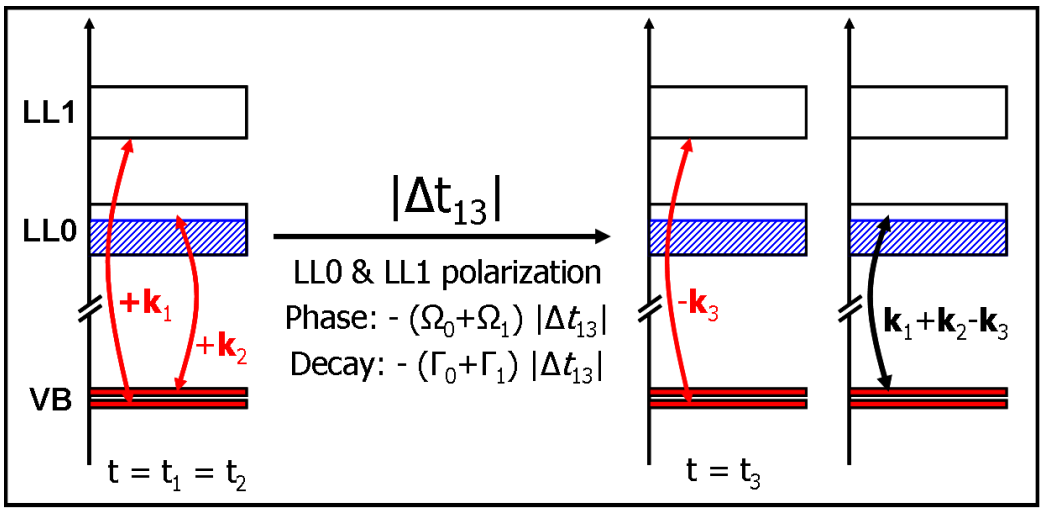


**Figure 4.6:** Interband dynamics along the $\Delta t_{13} < 0$ axis: Pulse $\mathbf{k}_1$ and $\mathbf{k}_2$ arrive together and create interband polarizations (LL0* and LL1* in this figure). They accumulate phase $\Omega_0|\Delta t_{13}|$ and $\Omega_1|\Delta t_{13}|$ and decay as $-\Gamma_0|\Delta t_{13}|$ and $-\Gamma_1|\Delta t_{13}|$ respectively. Pulse $\mathbf{k}_3$ then arrives and produces the FWM signal, which reflects the phase $(\Omega_0 + \Omega_1)|\Delta t_{13}|$ and the decay $-(\Gamma_0 + \Gamma_1)|\Delta t_{13}|$.

**Negative $\Delta t_{13}$ axis**

Along the negative $\Delta t_{13}$ axis, pulses $\mathbf{k}_1$ and $\mathbf{k}_2$ arrive first (Fig. 4.6). They either create interband polarizations independently, or second order interband excitations (like biexcitons), but they cannot create intraband excitations like intraband coherences or populations. The created interband excitations evolve in the sample for a time $|\Delta t_{13}|$, after which pulse $\mathbf{k}_3$ arrives, resulting in the $\mathbf{k}_1+\mathbf{k}_2-\mathbf{k}_3$ FWM signal. As the interband excitations decay over the time $\Delta t_{13}$, the FWM signal versus $|\Delta t_{13}|$ (for $\Delta t_{13}<0$) decays with the same decoherence rate, i.e. either the sum of the decay rates of the two polarizations created, or the decay rate of the second order interband excitation (biexciton).

In conclusion, the FWM signal in both the positive and negative $\Delta t_{13}$ axis reflects the dynamics of interband excitations. It decays with the dephasing rate of the polarization for $\Delta t_{13}>0$, and either with the sum of the dephasing rates of the polarizations or the dephasing rate of biexcitons for $\Delta t_{13}<0$.

### 4.4.2 The $\Delta t_{12}$ axis: intraband dynamics

Along the $\Delta t_{12}$ axis we access different dynamics. To show this, we solve Eqs. (4.1) and (4.10) vs. time $t$ and time delay $\Delta t_{12}$, as done earlier in the $\Delta t_{13}$ axis, by considering only resonant terms and delta pulses. Because of the symmetry between pulses $\mathbf{k}_1$ and $\mathbf{k}_2$, there two FWM processes that create each contribution to $P_0$ and $P_1$. For example, a term of the form $P_n^L P_m^L P_l^{L*}$ contributes as $P_n^L(t)P_m^L(t+\Delta t_{12})P_l^{L*}(t)$, as well as $P_n^L(t+\Delta t_{12})P_m^L(t)P_l^{L*}(t)$. Moreover, all densities and intraband coherences can be created either by pulses $\mathbf{k}_1$ and $\mathbf{k}_3$, or by pulses $\mathbf{k}_2$ and $\mathbf{k}_3$. To distinguish them, we will use a "13" or "23" subscript respectively.

Tables 4.3 and 4.4 list the contributions to the LL0 and LL1 polarizations for both positive and negative $\Delta t_{12}$. The first block describes PSF, the second X–X interactions, the third the contributions of X densities and X–X coherences, and the last the contributions of X–X+MP coherences. We have introduced effective decay rates $\tilde{\gamma}_0$ for $M_0$ and $N_{10}$, and $\tilde{\gamma}_1$ for $M_1$ and $N_1$. As seen from Eqs. (4.9) and (4.8), the coupling between the resonant $M_0$ and $N_{10}$ results in two almost degenerate states – as in the case of $P_1^L$ and $\bar{P}^L$ – with energies

$$\omega_{1,2} \simeq \Omega_1 - \Omega_0 \pm \sqrt{W - \left(\frac{\gamma_{M_0}-\gamma_{10}}{2}\right)^2} - i\frac{\gamma_{M_0}+\gamma_{10}}{2} \equiv \Omega_1 - \Omega_0 \pm \delta_0 - i\tilde{\gamma}_0 \tag{4.23}$$

Similarly, the coupling between the resonant $M_1$ and $N_1$ (Eqs. (4.10) and (4.7)) results in two almost degenerate states with energies

$$\omega_{1,2} \simeq \pm\sqrt{2W - \left(\frac{\gamma_{M_1} - \gamma_D}{2}\right)^2} - i\frac{\gamma_{M_1} + \gamma_D}{2} \equiv \pm\delta_1 - i\tilde{\gamma}_1 \qquad (4.24)$$

In Tables 4.3 and 4.4 we have ignored the time delay dependence on the small energies $\delta$, $\delta_0$ and $\delta_1$, since they are of the order of a few meV and thus are much smaller than the energy of the observed oscillations (§4.2).

These analytical expressions are particularly useful to compare with the experiment. We begin with the LL1 signal, where we expect that PSF dominates. The relevant terms in Table 4.4 show that when only PSF is considered, there are no oscillations and the signal decays with a rate of $2\gamma_1$ for $\Delta t_{12} > 0$, and $2\tilde{\gamma}_1$ or $4\gamma_1$ for $\Delta t_{12} < 0$, depending on which one is smaller. As shown in Fig. 4.3, the LL1 signal exhibits no oscillations, and decays much more slowly for $\Delta t_{12} < 0$ than for $\Delta t_{12} > 0$. Thus, we conclude that $\tilde{\gamma}_1 \ll \gamma_1$.

A similar analysis for the LL0 signal allows us to identify the possible sources of the observed oscillations at the inter-LL energy. It is clear from Table 4.3 that for $\Delta t_{12} > 0$, despite the many different terms, the oscillations with frequency $\Omega_1 - \Omega_0$ may decay only with a rate of $\Gamma_0 + \gamma_1$. In the $\Delta t_{12} < 0$ axis, the situation is sligtly more complicated. If we ignore the PSF terms (since they are insignificant for the experimental conditions of interest), the oscillations may decay with a rate of $\Gamma_0 + 3\gamma_1$, $\Gamma_0 + \gamma_1 + \tilde{\gamma}_1$, $\tilde{\gamma}_0 + 2\gamma_1$ or $\tilde{\gamma}_0 + \tilde{\gamma}_1$. However, in the experiment the oscillations decay symmetrically about $\Delta t_{12}$ and since $\gamma_1 \gg \Gamma_0$, the $\Gamma_0 + 3\gamma_1$ and $\tilde{\gamma}_0 + 2\gamma_1$ decay rates are ruled out. We thus end up with two possibilities: either $\Gamma_0 + \gamma_1 + \tilde{\gamma}_1 \approx \Gamma_0 + \gamma_1$, or $\tilde{\gamma}_0 + \tilde{\gamma}_1 \approx \Gamma_0 + \gamma_1$. Since we concluded from LL1 that $\tilde{\gamma}_1 \ll \gamma_1$, the former condition is already true. This implies that $\tilde{\gamma}_0 \gtrsim \gamma_1$, a requirement that diminishes the role of the $M_0$ – $N_{10}$ coherences because of the large $\gamma_1$ rate[3]. We thus reach the conclusion that the oscillations for $\Delta t_{12} < 0$ decay as $\Gamma_0 + \gamma_1 + \tilde{\gamma}_1$ and are due to beatings of either $M_1^{13}$ or $N_1^{13}$ with another term that decays as $\Gamma_0 + \gamma_1$. To find out which this term is, we need a full calculation that we will present in the following section.

Before discussing our numerical results, it is interesting to note that for $\Delta t_{12} > 0$ all contributions decay with the polarizations decay rates, while for $\Delta t_{12} < 0$, we get access to the decay rates of intraband coherences and densities. This is a direct consequence of the process that creates a FWM signal in the $\mathbf{k}_1 + \mathbf{k}_2 - \mathbf{k}_3$ direction along the $\Delta t_{12}$ axis. As a result, "the $\Delta t_{12}$ axis probes the intraband dynamics of the system". This is illustrated in

[3]The contributions of the different terms to the polarizations include a 1/(decay rate) coefficient, which makes them smaller.

Contributions to $P_0(\Omega_0)$ along the $\Delta t_{12}$ axis

| Term | if $\Delta t_{12} > 0$ | if $\Delta t_{12} < 0$ |
|---|---|---|
| $E(t)\ P_0^L(t+\Delta t_{12})\ P_0^{L*}$ | $e^{-i\Omega_0\Delta t_{12}}e^{-\Gamma_0\Delta t_{12}}$ | 0 |
| $E(t+\Delta t_{12})\ P_0^L(t)\ P_0^{L*}$ | 0 | $e^{-i\Omega_0\Delta t_{12}}e^{2\Gamma_0\Delta t_{12}}$ |
| $E(t)\ N_0^{23}$ | $e^{-i\Omega_0\Delta t_{12}}e^{-\Gamma_0\Delta t_{12}}$ | 0 |
| $E(t+\Delta t_{12})\ N_0^{13}$ | 0 | $e^{-i\Omega_0\Delta t_{12}}e^{2\Gamma_0\Delta t_{12}}$<br>$e^{-i\Omega_0\Delta t_{12}}e^{\gamma_D\Delta t_{12}}$ |
| $P_0^L(t)\ P_1^L(t+\Delta t_{12})\ P_1^{L*}$ | $e^{-i\Omega_1\Delta t_{12}}e^{-\gamma_1\Delta t_{12}}$ | $e^{-i\Omega_1\Delta t_{12}}e^{(\Gamma_0+\gamma_1)\Delta t_{12}}$ |
| $P_0^L(t+\Delta t_{12})\ P_1^L(t)\ P_1^{L*}$ | $e^{-i\Omega_0\Delta t_{12}}e^{-\Gamma_0\Delta t_{12}}$ | $e^{-i\Omega_0\Delta t_{12}}e^{2\gamma_1\Delta t_{12}}$ |
| $P_0^L(t)\ N_1^{23}$ | $e^{-i\Omega_1\Delta t_{12}}e^{-\gamma_1\Delta t_{12}}$ | $e^{-i\Omega_1\Delta t_{12}}e^{(\Gamma_0+\gamma_1)\Delta t_{12}}$ |
| $P_0^L(t+\Delta t_{12})\ N_1^{13}$ | $e^{-i\Omega_0\Delta t_{12}}e^{-\Gamma_0\Delta t_{12}}$ | $e^{-i\Omega_0\Delta t_{12}}e^{2\gamma_1\Delta t_{12}}$<br>$e^{-i\Omega_0\Delta t_{12}}e^{\tilde{\gamma}_1\Delta t_{12}}$ |
| $P_1^L(t)\ N_{01}^{23}$ | $e^{-i\Omega_0\Delta t_{12}}e^{-\Gamma_0\Delta t_{12}}$ | $e^{-i\Omega_0\Delta t_{12}}e^{2\gamma_1\Delta t_{12}}$ |
| $P_1^L(t+\Delta t_{12})\ N_{01}^{13}$ | $e^{-i\Omega_1\Delta t_{12}}e^{-\gamma_1\Delta t_{12}}$ | $e^{-i\Omega_1\Delta t_{12}}e^{(\Gamma_0+\gamma_1)\Delta t_{12}}$<br>$e^{-i\Omega_1\Delta t_{12}}e^{\tilde{\gamma}_0\Delta t_{12}}$ |
| $P_0^L(t)\ (M_1^{32})^*$ | $e^{-i\Omega_1\Delta t_{12}}e^{-\gamma_1\Delta t_{12}}$ | $e^{-i\Omega_1\Delta t_{12}}e^{(\Gamma_0+\gamma_1)\Delta t_{12}}$ |
| $P_0^L(t+\Delta t_{12})\ (M_1^{31})^*$ | $e^{-i\Omega_0\Delta t_{12}}e^{-\Gamma_0\Delta t_{12}}$ | $e^{-i\Omega_0\Delta t_{12}}e^{2\gamma_1\Delta t_{12}}$<br>$e^{-i\Omega_0\Delta t_{12}}e^{\tilde{\gamma}_1\Delta t_{12}}$ |
| $P_1^L(t)\ (M_0^{32})^*$ | $e^{-i\Omega_0\Delta t_{12}}e^{-\Gamma_0\Delta t_{12}}$ | $e^{-i\Omega_0\Delta t_{12}}e^{2\gamma_1\Delta t_{12}}$ |
| $P_1^L(t+\Delta t_{12})\ (M_0^{31})^*$ | $e^{-i\Omega_1\Delta t_{12}}e^{-\gamma_1\Delta t_{12}}$ | $e^{-i\Omega_1\Delta t_{12}}e^{(\Gamma_0+\gamma_1)\Delta t_{12}}$<br>$e^{-i\Omega_1\Delta t_{12}}e^{\tilde{\gamma}_0\Delta t_{12}}$ |
| $P_0^L(t)\ P_1^L(t+\Delta t_{12})\ \bar{P}^{L*}$ | $e^{-i\Omega_1\Delta t_{12}}e^{-\gamma_1\Delta t_{12}}$ | $e^{-i\Omega_1\Delta t_{12}}e^{(\Gamma_0+\gamma_1)\Delta t_{12}}$ |
| $P_0^L(t+\Delta t_{12})\ P_1^L(t)\ \bar{P}^{L*}$ | $e^{-i\Omega_0\Delta t_{12}}e^{-\Gamma_0\Delta t_{12}}$ | $e^{-i\Omega_0\Delta t_{12}}e^{2\gamma_1\Delta t_{12}}$ |

**Table 4.3:** Contributions of the resonant terms in the equation of motion Eq. (4.1) to the LL0 third order polarization $P_0(\omega = \Omega_0)$ along the $\Delta t_{12}$ axis ($\Delta t_{13} = 0$). The terms in the first block describe Pauli blocking (PSF), the ones in the second X–X interactions, the terms in the third block are the contributions of X populations and X–X intraband coherences, and the last block contains the contributions of intraband X–X+MP coherences.

Contributions to $P_1(\Omega_1)$ along the $\Delta t_{12}$ axis

| Term | if $\Delta t_{12} > 0$ | if $\Delta t_{12} < 0$ |
|---|---|---|
| $E(t)\ P_1^L(t+\Delta t_{12})\ P_1^{L*}$ | $e^{-i\Omega_1\Delta t_{12}}e^{-\gamma_1\Delta t_{12}}$ | 0 |
| $E(t+\Delta t_{12})\ P_1^L(t)\ P_1^{L*}$ | 0 | $e^{-i\Omega_1\Delta t_{12}}e^{2\gamma_1\Delta t_{12}}$ |
| $E(t)\ N_1^{23}$ | $e^{-i\Omega_1\Delta t_{12}}e^{-\gamma_1\Delta t_{12}}$ | 0 |
| $E(t+\Delta t_{12})\ N_1^{13}$ | 0 | $e^{-i\Omega_1\Delta t_{12}}e^{2\gamma_1\Delta t_{12}}$<br>$e^{-i\Omega_1\Delta t_{12}}e^{\tilde{\gamma}_1\Delta t_{12}}$ |
| $P_1^L(t)\ P_0^L(t+\Delta t_{12})\ P_0^{L*}$ | $e^{-i\Omega_0\Delta t_{12}}e^{-\Gamma_0\Delta t_{12}}$ | $e^{-i\Omega_0\Delta t_{12}}e^{(\Gamma_0+\gamma_1)\Delta t_{12}}$ |
| $P_1^L(t+\Delta t_{12})\ P_0^L(t)\ P_0^{L*}$ | $e^{-i\Omega_1\Delta t_{12}}e^{-\gamma_1\Delta t_{12}}$ | $e^{-i\Omega_1\Delta t_{12}}e^{2\Gamma_0\Delta t_{12}}$ |
| $P_0^L(t)\ N_{10}^{23}$ | $e^{-i\Omega_1\Delta t_{12}}e^{-\gamma_1\Delta t_{12}}$ | $e^{-i\Omega_1\Delta t_{12}}e^{2\Gamma_0\Delta t_{12}}$ |
| $P_0^L(t+\Delta t_{12})\ N_{10}^{13}$ | $e^{-i\Omega_0\Delta t_{12}}e^{-\Gamma_0\Delta t_{12}}$ | $e^{-i\Omega_0\Delta t_{12}}e^{(\Gamma_0+\gamma_1)\Delta t_{12}}$<br>$e^{-i\Omega_0\Delta t_{12}}e^{\tilde{\gamma}_0\Delta t_{12}}$ |
| $P_1^L(t)\ N_0^{23}$ | $e^{-i\Omega_0\Delta t_{12}}e^{-\Gamma_0\Delta t_{12}}$ | $e^{-i\Omega_0\Delta t_{12}}e^{(\Gamma_0+\gamma_1)\Delta t_{12}}$ |
| $P_1^L(t+\Delta t_{12})\ N_0^{13}$ | $e^{-i\Omega_1\Delta t_{12}}e^{-\gamma_1\Delta t_{12}}$ | $e^{-i\Omega_1\Delta t_{12}}e^{2\Gamma_0\Delta t_{12}}$<br>$e^{-i\Omega_1\Delta t_{12}}e^{\gamma_D\Delta t_{12}}$ |
| $P_0^L(t)\ M_0^{23}$ | $e^{-i\Omega_1\Delta t_{12}}e^{-\gamma_1\Delta t_{12}}$ | $e^{-i\Omega_1\Delta t_{12}}e^{2\Gamma_0\Delta t_{12}}$ |
| $P_0^L(t+\Delta t_{12})\ M_0^{13}$ | $e^{-i\Omega_0\Delta t_{12}}e^{-\Gamma_0\Delta t_{12}}$ | $e^{-i\Omega_0\Delta t_{12}}e^{(\Gamma_0+\gamma_1)\Delta t_{12}}$<br>$e^{-i\Omega_0\Delta t_{12}}e^{\tilde{\gamma}_0\Delta t_{12}}$ |
| $P_1^L(t)\ M_1^{23}$ | $e^{-i\Omega_1\Delta t_{12}}e^{-\gamma_1\Delta t_{12}}$ | $e^{-i\Omega_1\Delta t_{12}}e^{2\gamma_1\Delta t_{12}}$ |
| $P_1^L(t+\Delta t_{12})\ M_1^{13}$ | $e^{-i\Omega_1\Delta t_{12}}e^{-\gamma_1\Delta t_{12}}$ | $e^{-i\Omega_1\Delta t_{12}}e^{2\gamma_1\Delta t_{12}}$<br>$e^{-i\Omega_1\Delta t_{12}}e^{\tilde{\gamma}_1\Delta t_{12}}$ |

**Table 4.4:** Contributions of the resonant terms in the equation of motion Eq. (4.2) to the LL1 third order polarization $P_1(\omega = \Omega_1)$ along the $\Delta t_{12}$ axis ($\Delta t_{13} = 0$). The first two terms describe Pauli blocking (PSF), the third one X–X interactions and the rest are contributions of incoherent densities and intraband coherences.

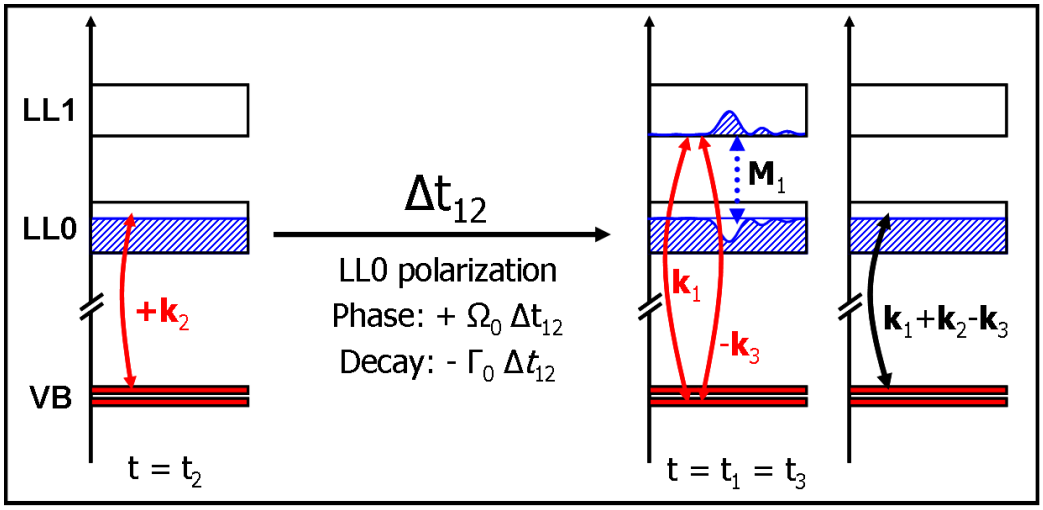


**Figure 4.7:** Interband dynamics along the $\Delta t_{12} > 0$ axis: Pulse $\mathbf{k}_2$ comes first, creates an interband polarization (LL0 in this figure), which accumulates a phase $-\Omega_0 \Delta t_{12}$ and decay $-\Gamma_0 \Delta t_{12}$. Pulses $\mathbf{k}_1$ and $\mathbf{k}_3$ then arrive and produce the FWM signal, which reflects the phase $-\Omega_0 \Delta t_{12}$ and decay $-\Gamma_0 \Delta t_{12}$.

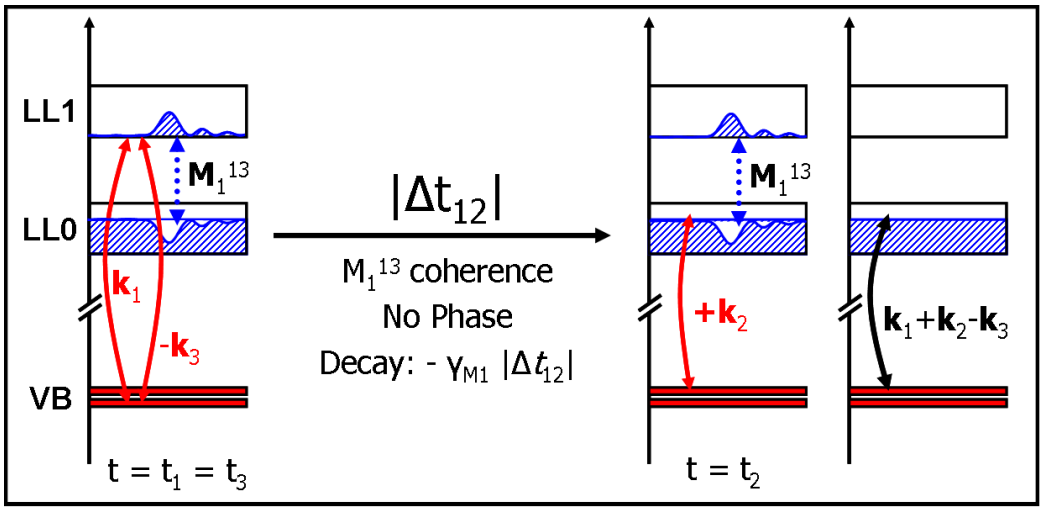


**Figure 4.8:** Interband dynamics along the $\Delta t_{12} < 0$ axis: Pulse $\mathbf{k}_1$ and $\mathbf{k}_3$ arrive first and create an intraband coherence ($M_1^{13}*$), which accumulates no phase and decays as $-\tilde{\gamma}_1 \Delta t_{12}$. Pulses $\mathbf{k}_1$ and $\mathbf{k}_3$ then arrive and produce the FWM signal, which reflects the zero phase and the decay $-\tilde{\gamma}_1 \Delta t_{12}$.

Figs. 4.7 and 4.8, which show the creation of the $M_1 = \langle |X_1\rangle\langle Y|\rangle_c$ coherence along the positive and negative $\Delta t_{12}$ axis.

Along the positive $\Delta t_{12}$ axis (Fig. 4.7) pulse $\mathbf{k}_2$ arrives first and creates a LL0 polarization in the sample. The polarization evolves with a phase frequency $\Omega_0$ and decay rate $\Gamma_0$ for a time $\Delta t_{12}$, after which pulses $\mathbf{k}_1$ and $\mathbf{k}_3$ arrive simultaneously, and create the $M_1$ coherence ($M_1^{13}$). The coherence is then probed by the decaying LL0 polarization, created by pulse $\mathbf{k}_2$, and results in the FWM signal at LL0 in the direction $\mathbf{k}_1 + \mathbf{k}_2 - \mathbf{k}_3$ that has a phase of $\Omega_0 \Delta t_{12}$ and decays as $\Gamma_0 \Delta t_{12}$. Because of the symmetry between the $\mathbf{k}_1$ and the $\mathbf{k}_2$ pulses, $M_1$ can be created by pulses $\mathbf{k}_2$ and $\mathbf{k}_3$ ($M_1^{23}$) and be probed by pulse $\mathbf{k}_1$. In both cases though, the decay of the signal along the positive $\Delta t_{12}$ axis reflects the decay of the interband polarization created by pulse $\mathbf{k}_2$.

Along the negative $\Delta t_{12}$ axis we access different information. Fig. 4.8 shows the process that creates the $M_1^{13}$ coherence. Here, pulses $\mathbf{k}_1$ and $\mathbf{k}_3$ arrive first and contribute a LL1 and a LL1$^*$ polarization respectively, which create the second order intraband coherence $M_1^{13}$ with wavevector $\mathbf{k}_1 - \mathbf{k}_3$. The $M_1$ coherence is a coherence between a LL1 exciton and the X+MP state $\{$1–MP + 1–LL0–e + 1–LL1–h$\}$, and since the two states are very close in energy, the coherence evolves in the sample with phase frequency $\bar{\Omega} - \Omega_1 \sim 0$ (this is also seen from Eq. (4.10)). As a result, the coherence evolves with almost no phase for time $|\Delta t_{12}|$. However, it does decay with decay rate $\tilde{g}_1$. After time $|\Delta t_{12}|$, pulse $\mathbf{k}_2$ arrives and probes the coherence, resulting in a FWM signal along the $\mathbf{k}_1 + \mathbf{k}_2 - \mathbf{k}_3$ direction that reflects the zero phase and the decay rate of the $M_1$ coherence.

## 4.5 Numerical calculations

Our physical arguments and analytical calculations in the previous section showed that $N_1$ or $M_1$ should contribute significantly to the LL0 signal, and that PSF should dominate the LL1 response. To check our conclusions and to identify the terms that are responsible for the oscillations, we solve Eqs. (4.1)–(4.11) numerically for the linear absorption of Fig. 3.4 and $\gamma_D = 0.1$ meV, $\gamma_{10} = 3$ meV, $\gamma_{M_1} = 0.3$ meV, and $\gamma_{M_0} = 0.6$ meV. Our conclusions are not sensitive to their precise values. Fig. 4.9 shows the calculated FWM signal for both axes, for photoexcitation of mostly LL1. The back panel shows the linear absorption spectrum and the optical pulse intensity. Our calculation reproduces well the experiment, shown in Figs. 4.1 and 4.3. These results reproduce the qualitative temporal and spectral features observed in the experiment within the femstosecond coherent regime, as a function of energy

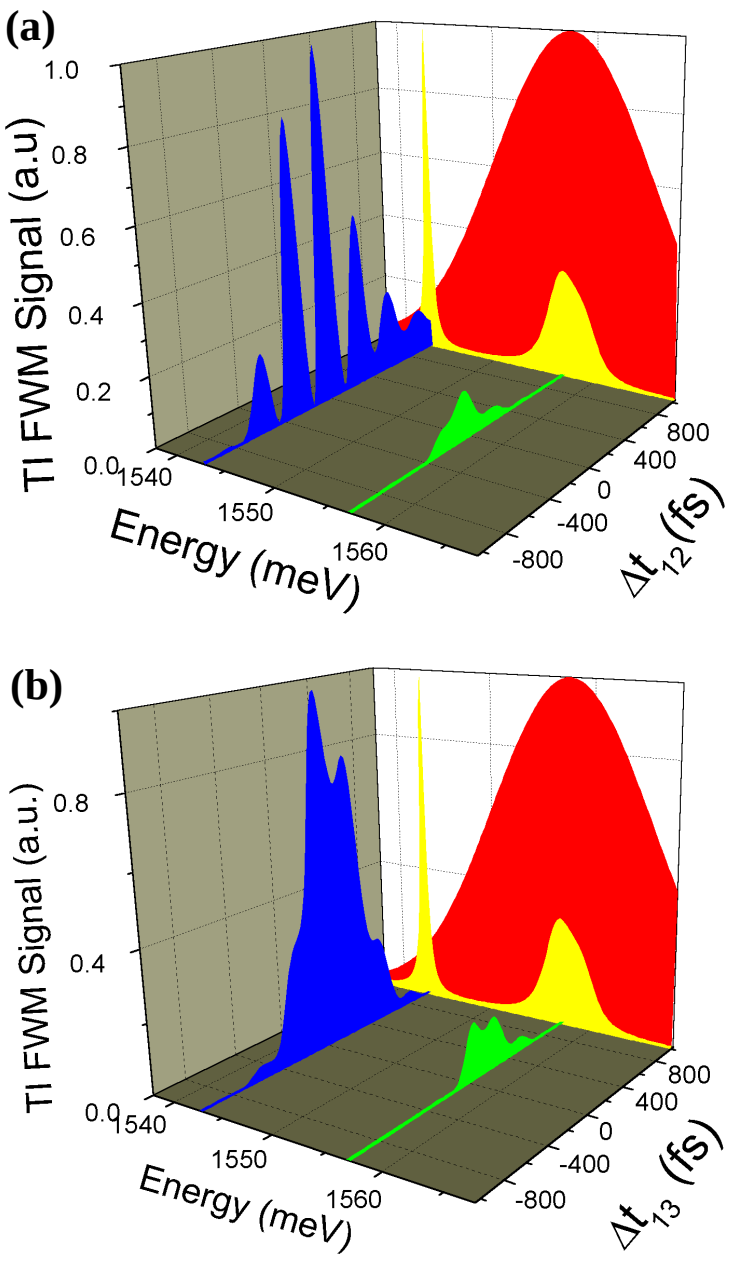


**Figure 4.9:** Numerical calculation of the SR–FWM signal along (a) the $\Delta t_{13}$ axis and (b) the $\Delta t_{12}$ axis, for mostly LL1 excitation. Back panel: Linear absorption spectrum and optical pulse intensity, showing the largely LL1 excitation conditions. The theoretical calculation is in good agreement with the experiment, shown in Figs. 4.1 and 4.3.

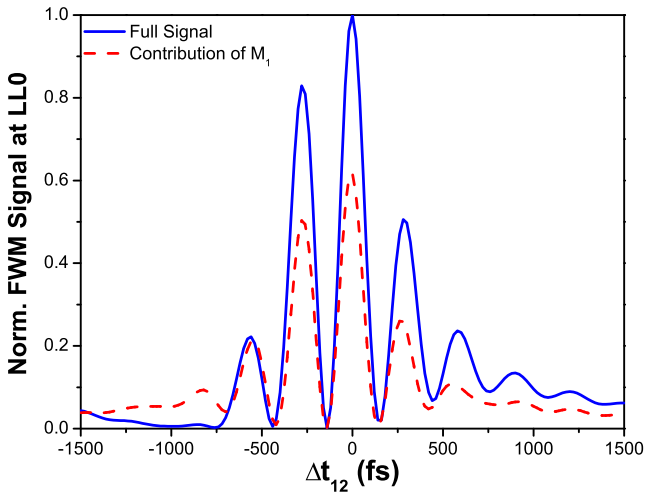


**Figure 4.10:** Numerical calculation of the LL0 SR–FWM signal along the $\Delta t_{12}$ axis and for mostly LL1 excitation. Dashed line: contribution of the $M_1$ intraband coherence.

and the two time delays. The main contribution to the calculated LL0 FWM signal comes from the $X_1 \leftrightarrow X_{01}$+MP coherence $M_1 = \langle |X_1\rangle\langle Y| \rangle_c$. This can be seen in Fig. 4.10, which compares to the calculation with the contribution of $M_1$ only.

### 4.5.1 Explanation of oscillations

As is shown in Fig. 4.10, the LL0 signal is dominated by the contribution of the $M_1$ coherence, and consequently the oscillations are due to this coherence. In particular, they are due to beatings between the two FWM processes that create $M_1$. As discussed in §4.4.2, because of the symmetry between pulses $\mathbf{k}_1$ and $\mathbf{k}_2$, the $M_1$ coherence (and any other process) can be created either by pulses $\mathbf{k}_1$ and $\mathbf{k}_3$ ($M_1^{13}$), or by pulses $\mathbf{k}_2$ and $\mathbf{k}_3$ ($M_1^{23}$). These two FWM contributions beat with each other and create the oscillations observed in experiment, as shown in Fig. 4.11. To illustate this, we will now discuss the two processes for both positive and negative $\Delta t_{12}$.

Fig. 4.12 shows the creation of the two FWM processes that create the $M_1$ coherence along the positive $\Delta t_{12}$ axis. In the case of $M_1^{13}$ (top panel of Fig. 4.12), pulse $\mathbf{k}_2$ arrives first, and creates a LL0 polarization which evolves for time $\Delta t_{12}$ with frequency $\Omega_0$ and decay rate $\Gamma_0$. Pulses $\mathbf{k}_1$ and $\mathbf{k}_3$ arrive at $t = \Delta t_{12}$ and create the $M_1^{13}$ coherence, which is then probed by

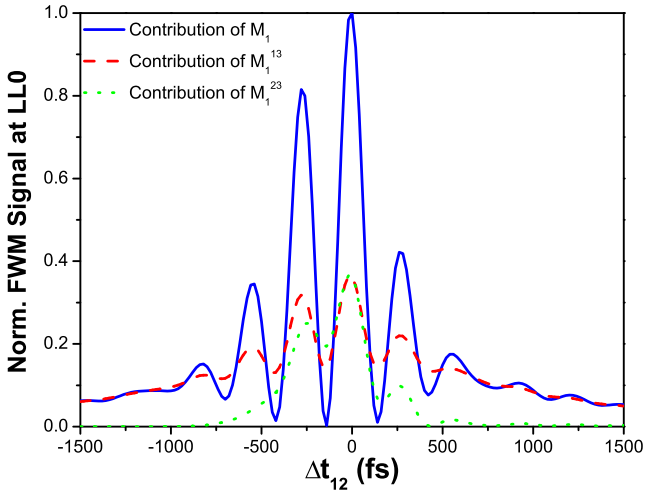


**Figure 4.11:** Numerical calculation of the FWM contributions of the $M_1$ (solid line), $M_1^{13}$ (dashed line), and $M_1^{23}$ (dotted line) coherences along the $\Delta t_{12}$ axis. It is clear that the oscillations are due to the interference between the signals of $M_1^{13}$ and $M_1^{23}$.

the decaying polarization created by pulse $\mathbf{k}_2$. The resulting FWM signal at LL0 is characterized by a relative phase of $\Omega_0 \Delta t_{12}$ and decays as $\Gamma_0 \Delta t_{12}$.

In the symmetric case that creates $M_1^{23}$ (bottom panel), pulse $\mathbf{k}_2$ creates a LL1 polarization, which evolves with frequency $\Omega_1$ and decay rate $\gamma_1$. At time $t = \Delta t_{12}$ pulses $\mathbf{k}_1$ and $\mathbf{k}_3$ arrive and create a LL0 and a LL1$^*$ polarization respectively. The decaying LL1 polarization from $\mathbf{k}_2$ and LL1$^*$ from $\mathbf{k}_3$ create the $M_1^{23}$ coherence, which is instantaneously probed by the LL0 polarization of $\mathbf{k}_1$. The resulting LL0 FWM signal has a relative phase of $\Omega_1 \Delta t_{12}$ and decay of $\gamma_1 \Delta t_{12}$. As a result the two contributions beat with each other with a frequency of $\Omega_1 - \Omega_0$ and a decay rate of $\Gamma_0 + \gamma_1$.

On the other hand, the negative $\Delta t_{12}$ axis gives us access to different information. Fig. 4.13 shows the creation of the two processes along this axis. Now pulses $\mathbf{k}_1$ and $\mathbf{k}_3$ arrive first and pulse $\mathbf{k}_2$ follows after time $t = |\Delta t_{12}|$. In the case of $M_0^{13}$ (top panel of Fig. 4.13), the two pulses create a LL1 and LL1$^*$ polarization respectively, which create the $M_1^{13}$ coherence. The latter evolves with a phase of $\bar{\Omega} - \Omega_1 \approx 0$ and its own decay rate $\gamma_{M_1}$. After time $t = |\Delta t_{12}|$, pulse $\mathbf{k}_2$ comes it and creates a LL0 polarization that probes the $M_0^{13}$ coherence. Thus, the LL0 signal in this case has (almost) no phase and decays as $-\gamma_{M_1} \Delta t_{12}$.

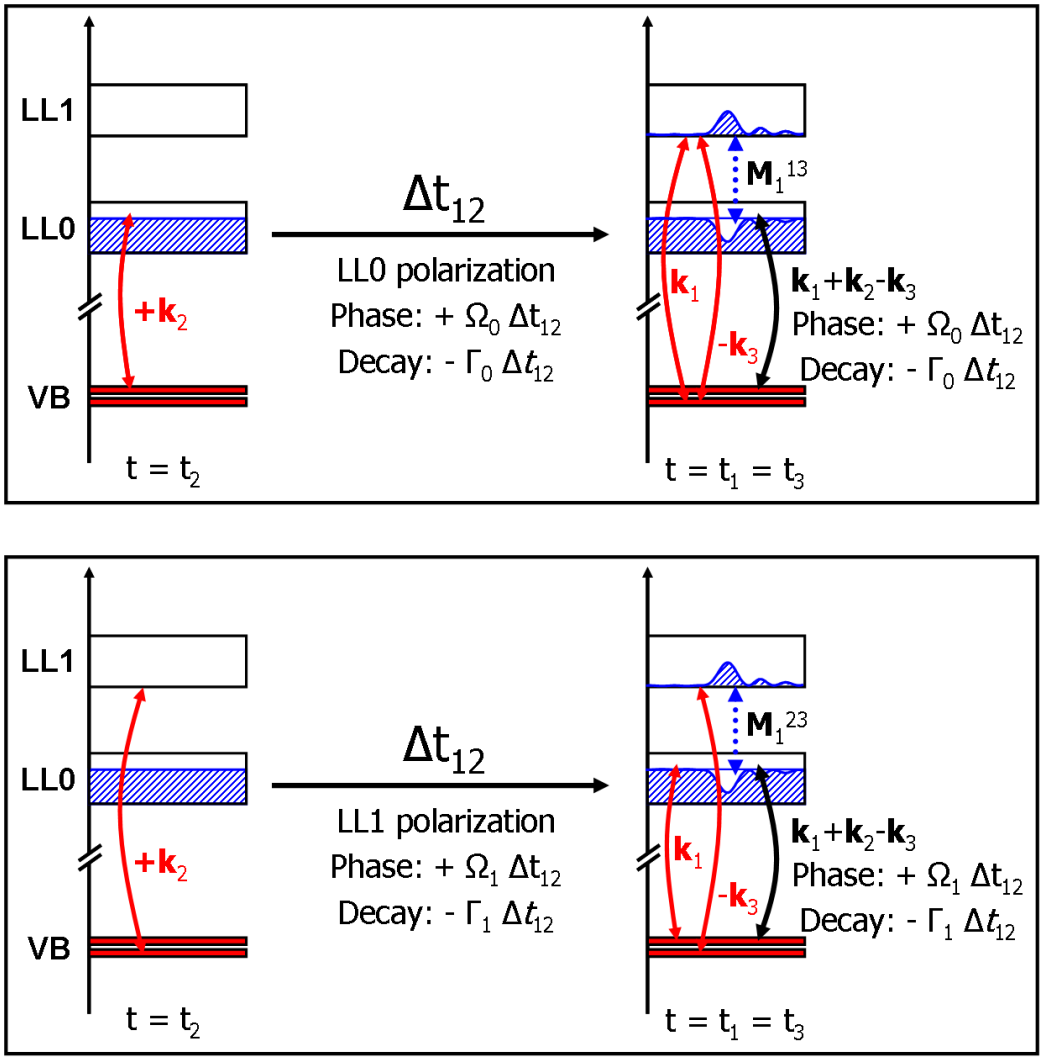


**Figure 4.12:** Schematic of the FWM processes that are responsible for the inter-LL oscillations along the $\Delta t_{12} > 0$ axis: The FWM contribution from the $M_1^{13}$ coherence (top panel) interferes with that of the $M_1^{23}$ (bottom panel). The two are symmetric processes obtained by exchanging the roles of $\mathbf{k}_1$ and $\mathbf{k}_2$. The superposition of the two results in inter-LL oscillations due to the different phase accumulated in the two processes during the $\Delta t_{12}$ time delay. The decay of the beats is thus $\Gamma_0 + \gamma_1$.

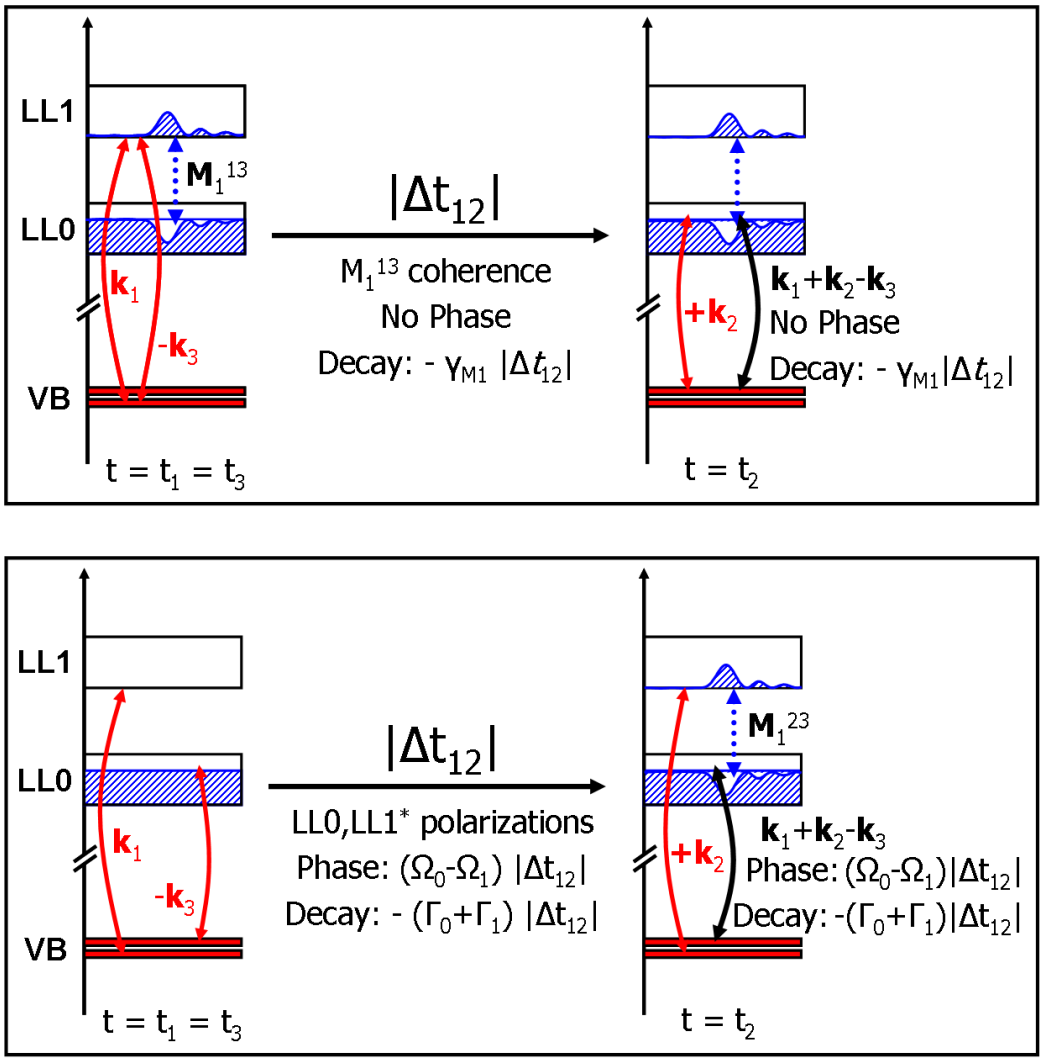


**Figure 4.13:** Schematic of the FWM processes that are responsible for the inter-LL oscillations along the $\Delta t_{12} < 0$ axis: The FWM contribution from the $M_1^{13}$ coherence (top panel) interferes with that of the $M_1^{23}$ (bottom panel). The two are symmetric processes obtained by exchanging the roles of $\mathbf{k}_1$ and $\mathbf{k}_2$. The superposition of the two results in inter-LL oscillations due to the different phase accumulated in the two processes during the $|\Delta t_{12}|$ time delay. The decay of the beats is thus $\Gamma_0 + \gamma_1 + \gamma_{M_1}$.

In the case of $M_1^{23}$ (bottom panel), pulses $\mathbf{k}_1$ and $\mathbf{k}_3$ create a LL0 and a LL1$^*$ polarization respectively, which evolve independently for a time $|\Delta t_{12}|$ each accumulating a phase of $\Omega_0 \Delta t_{12}$ and $-\Omega_1 \Delta t_{12}$ and a decay of $-\Gamma_0 |\Delta t_{12}|$ and $-\gamma_1 |\Delta t_{12}|$ respectively. Then pulse $\mathbf{k}_2$ arrives and contributes a LL1 polarization, which together with the LL1$^*$ polarization from $\mathbf{k}_3$ creates the $M_1^{23}$ coherence. Consequently, the two FWM contributions beat with frequency $\Omega_1 - \Omega_0$ and decay as $\Gamma_0 + \gamma_1 + \tilde{\gamma}_1 \approx \Gamma_0 + \gamma_1$. We thus conclude that $\tilde{\gamma}_1 \approx \gamma_{M_1} \ll (\Gamma_0 + \Gamma_1)$, i.e. the $X_1 \leftrightarrow$X+MP coherence $M_1$ dephases over a time interval of $1/\gamma_{M_1} \gg 1/(\Gamma_0 + \Gamma_1) \approx 300$fs.

## 4.6 Conclusions

In this chapter, we discussed a recent FWM experiment on the quantum Hall system, that showed a surpisingly large off-resonant signal at LL0 with strong oscillations. Using our theory, developed in Chapter 3, we derived an average polarization model and we calculated the LL0 FWM signal. We showed that the off-resonant signal is due to the X$\leftrightarrow$X+MP coherence $M_1 = \langle |X_1\rangle\langle Y| \rangle_c$. The observed oscillations are due to the interference of the two FWM processes that can create the $M_1$ coherence along the $\Delta t_{12}$ axis: $M_1$ can be created either by pulses $\mathbf{k}_1$ and $\mathbf{k}_3$, or by pulses $\mathbf{k}_2$ and $\mathbf{k}_3$. By comparing the decay of oscillations with our calculations, we are able to put an upper bound to the $M_1$ coherence decay rate.

In the following chapter, we will apply our theory in the case of an undoped quantum well in a large magnetic field. In this case, there is no 2DEG present in the ground state, but X$\leftrightarrow$X coherences are photoexcited and create interesting dynamics.

# Chapter 5

# Dynamics of coherences in an undoped quantum well

## 5.1 Outline

In the previous chapter, we discussed the nonlinear optical response of the quantum Hall system, and showed that we can access the dynamics of intraband coherences along the $\Delta t_{12}$ axis. This is not the case just for the quantum Hall system; it is a consequence of the configuration of pulses in any three–pulse FWM experiment. This opens the possibility of studying the dynamics of intraband coherences in other systems as well. Quantum coherences in general are at the heart of quantum mechanics and are central in determining the nonlinear optical properties of semiconductors and atomic systems. Raman coherences in three–level atomic systems lead to non-linear optical effects like electromagnetically induced transparency [116] and lasing without inversion [117]. In analogy to atomic systems, one would like to observe Raman coherences in semiconductors. In the past, quantum beats attributed to coherences between the heavy and light hole valence band continuum states have been observed in bulk GaAs [118]. Similarly, Raman coherences can be created in semiconductor quantum wells subject to a large perpendicular magnetic field. In this case, the quantum well confinement discretizes the eigenstates along the z-direction (growth direction). At the same time, the large B-field results in quasi-confinement in the x-y plane, thus discretizing the in-plane eigenstates into Landau levels. This discrete spectrum, similar to atomic systems, opens new possibilities for creating and controlling coherences.

Though similarities between atomic systems and semiconductors can be established, there are also important differences. Strong Coulomb interac-

tions exist between the optically excited states in semiconductors. This leads to novel effects like exciton-exciton scattering which have no analogue in atomic systems. The dynamics of coherences, like dephasing, result from the coupling of these optically excited states to other states or the environment. In a many-body system, it is not easy to treat such complex interactions theoretically. Thus measuring dynamical quantities like the dephasing rate is a valuable source of information on the behavior of complex systems. Moreover, if these coherences are long-lived, they are potentially useful in applications of quantum technology.

In this chapter, we will discuss the nonlinear response of an undoped quantum well in a perpendicular magnetic field. We will begin by describing the main results of a recent FWM experiment on this system in §5.2. In §5.3 we will present an average polarization model derived from the theory of Chapter 3, in the special case of no 2DEG carriers in the ground state. We will then present (§5.4) some simple analytical solutions, which in comparison with the experiment, will allow us to identify the signature of a Raman coherence and will extract its dephasing rate. Finally, in §5.5, we will present our numerical calculations and we will discuss the contributions of the different physical mechanisms to the nonlinear response of the undoped quantum well.

## 5.2 Experimental results

The sample under investigation is an undoped GaAs quantum well structure, which consists of 10 14 nm thick GaAs layers sandwiched between 10 nm thick layers of $Al_{0.3}Ga_{0.7}As$ [53]. The sample is kept at 1.5-4°K in a split-coil magneto-optical cryostat and a perpendicular magnetic field ($B = 0 - 7$ T) is applied along the growth direction of the quantum well. The system is photoexcited with three ∼100 fs pulses of right circularly polarized ($\sigma_+$) light. The experiment is similar to the one for the doped system, described in Refs. [45, 52] and §4.2. The pulses propagate in spatially distinct directions $\mathbf{k}_1$, $\mathbf{k}_2$ and $\mathbf{k}_3$ with a time delay $\Delta t_{12}$ ($\Delta t_{13}$) between pulse $\mathbf{k}_1$ and $\mathbf{k}_2$ ($\mathbf{k}_3$) (Fig. 2.6). For negative values of the above delays, pulse $\mathbf{k}_1$ arrives first. The signal is measured at the background–free direction $\mathbf{k}_1 + \mathbf{k}_2 - \mathbf{k}_3$ and is resolved with an interference filter to seperate the response from the LL0 and LL1 magnetoexcitons.

Fig. 5.1a shows the SR–FWM signal from LL0 and LL1 along the $\Delta t_{13}$ axis for mostly LL1 excitation. The back panel shows the linear absorption spectrum and pulse intensity. As expected, the LL1 signal is much larger than the one from LL0. For $\Delta t_{13} > 0$, both signals exhibit beatings at the

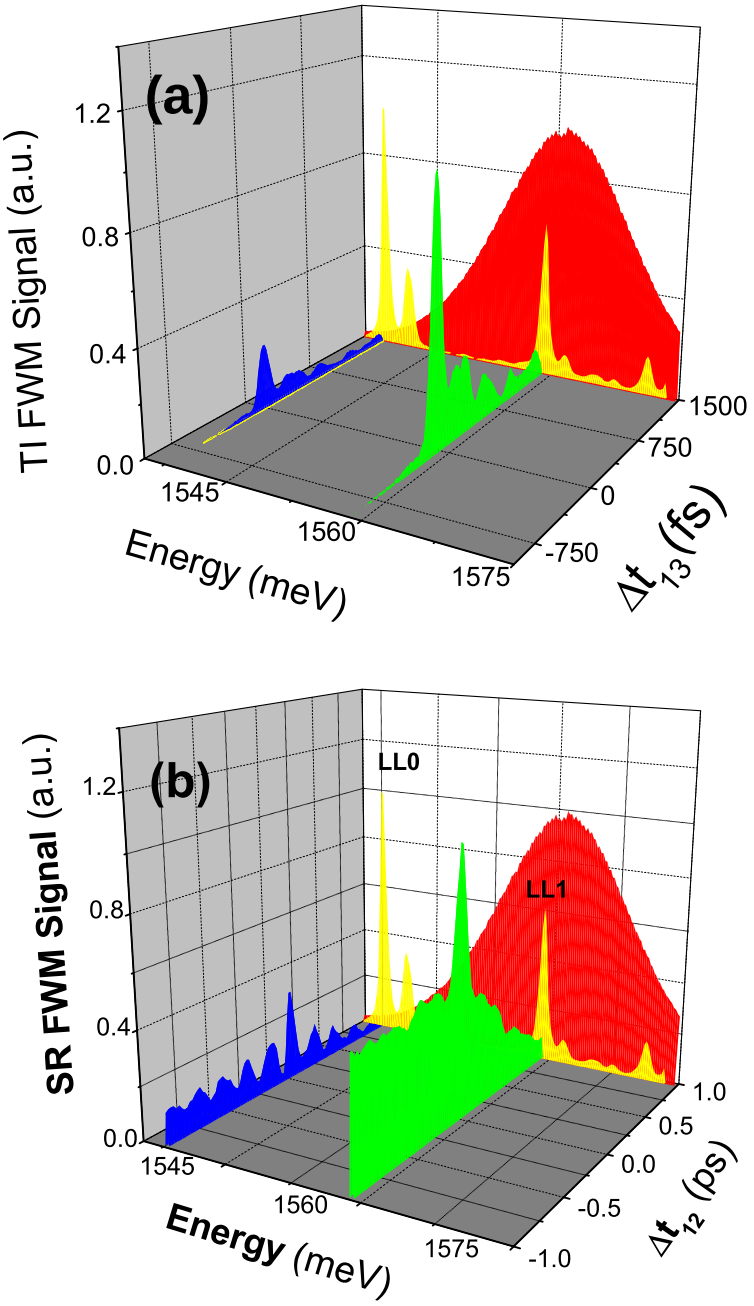


**Figure 5.1:** SR–FWM signal of the undoped quantum well along (a) the $\Delta t_{13}$ and (b) the $\Delta t_{12}$ axis, for mostly LL1 excitation. Back panel: Linear absorption spectrum and optical pulse intensity, showing the largely LL1 excitation conditions.

inter–LL frequency, which is also expected because of the interference of the two contributions. Along the negative axis, there are no oscillations and both signals decay much faster than along the positive axis. As discussed in §4.4.1, for $\Delta t_{13} < 0$ we access the dynamics of interband excitations, like polarizations and biexcitons. According to standard RPA theory, the decay rate for $\Delta t_{13} < 0$ is twice the decay rate along the positive axis [8]. Thus, any deviations from this asymmetric temporal profile are considered a signature of X–X correlations [2, 3].

Fig. 5.1b shows the LL0 and LL1 FWM signals along the $\Delta t_{12}$ axis for the same excitation conditions. Here we observe oscillations only in the LL0 signal, which are at the inter–LL energy, $\Omega_1 - \Omega_0$, measured from the linear absorption spectrum (back panel of Fig. 5.1). As discussed in §4.4.2, the positive and negative $\Delta t_{12}$ axes reflect different dynamics and thus, we analyse the decay rates seperately for the two halves. We substract a constant (exponential) background from the negative (positive) axis and take a Fourier transform of the signal. In both cases we see a strong peak at the $\Omega_1 - \Omega_0$ energy. However, there is a large difference in the linewidth for the two cases (as obtained by fitting a Lorentzian to the peak): 2.9 meV for the negative side vs. 5.6 meV for the positive. This indicates that the beats decay slower on the negative side. This will allow us to identify the decay rate of an X–X coherence created in the system. In the following, we will discuss an average polarization model derived from the theory of Chapter 3 for the case of the undoped system, which we will use to explain the above experimental results.

## 5.3 Average Polarization Model

### 5.3.1 Linear response

The linear response of the undoped quantum well is determined by the linear polarizations $P_n^L$ created in the system, described by Eq. (3.50). If we retain only the photoexcited LLs, LL0 and LL1, we end up with the following two equations of motion

$$i\partial_t P_0^L = (\Omega_0 - i\Gamma_0)P_0^L - V_{01}P_1^L - \mu E(t) \tag{5.1}$$

$$i\partial_t P_1^L = (\Omega_1 - i\Gamma_1)P_1^L - V_{10}P_0^L - \mu E(t) \tag{5.2}$$

where $\Gamma_n$ is the LL$n$ exciton decay rate, $\Omega_n$ is the exciton energy, $V_{nm}$ the inter–LL Coulomb induced coupling.

In the ideal system, exciton energies and inter–LL couplings can be easily

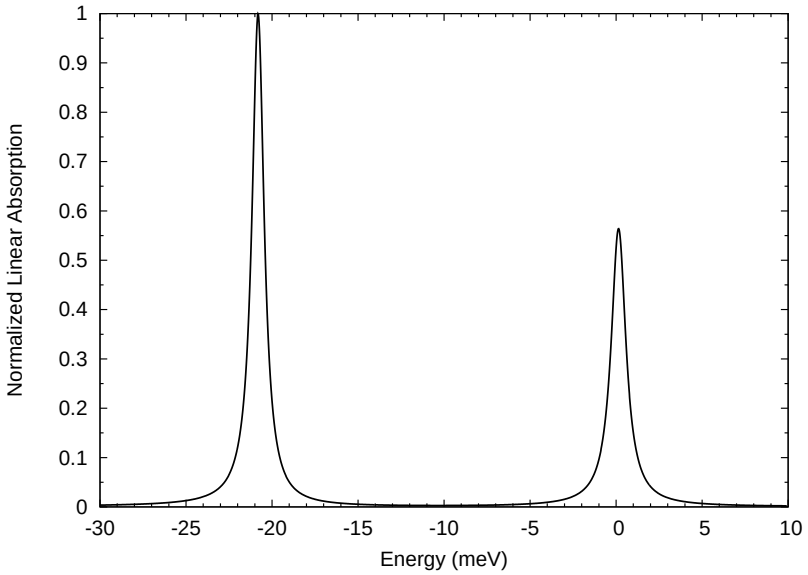


**Figure 5.2:** 3Numerical calculation of the linear absorption spectrum of the undoped quantum well that fits the $B = 7$ T data of Ref. [119], p. 60. Parameters used: $\Omega_1 - \Omega_0 = 20.9$ meV, $V_{01} = 1.4$ meV, $\Gamma_0 = 0.44$ meV and $\Gamma_1 = 0.6$ meV.

calculated analytically, using Eqs. (3.23) and (3.24):

$$\Omega_n = E_g + (n + 1/2)(\Omega_c^c + \Omega_c^v) - \int \frac{d\mathbf{q}}{(2\pi)^2} |\phi_{nn}(\mathbf{q})|^2 \tag{5.3}$$

$$\Rightarrow \Omega_1 - \Omega_0 = \Omega_c^c + \Omega_c^v - \frac{1}{4}\sqrt{\frac{\pi}{2}}\frac{e^2}{\epsilon\ell} \tag{5.4}$$

$$V_{nm} = \int \frac{d\mathbf{q}}{(2\pi)^2} |\phi_{nm}(\mathbf{q})|^2 \Rightarrow V_{01} = V_{10} = \frac{1}{2}\sqrt{\frac{\pi}{2}}\frac{e^2}{\epsilon\ell} \tag{5.5}$$

For $B = 7$ T, we obtain from the above expressions and Eq. (2.14) that $\Omega_1 - \Omega_0 = 18$ meV and $V_{01} = 7.21$ meV. However, here we use parameters that fit the experimentally measured linear absorption spectrum Ref. [119], since it is affected by higher LLs [85] that are not included here.

### 5.3.2 Nonlinear response

To describe the ultrafast nonlinear response of magnetoexcitons in the undoped system, we will use the theory of Chapter 3, in the special case of no ground state carriers. Since there is no 2DEG present, $\hat{Y}_n^\dagger|G\rangle = 0$ and $\hat{Y}_n = \hat{Y}_n^{\rm int}$ (Eqs. (3.29) and (3.27)) describes X–X interaction effects. In this case, our theory coincides with the DCTS, if phonons are included.

By retaining only the photoexcited states $|X_0\rangle$ and $|X_1\rangle$ and expanding the intraband matrix $\langle\hat{M}_n\rangle$ on the basis of X–X coherences and densities $\langle|X_n\rangle\langle X_m|\rangle$ $(n,m=0,1)$, we obtain the following equations of motion for the polarizations:

$$\begin{aligned} i\partial_t P_0 - (\Omega_0 - i\Gamma_0)P_0 + V_{01}P_1 &= 2\mu E(t)\left(P_0^L P_0^{L*} + N_0\right) \\ &- 2V_{01}\left[P_0^L\left(N_1 - N_{10}\right) - P_1^L\left(N_0 - N_{01}\right)\right] \\ &- 2V_{01}\left(P_1^L P_0^L + B_{10}^{01} + B_{01}^{01} + B_{10}^{10}\right)\left(P_1^{L*} - P_0^{L*}\right) \end{aligned} \tag{5.6}$$

$$\begin{aligned} i\partial_t P_1 - (\Omega_1 - i\Gamma_1)P_1 + V_{10}P_0 &= 2\mu E(t)\left(P_1^L P_1^{L*} + N_1\right) \\ &+ 2V_{10}\left[P_0^L\left(N_1 - N_{10}\right) - P_1^L\left(N_0 - N_{01}\right)\right] \\ &+ 2V_{10}\left(P_1^L P_0^L + B_{10}^{01} + B_{01}^{01} + B_{10}^{10}\right)\left(P_1^{L*} - P_0^{L*}\right) \end{aligned} \tag{5.7}$$

The first term in the right–hand side of Eqs. (5.6) and (5.7) describes phase space filling effects, while the second one describes the contributions of incoherent densities $N_n$ and intraband coherences $N_{nm}$, defined in Eqs. (4.3) and (4.4) respectively. The last term is the contribution of mean field X–X interactions and X–X correlations, described by $B_{nm}^{n'm'}$ (Eq. (3.6)).

The dynamics of the incoherent densities $N_n = \langle|X_n\rangle\langle X_n|\rangle_c$ is described by Eq. (6.30) without the contribution of the X–X+MP coherences $M_n = \langle|X_n\rangle\langle Y|\rangle_c$:

$$i\partial_t N_0 = -i\gamma_D N_0 + V_{10}N_{01} - V_{01}N_{10} + i(2\Gamma_0 - \gamma_D)P_0^L P_0^{L*} \tag{5.8}$$

$$i\partial_t N_1 = -i\gamma_D N_1 + V_{01}N_{10} - V_{10}N_{01} + i(2\Gamma_1 - \gamma_D)P_1^L P_1^{L*} \tag{5.9}$$

where $\gamma_D$ is the density decay rate, and $N_{10} = N_{01}^*$ is the $X_0$–$X_1$ coherence described by

$$i\partial_t N_{10} = (\Omega_1 - \Omega_0 - i\gamma_{10})N_{10} + V_{10}N_1 - V_{10}N_0 + i(\Gamma_0 + \Gamma_1 - \gamma_{10})P_1^L P_0^{L*} \tag{5.10}$$

where again $\gamma_{10}$ is the coherence decay rate.

Finally, X–X correlations are described by the following equations of motion, derived from Eq. (3.76):

$$i\partial_t B_{01}^{01} = \left(\Omega_{01} - i\gamma_{01}^{01}\right)B_{01}^{01} + W_B\left(P_0^L - P_1^L\right)^2 \tag{5.11}$$

$$i\partial_t B_{10}^{10} = \left(\Omega_{10} - i\gamma_{10}^{10}\right)B_{10}^{10} + W_B\left(P_0^L - P_1^L\right)^2 \tag{5.12}$$

$$i\partial_t B_{10}^{01} = \left(\Omega_{10}^{01} - i\gamma_{10}^{01}\right)B_{10}^{01} + 2W_B\left(P_0^L - P_1^L\right)^2 + i(\Gamma_0 + \Gamma_1 - \gamma_{10}^{01})P_0^L P_1^L \tag{5.13}$$

where $W_B = \langle B_{01}^{01}|B_{01}^{01}\rangle = \langle B_{10}^{10}|B_{10}^{10}\rangle$, verified easily from the definition of $B_{01}^{01}$ and $B_{10}^{10}$, given in Eq. (3.75). Using these definitions and Eqs. (3.4), (3.6) and (A.1), it is straightforward to calculate $W_B$ analytically:

$$W_B = \frac{1}{(\pi\ell^2 N)^2}\sum_{\mathbf{q}} v_q^2|\phi_{10}(\mathbf{q})|^2 = \frac{1}{2N}\left(\frac{e^2}{\epsilon\ell}\right)^2 \tag{5.14}$$

$\Omega_{nm}^{n'm'}$ and $\gamma_{nm}^{n'm'}$ are the energy and the decay rate of the correlated X–X amplitude $B_{nm}^{n'm'}$, respectively. Since e.g. $B_{01}^{01}$ describes a $\{$2–LL0–$e$ + 2–LL1–$h\}$ state, it is expected that it is amost resonant with two LL0 exciton states, i.e. $\Omega_{01}^{01} \simeq 2\Omega_0$. Similarly, $\Omega_{10}^{10} \simeq 2\Omega_1$, and $\Omega_{10}^{01} \simeq \Omega_0 + \Omega_1$.

## 5.4 Simple analytical solutions

As explained in §4.4, simple analytical solutions of the equations of motion of our model are particularly useful. They allow us to distinguish the signatures of the different physical mechanisms that contribute to the nonlinear response of the system. Thus, by comparing to experiment we can understand which processes dominate the FWM signal. Here, we will present our analytical solutions for Eqs. (5.6)–(5.13) that describe the third–order response of the undoped quantum well. As in §4.4, we assume delta pulses and ignore all non–resonant terms in our equations.

Tables 5.1 and 5.2 list the LL0 and LL1 contributions of PSF, incoherent densities and intraband coherences, as well as X–X interactions and correlations along the positive and negative $\Delta t_{13}$ axis. For $\Delta t_{13} > 0$, all contributions decay with the polarizations decay rate, which is expected since in this case pulse $\mathbf{k}_3$ arrives first and can only create a polarization that will decay until pulses $\mathbf{k}_1$ and $\mathbf{k}_2$ come in (see e.g. Fig. 4.5 or Fig. 5.3 where the creation of the $B_{10}^{01}$ excitation is depicted as an example). On the other hand, for $\Delta t_{13} < 0$, we access different dynamics. PSF does not contribute for negative time delays, in agreement with RPA [12]. The contributions of intraband coherences and mean–field X–X interactions decay as $2(\Gamma_0 + \Gamma_1)$, which is about twice as fast as the decay of their contributions along the positive $\Delta t_{13}$ axis, assuming that $\Gamma_0 \simeq \Gamma_1$ in the undoped system. This is also in agreement with the Hartree–Fock treetment of X–X interactions [8]. However, the contributions of 2X excitations decay with their own decay rates. This is illustrated in Fig. 5.4 where a schematic of the contribution of the $B_{10}^{01}$ excitation to the LL0 signal is shown. When $\Delta t_{13} < 0$, pulses $\mathbf{k}_1$ and $\mathbf{k}_2$ arrive first and create the $B_{10}^{01}$ excitation, which then evolves for time $t = |\Delta t_{13}|$ with its own frequency $\Omega_{10}^{01}$ and decay rate $\gamma_{10}^{01}$, until it is probed

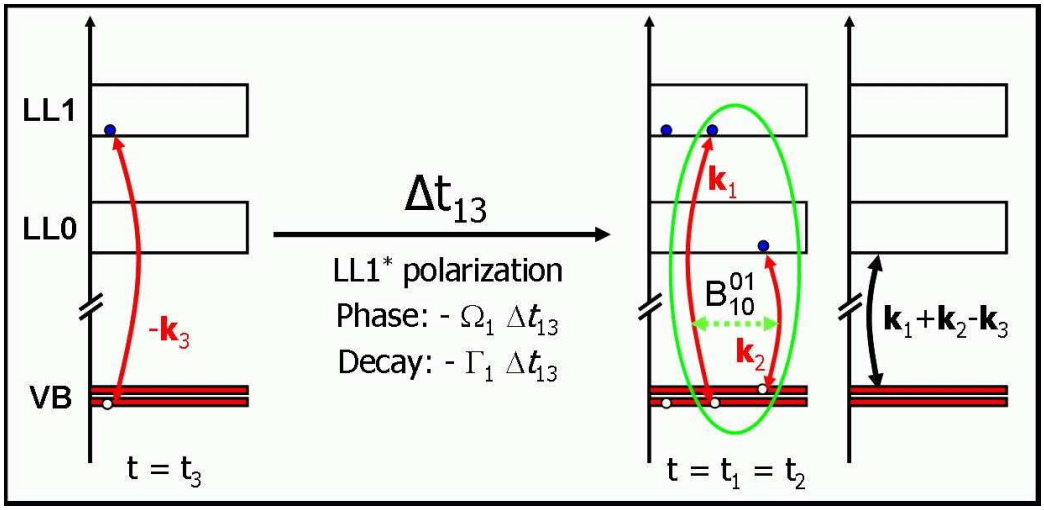


**Figure 5.3:** Dynamics of the interband 2X excitation $B_{10}^{01}$ along the $\Delta t_{13} > 0$ axis: pulse $\mathbf{k}_3$ arrives first and creates a LL1$^*$ polarization which evolves for time $t = \Delta t_{13}$ and accumulates a phase of $\Omega_1 \Delta t_{13}$ and decays as $-\Gamma_1 \Delta t_{13}$. Pulses $\mathbf{k}_1$ and $\mathbf{k}_2$ then arrive and create the 2X excitation $B_{10}01$, which describes the 4–particle $\{1\text{–LL0–}e + 1\text{–LL1–}e + 1\text{–LL0–}h + 1\text{–LL1–}h\}$ state, and is probed instantly by the decaying LL1$^*$ polarization. Thus the resulting FWM signal reflects the phase $\Omega_1 \Delta t_{13}$ and the decay $-\Gamma_1 \Delta t_{13}$.

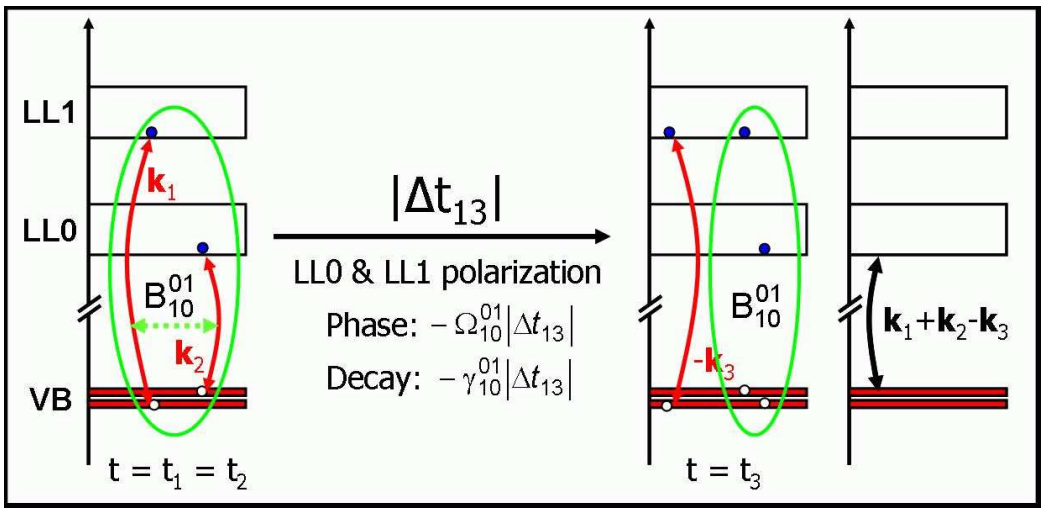


**Figure 5.4:** Dynamics of the interband 2X excitation $B_{10}^{01}$ along the $\Delta t_{13} < 0$ axis: pulses $\mathbf{k}_1$ and $\mathbf{k}_2$ arrive together and create the 2X excitation $B_{10}^{01}$. The excitation evolves for time $t = |\Delta t_{13}|$ during which it accumulates a phase of $(\Omega_{10}^{01} - \Omega_0)|\Delta t_{13}| \simeq \Omega_1 |\Delta t_{13}|$ and decays as $-\gamma_{10}^{01}|\Delta t_{13}|$. Pulse $\mathbf{k}_3$ then arrives and produces the FWM signal, which reflects the phase $\sim \Omega_1 |\Delta t_{13}|$ and the decay $-\gamma_{10}^{01}|\Delta t_{13}|$.

Contributions to $P_0(\Omega_0)$ along the $\Delta t_{13}$ axis

| Term | if $\Delta t_{13} > 0$ | if $\Delta t_{13} < 0$ |
|---|---|---|
| $E(t)P_0^L P_0^{L*}$ | $e^{i\Omega_0 \Delta t_{13}} e^{-\Gamma_0 \Delta t_{13}}$ | 0 |
| $E(t)N_0$ | $e^{i\Omega_0 \Delta t_{13}} e^{-\Gamma_0 \Delta t_{13}}$ | 0 |
| $P_0^L N_1$ | $e^{i\Omega_1 \Delta t_{13}} e^{-\Gamma_1 \Delta t_{13}}$ | $e^{i\Omega_1 \Delta t_{13}} e^{(\Gamma_0+\Gamma_1) \Delta t_{13}}$ |
| $P_1^L N_{01}$ | $e^{i\Omega_1 \Delta t_{13}} e^{-\Gamma_1 \Delta t_{13}}$ | $e^{i\Omega_1 \Delta t_{13}} e^{(\Gamma_0+\Gamma_1) \Delta t_{13}}$ |
| $P_0^L P_1^L P_1^{L*}$ | $e^{i\Omega_1 \Delta t_{13}} e^{-\Gamma_1 \Delta t_{13}}$ | $e^{i\Omega_1 \Delta t_{13}} e^{(\Gamma_0+\Gamma_1) \Delta t_{13}}$ |
| $B_{01}^{01} P_0^{L*}$ | $e^{i\Omega_0 \Delta t_{13}} e^{-\Gamma_0 \Delta t_{13}}$ | $e^{i\Omega_0 \Delta t_{13}} e^{2\Gamma_0 \Delta t_{13}}$<br>$e^{i\Omega_0 \Delta t_{13}} e^{\gamma_{01}^{01} \Delta t_{13}}$ |
| $B_{10}^{01} P_1^{L*}$ | $e^{i\Omega_1 \Delta t_{13}} e^{-\Gamma_1 \Delta t_{13}}$ | $e^{i\Omega_1 \Delta t_{13}} e^{(\Gamma_0+\Gamma_1) \Delta t_{13}}$<br>$e^{i\Omega_1 \Delta t_{13}} e^{\gamma_{10}^{01} \Delta t_{13}}$ |

**Table 5.1:** Contributions of the resonant terms in the equation of motion Eq. (5.6) to the LL0 third order polarization $P_0(\omega = \Omega_0)$ along the $\Delta t_{13}$ axis ($\Delta t_{12} = 0$) for the undoped quantum well. The first two terms describe Pauli blocking (PSF), the next two are the contributions of incoherent densities and X–X coherences, while the last three are the contributions of X–X interactions and correlations. For simplicity we assumed $\Omega_{01}^{01} \simeq 2\Omega_0$ and $\Omega_{10}^{01} \simeq \Omega_0 + \Omega_1$.

from pulse $\mathbf{k}_3$. Thus, the resulting FWM signal reflects the frequency and decay rate of the 2X excitation. In the experiment (Fig. 5.1), both LL0 and LL1 signals decay faster that $2(\Gamma_0 + \Gamma_1)$ for $\Delta t_{13} < 0$. We thus conclude that biexcitonic contributions cannot decay more slowly.

Tables 5.3 and 5.4 show the LL0 and LL1 contributions along the positive and negative $\Delta t_{12}$ axis. Along this axis, there two FWM contributions for every process, because of the symmetry between pulses $\mathbf{k}_1$ and $\mathbf{k}_2$. For $\Delta t_{12} > 0$, all contributions decay with the decay rates of the polarizations, as expected. Along the negative $\Delta t_{12}$, we access the dynamics of intraband coherences and densities, as explained in §4.4.2.

To understand the origin of the oscillations in the LL0 signal, we note that for $\Delta t_{12} > 0$ the oscillations between any terms beat at the inter–LL energy, $\Omega_1 - \Omega_0$, and decay with rate $\Gamma_0 + \Gamma_1$. Thus, by comparing to experiment we conclude that $\Gamma_0 + \Gamma_1 = 5.6$ meV. For $\Delta t_{12} < 0$, the observed decay of the oscillations is slower than for $\Delta t_{12} > 0$, i.e. slower than $\Gamma_0 + \Gamma_1$. The only possibility of such oscillations is, as shown from Table 5.3, the case of beatings between the contributions of the incoherent density $N_1$ ($P_0^L N_1^{13}$), and the X–X coherence $N_{01}$ ($P_1^L N_{01}^{13}$), which decay as

Contributions to $P_1(\Omega_1)$ along the $\Delta t_{13}$ axis

| Term | if $\Delta t_{13} > 0$ | if $\Delta t_{13} < 0$ |
|---|---|---|
| $E(t)P_1^L P_1^{L*}$ | $e^{i\Omega_1 \Delta t_{13}} e^{-\Gamma_1 \Delta t_{13}}$ | 0 |
| $E(t)N_1$ | $e^{i\Omega_1 \Delta t_{13}} e^{-\Gamma_1 \Delta t_{13}}$ | 0 |
| $P_0^L N_{10}$ | $e^{i\Omega_0 \Delta t_{13}} e^{-\Gamma_0 \Delta t_{13}}$ | $e^{i\Omega_0 \Delta t_{13}} e^{(\Gamma_0+\Gamma_1) \Delta t_{13}}$ |
| $P_1^L N_0$ | $e^{i\Omega_0 \Delta t_{13}} e^{-\Gamma_0 \Delta t_{13}}$ | $e^{i\Omega_0 \Delta t_{13}} e^{(\Gamma_0+\Gamma_1) \Delta t_{13}}$ |
| $P_1^L P_0^L P_0^{L*}$ | $e^{i\Omega_0 \Delta t_{13}} e^{-\Gamma_0 \Delta t_{13}}$ | $e^{i\Omega_0 \Delta t_{13}} e^{(\Gamma_0+\Gamma_1) \Delta t_{13}}$ |
| $B_{10}^{10} P_1^{L*}$ | $e^{i\Omega_1 \Delta t_{13}} e^{-\Gamma_1 \Delta t_{13}}$ | $e^{i\Omega_1 \Delta t_{13}} e^{2\Gamma_1 \Delta t_{13}}$<br>$e^{i\Omega_1 \Delta t_{13}} e^{\gamma_{10}^{10} \Delta t_{13}}$ |
| $B_{10}^{01} P_0^{L*}$ | $e^{i\Omega_0 \Delta t_{13}} e^{-\Gamma_0 \Delta t_{13}}$ | $e^{i\Omega_0 \Delta t_{13}} e^{(\Gamma_0+\Gamma_1) \Delta t_{13}}$<br>$e^{i\Omega_0 \Delta t_{13}} e^{\gamma_{10}^{01} \Delta t_{13}}$ |

**Table 5.2:** Contributions of the resonant terms in the equation of motion Eq. (5.6) to the LL1 third order polarization $P_1(\omega = \Omega_1)$ along the $\Delta t_{13}$ axis ($\Delta t_{12} = 0$) for the undoped quantum well. The first two terms describe Pauli blocking (PSF), the next two are the contributions of incoherent densities and X–X coherences, while the last three are the contributions of X–X interactions and correlations. For simplicity we assumed $\Omega_{10}^{10} \simeq 2\Omega_1$ and $\Omega_{10}^{01} \simeq \Omega_0 + \Omega_1$.

$\gamma_D + \gamma_{10}$. Moreover, since the lifetime of the incoherent density decays very slowly, $\gamma_D + \gamma_{10} \simeq \gamma_{10} = 2.9$ meV. Thus, we conclude that the longest lasting oscillations are due to beatings between the incoherent density and the X–X coherence the lifetime of which is of the order of $1/2.9$ meV$^{-1} \simeq 200$ fs.

## 5.5 Numerical calculations

In this section we discuss the results of our numerical calculations, where we solve Eqs. (5.6)–(5.13) with no further approximations. Fig. 5.5 shows our calculation for the LL0 and LL1 FWM signals along the $\Delta t_{13}$ and $\Delta t_{12}$ axes with a long density decay rate $\gamma_D = 0.08$ meV, short decay rates for biexcitonic contributions ($\gamma_{01}^{01} \simeq \gamma_{10}^{10} \simeq \gamma_{10}^{01} \simeq 2$ meV) and $\gamma_{10} = 0.75$ meV, so that $\gamma_D \ll \gamma_{10} < \Gamma_0 + \Gamma_1 \simeq 1$ meV. Our calculation captures the qualitative features of the experiment (Fig. 5.1).

Fig. 5.6 shows the contributions of the different terms to the LL0 and LL1 signals along the $\Delta t_{13}$ axis. As expected from the photoexcitation conditions, PSF contributes significantly to LL1 while it is negligible for the LL0 signal. X–X interactions are significant mostly for $\Delta t_{13} < 0$ where PSF is zero, while

Contributions to $P_0(\Omega_0)$ along the $\Delta t_{12}$ axis

| Term | if $\Delta t_{12} > 0$ | if $\Delta t_{12} < 0$ |
|---|---|---|
| $E(t)\ P_0^L(t+\Delta t_{12})\ P_0^{L*}$ | $e^{-i\Omega_0\Delta t_{12}}e^{-\Gamma_0\Delta t_{12}}$ | 0 |
| $E(t+\Delta t_{12})\ P_0^L(t)\ P_0^{L*}$ | 0 | $e^{-i\Omega_0\Delta t_{12}}e^{2\Gamma_0\Delta t_{12}}$ |
| $E(t)\ N_0^{23}$ | $e^{-i\Omega_0\Delta t_{12}}e^{-\Gamma_0\Delta t_{12}}$ | 0 |
| $E(t+\Delta t_{12})\ N_0^{13}$ | 0 | $e^{-i\Omega_0\Delta t_{12}}e^{2\Gamma_0\Delta t_{12}}$<br>$e^{-i\Omega_0\Delta t_{12}}e^{\gamma_D\Delta t_{12}}$ |
| $P_0^L(t)\ N_1^{23}$ | $e^{-i\Omega_1\Delta t_{12}}e^{-\Gamma_1\Delta t_{12}}$ | $e^{-i\Omega_1\Delta t_{12}}e^{(\Gamma_0+\Gamma_1)\Delta t_{12}}$ |
| $P_0^L(t+\Delta t_{12})\ N_1^{13}$ | $e^{-i\Omega_0\Delta t_{12}}e^{-\Gamma_0\Delta t_{12}}$ | $e^{-i\Omega_0\Delta t_{12}}e^{2\Gamma_1\Delta t_{12}}$<br>$e^{-i\Omega_0\Delta t_{12}}e^{\gamma_D\Delta t_{12}}$ |
| $P_1^L(t)\ N_{01}^{23}$ | $e^{-i\Omega_0\Delta t_{12}}e^{-\Gamma_0\Delta t_{12}}$ | $e^{-i\Omega_0\Delta t_{12}}e^{2\Gamma_1\Delta t_{12}}$ |
| $P_1^L(t+\Delta t_{12})\ N_{01}^{13}$ | $e^{-i\Omega_1\Delta t_{12}}e^{-\Gamma_1\Delta t_{12}}$ | $e^{-i\Omega_1\Delta t_{12}}e^{(\Gamma_0+\Gamma_1)\Delta t_{12}}$<br>$e^{-i\Omega_1\Delta t_{12}}e^{\gamma_{10}\Delta t_{12}}$ |
| $P_0^L(t)\ P_1^L(t+\Delta t_{12})\ P_1^{L*}$ | $e^{-i\Omega_1\Delta t_{12}}e^{-\Gamma_1\Delta t_{12}}$ | $e^{-i\Omega_1\Delta t_{12}}e^{(\Gamma_0+\Gamma_1)\Delta t_{12}}$ |
| $P_0^L(t+\Delta t_{12})\ P_1^L(t)\ P_1^{L*}$ | $e^{-i\Omega_0\Delta t_{12}}e^{-\Gamma_0\Delta t_{12}}$ | $e^{-i\Omega_0\Delta t_{12}}e^{2\Gamma_1\Delta t_{12}}$ |
| $B_{01}^{01}\ P_0^{L*}$ | $e^{-i\Omega_0\Delta t_{12}}e^{-\Gamma_0\Delta t_{12}}$ | $e^{-i\Omega_0\Delta t_{12}}e^{2\Gamma_0\Delta t_{12}}$ |
| $B_{10}^{01}\ P_1^{L*}$ | $e^{-i\Omega_0\Delta t_{12}}e^{-\Gamma_0\Delta t_{12}}$<br>$e^{-i\Omega_1\Delta t_{12}}e^{-\Gamma_1\Delta t_{12}}$ | $e^{-i\Omega_0\Delta t_{12}}e^{2\Gamma_1\Delta t_{12}}$<br>$e^{-i\Omega_1\Delta t_{12}}e^{(\Gamma_0+\Gamma_1)\Delta t_{12}}$ |

**Table 5.3:** Contributions of the resonant terms in the equation of motion Eq. (5.6) to the LL0 third order polarization $P_0(\omega = \Omega_0)$ along the $\Delta t_{12}$ axis ($\Delta t_{13} = 0$) for the undoped quantum well. The terms in the first block describe Pauli blocking (PSF), the ones in the second are the contributions of X populations and X–X intraband coherences, while the last block includes the contributions of X–X interactions and correlations.

Contributions to $P_1(\Omega_1)$ along the $\Delta t_{12}$ axis

| Term | if $\Delta t_{12} > 0$ | if $\Delta t_{12} < 0$ |
|---|---|---|
| $E(t)\ P_1^L(t+\Delta t_{12})\ P_1^{L*}$ | $e^{-i\Omega_1\Delta t_{12}}e^{-\Gamma_1\Delta t_{12}}$ | 0 |
| $E(t+\Delta t_{12})\ P_1^L(t)\ P_1^{L*}$ | 0 | $e^{-i\Omega_1\Delta t_{12}}e^{2\Gamma_1\Delta t_{12}}$ |
| $E(t)\ N_1^{23}$ | $e^{-i\Omega_1\Delta t_{12}}e^{-\Gamma_1\Delta t_{12}}$ | 0 |
| $E(t+\Delta t_{12})\ N_1^{13}$ | 0 | $e^{-i\Omega_1\Delta t_{12}}e^{2\Gamma_1\Delta t_{12}}$<br>$e^{-i\Omega_1\Delta t_{12}}e^{\gamma_D\Delta t_{12}}$ |
| $P_0^L(t)\ N_{10}^{23}$ | $e^{-i\Omega_1\Delta t_{12}}e^{-\Gamma_1\Delta t_{12}}$ | $e^{-i\Omega_1\Delta t_{12}}e^{2\Gamma_0\Delta t_{12}}$ |
| $P_0^L(t+\Delta t_{12})\ N_{10}^{13}$ | $e^{-i\Omega_0\Delta t_{12}}e^{-\Gamma_0\Delta t_{12}}$ | $e^{-i\Omega_0\Delta t_{12}}e^{(\Gamma_0+\Gamma_1)\Delta t_{12}}$<br>$e^{-i\Omega_0\Delta t_{12}}e^{\gamma_{10}\Delta t_{12}}$ |
| $P_1^L(t)\ N_0^{23}$ | $e^{-i\Omega_0\Delta t_{12}}e^{-\Gamma_0\Delta t_{12}}$ | $e^{-i\Omega_0\Delta t_{12}}e^{(\Gamma_0+\Gamma_1)\Delta t_{12}}$ |
| $P_1^L(t+\Delta t_{12})\ N_0^{13}$ | $e^{-i\Omega_1\Delta t_{12}}e^{-\Gamma_1\Delta t_{12}}$ | $e^{-i\Omega_1\Delta t_{12}}e^{2\Gamma_0\Delta t_{12}}$<br>$e^{-i\Omega_1\Delta t_{12}}e^{\gamma_D\Delta t_{12}}$ |
| $P_1^L(t)\ P_0^L(t+\Delta t_{12})\ P_0^{L*}$ | $e^{-i\Omega_0\Delta t_{12}}e^{-\Gamma_0\Delta t_{12}}$ | $e^{-i\Omega_0\Delta t_{12}}e^{(\Gamma_0+\Gamma_1)\Delta t_{12}}$ |
| $P_1^L(t+\Delta t_{12})\ P_0^L(t)\ P_0^{L*}$ | $e^{-i\Omega_1\Delta t_{12}}e^{-\Gamma_1\Delta t_{12}}$ | $e^{-i\Omega_1\Delta t_{12}}e^{2\Gamma_0\Delta t_{12}}$ |
| $B_{10}^{10}\ P_1^{L*}$ | $e^{-i\Omega_1\Delta t_{12}}e^{-\Gamma_1\Delta t_{12}}$ | $e^{-i\Omega_1\Delta t_{12}}e^{2\Gamma_1\Delta t_{12}}$ |
| $B_{10}^{01}\ P_0^{L*}$ | $e^{-i\Omega_0\Delta t_{12}}e^{-\Gamma_0\Delta t_{12}}$<br>$e^{-i\Omega_1\Delta t_{12}}e^{-\Gamma_1\Delta t_{12}}$ | $e^{-i\Omega_1\Delta t_{12}}e^{2\Gamma_0\Delta t_{12}}$<br>$e^{-i\Omega_0\Delta t_{12}}e^{(\Gamma_0+\Gamma_1)\Delta t_{12}}$ |

**Table 5.4:** Contributions of the resonant terms in the equation of motion Eq. (5.7) to the LL1 third order polarization $P_1(\omega = \Omega_1)$ along the $\Delta t_{12}$ axis ($\Delta t_{13} = 0$) for the undoped quantum well. The terms in the first block describe Pauli blocking (PSF), the ones in the second are the contributions of X populations and X–X intraband coherences, while the last block includes the contributions of X–X interactions and correlations.

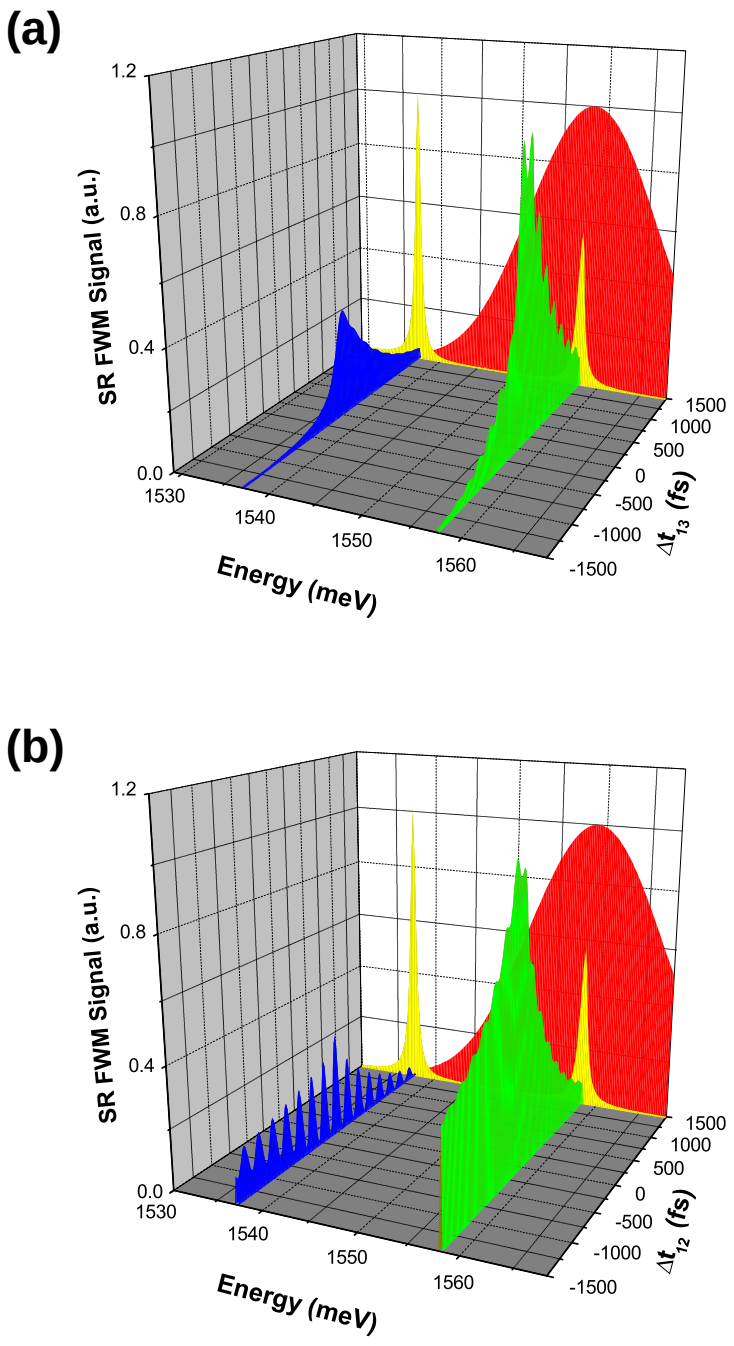


**Figure 5.5:** Calculated FWM signal from the undoped quantum well along (a) the $\Delta t_{13}$ and (b) the $\Delta t_{12}$ axis, for mostly LL1 excitation. Back panel: Linear absorption spectrum and optical pulse intensity, showing the largely LL1 excitation conditions.

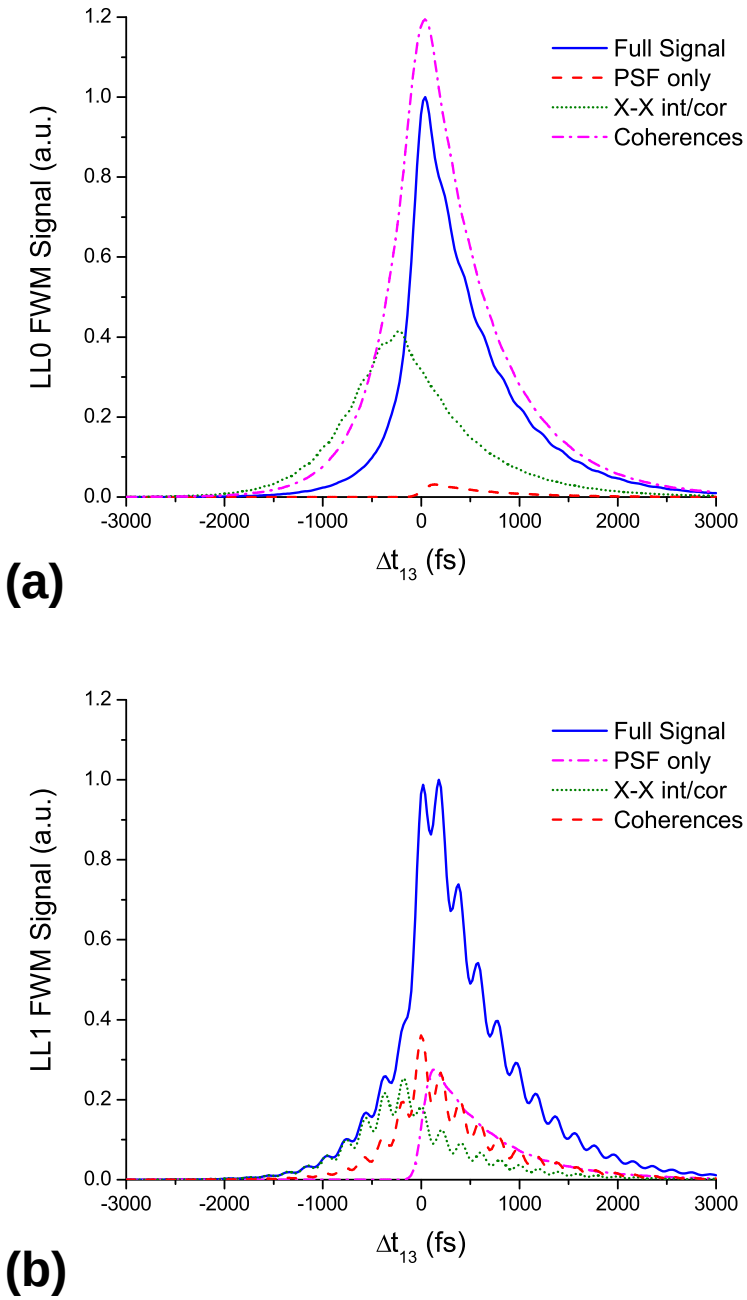


**Figure 5.6:** Contributions of the different terms to the (a) LL0 and (b) LL1 FWM signals along the $\Delta t_{13}$ axis for the undoped quantum well. Full signal is in blue, the contribution of PSF in red, X–X interactions and correlations in green and the contribition of intraband coherences and incoherent densities in magenta.

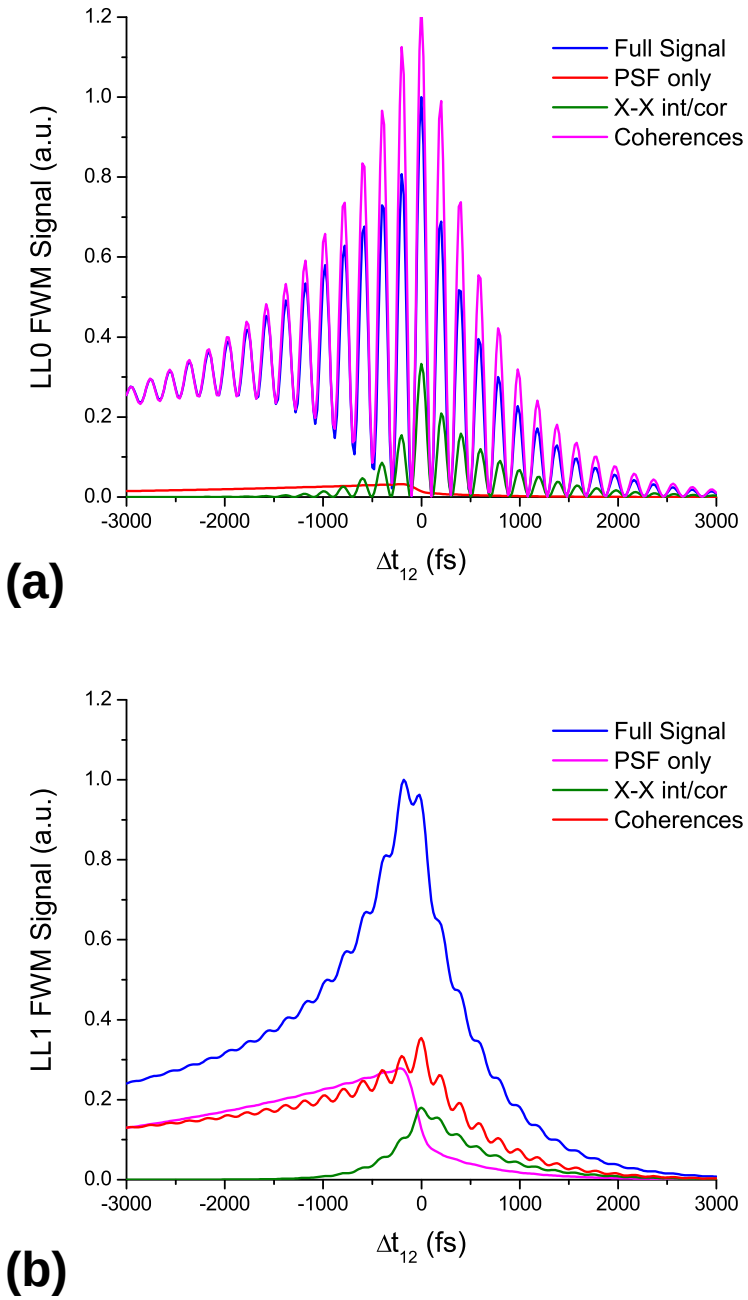


**Figure 5.7:** Contributions of the different terms to the (a) LL0 and (b) LL1 FWM signals along the $\Delta t_{12}$ axis for the undoped quantum well. Full signal is in blue, the contribution of PSF in red, X–X interactions and correlations in green and the contribition of intraband coherences and incoherent densities in magenta.

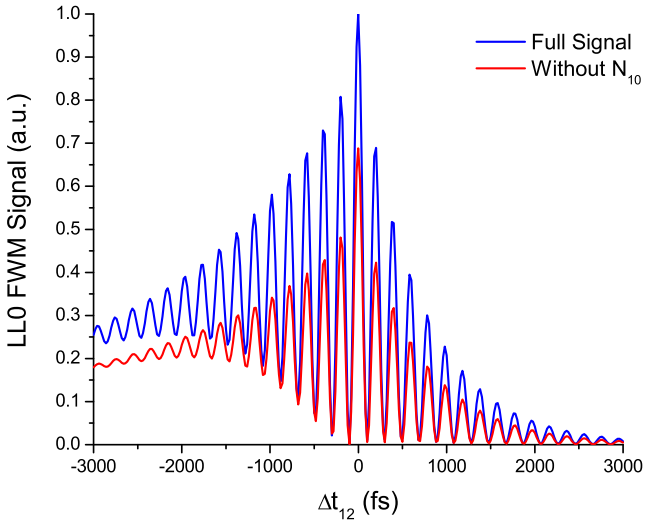


**Figure 5.8:** Numerical simulation of the LL0 FWM signal with and without the contribution of the X–X coherence.

intraband coherences and densities dominate the LL0 signal.

Fig. 5.7 shows the different contributions along the $\Delta t_{12}$ axis. The LL0 signal is dominated by intraband densities and coherences, which exhibit strong oscillations. As shown from Table 5.3, along the negative $\Delta t_{12}$ axis oscillations can be created from beatings between the 23 ans 13 contributions of the density $N_1$ or the coherence $N_{01}$. These oscillations decay with different decay rates depending on the source terms. The two slowest possible decay rates are (i) $\gamma_{10}+\gamma_D$ when $N_{01}^{13}$ beats with $N_1^{13}$ and (ii) $\Gamma_0+\Gamma_1+\gamma_D$ when $N_1^{13}$ beats with $N_1^{23}$. In the former case, the LL0 temporal profile is asymmetric, (all oscillations decay as $\Gamma_0+\Gamma_1$ for $\Delta t_{12} > 0$), while in the latter case the profile is symmetric. This is shown in Fig. 5.8 where the LL0 signal with and without the contribution of the $N_{01}$ coherence is plotted. Thus, the lifetime of the $N_{01}$ coherence can be extracted.

## 5.6 Conclusions

In this chapter we discussed the ultrafast nonlinear optical response of an undoped quantum well in a large magnetic field. To describe the dynamics of magnetoexcitons in this system, we used the theory described in Chapter 3 in the case of no carriers present in the ground state, which is equivalent to the DCTS [4–6] if phonons are included. By comparing our calculations

with the experiment [53], we identified the decay rate of a many body X–X coherence.

# Chapter 6

# The role of X+MP states at $\nu = 1$

## 6.1 Outline

In Chapter 4 we discussed the role of the 2DEG in the nonlinear response of the quantum Hall system by introducing a state $|Y\rangle$ which describes all X+MP effects. Although the major experimental results were explained with this approximation, we could not distinguish the role of the different X+MP states. Their effect was treated in Chapters 3 and 4 by introducing a dephasing rate to the X+MP coherence equation of motion. In this chapter, we develop a microscopic theory to study the effect of these X+MP states on the linear and nonlinear optical response of the quantum Hall system at filling factor $\nu = 1$.

In §6.2 we discuss the linear response and derive the equations of motion for the linear polarizations. We also study the energy dispersion of the X+MP states. We then calculate the linear absorption spectrum and we will show that it is strongly affected by X+MP states with non–zero momentum. In §6.3, we discuss the nonlinear response by deriving the equations of motion for the nonlinear polarizations, which are coupled to X–X, X–X+MP and X+MP–X+MP coherences. We finish by presenting a generalized average polarization model for the third–order polarization.

## 6.2 Linear Response

At filling factor $\nu = 1$, the 2DEG is spin–$\uparrow$ polarized and only LL0 is occupied. In this special case, the ground state excitations are distinguished from the photo–induced excitations, since the latter are spin–$\downarrow$ polarized. As

a result, the $\hat{Y}_n^{\rm int}$ operator, defined in Eq. (3.27), is orthogonal to all exciton states, i.e. $\hat{Y}_n^{\rm int} = \hat{Y}_n$, and

$$|Y_n\rangle = \frac{1}{2\pi\ell^2\sqrt{N}} \sum_{\substack{\mathbf{q}\neq 0 \\ mn'}} v_q \phi_{m0}(-\mathbf{q}) \left[\phi_{n'n}(\mathbf{q})|Y_{\mathbf{q}n'nm}\rangle - \phi_{nn'}(\mathbf{q})|Y_{\mathbf{q}nn'm}\rangle\right] \quad (6.1)$$

where

$$|Y_{\mathbf{q}nn'm}\rangle = \hat{Y}^\dagger_{\mathbf{q}nn'm}|G\rangle = \hat{X}^\dagger_{\mathbf{q}nn'}\hat{\rho}^e_{-\mathbf{q}m0\uparrow}|G\rangle \quad (6.2)$$

describe a continuum of X+MP states consisting of {1–LL$n$–$e$ + 1–LL$n'$–$h$ + 1–(LL0→LL$m$)–MP} that are orthogonal to all exciton states,

$$\langle X_l|Y_{\mathbf{q}nn'm}\rangle = 0 \quad (6.3)$$

and to each other

$$\langle Y_{\mathbf{q}_1 n_1 n_1' m_1}|Y_{\mathbf{q}_2 n_2 n_2' m_2}\rangle = \delta_{\mathbf{q}_1\mathbf{q}_2}\delta_{n_1 n_2}\delta_{n_1' n_2'}\delta_{m_1 m_2} \quad (6.4)$$

The above orthogonality relations are easily obtained by using Eq. (A.1) and taking into account that for $\nu = 1$, $\hat{\rho}^h_{\mathbf{q}nn'\sigma}|G\rangle = 0 = \hat{\rho}^e_{\mathbf{q}nn'\downarrow}|G\rangle$, as well as that $\mathbf{q} \neq 0$. The $\mathbf{q} = 0$ term is canceled by the direct interaction with the positive background [120], if we assume that the system is homogeneous.

Using the above expression for $|Y_n\rangle$, the equation of motion for the linear polarization, Eq. (3.50), becomes

$$\begin{aligned} i\partial_t P_n^L = (\Omega_n - i\Gamma_n)P_n^L - \sum_{m\neq n} V_{nm}P_m^L - d(t) \\ + \frac{1}{2\pi\ell^2\sqrt{N}} \sum_{\mathbf{q}mn'} v_{\mathbf{q}}\phi_{0m}(\mathbf{q}) \left[\phi_{nn'}(-\mathbf{q})\bar{P}^L_{\mathbf{q}n'nm} - \phi_{n'n}(-\mathbf{q})\bar{P}^L_{\mathbf{q}nn'm}\right] \end{aligned} \quad (6.5)$$

where

$$V_{nm} = \int \frac{d\mathbf{q}}{(2\pi)^2} v_q |\phi_{nm}(\mathbf{q})|^2 \quad (6.6)$$

is the static Coulomb induced inter–LL coupling,

$$\Omega_n = E_g + (n + 1/2)\left(\Omega_c^c + \Omega_c^v\right) - V_{nn} \quad (6.7)$$

is the LL$n$ exciton energy, and

$$\bar{P}^L_{\mathbf{q}nn'm} = \langle Y_{\mathbf{q}nn'm}|\psi_{1L}\rangle = \langle Y_{\mathbf{q}nn'm}|\bar{\psi}_{1L}\rangle \quad (6.8)$$

describes the time evolution of the $|Y_{\mathbf{q}nn'm}\rangle$ state. Its equation of motion is obtained by substituting $\hat{O} = \hat{Y}_{\mathbf{q}nn'm}$ in Eq. (3.34), using Eqs. (A.10) and (A.11) and keeping terms up to first order in the optical field:

$$\begin{aligned}
i\partial_t \bar{P}^L_{\mathbf{q}'nn'm} = {} & [E_g + (n+m+1/2)\Omega^c_c + (n'+1/2)\Omega^v_c + \sum_r V_{r0}]\bar{P}^L_{\mathbf{q}'nn'm} \\
& - \sum_r \bar{V}_{mr,00}(\mathbf{q})\bar{P}^L_{\mathbf{q}'nn'r} - \sum_{rr'} \bar{V}_{r'n',rn}(\mathbf{q})\bar{P}^L_{\mathbf{q}'rr'm} \\
& + \frac{1}{2\pi\ell^2\sqrt{N}} \sum_{\substack{\mathbf{q}'\neq 0 \\ rr'}} v_{q'}\phi_{0r}(\mathbf{q}') \Big[ \phi_{mr'}(-\mathbf{q}')\langle G|\hat{\rho}^e_{\mathbf{q}'0r\uparrow}\hat{\rho}^e_{\mathbf{q}-\mathbf{q}'0r'\uparrow}\hat{X}_{\mathbf{q}nn'}|\psi_{1L}\rangle e^{-i(\mathbf{q}\times\mathbf{q}')_z\ell^2/2} \\
& \qquad - \phi_{r'0}(-\mathbf{q}')\langle G|\hat{\rho}^e_{\mathbf{q}'0r\uparrow}\hat{\rho}^e_{\mathbf{q}-\mathbf{q}'r'm\uparrow}\hat{X}_{\mathbf{q}nn'}|\psi_{1L}\rangle e^{i(\mathbf{q}\times\mathbf{q}')_z\ell^2/2} \Big] \\
& + \frac{1}{2\pi\ell^2\sqrt{N}} \sum_{\substack{\mathbf{q}'\neq 0 \\ srr'}} v_{q'}\phi_{rr'}(\mathbf{q}') \Big[ \phi_{ms}(-\mathbf{q}')\langle G|\hat{\rho}^e_{\mathbf{q}0m\uparrow}\hat{\rho}^e_{\mathbf{q}'rr'\uparrow}\hat{X}_{\mathbf{q}+\mathbf{q}'sn'}|\psi_{1L}\rangle e^{i(\mathbf{q}\times\mathbf{q}')_z\ell^2/2} \\
& \qquad - \phi_{sn'}(-\mathbf{q}')\langle G|\hat{\rho}^e_{\mathbf{q}0m\uparrow}\hat{\rho}^e_{\mathbf{q}'rr'\uparrow}\hat{X}_{\mathbf{q}+\mathbf{q}'ns}|\psi_{1L}\rangle e^{-i(\mathbf{q}\times\mathbf{q}')_z\ell^2/2} \Big]
\end{aligned} \tag{6.9}$$

where

$$\bar{V}_{nn',mm'}(\mathbf{q}) = \int \frac{d\mathbf{q}'}{(2\pi)^2} v_{q'}\phi_{nn'}(\mathbf{q}')\phi^*_{mm'}(\mathbf{q}')e^{i(\mathbf{q}\times\mathbf{q}')_z\ell^2} \tag{6.10}$$

are a generalization of the Coulomb induced $V_{nm}$ couplings, Eq. (3.24), for non–zero momentum states.

In order to simplify the terms of the form $\langle G|\hat{\rho}^e\hat{\rho}^e\hat{X}|\psi_{1L}\rangle$ in Eq. (6.2), we expand the 1–$h$ many–particle wavefunction $|\psi_{1L}\rangle$ in terms of not only exciton states $|X_n\rangle$, but also X+MP states $|Y_{\mathbf{q}nn'm}\rangle$, in analogy with Eq. (3.48):

$$|\psi_{1L}\rangle = \sum_n P^L_n|X_n\rangle + \sum_{\substack{\mathbf{q}\neq 0 \\ nn'm\neq 0}} \bar{P}^L_{\mathbf{q}nn'm}|Y_{\mathbf{q}nn'm}\rangle + |\tilde{\psi}_{1L}\rangle \tag{6.11}$$

where $|\tilde{\psi}_{1L}\rangle$ is a $\{1$–$h/2\text{DEG}^*\}$ contribution, defined by the requirement $\langle X_n|\tilde{\psi}_{1L}\rangle = \langle Y_{\mathbf{q}nn'm}|\tilde{\psi}_{1L}\rangle = 0$, and describes X+2MP states and higher, i.e. contributions of the form $\hat{X}^\dagger\hat{\rho}^e\hat{\rho}^e|G\rangle$, $\hat{X}^\dagger\hat{\rho}^e\hat{\rho}^e\hat{\rho}^e|G\rangle$, etc. The above expansion is equivalent to separating the X+MP states from $|\bar{\psi}_{1L}\rangle$

$$|\bar{\psi}_{1L}\rangle \to \sum_{\substack{\mathbf{q}\neq 0 \\ nn'm\neq 0}} \bar{P}^L_{\mathbf{q}nn'm}|Y_{\mathbf{q}nn'm}\rangle + |\tilde{\psi}_{1L}\rangle \tag{6.12}$$

The $m \neq 0$ requirement in Eqs. (6.11) and (6.12) arises from the $\mathbf{q} \neq 0$ requirement when $\nu = 1$: in this case the ground state is full with spin–$\uparrow$

electrons, and a 2DEG electron – already in LL0 – cannot move within LL0 with non–zero momentum.

Substituting Eq. (6.11) in Eq. (6.2) and remembering that $\hat{\rho}^e_{qnm\uparrow}|G\rangle = (1-\delta_{n0})\ \delta_{m0}\ \hat{\rho}^e_{qn0\uparrow}|G\rangle$, we obtain the equation of motion for $\bar{P}^L_{\mathbf{q}nn'm}$:

$$\begin{aligned}
i\partial_t \bar{P}^L_{\mathbf{q}'nn'm} &= \left(\bar{\Omega}_{\mathbf{q}nn'm} - i\gamma_{\mathbf{q}nn'm}\right)\bar{P}^L_{\mathbf{q}'nn'm} + \frac{1}{\sqrt{N}}\alpha_{nn',0m}(\mathbf{q})\left(P^L_{n'} - P^L_n\right) \\
&- \sum_{r\neq 0,m}\left[\bar{V}_{mr,00}(\mathbf{q}) + \bar{V}_{0r,0m}(0) - \alpha_{or,om}(\mathbf{q})\right]\bar{P}^L_{\mathbf{q}'nn'r} \\
&- \sum_{r\neq n}\bar{V}_{n'n',rn}(\mathbf{q})\bar{P}^L_{\mathbf{q}'rn'm} - \sum_{r\neq n'}\bar{V}_{rn',nn}(\mathbf{q})\bar{P}^L_{\mathbf{q}'nrm} - \sum_{\substack{r\neq n\\ r'\neq n'}}\bar{V}_{r'n',rn}(\mathbf{q})\bar{P}^L_{\mathbf{q}'rr'm} \\
&+ \frac{1}{N}\sum_{\substack{\mathbf{q}'\neq 0,\mathbf{q}\\ r,t\neq 0}}\left[\alpha_{mt,rn}(\mathbf{q}'-\mathbf{q})\bar{P}^L_{\mathbf{q}'rn't}e^{i(\mathbf{q}\times\mathbf{q}')_z\ell^2/2} - \alpha_{mt,n'r}(\mathbf{q}'-\mathbf{q})\bar{P}^L_{\mathbf{q}'nrt}\right] \\
&- \frac{1}{N}\sum_{\substack{\mathbf{q}'\neq 0,\mathbf{q}\\ r}}\left[\alpha_{00,rn}(\mathbf{q}'-\mathbf{q})\bar{P}^L_{\mathbf{q}'rn'm} - \alpha_{00,n'r}(\mathbf{q}'-\mathbf{q})\bar{P}^L_{\mathbf{q}'nrm}e^{-i(\mathbf{q}\times\mathbf{q}')_z\ell^2/2}\right]
\end{aligned} \tag{6.13}$$

where we introduced a phenomenological decay rate $\gamma_{\mathbf{q}nn'm}$ and

$$\alpha_{nn',mm'}(\mathbf{q}) = \frac{1}{2\pi\ell^2}v_q\phi_{nn'}(\mathbf{q})\phi^*_{mm'}(\mathbf{q}) \tag{6.14}$$

to simplify the expression. The energy of the X+MP state $|Y_{\mathbf{q}nn'm}\rangle$ is the sum of the X and MP energies,

$$\bar{\Omega}_{\mathbf{q}nn'm} = \frac{\langle Y_{\mathbf{q}nn'm}|H|Y_{\mathbf{q}nn'm}\rangle}{\langle Y_{\mathbf{q}nn'}|Y_{\mathbf{q}nn'm}\rangle} = \Omega^X_{\mathbf{q}nn'} + \Omega^{MP}_{-\mathbf{q}m0} \tag{6.15}$$

where

$$\Omega^X_{\mathbf{q}nn'} = \frac{\langle X_{\mathbf{q}nn'}|H|X_{\mathbf{q}nn'}\rangle}{\langle X_{\mathbf{q}nn'}|X_{\mathbf{q}nn'}\rangle} = E_g + (n+1/2)\Omega^c_c + (n'+1/2)\Omega^v_c - \bar{V}_{n'n',nn}(\mathbf{q}) \tag{6.16}$$

is the energy of an exciton of momentum $\mathbf{q}$ with an electron in conduction band LL$n$ and a hole in valence band LL$n'$, while

$$\Omega^{MP}_{-\mathbf{q}m0} = \frac{\langle G|\hat{\rho}^e_{\mathbf{q}0m\uparrow}H\hat{\rho}^e_{-\mathbf{q}m0\uparrow}|G\rangle}{\langle G|\hat{\rho}^e_{\mathbf{q}0m\uparrow}\hat{\rho}^e_{-\mathbf{q}m0\uparrow}|G\rangle} = m\Omega^c_c - \bar{V}_{mm,00}(\mathbf{q}) + V_{00} - V_{0m} + \alpha_{0m,0m}(\mathbf{q}) \tag{6.17}$$

is the energy of a MP excitation of momentum $-\mathbf{q}$, created by destroying a conduction band electron from LL0 and creating another electron in LL$m$.

Fig. 6.1a shows the energy shift of the $|Y_{\mathbf{q}011}\rangle$ state from LL1, $\bar{\Omega}_{\mathbf{q}011} - \Omega_1$, as well its two components, $\Omega^X_{\mathbf{q}01} - (E_g + \frac{1}{2}\Omega^c_c + \frac{3}{2}\Omega^v_c)$ and $\Omega^{MP}_{-\mathbf{q}10} - \Omega^c_c$. The latter can be easily calculated analytically from Eq. (6.17) using Eqs. (3.4), (3.6) and (6.14)

$$\Omega^{MP}_{-\mathbf{q}10} - \Omega^c_c = \frac{e^2}{\epsilon\ell}\frac{q\ell}{\sqrt{2}}e^{-q^2\ell^2/2} + \frac{e^2}{\epsilon\ell}\frac{1}{2}\sqrt{\frac{\pi}{2}}\left\{1 - e^{-q^2\ell^2/4}\left[\left(1+\frac{q^2\ell^2}{2}\right)I_0\left(\frac{q^2\ell^2}{4}\right) - \frac{q^2\ell^2}{2}I_1\left(\frac{q^2\ell^2}{4}\right)\right]\right\} \tag{6.18}$$

where $I_n$ is a modified Bessel function of the first kind. The resulting curve is plotted in Fig. 6.1b. It has a maximum at $q\ell \sim 0.9$ and a minimum at $q\ell \sim 2$. For $q \to 0$, $\Omega^{MP}_{\mathbf{q}10} \to \Omega^c_c$, in accordance with Kohn's theorem [72]. For $q\ell \ll 1$, the spectrum increases linearly $\Omega^{MP}_{-\mathbf{q}10} - \Omega^c_c \simeq \frac{1}{2}q\ell$. Our result is in agreement with previous calculations of the energy dispersion of the magnetoplasmon for filling factor $\nu = 1$ [67]. The first term in the right–hand side of Eq. (6.18) is the energy dispersion of the magnetoplasmon when calculated within the RPA and is plotted in Fig. 6.1b. Although it describes the mode well for $q\ell \ll 1$, it is clearly inadequate for $q\ell \gg 1$ [67].

### 6.2.1 Linear Absorption

By solving the system of Eqs. (3.50) and (6.13), we can calculate the linear polarizations that are photoexcited in the system, and thus the linear absorption spectrum. If we retain the first two LLs only, LL0 and LL1, we need to calculate (besides $P^L_0$ and $P^L_1$) $\bar{P}^L_{\mathbf{q}001}$, $\bar{P}^L_{\mathbf{q}011}$, $\bar{P}^L_{\mathbf{q}101}$ and $\bar{P}^L_{\mathbf{q}111}$. The last two are resonant to LL2 and thus can be ignored, since they are not excited by the optical pulse. We then end up with the following equations of motion for the polarizations:

$$i\partial_t P^L_0 = (\Omega_0 - i\Gamma_0)P^L_0 - V_{01}P^L_1 - \mu E(t) - \frac{1}{N}\sum_{\mathbf{q}}\alpha_{01,01}(\mathbf{q})\bar{P}^L_{\mathbf{q}011} \tag{6.19}$$

$$i\partial_t P^L_1 = (\Omega_1 - i\Gamma_1)P^L_1 - V_{10}P^L_0 - \mu E(t) + \frac{1}{N}\sum_{\mathbf{q}}\alpha_{01,01}(\mathbf{q})\bar{P}^L_{\mathbf{q}011} \tag{6.20}$$

where we have made the transformation $P^L_n \to \sqrt{N}P^L_n$. We note that the symmetry between $\hat{Y}_0$ and $\hat{Y}_1$, Eq. (3.30) is satisfied.

In Eqs. (6.19) and (6.20) the polarizations are not coupled to $\bar{P}^L_{\mathbf{q}001}$, and thus we will ignore it. The only quantity left then is $\bar{P}^L_{\mathbf{q}011}$, whose dynamics

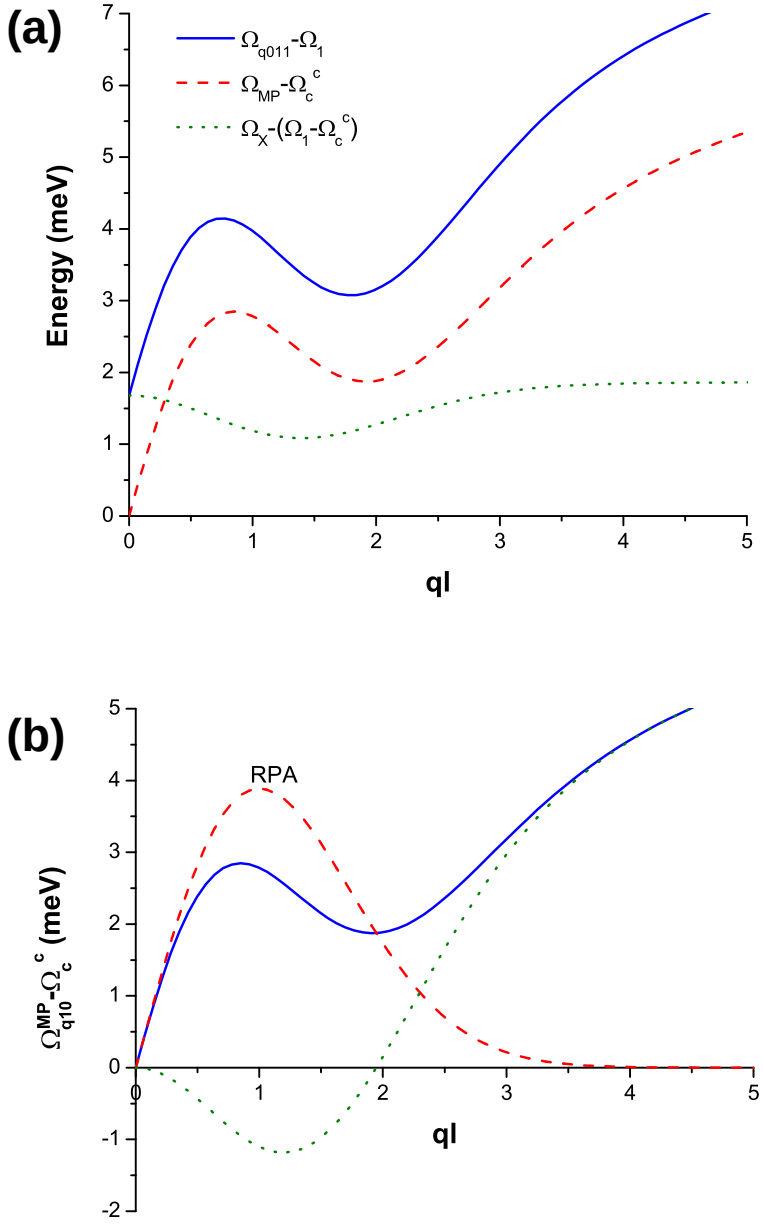


**Figure 6.1:** (a) Energy shift of the X+MP $|Y_{\mathbf{q}011}\rangle$ state at $\nu = 1$ in comparison with the LL1 exciton $|X_1\rangle$ energy. The solid line denotes the energy shift $\bar{\Omega}_{\mathbf{q}011} - \Omega_1$, which is the sum of the $X_{\mathbf{q}01}$ energy (dashed line) and the MP energy (dotted line). (b) Dispersion curve of the MP energy (solid line). The dashed line denotes the RPA contribution, and the dotted line the rest. Our calculation reproduces older results [67].

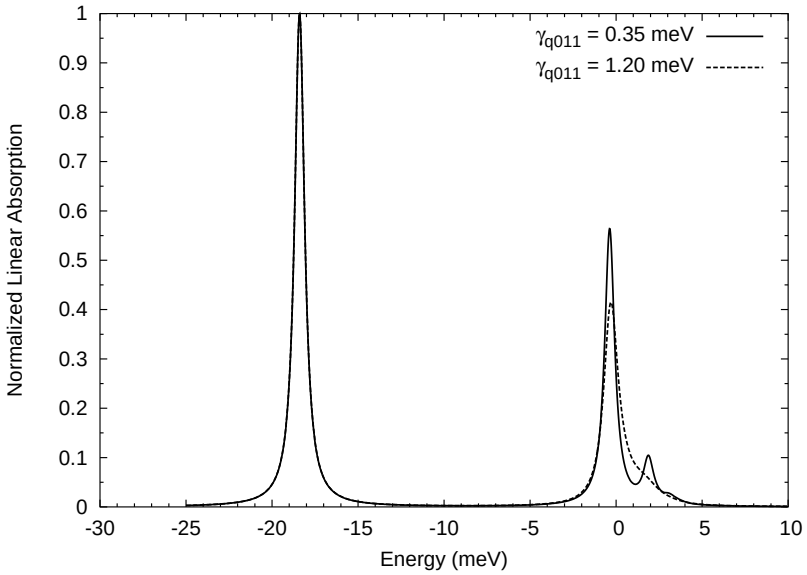


**Figure 6.2:** Calculation of the linear absorption spectrum of the quantum Hall system at $\nu = 1$ ($B = 8.68$ T for the system of Ref. [52]) by retaining the $|X_0\rangle$, $|X_1\rangle$, and $|Y_{\mathbf{q}011}\rangle$ states. The zero of energy is the energy of the LL1 exciton ($\Omega_1$). The X+MP states create a second peak close to the LL1 peak. When the dephasing is large, the two peaks merge into a broad one.

is described by the equation of motion

$$i\partial_t \bar{P}^L_{\mathbf{q}011} = \left(\bar{\Omega}_{\mathbf{q}011} - i\gamma_{\mathbf{q}011}\right) \bar{P}^L_{\mathbf{q}011} + \frac{1}{\sqrt{N}} \alpha_{01,01}(\mathbf{q}) \left(P^L_1 - P^L_0\right) + \frac{1}{N} \sum_{\mathbf{q}' \neq 0, \mathbf{q}} W(\mathbf{q}, \mathbf{q}') \bar{P}^L_{\mathbf{q}'011} \tag{6.21}$$

where we defined

$$W(\mathbf{q}, \mathbf{q}') = 2\alpha_{11,00}(\mathbf{q}' - \mathbf{q}) \cos\left[\frac{(\mathbf{q} \times \mathbf{q}')_z \ell^2}{2}\right] - \alpha_{11,11}(\mathbf{q}' - \mathbf{q}) - \alpha_{00,00}(\mathbf{q}' - \mathbf{q}) \tag{6.22}$$

the coupling between different momentum states that describes rescattering many–body effects.

Fig. 6.2 shows the linear absorption spectrum that is calculated by solving Eqs. (6.19), (6.20) and (6.21) for the quantum Hall system of Ref. [52] at $\nu = 1$, which corresponds to a magnetic field $B = 8.68$ T. The contribution of the X+MP states $|Y_{\mathbf{q}011}\rangle$ creates a second peak next to the LL1 peak. If the dephasing of these states is strong, the two peaks merge into a broad one, similar to the experiment [52]. Fig. 6.3 shows the linear absorption

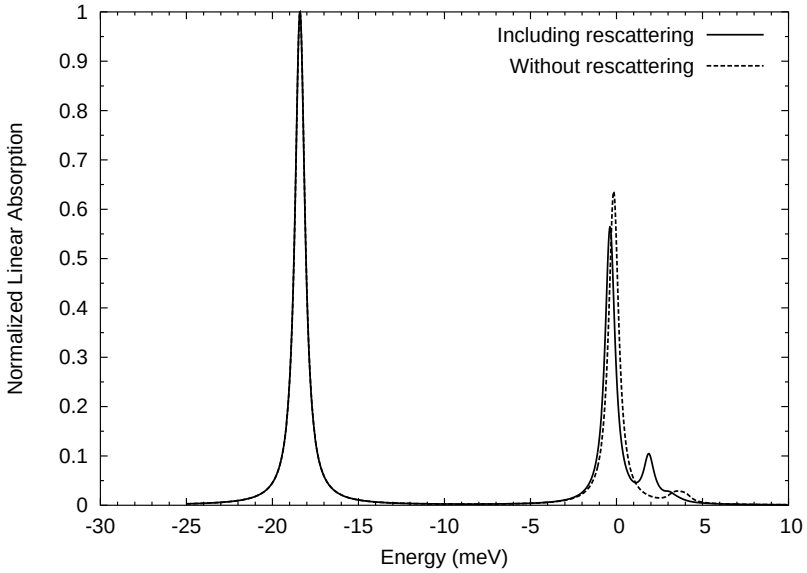


**Figure 6.3:** Effect of rescattering many–body processes on the linear absorption spectrum of the quantum Hall system at $\nu = 1$.

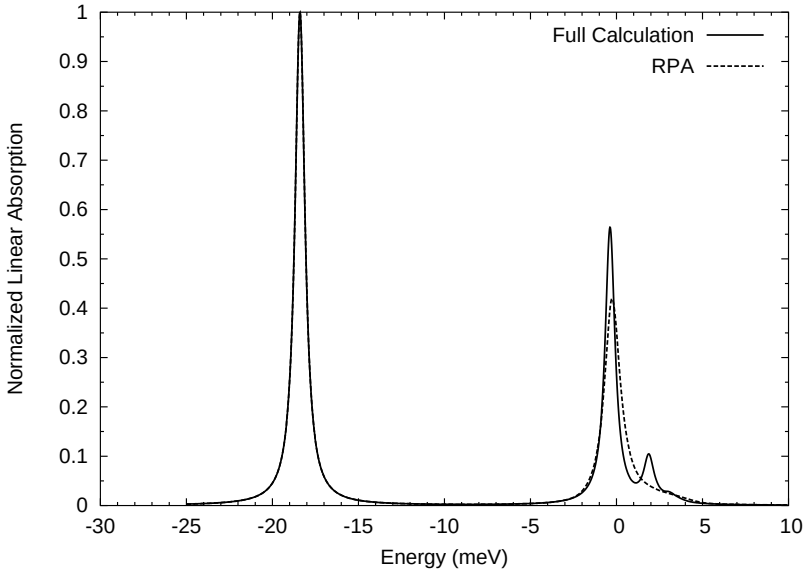


**Figure 6.4:** Calculation of the linear absorption spectrum within the RPA.

spectrum without the last term in Eq. (6.21), which describes rescattering effects. These effects bring the two peaks closer to each other. Fig. 6.4 shows the linear absoprtion spectrum when calculated within RPA, which does not reproduce the second peak. This indicates that the role of the X+MP states for $q\ell > 1$, where RPA is inadequate, is important.

## 6.3 Nonlinear Response

To calculate the nonlinear polarization, we use Eq. (3.34) for $\hat{O} = \hat{X}_n$, as in §3.4:

$$\begin{aligned} i\partial_t P_n =&(\Omega_n - i\Gamma_n)P_n - \sum_{m\neq n} V_{nm}P_m - d(t)\sum_m \langle[\hat{X}_n, \hat{X}_m^\dagger]\rangle_{(2)} \\ &+ \frac{1}{2\pi\ell^2\sqrt{N}} \sum_{\mathbf{q}\neq 0}\sum_m v_{\mathbf{q}} \left[\phi_{nm}(-\mathbf{q})\langle\hat{\rho}_{\mathbf{q}}\hat{X}_{\mathbf{q}mn}\rangle_{(3)} - \phi_{mn}(-\mathbf{q})\langle\hat{\rho}_{\mathbf{q}}\hat{X}_{\mathbf{q}nm}\rangle_{(3)}\right] \end{aligned} \tag{6.23}$$

where the subscript $(n)$ denotes that we only keep the contributions to the matrix element that are of $n$th–order in the optical field.

To calculate the second–order contribution of $\langle[\hat{X}_n, \hat{X}_m^\dagger]\rangle$, we expand the intraband commutator $[\hat{X}_n, \hat{X}_m^\dagger]$ on the strongly correlated basis $|X_n\rangle\langle X_m|$, $|X_l\rangle\langle Y_{\mathbf{q}nn'm}|$, and $|Y_{\mathbf{q}nn'm}\rangle\langle Y_{\mathbf{q}'rr's}|$, and obtain:

$$\begin{aligned} \langle[\hat{X}_n, \hat{X}_m^\dagger]\rangle_{(2)} =& -\frac{\delta_{nm}}{N}\Big[2\langle|X_n\rangle\langle X_n|\rangle \\ &+ \sum_{\substack{\mathbf{q}\neq 0\\ r,t\neq 0}} \left(\langle|Y_{\mathbf{q}rnt}\rangle\langle Y_{\mathbf{q}rnt}|\rangle + \langle|Y_{\mathbf{q}nrt}\rangle\langle Y_{\mathbf{q}nrt}|\rangle\right)\Big] \\ =& -\frac{\delta_{nm}}{N}\Big[2\langle|X_n\rangle\langle X_n|\rangle_c + 2P_n^L P_n^{L*} \\ &+ \sum_{\substack{\mathbf{q}\neq 0\\ r,t\neq 0}} \left(\langle|Y_{\mathbf{q}rnt}\rangle\langle Y_{\mathbf{q}rnt}|\rangle_c + \langle|Y_{\mathbf{q}nrt}\rangle\langle Y_{\mathbf{q}nrt}|\rangle_c\right)\Big] \end{aligned} \tag{6.24}$$

In the last line of the above expression we seperated the coherent contributions in the X populations using Eq. (3.67), while it is straightforward to verify from Eq. (3.64) that $\langle|Y_{\mathbf{q}nn'm}\rangle\langle Y_{\mathbf{q}rr's}|\rangle = \langle|Y_{\mathbf{q}nn'm}\rangle\langle Y_{\mathbf{q}rr'm}|\rangle_c$. Eq. (6.24) will give the PSF contribution to our equations of motion.

To calculate matrix elements of the form $\langle\hat{\rho}_{\mathbf{q}}\hat{X}_{\mathbf{q}mn}\rangle$ we note that these are interband density matrices and thus we may expand them into correlated

and uncorrelated contributions, as in Eq. (3.70):

$$\begin{aligned}\langle\hat{\rho}_{\mathbf{q}}\hat{X}_{\mathbf{q}mn}\rangle =& \sum_r P_r^{L*}\langle G|[\hat{X}_r, \hat{\rho}_{\mathbf{q}}\hat{X}_{\mathbf{q}mn}]|\psi_2\rangle + \sum_r P_r^L\langle[\hat{\rho}_{\mathbf{q}}\hat{X}_{\mathbf{q}mn}, \hat{X}_r^\dagger]\rangle_c \\ &+ \frac{1}{2}\sum_{rr'} P_s^L P_{s'}^L\langle\bar{\psi}_{1L}|[[\hat{\rho}_{\mathbf{q}}\hat{X}_{\mathbf{q}mn}, \hat{X}_s^\dagger], \hat{X}_{s'}^\dagger]|G\rangle + \langle\hat{\rho}_{\mathbf{q}}\hat{X}_{\mathbf{q}mn}\rangle_c \quad (6.25)\end{aligned}$$

The commutators in the above equation are easily calculated with Eqs. (3.21) and (A.1). Moreover, using the expansion of the 2–$h$ state Eq. (3.60) and Eq. (6.12), we obtain:

$$\begin{aligned}\langle\hat{\rho}_{\mathbf{q}}\hat{X}_{\mathbf{q}mn}\rangle =& -\frac{1}{N\sqrt{N}}\phi_{mn}(\mathbf{q})(P_m^{L*} - P_n^{L*})P_n^L P_m^L - \frac{1}{N}\sum_{t\neq 0}\phi_{t0}(\mathbf{q})\bar{P}^{L*}_{\mathbf{q}nmt}P_n^L P_m^L \\ &+ \frac{1}{\sqrt{N}}\sum_{rr'}\phi_{rr'}(\mathbf{q})(P_{r'}^L - P_r^L)\langle\hat{X}^\dagger_{\mathbf{q}rr'}\hat{X}_{\mathbf{q}mn}\rangle_c \\ &- \frac{1}{\sqrt{N}}P_m^L\langle\hat{\rho}_{\mathbf{q}}\hat{\rho}^h_{-\mathbf{q}mn\downarrow}\rangle_c - \frac{1}{\sqrt{N}}P_n^L\langle\hat{\rho}_{\mathbf{q}}\hat{\rho}^e_{-\mathbf{q}nm\downarrow}\rangle_c + \langle\hat{\rho}_{\mathbf{q}}\hat{X}_{\mathbf{q}mn}\rangle_c \\ & \quad (6.26)\end{aligned}$$

where we have treated X–X interactions within the Hartree–Fock approximation. The intraband density matrices of the form $\langle\hat{X}^\dagger\hat{X}\rangle$ and $\langle\hat{\rho}\hat{\rho}\rangle$ in Eq. (6.26) can be calculated by expanding the corresponding operators in our basis consisiting of $|X_n\rangle\langle X_m|$, $|X_l\rangle\langle Y_{\mathbf{q}nn'm}|$, and $|Y_{\mathbf{q}nn'm}\rangle\langle Y_{\mathbf{q}'rr's}|$. Using Eqs. (A.1), (A.3) and (A.4), we obtain

$$\langle\hat{X}^\dagger_{\mathbf{q}rr'}\hat{X}_{\mathbf{q}mn}\rangle_c = \sum_{t\neq 0}\langle|Y_{\mathbf{q}rr't}\rangle\langle Y_{\mathbf{q}mnt}|\rangle_c \quad (6.27)$$

and after some algebra,

$$\begin{aligned}
\langle \hat{\rho}_{\mathbf{q}} \hat{\rho}^h_{-\mathbf{q}mn\downarrow} \rangle_c &= \frac{1}{N} \phi_{mn}(\mathbf{q}) \left[ \langle |X_m\rangle\langle X_n| \rangle_c - \langle |X_n\rangle\langle X_n| \rangle_c \right] \\
&+ \frac{1}{\sqrt{N}} \sum_{t\neq 0} \left[ \phi_{0t}(\mathbf{q}) \langle |X_m\rangle\langle Y_{\mathbf{q}mnt}| \rangle_c + \phi_{t0}(\mathbf{q}) \langle |X_n\rangle\langle Y_{-\mathbf{q}nmt}| \rangle^*_c \right] \\
&+ \frac{1}{N} \sum_{\substack{r,\ \mathbf{q}'\neq 0 \\ t\neq 0, t'\neq 0}} \left[ \phi_{tt'}(\mathbf{q}) - \delta_{tt'} \phi_{00}(\mathbf{q}) e^{i(\mathbf{q}\times\mathbf{q}')_z \ell^2} \right] \langle |Y_{\mathbf{q}'-\mathbf{q}rmt}\rangle\langle Y_{\mathbf{q}'rnt'}| \rangle_c \\
&+ \frac{1}{N} \sum_{\substack{\mathbf{q}'\neq 0 \\ rr',\ t\neq 0}} \phi_{rr'}(\mathbf{q}) \langle |Y_{\mathbf{q}'rmt}\rangle\langle Y_{\mathbf{q}'r'nt}| \rangle_c e^{i(\mathbf{q}\times\mathbf{q}')_z \ell^2} \\
&- \frac{1}{N} \sum_{\substack{\mathbf{q}'\neq 0 \\ rr',\ t\neq 0}} \phi_{mr'}(\mathbf{q}) \langle |Y_{\mathbf{q}'rr't}\rangle\langle Y_{\mathbf{q}'rnt}| \rangle_c \qquad (6.28) \\
\langle \hat{\rho}_{\mathbf{q}} \hat{\rho}^e_{-\mathbf{q}nm\downarrow} \rangle_c &= \frac{1}{N} \phi_{mn}(\mathbf{q}) \left[ \langle |X_m\rangle\langle X_m| \rangle_c - \langle |X_n\rangle\langle X_m| \rangle_c \right] \\
&+ \frac{1}{\sqrt{N}} \sum_{t\neq 0} \left[ \phi_{0t}(\mathbf{q}) \langle |X_n\rangle\langle Y_{\mathbf{q}mnt}| \rangle_c + \phi_{t0}(\mathbf{q}) \langle |X_m\rangle\langle Y_{-\mathbf{q}nmt}| \rangle^*_c \right] \\
&+ \frac{1}{N} \sum_{\substack{r,\ \mathbf{q}'\neq 0 \\ t\neq 0, t'\neq 0}} \left[ \phi_{tt'}(\mathbf{q}) e^{-i(\mathbf{q}\times\mathbf{q}')_z \ell^2} - \delta_{tt'} \phi_{00}(\mathbf{q}) \right] \langle |Y_{\mathbf{q}'-\mathbf{q}nrt}\rangle\langle Y_{\mathbf{q}'mrt'}| \rangle_c \\
&- \frac{1}{N} \sum_{\substack{\mathbf{q}'\neq 0 \\ rr',\ t\neq 0}} \phi_{rr'}(\mathbf{q}) \langle |Y_{\mathbf{q}'nr't}\rangle\langle Y_{\mathbf{q}'mrt}| \rangle_c e^{-i(\mathbf{q}\times\mathbf{q}')_z \ell^2} \\
&+ \frac{1}{N} \sum_{\substack{\mathbf{q}'\neq 0 \\ rr',\ t\neq 0}} \phi_{rn}(\mathbf{q}) \langle |Y_{\mathbf{q}'rr't}\rangle\langle Y_{\mathbf{q}'mr't}| \rangle_c \qquad (6.29)
\end{aligned}$$

Th advantage of these expansions is that despite the long expressions, we have now reduced the dynamics of all intraband density matrices to the dynamics of $\langle |X_n\rangle\langle X_m| \rangle_c$, $\langle |X_n\rangle\langle Y_{\mathbf{q}rr't}| \rangle_c$ and $\langle |Y_{\mathbf{q}nn'm}\rangle\langle Y_{\mathbf{q}'rr't}| \rangle_c$, which is described by equations of motion derived from Eq. (3.66), in analogy with Eqs. (6.30) and (3.69). We thus obtain the following equation of motion for the X populations

and X–X coherences, taking into account Eqs. (6.12), (6.3) and (3.26):

$$\begin{aligned} i\partial_t\langle|X_n\rangle\langle X_m|\rangle_c &= (\Omega_m - \Omega_n - i\gamma_{nm})\langle|X_n\rangle\langle X_m|\rangle_c + i(\Gamma_n + \Gamma_m - \gamma_{nm})P_n^{L*}P_m^L \\ &\quad - \sum_{r\neq m} V_{rm}\langle|X_n\rangle\langle X_r|\rangle_c + \sum_{r\neq n} V_{nr}\langle|X_r\rangle\langle X_m|\rangle_c \\ &\quad + \frac{1}{\sqrt{N}}\sum_{\substack{\mathbf{q}\neq 0\\ r,t\neq 0}} [\alpha_{0t,rm}(\mathbf{q})\langle|X_n\rangle\langle Y_{\mathbf{q}rmt}|\rangle_c - \alpha_{0t,mr}(\mathbf{q})\langle|X_n\rangle\langle Y_{\mathbf{q}mrt}|\rangle_c] \\ &\quad - \frac{1}{\sqrt{N}}\sum_{\substack{\mathbf{q}\neq 0\\ r,t\neq 0}} [\alpha_{rn,0t}(\mathbf{q})\langle|Y_{\mathbf{q}rnt}\rangle\langle X_m|\rangle_c - \alpha_{nr,0t}(\mathbf{q})\langle|Y_{\mathbf{q}nrt}\rangle\langle X_m|\rangle_c] \end{aligned} \tag{6.30}$$

where $\gamma_{nm}$ is the decay rate of the $X_n \leftrightarrow X_m$ coherence (if $n \neq m$) or $X_n$ density (if $n = m$). Similarly, we obtain for the X–X+MP coherences:

$$\begin{aligned} i\partial_t\langle|X_l\rangle\langle Y_{\mathbf{q}nn'm}|\rangle_c &= (\bar{\Omega}_{\mathbf{q}nn'm} - \Omega_l - i\gamma^l_{\mathbf{q}nn'm})\langle|X_l\rangle\langle Y_{\mathbf{q}nn'm}|\rangle_c \\ &\quad + i(\Gamma_l + \gamma_{\mathbf{q}nn'm} - \gamma^l_{\mathbf{q}nn'm})P_l^{L*}\bar{P}^L_{\mathbf{q}nn'm} \\ &\quad + \frac{1}{\sqrt{N}}\sum_{\substack{\mathbf{q}'\neq 0\\ s\ t\neq 0}} \left[\alpha_{sl,0t}(\mathbf{q}')\bar{P}^{L*}_{\mathbf{q}'slt} - \alpha_{ls,0t}(\mathbf{q}')\bar{P}^{L*}_{\mathbf{q}'lst}\right]\bar{P}^L_{\mathbf{q}nn'm} \\ &\quad - \sum_{t\neq 0,m}\left[\bar{V}_{mt,00}(\mathbf{q}) - \alpha_{m0,t0}(-\mathbf{q}) + \frac{1}{N}\sum_{\mathbf{q}'\neq 0}\alpha_{m0,t0}(\mathbf{q}')\right]\langle|X_l\rangle\langle Y_{\mathbf{q}nn't}|\rangle_c \\ &\quad - \sum_{s\neq n}\bar{V}_{n'n',sn}(\mathbf{q})\langle|X_l\rangle\langle Y_{\mathbf{q}sn'm}|\rangle_c - \sum_{s\neq n'}\bar{V}_{sn',nn}(\mathbf{q})\langle|X_l\rangle\langle Y_{\mathbf{q}nsm}|\rangle_c \\ &\quad - \sum_{s\neq n\ s'\neq n'}\bar{V}_{s'n',sn}(\mathbf{q})\langle|X_l\rangle\langle Y_{\mathbf{q}ss'm}|\rangle_c + \sum_{s\neq l}V_{ls}\langle|X_s\rangle\langle Y_{\mathbf{q}nn'm}|\rangle_c \\ &\quad + \frac{1}{\sqrt{N}}\alpha_{m0,n'n}(-\mathbf{q})\left[\langle|X_l\rangle\langle X_{n'}|\rangle_c - \langle|X_l\rangle\langle X_n|\rangle_c\right] \\ &\quad - \frac{1}{\sqrt{N}}\sum_{\substack{\mathbf{q}'\neq 0\\ s\ t\neq 0}}[\alpha_{sl,0t}(\mathbf{q}')\langle|Y_{\mathbf{q}'slt}\rangle\langle Y_{\mathbf{q}nn'm}|\rangle_c - \alpha_{ls,0t}(\mathbf{q}')\langle|Y_{\mathbf{q}'lst}\rangle\langle Y_{\mathbf{q}nn'm}|\rangle_c] \\ &\quad + \frac{1}{N}\sum_{\substack{\mathbf{q}'\neq 0,\mathbf{q}\\ s\ t\neq 0}}\left[\alpha_{mt,sn}(\mathbf{q}'-\mathbf{q})e^{i(\mathbf{q}\times\mathbf{q}')_z\ell^2} - \delta_{tm}\alpha_{00,sn}(\mathbf{q}'-\mathbf{q})\right]\langle|X_l\rangle\langle Y_{\mathbf{q}'sn't}|\rangle_c \\ &\quad - \frac{1}{N}\sum_{\substack{\mathbf{q}'\neq 0,\mathbf{q}\\ s\ t\neq 0}}\left[\alpha_{mt,n's}(\mathbf{q}'-\mathbf{q}) - \delta_{tm}\alpha_{00,n's}(\mathbf{q}'-\mathbf{q})e^{-i(\mathbf{q}\times\mathbf{q}')_z\ell^2}\right]\langle|X_l\rangle\langle Y_{\mathbf{q}'nst}|\rangle_c \end{aligned} \tag{6.31}$$

where we used Eqs. (A.10), (A.11) and (3.66), and introduced a decay rate $\gamma^l_{\mathbf{q}nn'm}$ for the $\langle|X_l\rangle\langle Y_{\mathbf{q}nn'm}|\rangle_c$ coherence.

In analogy with Eqs. (6.30) and (6.31), we can also write the equation of motion for $\langle|Y_{\mathbf{q}nn'm}\rangle\langle Y_{\mathbf{q}'rr't}|\rangle_c$ and thus together with Eq. (6.23) and Eqs. (6.26)–(6.28), we can calculate the third–order polarizations induced in the system. In the following sections, we will present a simplified form of the above equations when photoexcitating the lowest two LLs and ignoring X+MP–X+MP contributions and we will calculate the FWM signal.

## 6.4 Calculation of the FWM signal

To simplify the equations of motion discussed above, we keep the lowest two LLs, LL0 and LL1, assuming that they are the only photoexcited levels. We also ignore density matrices of the $\langle|Y\rangle\langle Y|\rangle_c$ form, as they describe X+MP–X+MP coherences, which we assume they dephase fast and thus their contribution can be described within the relaxation time approximation.

To simplify our expresions, we use the definitions introduced in Eqs. (4.3) and (4.4) for the X populations and X–X coherences respectively, as well as

$$M_{l,nn'}(\mathbf{q}) = \langle|X_l\rangle\langle Y_{\mathbf{q}nn'1}|\rangle_c \tag{6.32}$$

in analogy with Eq. (4.5) and taking into account that the $m \neq 0$ requirement in the $|Y_{\mathbf{q}nn'm}\rangle$ states implies $m = 1$ when keeping 2 LLs only. We also introduce the transformations $P^L_n \to \sqrt{N}P^L_n$ [which we also used in Eqs. (6.19)–(6.21)] $N_n \to NN_n$, $N_{nm} \to NN_{nm}$, and $M_{l,nn'}(\mathbf{q}) \to \sqrt{N}M_{l,nn'}(\mathbf{q})$. Finally, for simplicity we assume that the $M_{l,nn'}(\mathbf{q})$ density matrices depend only on the amplitude $|\mathbf{q}|$. We thus obtain the following equations of motion for the third–order polarizations:

$$\begin{aligned}
i\partial_t P_0 =&(\Omega_0 - i\Gamma_0)P_0 - V_{01}P_1 + 2\mu E(t)\left[P^L_0 P^{L*}_0 + N_0\right] \\
&- 2V_{01}P^L_0 P^L_1(P^{L*}_1 - P^{L*}_0) - \frac{1}{N}P^L_0 P^L_1 \sum_{\mathbf{q}} \alpha_{01,01}(\mathbf{q})\bar{P}^{L*}_{\mathbf{q}011} \\
&- 2V_{01}\left[P^L_1(N_{01} - N_0) - P^L_0(N_{10} - N_1)\right] \\
&- \frac{1}{N}P^L_0 \sum_{\mathbf{q}} \alpha_{01,01}(\mathbf{q})\left[M^*_{1,01}(\mathbf{q}) - M_{0,01}(\mathbf{q})\right] \\
&- \frac{1}{N}P^L_1 \sum_{\mathbf{q}} \alpha_{01,01}(\mathbf{q})\left[M^*_{0,01}(\mathbf{q}) - M_{1,01}(\mathbf{q})\right]
\end{aligned} \tag{6.33}$$

$$
\begin{aligned}
i\partial_t P_1 =&(\Omega_1 - i\Gamma_1)P_1 - V_{10}P_0 + 2\mu E(t)\left[P_1^L P_1^{L*} + N_1\right] \\
&+ 2V_{10}P_0^L P_1^L(P_1^{L*} - P_0^{L*}) + \frac{1}{N}P_0^L P_1^L \sum_{\mathbf{q}} \alpha_{01,01}(\mathbf{q})\bar{P}^{L*}_{\mathbf{q}011} \\
&+ 2V_{10}\left[P_1^L(N_{01} - N_0) - P_0^L(N_{10} - N_1)\right] \\
&+ \frac{1}{N}P_0^L \sum_{\mathbf{q}} \alpha_{01,01}(\mathbf{q})\left[M^*_{1,01}(\mathbf{q}) - M_{0,01}(\mathbf{q})\right] \\
&+ \frac{1}{N}P_1^L \sum_{\mathbf{q}} \alpha_{01,01}(\mathbf{q})\left[M^*_{0,01}(\mathbf{q}) - M_{1,01}(\mathbf{q})\right] \qquad (6.34)
\end{aligned}
$$

The above equations are in exact analogy with Eqs. (4.1) and (4.2). As before, the third term in Eqs. (6.33) and (6.34) is the contribution of Pauli blocking effects (PSF), the fourth describes X–X interactions, and the sixth is the contributions of incoherent X populations and X–X coherences. The fifth and seventh terms are contributions of X–X+MP coherences. They are a generalization of the relevant terms in Eqs. (4.1) and (4.2) so as to include the contribution of each momentum $\mathbf{q}$ seperately. The only density matrices that contribute to the LL0 and LL1 polarizations are $M_{0,01}(q)$ and $M_{1,01}(q)$, in analogy with the $M_0$ and $M_1$ matrices discussed in Chapter 4. We thus ignore all other matrices (like $M_{0,00}$, $M_{0,10}$, etc.). Using Eqs. (6.30) and (6.31), we then obtain the following equations of motion for the X populations, and X–X and X–X+MP coherences:

$$
\begin{aligned}
i\partial_t N_0 =& -i\gamma_D N_0 + i(2\Gamma_0 - \gamma_D)P_0^{L*}P_0^L - V_{10}N_{10} + V_{01}N^*_{10} \\
&+ \frac{1}{N}\sum_{\mathbf{q}\neq 0}\left[-\alpha_{01,01}(\mathbf{q})M_{0,01}(\mathbf{q}) + \alpha_{01,01}(\mathbf{q})M^*_{0,01}(\mathbf{q})\right] \qquad (6.35)
\end{aligned}
$$

$$
\begin{aligned}
i\partial_t N_1 =& -i\gamma_D N_1 + i(2\Gamma_1 - \gamma_D)P_1^{L*}P_1^L + V_{10}N_{10} - V_{01}N^*_{10} \\
&+ \frac{1}{N}\sum_{\mathbf{q}\neq 0}\left[\alpha_{01,01}(\mathbf{q})M_{1,01}(\mathbf{q}) - \alpha_{01,01}(\mathbf{q})M^*_{1,01}(\mathbf{q})\right] \qquad (6.36)
\end{aligned}
$$

$$
\begin{aligned}
i\partial_t N_{10} =&(\Omega_1 - \Omega_0 - i\gamma_{10})N_{10} + i(\Gamma_0 + \Gamma_1 - \gamma_{10})P_0^{L*}P_1^L - V_{01}N_0 + V_{01}N_1 \\
&+ \frac{1}{N}\sum_{s,\mathbf{q}\neq 0}\left[\alpha_{01,01}(\mathbf{q})M_{0,01}(\mathbf{q}) + \alpha_{01,01}(\mathbf{q})M^*_{1,01}(\mathbf{q})\right] \qquad (6.37)
\end{aligned}
$$

$$
\begin{aligned}
i\partial_t M_{0,01} =& (\bar{\Omega}_{\mathbf{q}011} - \Omega_0 - i\gamma^0_{\mathbf{q}011})M_{0,01} + i(\Gamma_0 + \gamma_{\mathbf{q}011} - \gamma^0_{\mathbf{q}011})P_0^{L*}\bar{P}^L_{\mathbf{q}011} \\
&+ V_{01}M_{1,01}(\mathbf{q}) + \alpha_{01,01}(\mathbf{q})\left[N_{10} - N_0\right] + \frac{1}{N}\sum_{\mathbf{q}'\neq 0,\mathbf{q}} W(\mathbf{q},\mathbf{q}')M_{0,01}(\mathbf{q}') \qquad (6.38)
\end{aligned}
$$

$$i\partial_t M_{1,01} = (\bar{\Omega}_{\mathbf{q}011} - \Omega_1 - i\gamma^1_{\mathbf{q}011})M_{1,01} + i(\Gamma_1 + \gamma_{\mathbf{q}011} - \gamma^1_{\mathbf{q}011})P_1^{L*}\bar{P}^L_{\mathbf{q}011} + V_{10}M_{0,01}(\mathbf{q}) + \alpha_{01,01}(\mathbf{q})\left[N_1 - N_{01}\right] + \frac{1}{N}\sum_{\mathbf{q}'\neq 0,\mathbf{q}} W(\mathbf{q},\mathbf{q}')M_{1,01}(\mathbf{q}') \tag{6.39}$$

The system of Eqs. (6.19)–(6.39) can be solved numerically thus we can calculate the FWM signal created at the LL0 and LL1 energies. In the following, we present our numerical calculations where we have included only the factorizable parts of the X–X+MP coherences, i.e. terms of the form $P_0^L P_1^L \bar{P}^{L^*}_{\mathbf{q}011}$. Calculations of the FWM signal including non-factorizable parts are in progress.

Fig. 6.5 shows the calculated FWM signal along the $\Delta t_{12}$ axis for mostly LL1 photoexcitation in two cases: when including the contributions of the X+MP states and when they are ignored. It is clear that their presence strongly affects the nonlinear signal, as it creates a transfer of oscillator strength from LL1 to LL0. In the absence of the continuum of the X+MP states (Fig. 6.5b), the FWM signal is similar to the one from the undoped system.

Fig. 6.6 shows the LL0 FWM signal when calculated within the RPA in comparison with the signal obtained from the full X+MP dispersion. This comparison that the large–momentum X+MP states, for which the RPA is inadequate, can affect the decay of the FWM signal. This is more clear in Fig. 6.6b where a small dephasing rate of the X+MP states is assumed.

## 6.5 Conclusions

In this chapter we studied the role of the X+MP states, described by $|Y_{\mathbf{q}nn'm}\rangle = \hat{X}^\dagger_{\mathbf{q}nn'}\hat{\rho}^e_{-\mathbf{q}m0\uparrow}|G\rangle$, in the linear and nonlinear response of the quantum Hall system for filling factor $\nu = 1$. We showed that the energy dispersion of these states approximately follows the energy dispersion of the magnetoplasmon excitation, which exhibits a local minimum at a non–zero momentum. These large momentum states affect the linear and nonlinear response of the quantum Hall system and cannot be described within the RPA. The linear absorption spectrum exhibits a peak close to the LL1 peak because of the X+MP states, which due to strong dephasing merge into a broad peak that is observed in experiment.

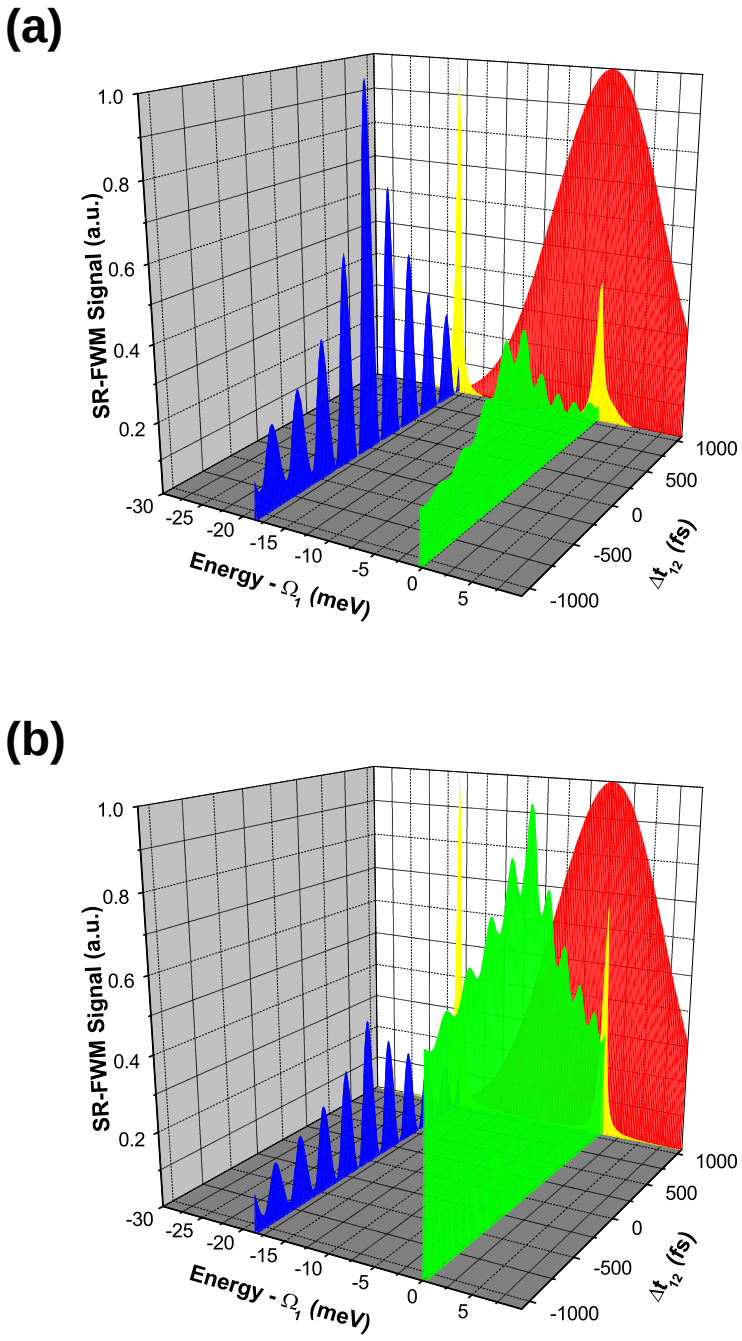


**Figure 6.5:** Theoretical calculation of the FWM signal along the $\Delta t_{12}$ axis for mostly LL1 photoexcitation, (a) with and (b) without the contribution of the X+MP states. The presence of these states strongly affects the nonlinear signal and creates a transfer of oscillator strength from LL1 to LL0. In the absence of the X+MP states, we obtain the LL1/LL0 signal ratio similar to the undoped system.

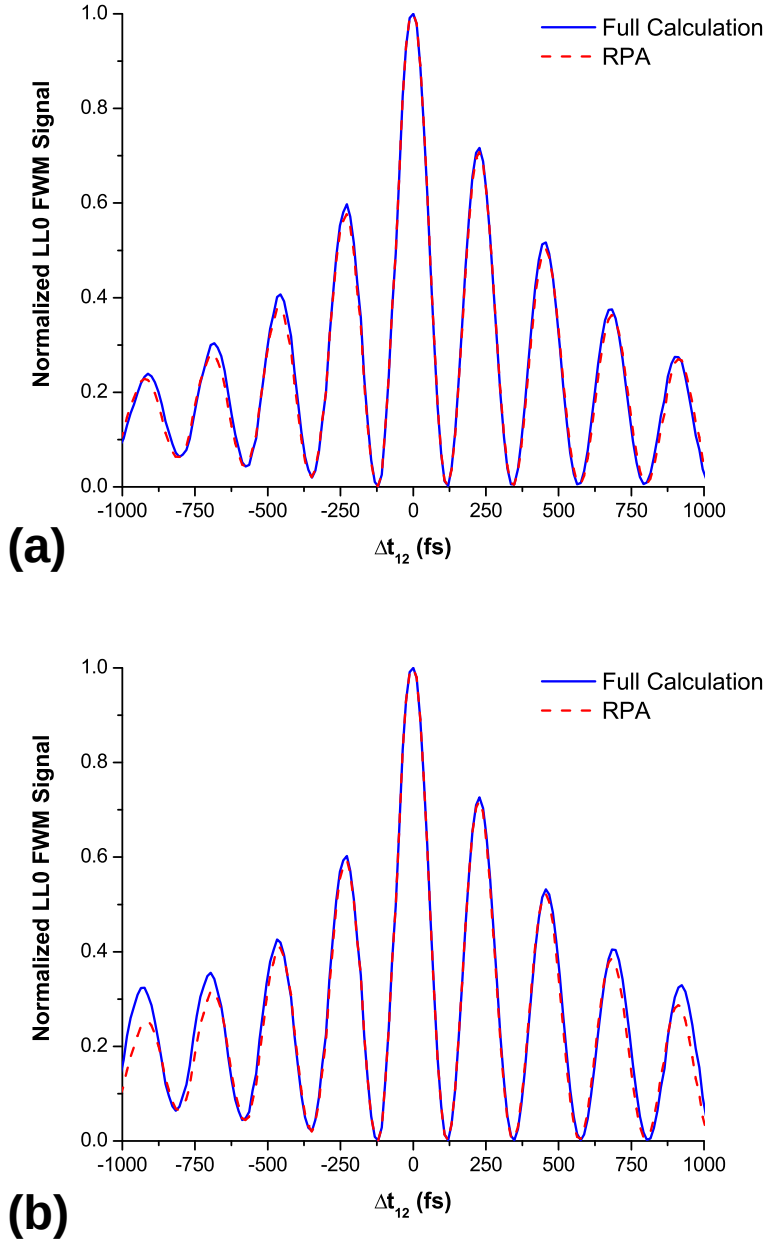


**Figure 6.6:** Calculation of the LL0 FWM signal and comparison with calculation within the RPA, for (a) large and (b) small dephasing of the X+MP states. The large momentum X+MP states, which are not described by the RPA, affect the decay of the signal.

# Chapter 7

# Conclusions

## 7.1 Summary

In this thesis, we discussed a theoretical formulation to study the ultrafast nonlinear optical response of the quantum Hall system. Our approach goes beyond the DCTS, widely used to describe the ultrafast coherent dynamics of excitons in undoped semiconductors, the assumptions of which break down in systems with a strongly correlated ground state, such as the quantum Hall system. Our theory is based on the projection of the exciton states and the separation of the uncorrelated contributions to the third–order nonlinear optical response from the contributions due to correlations among the interband and intraband elementary excitations. We also use an expansion in terms of the optical field in order to eliminate the number of independent dynamical variables that need to be considered, similar to the DCTS [4–6].

We discussed and compared to recent ultrafast three–pulse FWM results that demonstrate the important role of correlations between photoexcited excitons and the inter–LL collective excitations of the 2DEG. We showed that three–pulse transient FWM spectroscopy can be used to access simultaneously the intraband and interband coherent dynamics of the quantum Hall system. Even for very small excitation of the LL0 transition, the FWM signal in the quantum Hall system is dominated by a large off–resonant peak at the LL0 energy with strong coherent oscillations and symmetric temporal profile. Using a microscopic many-body theory we showed that this signal is due to many-particle coherences created via the non-instantaneous interactions of photoexcited carriers and MPs. In particular, the non–instantaneous $X_1 \rightarrow X_{01}$+MP interaction process both creates an intraband coherence and leads to strong LL1 exciton dephasing. Such effects govern the LL0 FWM temporal and spectral profiles. We showed for example that strong tempo-

ral oscillations result from the interference of different FWM contributions of the above intraband coherences. The combination of ultrafast nonlinear spectroscopy and quantum Hall physics initiates a new field of quantum Hall ultrafast dynamics. Future experimental and theoretical activity in this area will further progress our understanding and manipulation of non–equilibrium correlations and quantum coherent phenomena in nanostructures.

From a theoretical point of view, the theoretical formulation developed in this thesis can be used to study the ultrafast nonlinear optical dynamics due to excitations such as the trion and skyrmion states. Such effects have not been explored before. In addition, a new more sensitive experimental technique called two–dimensional correlation spectroscopy that was very recently developed can provide new insight into the ultrafast dynamics of the quantum Hall system. To guide such experiments, theoretical calculations of the experimentally observable signal must be performed based on the present theory.

# Appendix A

# Useful commutators

Here we include several commutators that have been used in Chapter 6. The calculations are often lengthy but always straightforward, by using the definitions Eqs. (3.11), (3.17) and (3.18), as well as Eq. (3.1).

X–X interactions are described by the commutator

$$\left[\hat{X}_{\mathbf{q}_1 n_1 n_1'}, \hat{X}^{\dagger}_{\mathbf{q}_2 n_2 n_2'}\right] = \delta_{\mathbf{q}_1\mathbf{q}_2}\delta_{n_1 n_2}\delta_{n_1' n_2'} - \frac{1}{\sqrt{N}}\delta_{n_1 n_2} e^{i(\mathbf{q}_1\times\mathbf{q}_2)_z \ell^2/2}\hat{\rho}^{h}_{\mathbf{q}_2-\mathbf{q}_1 n_2' n_1'\downarrow} - \frac{1}{\sqrt{N}}\delta_{n_1' n_2'} e^{-i(\mathbf{q}_1\times\mathbf{q}_2)_z \ell^2/2}\hat{\rho}^{e}_{\mathbf{q}_2-\mathbf{q}_1 n_2 n_1\downarrow} \tag{A.1}$$

When $\mathbf{q}_1 = \mathbf{q}_2 = \mathbf{q}$ and $n_1 = n_1' = n$, $m_1 = m_1' = m$ Eq. (A.1) is simplified to Eq. (3.15), written also as

$$\left[\hat{X}_n, \hat{X}^{\dagger}_m\right] = \delta_{nm}\left(1 - \frac{1}{\sqrt{N}}\hat{\rho}^{h}_{0nn\downarrow} - \frac{1}{\sqrt{N}}\hat{\rho}^{e}_{0nn\downarrow}\right) \tag{A.2}$$

Similarly, X–MP interactions are described by

$$\left[\hat{\rho}^{e}_{\mathbf{q}nm\sigma}, \hat{X}^{\dagger}_{\mathbf{q}'n'm'}\right] = \frac{1}{\sqrt{N}}\delta_{\sigma\downarrow}\delta_{mn'} e^{i(\mathbf{q}\times\mathbf{q}')_z \ell^2/2}\hat{X}^{\dagger}_{\mathbf{q}+\mathbf{q}'nm'} \tag{A.3}$$

In analogy of the above commutator,

$$\left[\hat{\rho}^{h}_{\mathbf{q}nm\sigma}, \hat{X}^{\dagger}_{\mathbf{q}'n'm'}\right] = \frac{1}{\sqrt{N}}\delta_{\sigma\downarrow}\delta_{mm'} e^{-i(\mathbf{q}\times\mathbf{q}')_z \ell^2/2}\hat{X}^{\dagger}_{\mathbf{q}+\mathbf{q}'n'n} \tag{A.4}$$

It is also useful to describe the interactions between magnetoplasmons by the commutator

$$\left[\hat{\rho}^{e}_{\mathbf{q}nn'\sigma}, \hat{\rho}^{e}_{\mathbf{q}'mm'\sigma'}\right] = \frac{1}{\sqrt{N}}\delta_{\sigma\sigma'}\delta_{n'm} e^{i(\mathbf{q}\times\mathbf{q}')_z \ell^2/2}\hat{\rho}^{e}_{\mathbf{q}+\mathbf{q}'nm'\sigma} - \frac{1}{\sqrt{N}}\delta_{\sigma\sigma'}\delta_{nm'} e^{-i(\mathbf{q}\times\mathbf{q}')_z \ell^2/2}\hat{\rho}^{e}_{\mathbf{q}+\mathbf{q}'mn'\sigma} \tag{A.5}$$

Moreover,

$$\begin{aligned}\left[\hat{\rho}^h_{\mathbf{q}nn'\sigma},\hat{\rho}^h_{\mathbf{q}'mm'\sigma'}\right] = &\ \frac{1}{\sqrt{N}}\delta_{\sigma\sigma'}\delta_{n'm}e^{-i(\mathbf{q}\times\mathbf{q}')_z\ell^2/2}\hat{\rho}^h_{\mathbf{q}+\mathbf{q}'nm'\sigma}\\ &-\frac{1}{\sqrt{N}}\delta_{\sigma\sigma'}\delta_{nm'}e^{i(\mathbf{q}\times\mathbf{q}')_z\ell^2/2}\hat{\rho}^h_{\mathbf{q}+\mathbf{q}'mn'\sigma}\end{aligned} \tag{A.6}$$

and

$$\left[\hat{\rho}^e_{\mathbf{q}nn'\sigma},\hat{\rho}^h_{\mathbf{q}'mm'\sigma'}\right]=0 \tag{A.7}$$

Another useful commutator, which is easily calculated using Eqs. (A.1) and (A.3), is

$$[\hat{X}_l,\hat{Y}^\dagger_{\mathbf{q}nn'm}]=-\frac{1}{\sqrt{N}}\left(\delta_{ln}\hat{\rho}^h_{\mathbf{q}n'n\downarrow}+\delta_{ln'}\hat{\rho}^e_{\mathbf{q}nn'\downarrow}\right)\hat{\rho}^e_{-\mathbf{q}m0\uparrow} \tag{A.8}$$

where $\hat{Y}^\dagger_{\mathbf{q}nn'm}$ is defined in Eq. (6.2). Eq. (A.8) describes the interaction of an exciton with an X+MP configuration. Similarly, X+MP–X+MP interactions are described by

$$\begin{aligned}[\hat{Y}_{\mathbf{q}_1n_1n_1'm_1},\hat{Y}^\dagger_{\mathbf{q}_2n_2n_2'm_2}] =&\frac{1}{\sqrt{N}}\Big[\delta_{m_1m_2}e^{-i(\mathbf{q}_1\times\mathbf{q}_2)_z\ell^2/2}\hat{\rho}^e_{\mathbf{q}_1-\mathbf{q}_200\uparrow}\\ &-e^{i(\mathbf{q}_1\times\mathbf{q}_2)_z\ell^2/2}\hat{\rho}^e_{\mathbf{q}_1-\mathbf{q}_2m_2m_1\uparrow}\Big]\hat{X}^\dagger_{\mathbf{q}_2n_2n_2'}\hat{X}_{\mathbf{q}_1n_1n_1'}\\ &+\Big[\delta_{\mathbf{q}_1\mathbf{q}_2}\delta_{n_1n_2}\delta_{n_1'n_2'}-\frac{\delta_{n_1n_2}}{\sqrt{N}}e^{-i(\mathbf{q}_1\times\mathbf{q}_2)_z\ell^2/2}\hat{\rho}^h_{\mathbf{q}_2-\mathbf{q}_1n_2'n_1'\downarrow}\\ &-\frac{\delta_{n_1'n_2'}}{\sqrt{N}}e^{i(\mathbf{q}_1\times\mathbf{q}_2)_z\ell^2/2}\hat{\rho}^e_{\mathbf{q}_2-\mathbf{q}_1n_2n_1\downarrow}\Big]\hat{\rho}^e_{\mathbf{q}_10m_1\uparrow}\hat{\rho}^e_{\mathbf{q}_2m_20\uparrow}\end{aligned} \tag{A.9}$$

The interactions between excitons and the ground state 2DEG are described by the commutator of the exciton operator with the Hamiltonian:

$$\begin{aligned}\left[\hat{X}_{\mathbf{q}nn'},H\right] =&\Big[E_g+\Omega^c_c(n+\frac{1}{2})+\Omega^v_c(n'+\frac{1}{2})\Big]\hat{X}_{\mathbf{q}nn'}-\sum_{rr'}\bar{V}_{r'n',rn}(\mathbf{q})\hat{X}_{\mathbf{q}rr'}\\ &+\frac{1}{2\pi\ell^2\sqrt{N}}\sum_{\mathbf{q}'r}v_{q'}\hat{\rho}_{\mathbf{q}'}\Big[\phi_{nr}(-\mathbf{q}')\hat{X}_{\mathbf{q}+\mathbf{q}'rn'}e^{i(\mathbf{q}\times\mathbf{q}')_z\ell^2/2}\\ &-\phi_{rn'}(-\mathbf{q}')\hat{X}_{\mathbf{q}+\mathbf{q}'nr}e^{-i(\mathbf{q}\times\mathbf{q}')_z\ell^2/2}\Big]\end{aligned} \tag{A.10}$$

Similarly,

$$\begin{aligned}\left[\hat{\rho}^{e}_{\mathbf{q}mm'\sigma}, H\right] =& \Big[\Omega^{c}_{c}(m'-m) + \sum_{r} V_{rm}\Big]\hat{\rho}^{e}_{\mathbf{q}mm'\sigma} - \sum_{rr'} \bar{V}_{m'r',mr}(\mathbf{q})\hat{\rho}^{e}_{\mathbf{q}rr'\sigma} \\ &+ \frac{1}{2\pi\ell^2\sqrt{N}} \sum_{\mathbf{q}'r} v_{q'}\hat{\rho}_{-\mathbf{q}'}\Big[\phi_{m'r}(\mathbf{q}')\hat{\rho}^{e}_{\mathbf{q}+\mathbf{q}'mr\sigma} e^{i(\mathbf{q}\times\mathbf{q}')_z\ell^2/2} \\ &\qquad - \phi_{rm}(\mathbf{q}')\hat{\rho}^{e}_{\mathbf{q}+\mathbf{q}'rm'\sigma} e^{-i(\mathbf{q}\times\mathbf{q}')_z\ell^2/2}\Big]\end{aligned} \tag{A.11}$$

and

$$\begin{aligned}\left[\hat{\rho}^{h}_{\mathbf{q}mm'\sigma}, H\right] =& \Big[\Omega^{v}_{c}(m'-m) + \sum_{r} V_{mr}\Big]\hat{\rho}^{h}_{\mathbf{q}mm'\sigma} - \sum_{rr'} \bar{V}_{mr,m'r'}(\mathbf{q})\hat{\rho}^{h}_{\mathbf{q}rr'\sigma} \\ &+ \frac{1}{2\pi\ell^2\sqrt{N}} \sum_{\mathbf{q}'r} v_{q'}\hat{\rho}_{-\mathbf{q}'}\Big[\phi_{mr}(\mathbf{q}')\hat{\rho}^{h}_{\mathbf{q}+\mathbf{q}'rm'\sigma} e^{i(\mathbf{q}\times\mathbf{q}')_z\ell^2/2} \\ &\qquad - \phi_{rm'}(\mathbf{q}')\hat{\rho}^{h}_{\mathbf{q}+\mathbf{q}'mr\sigma} e^{-i(\mathbf{q}\times\mathbf{q}')_z\ell^2/2}\Big]\end{aligned} \tag{A.12}$$

# Bibliography


[1] N. W. Ashcroft and N. D. Mermin, *Solid State Physics*, Saunders College Publishing (1975).

[2] D. S. Chemla and J. Shah, *Many-body and correlation effects in semiconductors*, Nature **411** (6837), 549 (2001).

[3] D. S. Chemla, *Ultrafast transient nonlinear optical processes in semiconductors*, in *Non-linear Optics in Semiconductors*, edited by R. K. Willardson and A. C. Beers, Academic Press, New York (1999).

[4] V. M. Axt and A. Stahl, *A dynamics-controlled truncation scheme for the hierarchy of density matrices in semiconductor optics*, Z. Phys. B Condens. Matter **93** (2), 195 (1994).

[5] V. M. Axt, K. Victor, and A. Stahl, *Influence of a phonon bath on the hierarchy of electronic densities in an optically excited semiconductor*, Phys. Rev. B **53** (11), 7244 (1996).

[6] V. M. Axt and S. Mukamel, *Nonlinear optics of semiconductor and molecular nanostructures; a common perspective*, Rev. Mod. Phys. **70** (1), 145 (1998).

[7] F. Rossi and T. Kuhn, *Theory of ultrafast phenomena in photoexcited semiconductors*, Rev. Mod. Phys. **74** (3), 895 (2002).

[8] W. Schäfer and M. Wegener, *Semiconductor Optics and Transport Phenomena*, Springer (2002).

[9] H. Haug and S. W. Koch, *Quantum Theory of the Optical and Electronic Properties of Semiconductors*, World Scientific (1993).

[10] S. T. Cundiff, M. Koch, W. H. Knox, J. Shah, and W. Stolz, *Optical Coherence in Semiconductors: Strong Emission Mediated by Nondegenerate Interactions*, Phys. Rev. Lett. **77** (6), 1107 (1996).

[11] S. Wu, X.-C. Zhang, and R. L. Fork, *Direct experimental observation of interactive third and fifth order nonlinearities in a time- and space-resolved four-wave mixing experiment*, Applied Physics Letters **61** (8), 919 (1992).

[12] R. W. Boyd, *Nonlinear Optics*, Academic Press, San Diego, CA, 2nd ed. (2003).

[13] J. Shah, *Ultrafast Spectroscopy of Semiconductors and Semiconductor Nanostructures*, vol. 115 of *Springer Series in Solid–State Sciences*, Springer-Verlag, Berlin Heidelberg New York, 2nd ed. (1999).

[14] L. J. Sham, *Theory of the Shallow Impurity States in Semiconductors*, Phys. Rev. **150** (2), 720 (1966).

[15] *Topics in Computational Materials Science*, chap. First-Principles Theory of Electron Excitation Energies in Solids, Surfaces, and Defects, World Scientific, Singapore (1998).

[16] M. I. Salkola and J. R. Schrieffer, *Collective excitations in high-temperature superconductors*, Phys. Rev. B **58** (10), R5944 (1998).

[17] M. Rübhausen, *The different energy scales of cuprate uperconductors investigated by inelastic light scattering*, Journal of Physics and Chemistry of Solids **59** (10-12), 1947 (1998).

[18] E. Y. Andrei, D. C. Glattli, F. I. B. Williams, and M. Heiblum, *Low frequency collective excitations in the quantum-hall system*, Surface Science **196** (1–3), 501 (1988).

[19] M. A. Eriksson, A. Pinczuk, B. S. Dennis, S. H. Simon, L. N. Pfeiffer, and K. W. West, *Collective Excitations in the Dilute 2D Electron System*, Phys. Rev. Lett. **82** (10), 2163 (1999).

[20] A. Pinczuk, *Perspectives in Quantum Hall Effects:Novel Quantum Liquids in Low-Dimensional Semiconductor Structures*, chap. 8, Wiley, New York (1996).

[21] T. Chakraborty and P. Pietilainen, *The Quantum Hall Effects, Fractional and Integral*, Springer, 2nd ed. (1995).

[22] S. D. Sarma and A. Pinczuk (Eds.), *Perspectives in Quantum Hall Effects:Novel Quantum Liquids in Low-Dimensional Semiconductor Structures*, Wiley, New York (1996).

[23] K. v. Klitzing, G. Dorda, and M. Pepper, *New Method for High-Accuracy Determination of the Fine-Structure Constant Based on Quantized Hall Resistance*, Phys. Rev. Lett **45** (6), 494 (1980).

[24] D. C. Tsui, H. L. Stormer, and A. C. Gossard, *Two-Dimensional Magnetotransport in the Extreme Quantum Limit*, Phys. Rev. Lett. **48** (22), 1559 (1982).

[25] A. T. Karathanos, I. E. Perakis, N. A. Fromer, and D. S. Chemla, *Ultrafast nonlinear optical response of strongly correlated systems: Dynamics in the quantum Hall effect regime*, Phys. Rev. B **67**, 035316 (2003).

[26] I. E. Perakis and T. V. Shahbazyan, *Many-body correlation effects in the ultrafast non-linear optical response of confined Fermi seas*, Surface Science Reports **40** (1–2), 1 (2000).

[27] I. E. Perakis, *Many-body effects in nonlinear spectroscopy: a time-dependent transformation approach*, Chemical Physics **210** (1–2), 259 (1996).

[28] I. Brener, W. H. Knox, and W. Schäefer, *Virtual excitation of the Fermi-edge singularity in modulation-doped quantum wells*, Phys. Rev. B **51** (3), 2005 (1995).

[29] S. Bar-Ad, I. Bar-Joseph, Y. Levinson, and H. Shtrikman, *Coherent optical spectroscopy of electron scattering in a two-dimensional electron gas in high magnetic fields*, Phys. Rev. Lett. **72** (5), 776 (1994).

[30] I. E. Perakis and D. S. Chemla, *ac Stark effect of the Fermi edge singularity: Observation of "excitonic polarons"?*, Phys. Rev. Lett. **72** (20), 3202 (1994).

[31] N. Primozich, T. V. Shahbazyan, I. E. Perakis, and D. S. Chemla, *Coherent ultrafast optical dynamics of the Fermi-edge singularity*, Phys. Rev. B **61** (3), 2041 (2000).

[32] T. V. Shahbazyan, N. Primozich, I. E. Perakis, and D. S. Chemla, *Femtosecond Coherent Dynamics of the Fermi-Edge Singularity and Exciton Hybrid*, Phys. Rev. Lett. **84** (9), 2006 (2000).

[33] M. Shayegan, J. K. Wang, M. Santos, T. Sajoto, and B. B. Goldberg, *Fractional quantum Hall effect in a high-mobility $GaAs/Al_xGa_{1-x}As$ multiple quantum well heterostructure*, Applied Physics Letters **54** (1), 27 (1989).

[34] T. Sajoto, Y. W. Suen, L. W. Engel, M. B. Santos, and M. Shayegan, *Fractional quantum Hall effect in very-low-density $GaAs/Al_xGa_{1-x}As$ heterostructures*, Phys. Rev. B **41** (12), 8449 (1990).

[35] A. H. MacDonald, H. C. A. Oji, and S. M. Girvin, *Magnetoplasmon Excitations from Partially Filled Landau Levels in Two Dimensions*, Phys. Rev. Lett. **55**, 2208 (1985).

[36] P. Pietiläinen and T. Chakraborty, *Collective Excitations in the Fractionally Quantized Hall Effect and the Magnetoplasmon Mode*, Europhys. Lett. **5** (2), 157 (1988).

[37] I. K. Marmorkos and S. D. Sarma, *Magnetoplasmon excitation spectrum for integral filling factors in a two-dimensional electron system*, Phys. Rev. B **45** (23), 13396 (1992).

[38] N. A. Fromer, C. E. Lai, D. S. Chemla, I. E. Perakis, D. Driscoll, and A. C. Gossard, *Dynamics of Inter-Landau-Level Excitations of a Two-Dimensional Electron Gas in the Quantum Hall Regime*, Phys. Rev. Lett. **89**, 067401 (2002).

[39] N. A. Fromer, C. Schüller, D. S. Chemla, T. V. Shahbazyan, I. E. Perakis, K. Maranowski, and A. C. Gossard, *Electronic Dephasing in the Quantum Hall Regime*, Phys. Rev. Lett **83** (22), 4646 (1999).

[40] N. A. Fromer, C. Schüller, C. W. Lai, D. S. Chemla, I. E. Perakis, D. Driscoll, and A. C. Gossard, *Coulomb correlations in a two-dimensional electron gas in large magnetic fields*, Phys. Rev. B **66**, 205314 (2002).

[41] I. E. Perakis and D. S. Chemla, *Ultrafast Dephasing and Collective Effects in the Quantum Hall Effect Regime*, physica status solidi (b) **234** (1), 242 (2002).

[42] I. E. Perakis and D. S. Chemla, *Coherent ultrafast dynamics in the quantum Hall effect regime*, Solid State Communications (2003).

[43] I. E. Perakis, *Ultrafast dephasing in strongly correlated systems*, physica status solidi (b) **238** (3), 502 (2003).

[44] C. Schüller, I. E. Perakis, N. A. Fromer, and D. S. Chemla, *Ultrafast Spectroscopy in the Quantum Hall Regime*, in *Nonequilibrium Physics at Short Time Scales: Formation of Correlations*, edited by K. Morawetz, pp. 209–230, Springer Verlag, Berlin, Heidelberg, New York (2004).

[45] K. M. Dani, J. Tignon, M. Breit, D. S. Chemla, E. G. Kavousanaki, and I. E. Perakis, *Ultrafast Dynamics of Coherences in a Quantum Hall System*, Phys. Rev. Lett. **97**, 057401 (2006).

[46] K. M. Dani, E. G. Kavousanaki, J. Tignon, D. S. Chemla, and I. E. Perakis, *Nonlinear optical studies of the transient coherence in the Quantum Hall system*, Solid State Communications **140** (2), 72 (2006).

[47] K. M. Dani, J. Tignon, M. Breit, D. S. Chemla, E. G. Kavousanaki, and I. E. Perakis, *Dynamics of the collective excitations of the quantum Hall system*, Physica E: Low-dimensional Systems and Nanostructures **34** (1-2), 206 (2006).

[48] E. G. Kavousanaki, K. M. Dani, J. Tignon, D. S. Chemla, and I. E. Perakis, *Correlation effects in the ultrafast dynamics of the Quantum Hall system close to* $\nu = 1$, physica status solidi (b) **243** (10), 2397 (2006).

[49] D. Yoshioka, *The Quantum Hall Effect*, vol. 133 of *Springer Series in Solid–State Sciences*, Springer–Verlag, Berlin Heidelberg New York (2002).

[50] M. Wegener and D. S. Chemla, *Coherent control of electron-phonon quantum kinetics: exploring the weak and the strong coupling regime*, Chemical Physics **251** (1-3), 269 (2000).

[51] V. M. Axt and T. Kuhn, *Femtosecond spectroscopy in semiconductors: a key to coherences, correlations and quantum kinetics*, Rep. Prog. Phys. **67** (4), 433 (2004).

[52] K. M. Dani, *Dynamics of the Quantum Hall System via Ultrafast Non-Linear Optical Spectroscopy*, Ph.D. thesis, Ernest Orlando Lawrence Berkeley National Laboratory and University of California at Berkeley, Berkeley, CA (2006).

[53] K. M. Dani, I. A. Cotoros, J. Wang, J. Tignon, D. S. Chemla, E. G. Kavousanaki, and I. E. Perakis, *Observation of Inter-Landau-level Quantum Coherence in Semiconductor Quantum Wells*, in preparation.

[54] *Electronic archive: New Semiconductor Materials. Characteristics and Properties*, Ioffe Physico-Technical Institute.
`http://www.ioffe.ru/SVA/NSM//Semicond/GaAs/bandstr.html`

[55] A. H. MacDonald and D. S. Ritchie, *Hydrogenic energy levels in two dimensions at arbitrary magnetic fields*, Phys. Rev. B **33** (12), 8336 (1986).

[56] O. Akimoto and H. Hasegawa, *nterband Optical Transitions in Extremely Anisotropic Semiconductors. II. Coexistence of Exciton and the Landau Levels*, Journal of the Physical Society of Japan **22** (1), 181 (1967).

[57] M. Shinada and S. Sugano, *Interband Optical Transitions in Extremely Anisotropic Semiconductors. I. Bound and Unbound Exciton Absorption*, Journal of the Physical Society of Japan **21** (10), 1936 (1966).

[58] M. Shinada and K. Tanaka, *Interband Optical Transitions in Extremely Anisotropic Semiconductors. III. Numerical Studies of Magneto-Optical Absorption*, Journal of the Physical Society of Japan **29** (5), 1258 (1970).

[59] M. Altarelli, U. Ekenberg, and A. Fasolino, *Calculations of hole subbands in semiconductor quantum wells and superlattices*, Phys. Rev. B **32** (8), 5138 (1985).

[60] G. E. W. Bauer and T. Ando, *Theory of magnetoexcitons in quantum wells*, Phys. Rev. B **37** (6), 3130 (1988).

[61] D. A. Broido and L. J. Sham, *Effective masses of holes at GaAs-AlGaAs heterojunctions*, Phys. Rev. B **31** (2), 888 (1985).

[62] U. Ekenberg and M. Altarelli, *Subbands and Landau levels in the two-dimensional hole gas at the GaAs-$Al_xGa_{1-x}As$ interface*, Phys. Rev. B **32** (6), 3712 (1985).

[63] S.-R. E. Yang, D. A. Broido, and L. J. Sham, *Holes at GaAs-$Al_xGa_{1-x}As$ heterojunctions in magnetic fields*, Phys. Rev. B **32** (10), 6630 (1985).

[64] S.-R. E. Yang and L. J. Sham, *Theory of magnetoexcitons in quantum wells*, Phys. Rev. Lett. **58** (24), 2598 (1987).

[65] J. M. Luttinger, *Quantum Theory of Cyclotron Resonance in Semiconductors: General Theory*, Phys. Rev. **102** (4), 1030 (1956).

[66] S. M. Girvin, A. H. MacDonald, and P. M. Platzman, *Collective-Excitation Gap in the Fractional Quantum Hall Effect*, Phys. Rev. Lett. **54**, 581 (1985).

[67] C. Kallin and B. I. Halperin, *Excitations from a filled Landau level in the two-dimensional electron gas*, Phys. Rev. B **30** (10), 5655 (1984).

[68] J. P. Eisenstein, L. N. Pfeiffer, and K. W. West, *Coulomb barrier to tunneling between parallel two-dimensional electron systems*, Phys. Rev. Lett. **69** (26), 3804 (1992).

[69] A. Pinczuk, B. S. Dennis, L. N. Pfeiffer, and K. West, *Observation of collective excitations in the fractional quantum Hall effect*, Phys. Rev. Lett. **70** (25), 3983 (1993).

[70] A. Pinczuk, J. P. Valladares, D. Heiman, A. C. Gossard, J. H. English, C. W. Tu, L. Pfeiffer, and K. West, *Observation of roton density of states in two-dimensional Landau-level excitations*, Phys. Rev. Lett. **61** (23), 2701 (1988).

[71] R. P. Feynmann, *Statistical Mechanics: A Set of Lectures*, Benjamin/Cummings, Massachusetts (1972).

[72] W. Kohn, *Cyclotron Resonance and de Haas-van Alphen Oscillations of an Interacting Electron Gas*, Phys. Rev. **123** (4), 1242 (1961).

[73] M. L. Cohen and J. R. Chelikowsky, *Electronic Structure and Optical Properties of Semiconductors*, vol. 75 of *Solid State Physics*, Springer, Berlin, Heidelberg, 2nd ed. (1989).

[74] E. J. Mayer, G. O. Smith, V. Heuckeroth, J. Kuhl, K. Bott, A. Schulze, T. Meier, S. W. Koch, P. Thomas, R. Hey, and K. Ploog, *Polarization dependence of beating phenomena at the energetically lowest exciton transition in GaAs quantum wells*, Phys. Rev. B **51** (16), 10909 (1995).

[75] L. Schultheis, J. Kuhl, A. Honold, and C. W. Tu, *Picosecond Phase Coherence and Orientational Relaxation of Excitons in GaAs*, Phys. Rev. Lett. **57** (14), 1797 (1986).

[76] M. Lindberg and S. W. Koch, *Effective Bloch equations for semiconductors*, Phys. Rev. B 38 **38** (5), 3342 (1988).

[77] S. Schmitt-Rink and D. S. Chemla, *Collective Excitations and the Dynamical Stark Effect in a Coherently Driven Exciton System*, Phys. Rev. Lett. **57** (21), 2752 (1986).

[78] S. Schmitt-Rink, D. S. Chemla, and H. Haug, *Nonequilibrium theory of the optical Stark effect and spectral hole burning in semiconductors*, Phys. Rev. B **37**, 941 (1988).

[79] S. Weiss, M.-A. Mycek, J.-Y. Bigot, S. Schmitt-Rink, and D. S. Chemla, *Collective effects in excitonic free induction decay: Do semiconductors and atoms emit coherent light in different ways?*, Phys. Rev. Lett. **69** (18), 2685 (1992).

[80] S. Glutsch, U. Siegner, and D. S. Chemla, *Spatiotemporal dynamics of photon echoes from continuum states in semiconductors*, Phys. Rev. B **52** (7), 4941 (1995).

[81] M. Lindberg, R. Binder, and S. W. Koch, *Theory of the semiconductor photon echo*, Phys. Rev. A **45** (3), 1865 (1992).

[82] K. Leo, M. Wegener, J. Shah, D. S. Chemla, E. O. Göbel, T. C. Damen, S. Schmitt-Rink, and W. Schäfer, *Effects of coherent polarization interactions on time-resolved degenerate four-wave mixing*, Phys. Rev. Lett. **65** (11), 1340 (1990).

[83] M. Wegener, D. S. Chemla, S. Schmitt-Rink, and W. Schäfer, *Line shape of time-resolved four-wave mixing*, Phys. Rev. A **42** (9), 5675 (1990).

[84] F. Jahnke, M. Koch, T. Meier, J. Feldmann, W. Schäfer, P. Thomas, S. Koch, E. Göbel, and H. Nickel, *Simultaneous influence of disorder and Coulomb interaction on photon echoes in semiconductors*, Phys. Rev. B **50** (11), 8114 (1994).

[85] C. Stafford, S. Schmitt-Rink, and W. Schaefer, *Nonlinear optical response of two-dimensional magnetoexcitons*, Phys. Rev. B **41** (14), 10000 (1990).

[86] S. Schmitt-Rink, J. B. Stark, W. H. Knox, D. S. Chemla, and W. Schäfer, *Optical properties of quasi-zero-dimensional magneto-excito ns*, Applied Physics A: Materials Science & Processing **53** (6), 491 (1991).

[87] S. Bar-Ad and I. Bar-Joseph, *Exciton spin dynamics in GaAs heterostructures*, Phys. Rev. Lett. **68** (3), 349 (1992).

[88] D. J. Lovering, R. T. Phillips, G. J. Denton, and G. W. Smith, *Resonant generation of biexcitons in a GaAs quantum well*, Phys. Rev. Lett. **68** (12), 1880 (1992).

[89] P. Kner, S. Bar-Ad, M. V. Marquezini, D. S. Chemla, and W. Schäfer, *Magnetically Enhanced Exciton-Exciton Correlations in Semiconductors*, Phys. Rev. Lett. **78** (7), 1319 (1997).

[90] K. Victor, V. M. Axt, and A. Stahl, *Hierarchy of density matrices in coherent semiconductor optics*, Phys. Rev. B **51** (20), 14164 (1995).

[91] W. Schäfer, D. S. Kim, J. Shah, T. C. Damen, J. E. Cunningham, K. W. Goossen, L. N. Pfeiffer, and K. Köhler, *Femtosecond coherent fields induced by many-particle correlations in transient four-wave mixing*, Phys. Rev. B **53** (24), 16429 (1996).

[92] G. Bartels, A. Stahl, V. M. Axt, B. Haase, U. Neukirch, and J. Gutowski, *Identification of Higher-Order Electronic Coherences in Semiconductors by their Signature in Four-Wave-Mixing Signals*, Phys. Rev. Lett. **81** (26), 5880 (1998).

[93] L. J. S. S. R. Bolton, U. Neukirch, D. S. Chemla, and V. M. Axt, *Demonstration of Sixth-Order Coulomb Correlations in a Semiconductor Single Quantum Well*, Phys. Rev. Lett. **85** (9), 2002 (2000).

[94] R. L. P. Kner, W. Schäfer and D. S. Chemla, *Coherence of Four-Particle Correlations in Semiconductors*, Phys. Rev. Lett. **81** (24), 5386 (1998).

[95] N. A. Fromer, P. Kner, D. S. Chemla, R. Lövenich, and W. Schäfer, *Correlation effects beyond Hartree-Fock theory and polarization dependence of four-wave mixing in bulk GaAs at high magnetic field*, Phys. Rev. B **62** (4), 2516 (2000).

[96] U. Neukirch, S. R. Bolton, N. A. Fromer, L. J. Sham, and D. S. Chemla, *Polariton-Biexciton Transitions in a Semiconductor Microcavity*, Phys. Rev. Lett. **84** (10), 2215 (2000).

[97] U. Neukirch, S. R. Bolton, L. J. Sham, and D. S. Chemla, *Electronic four-particle correlations in semiconductors: Renormalization of coherent pump-probe oscillations*, Phys. Rev. B **61** (12), R7835 (2000).

[98] I. E. Perakis and T. V. Shahbazyan, *Canonical transformation approach to the ultrafast nonlinear optical dynamics of semiconductors*, International Journal of Modern Physics B **13** (8), 869 (1999).

[99] S. Mukamel, *Principles of Nonlinear Optical Spectroscopy*, Oxford University Press (1995).

[100] M. Z. Maialle and L. J. Sham, *Interacting Electron Theory of Coherent Nonlinear Response*, Phys. Rev. Lett. **73** (24), 3310 (1994).

[101] T. Östreich, K. Schönhammer, and L. J. Sham, *Exciton-Exciton Correlation in the Nonlinear Optical Regime*, Phys. Rev. Lett. **74** (23), 4698 (1995).

[102] W. Schäfer, R. Lövenich, N. A. Fromer, and D. S. Chemla, *From Coherently Excited Highly Correlated States to Incoherent Relaxation Processes in Semiconductors*, Phys. Rev. Lett. **86** (2), 344 (2001).

[103] H. C. A. Oji and A. H. MacDonald, *Magnetoplasma modes of the two-dimensional electron gas at nonintegral filling factors*, Phys. Rev. B **33** (6), 3810 (1986).

[104] E. Feenberg, *Theory of Quantum Fluids*, Academic Press, New York (1969).

[105] V. M. Apalkov and E. I. Rashba, *Interaction of excitons with an incompressible quantum liquid*, Phys. Rev. B **46** (3), 1628 (1992).

[106] A. Pinczuk, B. S. Dennis, D. Heiman, C. Kallin, L. Brey, C. Tejedor, S. Schmitt-Rink, L. N. Pfeiffer, and K. W. West, *Spectroscopic measurement of large exchange enhancement of a spin-polarized 2D electron gas*, Phys. Rev. Lett. **68** (24), 3623 (1992).

[107] S. M. Girvin and A. H. MacDonald, *Novel Quantum Liquids in Low Dimensional Semiconductor Structures*, Wiley, New York (1996).

[108] N. R. Cooper and D. B. Chklovskii, *Theory of photoluminescence of the $\nu = 1$ quantum Hall state: Excitons, spin waves, and spin textures*, Phys. Rev. B **55** (4), 2436 (1997).

[109] E. H. Aifer, B. B. Goldberg, and D. A. Broido, *Evidence of Skyrmion Excitations about $\nu = 1$ in n-Modulation-Doped Single Quantum Wells by Interband Optical Transmission*, Phys. Rev. Lett. **76** (4), 680 (1996).

[110] A. H. MacDonald, *Hartree-Fock approximation for response functions and collective excitations in a two-dimensional electron gas with filled Landau levels*, J. Phys. C: Solid State Phys. 18 1003-1016 **18** (5), 1003 (1985).

[111] T. V. Shahbazyan, N. Primozich, and I. E. Perakis, *Ultrafast Coulomb-induced dynamics of quantum well magnetoexcitons*, Phys. Rev. B **62** (23), 15925 (2000).

[112] T. Östreich, K. Schönhammer, and L. J. Sham, *Theory of exciton-exciton correlation in nonlinear optical response*, Phys. Rev. B **58** (19), 12920 (1998).

[113] R. Haydock, *The Recursive Solution of the Schrödinger Equation*, in *Solid State Physics*, edited by H. Ehrenreich, F. Seitz, and D. Turnbull, vol. 35, pp. 215–294, Academic Press Inc. (1980).

[114] I. E. Perakis and E. G. Kavousanaki, *Theory of ultrafast exciton dynamics in the Quantum Hall system*, Chemical Physics **318** (1-2), 118 (2005).

[115] T. D. H. K. G. Bartels, G. C. Cho, A. Stahl, and K. Köhler, *Coherent signature of differential transmission signals in semiconductors: Theory and experiment*, Phys. Rev. B **55** (24), 16404 (1997).

[116] K.-J. Boller, A. Imamoğlu, and S. E. Harris, *Observation of electromagnetically induced transparency*, Phys. Rev. Lett. **66** (20), 2593 (1991).

[117] A. S. Zibrov, M. D. Lukin, D. E. Nikonov, L. Hollberg, M. O. Scully, V. L. Velichansky, and H. G. Robinson, *Experimental Demonstration of Laser Oscillation without Population Inversion via Quantum Interference in Rb*, Phys. Rev. Lett. **75** (8), 1499 (1995).

[118] M. E. Donovan, A. Schülzgen, J. Lee, P. A. Blanche, N. Peyghambarian, G. Khitrova, H. M. Gibbs, I. Rumyantsev, R. T. N. H. Kwong, Z. S. Yang, , and R. Binder, *Evidence for Intervalence Band Coherences in Semiconductor Quantum Wells via Coherently Coupled Optical Stark Shifts*, Phys. Rev. Lett. **87** (2001).

[119] N. A. Fromer, *Dynamics of Coulomb Correlations in Semiconductors in High Magnetic Fields*, Ph.D. thesis, Ernest Orlando Lawrence Berkeley National Laboratory and University of California at Berkeley, Berkeley, CA (2002).

[120] G. D. Mahan, *Many–Particle Physics*, Plenum Press (1990).